Atmospheric mechanisms of central Saharan dust storm formation in boreal summer: observations from the Fennec campaign

Christopher J. T. Allen

Climate Research Lab, School of Geography and the Environment,
University of Oxford

Thesis submitted to the University of Oxford for the degree of
Doctor of Philosophy in Geography and the Environment

Hilary Term 2015 (accepted Trinity Term 2015)

Concise Abstract

In boreal summer, satellite measurements show that the central Sahara is the dustiest region of the planet. However, ground-based observations of the central Sahara have been limited to its outer edges, leaving a void in observations approximately 1 million km^2 in area. The Fennec Project has been the first campaign to instrument this remote but climatologically important region. This thesis uses these new observations to detect and explain the atmospheric mechanisms that make the central Sahara the summer global dust maximum.

Four atmospheric mechanisms are found to cause dust storms in the central Sahara in June 2011 and June 2012. These are cold pool outflows, low-level jets (LLJs), monsoon surges and dry convective plumes. Dust may be emitted locally by these phenomena, or be advected, principally by cold pools. In both field seasons, dust emission by cold pool outflows is the most important dust mechanism, causing roughly half of the total dust loadings at the Fennec supersite of Bordj-Badji Mokhtar (BBM), the closest station to the dust maximum. The second most important mechanism is dust advection by cold pools (roughly 30% dust), followed by dust emission by monsoon surges, LLJs and finally dry convective plumes (only 2% dust). Choice of instrumentation is very important: because cold pools frequently occur at night or under cloud, the sun photometer misses about half of cold pool dust at BBM.

Although LLJs occurred on 21/28 mornings at BBM in June 2011, only five of these jets led to dust emission. Calculations of momentum exchanges through the atmospheric column show that momentum mix-down from the jet core is the cause of dust emission on these occasions, but that the LLJ has to be particularly strong ($\geq$ 16 m s^{-1}) to result in dust emission at the surface.

The Met Office Africa-Limited Area Model (LAM) underestimates monsoon LLJ wind profiles, and ERA-Interim reanalysis underestimates both monsoon and Harmattan LLJ wind profiles. At the surface, the Met Office Africa-LAM and GLOBAL models significantly underpredict the frequency of observed wind speeds >6 m s^{-1}. This will cause them to significantly underestimate dust emission, as emission is a threshold process proportional to the cube of wind speed.

Full Abstract

In boreal summer, satellite measurements show that the central Sahara is the dustiest region of the planet. However, ground-based observations of the central Sahara have been limited to its outer edges, leaving a void in observations approximately 1 million km^2 in area. The Fennec Project has been the first campaign to instrument this remote but climatologically important region. This thesis uses these new observations to detect and explain the atmospheric mechanisms that make the central Sahara the summer global dust maximum.

Four atmospheric mechanisms are found to cause dust storms in the central Sahara in June 2011 and June 2012. These are cold pool outflows, low-level jets (LLJs), monsoon surges and dry convective plumes. Dust may be emitted locally by these phenomena, or be advected, principally by cold pools. In both field seasons, dust emission by cold pool outflows is the most important dust mechanism, causing roughly half of the total dust loadings at the Fennec supersite of Bordj-Badji Mokhtar (BBM), the closest station to the dust maximum. The second most important mechanism is dust advection by cold pools (roughly 30% dust at BBM), followed by dust emission by monsoon surges, LLJs and finally dry convective plumes (only 2% dust at BBM). Although June 2012 was significantly more dusty than June 2011, the relative importance of the different atmospheric dust mechanisms at BBM did not change.

At the automatic weather stations (AWSs) across the remote desert, cold pools and LLJs are by far the most frequently detected atmospheric dust mechanisms. LLJs are particularly common in the Atlantic Inflow in western Mauritania and in the north-easterly Harmattan in western Algeria. Cold pools are much more frequent at BBM, the station under the greatest moist monsoon influence, than at the AWSs to the north.

Detection of advected dust is a particular difficulty without dedicated dust-detection instrumentation or human observers (e.g. at the AWSs). Detection of dust *emission* mechanisms can be very successful with only routine ground observations and satellite measurements, but quantifying the associated dust burden without dedicated dust instruments is problematic. The choice of instrumentation for dust measurement is crucial. Because cold pool outflows - the most important dust mechanism - frequently occur at night or under cloud, sun photometers miss about half of cold pool dust. Lidars have the advantage of providing height resolved dust profiles, but they suffer from attenuation in thick dust. The nephelometer proved to be the most reliable dust instrument.

Although LLJs occurred on 21/28 mornings at BBM in June 2011, only five of these jets led to dust emission. Calculations of momentum exchanges through the atmospheric column show that momentum mix-down from the jet core is the cause of dust emission on these occasions, but that the LLJ has to be particularly strong ($\geq$ 16 m s^{-1}) to result in dust emission at the surface. Met Office Africa-LAM underestimates monsoon LLJ wind profiles and ERA-Interim reanalysis underestimates both monsoon and Harmattan LLJ wind profiles. At the surface, the Met Office Africa-LAM and GLOBAL models significantly underpredict the frequency of observed wind speeds >6 m s^{-1}. This will cause them to significantly underestimate dust emission, as emission is a threshold process proportional to the cube of wind speed.

A particularly interesting implication of the research presented here is that the central Sahara is likely much more dusty than previously thought. This is because almost all of the techniques currently used to study dust in the region are systematically biased to result in underestimates of dust burden. Cold pools are the most important dust mechanism but, since they rarely occur during the daytime or in cloud-free conditions they are often missed by sun photometers. Many will be missed by satellites that cannot retrieve below cloud and satellites that pass over the Sahara in daylight hours (e.g. the A-train). A commonly-used satellite dust detection algorithm often misses dust under moist (i.e. cold pool) conditions. Cold pools cannot be simulated by models without explicit convection, which requires very high spatial resolution. Finally, the numerical models assessed here significantly underpredict the frequency of wind speeds over the dust emission threshold. The Sahara is probably much dustier than current estimates suggest.

Acknowledgements

There are a great many people to whom I am indebted for help writing my thesis. Firstly I would like to sincerely thank Professor Richard Washington for supervising me, for being an inexhaustible source of ideas, and for always being ready to fight my corner with me. I am very grateful to all the members of the Climate Research Lab at Oxford University, past and present, for support, technical assistance and good humour at all stages of my DPhil. I am particularly grateful to Drs. Ian Ashpole, Sebastian Engelstaedter and Karsten Haustein. The Fennec Project would not have been possible without all of the individuals who undertook difficult fieldwork with us or for us in the Sahara. Their names are listed in later chapters; here I would like to thank Azzedine Saci of the Algerian Meteorological Service in particular. I am also grateful to all other members and partners of Fennec, especially those who worked hard to provide the model and satellite data used here. I thank the reviewers and editors of the *Journal of Geophysical Research: Atmospheres* for their rigorous examination of three of my research chapters which significantly elevated their scientific quality. Thank you to Dr Simon Dadson (University of Oxford) and Dr Ron Miller (NASA/Columbia University) for a challenging but stimulating and (largely!) enjoyable viva.

I would like to formally thank the Natural Environment Research Council for my doctoral studentship (grant NE/J500045/1), Oriel College for a Graduate Scholarship and two travel grants, and the European Space Agency for sponsoring my attendance at the European Geosciences Union conference in April 2013. Fennec was funded by the Natural Environment Research Council (grant NE/G017166/1). I am also grateful to Dr Peter Bull for providing me with undergraduate teaching opportunities at Hertford College which have been a great experience and a welcome source of additional funding.

Finally I extend heartfelt thanks to my friends and my family for supporting me through the last four years. My DPhil would not have been possible without you.

Contents

List of figures

List of tables

Acronyms

AEJ	African Easterly Jet
AERONET	Aerosol Robotic Network
AEW	African Easterly Wave
AGCM	Atmospheric General Circulation Model
agl	above ground level
ALAM	Africa Limited Area Model
AMMA	African Monsoon Multidisciplinary Analysis
AOD	Aerosol Optical Depth (equivalent to AOT)
AOT	Aerosol Optical Thickness (equivalent to AOD)
AVHRR	Advanced Very High Resolution Radiometer
AWS	Automatic Weather Station
BBM	Bordj Badji Mokhtar
BoDEx	Bodélé Dust Experiment
CALIPSO	Cloud-Aerosol Lidar and Infrared Pathfinder Satellite Observation
CBL	Convective Boundary Layer
CMIP5	Coupled Model Intercomparison Project 5
COSMO-ART	Consortium for Small-scale Modelling Aerosols and Reactive Trace gases model
COSMO-MUSCAT	Consortium for Small-scale Modelling Multi-Scale Chemistry Aerosol Transport model
CWS	Central-western Sahara
ECMWF	European Centre for Medium-range Weather Forecasts
EOP	Extended Observation Period
ERAI	ERA-Interim reanalysis product
EUMETSAT	European Organisation for the Exploitation of Meteorological Satellites
GLOBAL	Met Office Unified Model in NWP configuration, global domain
IOP	Intensive Observation Period
IOP1	Intensive Observation Period 1 (June 2011)
IOP2	Intensive Observation Period 2 (June 2012)
ITCZ	Inter-Tropical Convergence Zone
ITD	Inter-Tropical Discontinuity
LAM	Limited Area Model
LLJ	Low Level Jet
MCC	Mesoscale Convective Complex
MODIS	Moderate Resolution Imaging Spectroradiometer
NASA GISS	National Aeronautics and Space Administration Goddard Institude for Space Studies model
NWP	Numerical Weather Prediction
RCM	Regional Climate Model
SAMUM	Saharan Mineral Dust Experiment

SDF	SEVIRI Dust Flag
SEVIRI	Spinning Enhanced Visible and InfraRed Imager
SHL	Saharan Heat Low
SOMs	Self Organising Maps
TOA	Top Of Atmosphere
TOMS	Total Ozone Mapping Spectrometer
WAM	West African Monsoon (moist onshore flow only)

1. Introduction

1.1 Preface

It might seem unlikely that the influence of the Sahara Desert stretches to the Amazon Rainforest or the beaches of Miami. And yet, every year, millions of tonnes of desert dust are lofted west from North Africa and deposited along the way over the Atlantic Ocean, the Caribbean and the northern reaches of South America [*Prospero*, 1999; *Kaufman et al.*, 2005; *Engelstaedter et al.*, 2006; *Schepanski et al.*, 2009a; *Ridley et al.*, 2012; *Touré et al.*, 2012]. This is much more than an interesting geographical anecdote: desert dust[1] is not a passive constituent of the Earth System but a component that actively influences atmospheric, biogeochemical and oceanic processes [*Jickells et al.*, 2005]. Dust can absorb or scatter radiation, changing how the atmosphere is heated, with consequent effects on atmospheric dynamics [*Miller and Tegen*, 1998; *Choobari et al.*, 2014]; it can modify cloud properties with consequences for radiation and precipitation [*Shao et al.*, 2011] and it provides nutrients (particularly iron and phosphorous) to ocean and terrestrial ecosystems, influencing primary productivity and ultimately atmospheric carbon dioxide concentrations [*Ravi et al.*, 2011]. North Africa is not the only dust source in the world – other major sources can be found in the Middle East, southwest Africa, the Taklamakan, the U.S. Great Basin and central Australia [*Washington et al.*, 2003] – but it is widely viewed as the most important [*Washington et al.*, 2003; *Tanaka and Chiba*, 2006; *Choobari et al.*, 2014], contributing perhaps 55% of global dust emissions [*Ginoux et al.*, 2012]. As such, North Africa, and the Sahara in particular, plays a key role in influencing the Earth's climate.

[1] Variously reported as 'mineral dust', 'mineral aerosol', 'aeolian dust' and 'atmospheric dust'

For the dust to have any impact on climate however, it must enter the atmosphere. Whether this happens depends on the local erodibility (how susceptible the substrate is to erosion) and the local erosivity (the forces acting to entrain a particle into the airflow). Erosivity can be divided into two components: 'deflation processes' (which occur at or within centimetres of the surface) and 'atmospheric mechanisms'[2]: the meteorological phenomena which generate the winds which result in deflation (if the surface is erodible). Understanding these meteorological phenomena – the atmospheric mechanisms – is important because they are arguably the start of the dust cycle.

With numerical weather prediction (NWP) models now able to cover the globe at a resolution of 17km (e.g. the Met Office Unified Model), understanding the atmospheric mechanisms that generate dust storms may seem a fairly straightforward task. But the attraction of such high resolution on a global scale masks the fact that, due to their remoteness and harsh conditions, the most important dust source regions provide very few observations with which to validate the model output. Uncritical users run the risk of conflating high model resolution with model accuracy.

In boreal summer, the central Sahara is the dustiest place in the world [*Engelstaedter and Washington*, 2007; *Ashpole and Washington*, 2012]. However, it is a region that has, until the Fennec Project, been almost entirely devoid of ground-based observations [*Washington et al.*, 2012]. Without these observations, the processes that make it so dusty are very difficult to study and it is almost impossible to know how well numerical models are simulating the atmospheric mechanisms and other related variables. Since dust emission – specifically saltation bombardment – is proportional to the cube of wind speed rather than wind speed alone [*Bagnold*, 1941; *Gillette*, 1974; *Marticorena and*

[2] Also termed 'atmospheric dust mechanisms' or simply 'dust mechanisms' in this thesis

Bergametti, 1995], errors in wind speeds can potentially cube errors in dust emission. Without observations, it is also not possible to know how to improve the models, or what atmospheric mechanisms might be entirely missing. Knowing that the wind speeds or friction velocities are wrong is not enough: improvements will only be made if the atmospheric mechanisms that generate the winds are simulated correctly. As *Shao et al.* [2011: 200] explain:

> "The accurate simulation of meteorological conditions remains a critical issue for the quantification of the dust cycle. *Timmreck and Schulz* [2004] and *Menut* [2008] showed that dust emission is sensitive to the way winds are represented in dust models. In particular, meso-scale atmospheric systems which are mostly unresolved in global and regional dust models are often responsible for intense dust emissions, such as haboobs[3] [*Knippertz et al.*, 2007], gusty winds [*Engelstaedter and Washington*, 2007], low level jets [*Schepanski et al.*, 2009b], dust devils and convective turbulence [*Klose et al.*, 2010]."

The DPhil will therefore focus on understanding the atmospheric mechanisms which make the central Sahara the dustiest place in the world in summer. It will do this by exploiting new ground-based measurements from the Fennec Project [*Washington et al.*, 2012]. These measurements will be used not only to research the atmospheric mechanisms themselves but also to understand how well models represent them, how well instrumentation detects them, and the subsequent implications for our understanding of dust and Saharan climate.

1.2 Thesis structure

The thesis is composed of nine chapters, of which this is the first. Chapter 2 reviews the state of current understanding about atmospheric dust, with a focus on the Sahara. Following this survey, Chapter 3 presents the formal motivation and research aims for the thesis. Chapter 4 briefly discusses the Fennec Project, the datasets used in the thesis

[3] A term used in North Africa and the Arabian Peninsula for dust storms caused by cold pool outflows

and its geographical scope. Chapters 5-8 are the main research chapters. The first three research chapters have been published as individual articles in *Journal of Geophysical Research: Atmospheres.* The fourth research chapter has been submitted for publication in *Aeolian Research*. The second article (Chapter 6) was highlighted as a 'contribution of special significance' by the Editor of the *Journal of Geophysical Research: Atmospheres* and was featured as a 'Research Spotlight' in *Eos.* The four research chapters (Chapters 5-8) are described briefly below.

- Chapter 5: *Dust emission and transport mechanisms in the central Sahara: Fennec ground-based observations from Bordj-Badji Mokhtar, June 2011*. This chapter provides detailed case studies of the different dust emission and transport mechanisms observed at the Fennec supersite of Bordj-Badji Mokhtar in Algeria in June 2011 then moves to quantifying their relative importance for dust production and their relationship with wind speeds.
- Chapter 6: *The low-level jet dust emission mechanism in the central Sahara: Observations from Bordj-Badji Mokhtar during the June 2011 Fennec Intensive Observation Period*. This chapter focuses on understanding the characteristics of low-level jets, in particular their development and why they do not result in dust emission at the surface as frequently as might be expected. It also evaluates model and reanalysis simulation of jet wind profiles.
- Chapter 7: *Dust detection from ground-based observations in the summer global dust maximum: results from Fennec 2011 and 2012 and implications for modelling and field observations.* This chapter develops a methodology to detect dust mechanisms at Bordj-Badji Mokhtar during the second Fennec field season when instrumentation was more limited. It then compares the dust mechanisms

between the two field seasons and discusses the implications of the findings for interpretation of model, satellite and field data in the region.

- Chapter 8: *Dust mechanisms across the central-western Sahara in June 2011: observations and modelling* develops a methodology to detect dust mechanisms at the Fennec automatic weather stations across the remote central-western Sahara, explains the geographical variability of the dust mechanisms, then moves on to evaluate model simulation of surface wind speeds.

The last thesis chapter, Chapter 9, discusses the findings of all of the chapters and presents the final conclusions and implications.

1.3 References

Ashpole, I., and R. Washington (2012), An automated dust detection using SEVIRI: A multiyear climatology of summertime dustiness in the central and western Sahara, *J. Geophys. Res.*, *117*(D8), D08202, doi: 10.1029/2011jd016845.

Bagnold, R. A. (1941), *The Physics of Blown Sand and Desert Dunes*, Methuen, London.

Choobari, O. A., P. Zawar-Reza, and A. Sturman (2014), The global distribution of mineral dust and its impacts on the climate system: A review, *Atmospheric Research*, *138*(0), 152-165, doi: 10.1016/j.atmosres.2013.11.007.

Engelstaedter, S., and R. Washington (2007), Temporal controls on global dust emissions: The role of surface gustiness, *Geophys. Res. Lett.*, *34*(15), L15805, doi: 10.1029/2007gl029971.

Engelstaedter, S., I. Tegen, and R. Washington (2006), North African dust emissions and transport, *Earth-Science Reviews*, *79*(1–2), 73-100, doi: 10.1016/j.earscirev.2006.06.004.

Gillette, D. A. (1974), On the production of soil wind erosion aerosols having the potential for long-range transport, *J. Rech. Atmos.*, *8*, 735-744.

Ginoux, P., J. M. Prospero, T. E. Gill, N. C. Hsu, and M. Zhao (2012), Global-scale attribution of anthropogenic and natural dust sources and their emission rates based on MODIS Deep Blue aerosol products, *Reviews of Geophysics*, *50*(3), doi: 10.1029/2012RG000388.

Jickells, T. D., Z. S. An, K. K. Andersen, A. R. Baker, G. Bergametti, N. Brooks, J. J. Cao, P. W. Boyd, R. A. Duce, K. A. Hunter, H. Kawahata, N. Kubilay, J. laRoche, P. S. Liss, N. Mahowald, J. M. Prospero, A. J. Ridgwell, I. Tegen, and R. Torres (2005), Global Iron Connections Between Desert Dust, Ocean Biogeochemistry, and Climate, *Science*, *308*(5718), 67-71, doi: 10.1126/science.1105959.

Kaufman, Y. J., I. Koren, L. A. Remer, D. Tanré, P. Ginoux, and S. Fan (2005), Dust transport and deposition observed from the Terra-Moderate Resolution Imaging Spectroradiometer (MODIS) spacecraft over the Atlantic Ocean, *J. Geophys. Res.*, *110*(D10), D10S12, doi: 10.1029/2003jd004436.

Klose, M., Y. Shao, M. K. Karremann, and A. H. Fink (2010), Sahel dust zone and synoptic background, *Geophysical Research Letters*, *37*(9), L09802, doi: 10.1029/2010gl042816.

Knippertz, P., C. Deutscher, K. Kandler, T. Müller, O. Schulz, and L. Schütz (2007), Dust mobilization due to density currents in the Atlas region: Observations from the Saharan Mineral Dust Experiment 2006 field campaign, *J. Geophys. Res.*, *112*(D21), D21109, doi: 10.1029/2007jd008774.

Marticorena, B., and G. Bergametti (1995), Modeling the atmospheric dust cycle: 1. Design of a soil-derived dust emission scheme, *J. Geophys. Res.*, *100*(D8), 16415-16430, doi: 10.1029/95jd00690.

Menut, L. (2008), Sensitivity of hourly Saharan dust emissions to NCEP and ECMWF modeled wind speed, *Journal of Geophysical Research: Atmospheres*, *113*(D16), doi: 10.1029/2007jd009522.

Miller, R. L., and I. Tegen (1998), Climate Response to Soil Dust Aerosols, *Journal of Climate*, *11*(12), 3247-3267, doi: 10.1175/1520-0442(1998)011<3247:crtsda>2.0.co;2.

Prospero, J. M. (1999), Long-range transport of mineral dust in the global atmosphere: Impact of African dust on the environment of the southeastern United States, *Proceedings of the National Academy of Sciences*, *96*(7), 3396-3403, doi: 10.1073/pnas.96.7.3396.

Ravi, S., P. D'Odorico, D. D. Breshears, J. P. Field, A. S. Goudie, T. E. Huxman, J. Li, G. S. Okin, R. J. Swap, A. D. Thomas, S. Van Pelt, J. J. Whicker, and T. M. Zobeck (2011), Aeolian processes and the biosphere, *Rev. Geophys.*, *49*(3), RG3001, doi: 10.1029/2010rg000328.

Ridley, D. A., C. L. Heald, and B. Ford (2012), North African dust export and deposition: A satellite and model perspective, *Journal of Geophysical Research: Atmospheres*, *117*(D2), D02202, doi: 10.1029/2011jd016794.

Schepanski, K., I. Tegen, and A. Macke (2009a), Saharan dust transport and deposition towards the tropical northern Atlantic, *Atmos. Chem. Phys.*, *9*(4), 1173-1189, doi: 10.5194/acp-9-1173-2009.

Schepanski, K., I. Tegen, M. C. Todd, B. Heinold, G. Bönisch, B. Laurent, and A. Macke (2009b), Meteorological processes forcing Saharan dust emission inferred from MSG-SEVIRI observations of subdaily dust source activation and numerical models, *J. Geophys. Res.*, *114*(D10), D10201, doi: 10.1029/2008jd010325.

Shao, Y., K.-H. Wyrwoll, A. Chappell, J. Huang, Z. Lin, G. H. McTainsh, M. Mikami, T. Y. Tanaka, X. Wang, and S. Yoon (2011), Dust cycle: An emerging core theme in Earth system science, *Aeolian Research*, *2*(4), 181-204, doi: 10.1016/j.aeolia.2011.02.001.

Tanaka, T. Y., and M. Chiba (2006), A numerical study of the contributions of dust source regions to the global dust budget, *Global and Planetary Change*, *52*(1–4), 88-104, doi: 10.1016/j.gloplacha.2006.02.002.

Timmreck, C., and M. Schulz (2004), Significant dust simulation differences in nudged and climatological operation mode of the AGCM ECHAM, *Journal of Geophysical Research: Atmospheres*, *109*(D13), doi: 10.1029/2003jd004381.

Touré, N. E., A. Konaré, and S. Silué (2012), Intercontinental Transport and Climatic Impact of Saharan and Sahelian Dust, *Advances in Meteorology*, *2012*, 14, doi: 10.1155/2012/157020.

Washington, R., M. C. Todd, N. J. Middleton, and A. S. Goudie (2003), Dust-Storm Source Areas Determined by the Total Ozone Monitoring Spectrometer and Surface Observations, *Annals of the Association of American Geographers*, *93*(2), 297-313, doi: 10.1111/1467-8306.9302003.

Washington, R., C. Flamant, D. J. Parker, J. H. Marsham, J. B. McQuaid, H. Brindley, M. C. Todd, E. Highwood, C. Ryder, J. P. Chaboureau, C. Kocha, M. Bechir, and A. Saci (2012), Fennec - The Saharan Climate System, *CLIVAR Exchanges*, *17*(3), 31-33.

2. Literature review

This literature review sets the context of the thesis, describing the current state of scientific research on atmospheric dust, focusing particularly on North Africa. It is not intended to be an exhaustive survey. The review examines the concepts of erosivity and erodibility, the impacts of dust on climate, the distribution of dust sources, the annual cycle of dust emission in North Africa and finally the atmospheric mechanisms of dust emission and advection. The literature review provides the background for the formal thesis motivation and thesis aims, which are the subject of the following chapter (Chapter 3).

2.1. Erosivity and erodibility

There are two fundamental controls on wind erosion: erosivity and erodibility. Erosivity can be thought of as the sum of the forces acting to entrain a particle into the airflow whilst erodibility is the susceptibility of the soil to these forces. Thus maximum erosion occurs when erosivity is high and erodibility is high.

Erosivity is a function of the power of the wind. However, it is not the wind itself which entrains particles into the airflow: aerodynamic entrainment is accomplished by the forces of lift and drag. Lift occurs when wind flowing over a particle generates an area of low pressure above the particle, 'sucking' it into the airflow. Drag is the shear stress imparted on the particle, caused by the rapid increase in wind speed with height in the first few centimetres above the ground surface. The gradient of this velocity profile is called the shear velocity (or friction velocity, u_*). Shear velocity is the preferred measurement for describing erosivity. Increasing the overall environmental wind speed will increase the shear velocity [*Wiggs,* 2011].

Erodibility is a function of a number of factors. For particles larger than about 60μm diameter, increasing the grain size increases the shear velocity required for entrainment [*Chepil*, 1945]. However, as grain size decreases below 60μm and further, inter-particle molecular and electrostatic cohesive forces again increase the shear velocity required for entrainment [e.g. *Iverson and White,* 1982; *Marticorena and Bergametti*, 1995]. Erodibility also generally decreases with increasing moisture content (because of increased surface tension associated with pore moisture), with surface crusting (which provides a protective cover), with the presence of non-erodible roughness elements (e.g. cobbles and rocks, which deepen the layer of zero flow velocity) and with vegetation (which reduces the wind velocity near the surface and binds sediment together in root systems) [*Ravi et al.*, 2011]. However, all these effects are highly non-linear and poorly understood [*Wiggs*, 2011]. *Bagnold* [1941] first proposed that under different conditions, there would be a different threshold of shear velocity (u_{*t}) required for particle entrainment. The threshold shear velocity is still very commonly used in both empirical and modelling contexts as a single value which represents local erodibility. In the hyper-arid central Sahara, where rainfall and vegetation are negligible [e.g. *Loveland and Belward*, 1997], it is reasonable to assume that u_{*t} will be primarily controlled by the soil type and the presence of other roughness elements**.**

2.1.1. Dust deflation processes

Since dust is commonly defined as particles with diameter < 60μm , inter-particle cohesive forces are strong and direct entrainment of dust by aerodynamic lift and drag is thought to be small [*Goudie and Middleton*, 2006; *Shao*, 2008]. Two other processes, probably of roughly equal importance, are responsible for the majority of dust deflation: saltation bombardment and aggregate disintegration [*Shao*, 2008]. Saltation

bombardment occurs when a saltating sand grain strikes the surface with enough force to overcome dust inter-particle cohesive forces and 'splashes' dust particles into the airflow [*Gillette*, 1981]. Wind tunnel experiments [*Shao et al.*, 1993] demonstrate that dust emission by saltation bombardment can be an order of magnitude greater than by aerodynamic entrainment. The widely used dust emission parameterization scheme of *Marticorena and Bergametti* [1995] is based on saltation bombardment. The second major dust deflation process, aggregate disintegration, occurs when aggregates of dust particles (or sand particles coated with dust) behave as an individual saltating particle but upon impact with the surface disaggregate, releasing dust into the atmosphere [*Shao*, 2001]. This process has also been parameterized for use in numerical models [e.g. *Shao*, 2004]. *Kok* [2011] shows that the size distribution of emitted dust can be well-predicted compared to measurements by considering aggregate disintegration to be analogous to the fragmentation of a brittle material such as glass. The three main dust deflation processes are illustrated in Figure 2-1.

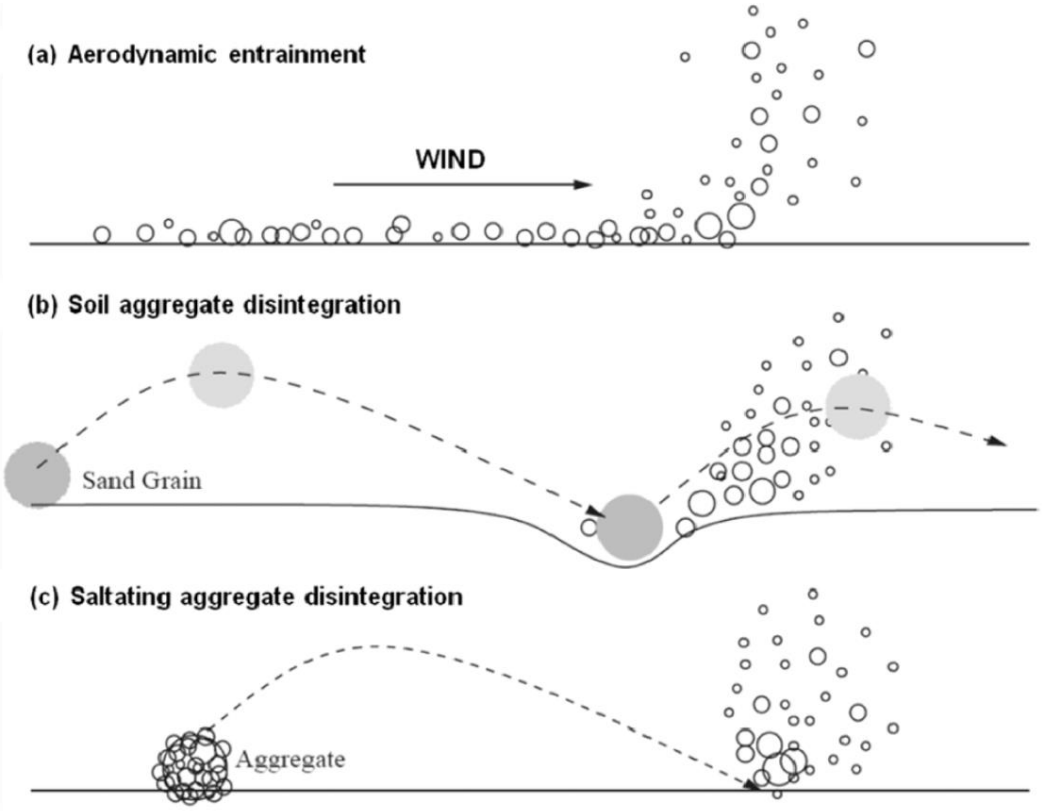

Figure 2-1: The three main dust deflation processes. 'Soil aggregate disintegration' (panel b) is more often termed saltation bombardment. Source: Figure 7.5 of Shao, Y. (2008), Physics and Modelling of Wind Erosion, 2 ed., 452 pp., Springer Netherlands. Reproduced with permission of Springer Science+Business Media.

2.2. Dust and climate

2.2.1. Dust properties and radiative effects

Once dust particles enter the atmosphere, they can exert a multitude of effects on the climate system. The average size range of airborne dust particles has historically been given as diameter 0.1 to 10μm [*Jickells et al.*, 2005], with particle diameters >1μm usually referred to as 'coarse mode' [*Mahowald et al.*, 2013]. However, recent field campaigns closer to desert dust sources have demonstrated that a substantial fraction of airborne dust is larger than 10μm [*Mahowald et al.*, 2013]. For example, airborne measurements in the central Sahara as part of the Fennec campaign recorded dust

particles up to 300μm in size, with particles up to 100μm always present between the surface and 3km [*Ryder et al.*, 2013a; *Ryder et al.*, 2013b]. This is significant because (i) dust emission is usually thought of in terms of particles with diameter <60μm [*Goudie and Middleton*, 2006] (ii) models do not usually include particles over 10μm [*Huneeus et al.*, 2011] (iii) the inversion techniques of the Aerosol Robotic Network (AERONET) of sun photometers, a benchmark observational network, were developed for finer particles [*Mahowald et al.*, 2013] and most importantly (iv) dust size is an important factor in determining the radiative effects of dust [e.g. *Tegen and Lacis*, 1996; *Kok*, 2011].

Since mineral aerosols are one of the largest aerosol groups by optical thickness [*Tegen et al.*, 1997] it is important to understand their effects on the radiation budget. The radiative effects of dust are complicated since as well as depending on particle size [e.g. *Ryder et al.*, 2013b], they also depend on dust composition [e.g. *Formenti et al.*, 2011; *Moosmüller et al.*, 2012], dust concentration and optical thickness [*Redmond et al.*, 2010; *Gu et al.*, 2012; *di Sarra et al.*, 2013], dust shape [e.g. *Redmond et al.*, 2010; *Formenti et al.*, 2011; *Z Wang et al.*, 2013], dust altitude [e.g. *Perrone et al.*, 2012], and interactions within, below or above cloud [e.g. *Smoydzin et al.*, 2012; *Naeger et al.*, 2013; *Santos et al.*, 2013]. The net radiative forcing at the top of the atmosphere (TOA), in the atmosphere or at the surface can be different in magnitude or even in sign depending on the exact combination of these properties present. Indeed, net global dust radiative forcing is estimated by the Intergovernmental Panel on Climate Change to be between -0.3 and +0.1 W m^{-2} [*Boucher et al.*, 2013]. Local dust effects are much more marked: *Haywood et al.* [2005] found that dust over the Sahara could exert a longwave radiative forcing of up to 50 W m^{-2} in cloud-free areas. In general, the larger the dust particles the larger their absorption in both the shortwave and longwave spectrum and

therefore their atmospheric heating [*Mahowald et al.*, 2013; *Ryder et al.*, 2013b]. A simplified schematic of dust-radiation interactions is shown in Figure 2-2.

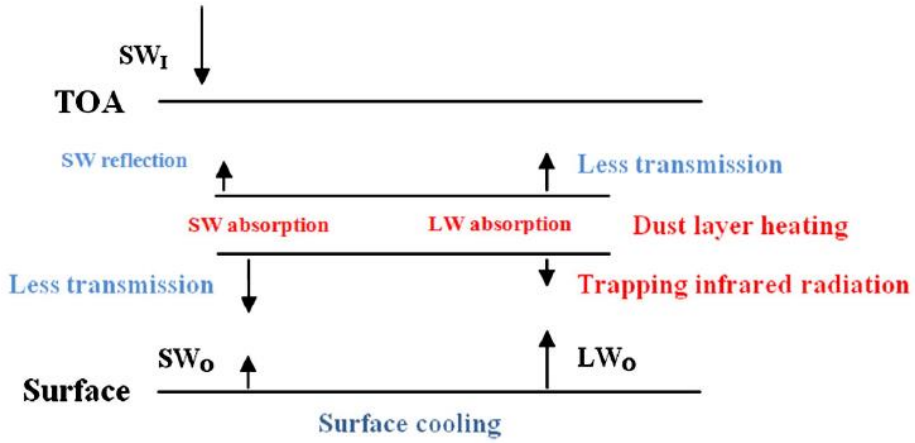

Figure 2-2: Simplified schematic of dust-radiation interactions. SW=shortwave, LW=longwave, subscripts I and O stand for 'incoming' and 'outgoing' respectively. Note that the surface may warm despite negative surface forcing, since it also depends on forcing at TOA. 'Surface cooling' in the schematic would be more precisely described as 'negative surface radiative forcing' (R L Miller, pers. comm.). Reprinted from Choobari, O. A., P. Zawar-Reza, and A. Sturman (2014) (Figure 2), The global distribution of mineral dust and its impacts on the climate system: A review, Atmospheric Research, 138(0), 152-165, doi: 10.1016/j.atmosres.2013.11.007) with permission from Elsevier.

Aerosol radiative effects are divided into direct, semi-direct and indirect effects. The direct effect is the scattering or absorption of radiation by dust particles themselves [e.g. *Haywood et al.*, 2005]. The semi-direct effect is a change in cloud-cover caused by heating of the air column by dust [e.g. *Gu et al.*, 2012]. Changes to cloud properties caused by aerosol modification of cloud microphysics are known as aerosol indirect effects. Since aerosol particles act as cloud condensation or ice nuclei [e.g. *DeMott et al.*, 2003], there can be a reduction in the size of cloud droplets in the presence of dust and an increase in their number, leading to brighter clouds and greater reflection of solar radiation [*Twomey*, 1977]. Laboratory studies suggest that feldspar, a minor component

in desert dust, is the most effective mineral for ice nucleation [*Atkinson et al.*, 2013]. Another consequence of smaller cloud particles is that the number of collisions in the cloud is reduced, leading to less precipitation and longer cloud lifetimes [e.g. *Mahowald and Kiehl*, 2003]. In general, aerosol indirect effects are poorly understood [*Boucher et al.*, 2013].

2.2.2. Effect on atmospheric dynamics

As a result of the radiative effects described above, dust can have marked effects on atmospheric dynamics. Over Saudi Arabia, for example, it has been demonstrated that dust storms can strengthen the summer heat low. *Mohalfi et al.* [1998] ran two model simulations for a 6-day dust event in June 1979, one run with and one without dust. The authors found that in the control run, the radiative heating was not sufficient for the low pressure region to deepen as found in the observations. Only with the addition of dust did the heat low develop in a comparable way to the observed system. In the Sahara, the heat low is climatologically collocated with the Saharan dust maximum [*Ashpole and Washington*, 2012]. Here there is also an interaction between the heat low and dust emission, with the heat low promoting dust emission, and the suspended dust in turn modifying the atmospheric circulation [e.g. *Stanelle et al.*, 2010; *Lavaysse et al.*, 2011]. The cyclonic circulation of the heat low at low levels leads to a convergence of south-westerly moist monsoon air from the Gulf of Guinea and dry Saharan air within the north-easterly Harmattan winds [*Parker et al.*, 2005; *Engelstaedter et al.*, 2015]. Low level jets, which can raise and transport dust, can be embedded in both the monsoon flow and the Harmattan [*Schepanski et al.*, 2009b]. Thus important feedbacks exist between dust and the heat low.

One of the current challenges in climate prediction is Sahel rainfall. It is an important scientific goal but also a societal one. Over 60 million people live in the Sahel, and over 60% of the active population work in agriculture, which is almost totally reliant on rainfall [*Kandji et al.*, 2006]. A review by [*Druyan*, 2011: 1415] concluded that "no consensus emerges regarding the impact of anticipated greenhouse gas forcing on the hydrology of the Sahel in the second half of the 21st century". This discrepancy, however, may be due to how different models simulate the Saharan heat low [*Biasutti et al.*, 2009] which, as has been seen, both drives and responds to dust emission. *Biasutti et al.* [2009] show that models which generate a strong heat low project future Sahel wetting, and that models which produce a weak heat low project future Sahel drying (+1 mm day^{-1} century^{-1} and -1.5 mm day^{-1} century^{-1} respectively). Thus they argue that work must look to the Sahara as well as at ocean sea surface temperatures in order to assess future precipitation trends in the Sahel.

Dust-atmosphere interactions have been shown to both suppress and increase dust emission. Using an atmospheric general circulation model (AGCM) which incorporated the radiative effects of mineral dust, *R L Miller et al.* [2004b] and *Pérez et al.* [2006] found that, by reducing incoming solar radiation, the dust led to a reduction in boundary layer turbulent mixing and a reduction in downward transport of momentum to the surface, resulting in lower surface wind speeds and less dust emission. By contrast, *Stanelle et al.* [2010] demonstrate with the COSMO-ART model that the presence of dust can lead to a horizontal temperature gradient which strengthens surface winds. Where dust is close to the surface, it leads to an increase in 2m temperature. Where dust is elevated, the 2m temperature is reduced (by up to 4°C at noon for the June 2007 case study of *Stanelle et al.* [2010]). This temperature gradient leads to higher wind speeds and possibly further dust emission. Using the COSMO-MUSCAT model *Heinold et al.*

[2011] even argue that dust emissions can induce pressure changes that strengthen the Hadley circulation.

Through experiments with the NASA GISS AGCM, *R L Miller et al.* [2004a] show that, over the Sahara, the presence of dust leads to increased evaporation, despite the reduction in incoming shortwave radiation. This occurs when the radiation absorbed by the aerosol layer is enough to induce anomalous diabatic heating, which promotes ascending air and can lead to precipitation. This change acts in an opposite direction to the indirect aerosol effect, which acts to reduce precipitation. Suspended dust particles increase the number of cloud condensation nuclei available, reducing the average cloud droplet size and increasing the number of collisions necessary to form a raindrop, thereby suppressing precipitation. As a result of the AGCM experiments, *R L Miller et al.* [2004a] conclude that if dust causes a negative TOA forcing it tends to reduce precipitation but that if the TOA forcing is positive, precipitation can increase over deserts.

Research has also been done on the influence of Saharan dust on the Atlantic Ocean, since this is the principal transport pathway of Saharan dust in summer and winter [*Engelstaedter et al.*, 2006]. It is generally thought that the presence of dust over the Atlantic lowers SSTs, principally by scattering incoming solar radiation [e.g. *Evan et al.*, 2009; *Martínez Avellaneda et al.*, 2010; *C Wang et al.*, 2012]. *Evan et al.* [2011] even argue that dust 'excites' the Atlantic Meridional Mode on interannual to decadal timescales.

Evan et al. [2006] find that there is an anticorrelation between Atlantic atmospheric dust and tropical cyclone activity (correlation coefficient -0.53, $p<0.05$; correlation -0.71 when strong El Niño and La Niña years are removed). This relationship does not prove

that dust reduces hurricane activity, although there are two ways that it might. Firstly, by absorbing solar radiation and subsequently heating the mid-troposphere, it has been argued that the dust layer stabilises the atmosphere, suppressing hurricane development [e.g. *Dunion and Velden*, 2004]. However, this radiative-dynamical effect has been shown to be much more complex, with other studies showing it both inhibiting and enhancing hurricane formation [e.g. *Bretl et al.*, 2015]. The second hypothesised effect of dust on hurricane formation is microphysical: submicron dust particles increase the number of available cloud condensation nuclei and slow the coalescence of cloud droplets into raindrops, resulting in less rainout and an invigoration of convection at the periphery of the storm that weakens convection at the eyewall [*Rosenfeld et al.*, 2012].

Accurate representation of aerosols in numerical models improves the quality of simulations. Using a convective-scale operational model, *Kocha et al.* [2012] show that simulations using interactive dust significantly improve representation of a major Saharan dust storm in March 2006, in particular the intense (>2°C) heating in the centre of the dust plume and the associated circulation changes. A more permanent feature over Africa whose simulation has been improved thanks to better dust representation is the African Easterly Jet (AEJ). Prior to the introduction of a new aerosol climatology in June 2003, the 700hPa AEJ in 5-day European Centre for Medium-Range Weather Forecasts (ECMWF) forecasts tended to be too weak and too zonal in structure. This was in spite of the observations available for assimilation generating the AEJ reasonably accurately. After the introduction of the new aerosol climatology, which reduced aerosol optical depth over the Sahara, *Tompkins et al.* [2005] found that the 5-day forecast of the AEJ developed much more in line with dropsonde data. Since the AEJ is an integral part of the West African Monsoon system, playing a key role in generating African Easterly Waves (AEWs) and mesoscale convective complexes

(MCCs), it is evident that solid understanding of dust aerosol is necessary for weather prediction beyond the Sahara. Indeed, *Rodwell and Jung* [2008] extend the work of *Tompkins et al.* [2005] to show that the new ECMWF aerosol climatology results in improvements in the precipitation field across the tropics and reduced atmospheric circulation errors in the extratropics.

Conversely, wrongly estimating dust properties can have significant ramifications in simulations. *Kok* [2011] argues that general and regional circulation models overestimate the emitted fraction of clay aerosols (<2 μm diameter) by a factor of 2–8 relative to measurements. Since the global radiative cooling caused by an over-abundance of these small particles is found to be an overestimate, dust emission rates are (wrongly) tuned down.

2.2.3. Biogeochemistry

As well as having an effect on climate through interactions with radiation, dust can modify biogeochemical cycles, which may in turn modify the climate. Large areas of the ocean are iron-limited, and iron input through dust deposition into the ocean is crucial for phytoplankton primary production [*Jickells et al.*, 2005]. *Mahowald et al.* [2010] argue that, over the course of the 20th century, supply of iron to the oceans by desert dust increased ocean productivity by 6%, resulting in a drawdown of carbon dioxide of 4ppm. Using Moderate Resolution Imaging Spectroradiometer (MODIS) satellite data, *Kaufman et al.* [2005] estimate that, of the 240 ± 80 Tg of dust that are transported from the Sahara across the Atlantic Ocean, 50 Tg reach and fertilise the Amazon Rainforest. *Kaufman et al.* [2005] note that this figure represents the 'missing' nutrients required by the rainforest, as described by *Swap et al.* [1992]. On millennial scales, it has been suggested that high dust loading during glacials supplied the oceans

with more nutrients, enhancing primary production and CO_2 drawdown, helping explain glacial-interglacial CO_2 differences [*Martin et al.,* 1990].

It is clear that mineral dust has complicated but important interactions with the climate system. Reducing our uncertainty of these effects depends not only on understanding the complexities of dust radiative or biogeochemical processes in isolation; it also depends on understanding how and how much dust is emitted from the surface, and where this emission occurs. At present this is a real challenge for the Coupled Model Intercomparison Project Phase 5 (CMIP5) models (Figure 2-3). *Evan et al.* [2014: 5-6] compare CMIP5 dust emission and transport from North Africa with satellite retrievals from two instruments and conclude:

> "Based on the results presented here CMIP5 models are unable to capture any of the salient features of northern African dust emission and transport… there is no reason to assume that the projections of dust emission and concentration for the 21st century have any validity."

There are caveats to this claim, in particular (i) dust mass path (Figure 2-3) is not directly observed but instead is retrieved subject to assumptions (especially about shortwave extinction) and (ii) dust modellers may not actively participate in their model's IPCC simulations, so a more accurate simulation may be described elsewhere. (This caveat is probably generally true of multi-aerosol intercomparison exercises where the participants do not specialize in dust.) The findings of *Evan et al* [2014] nevertheless underline the importance of understanding the distribution of dust sources and observed and modelled atmospheric dust emission and transport mechanisms.

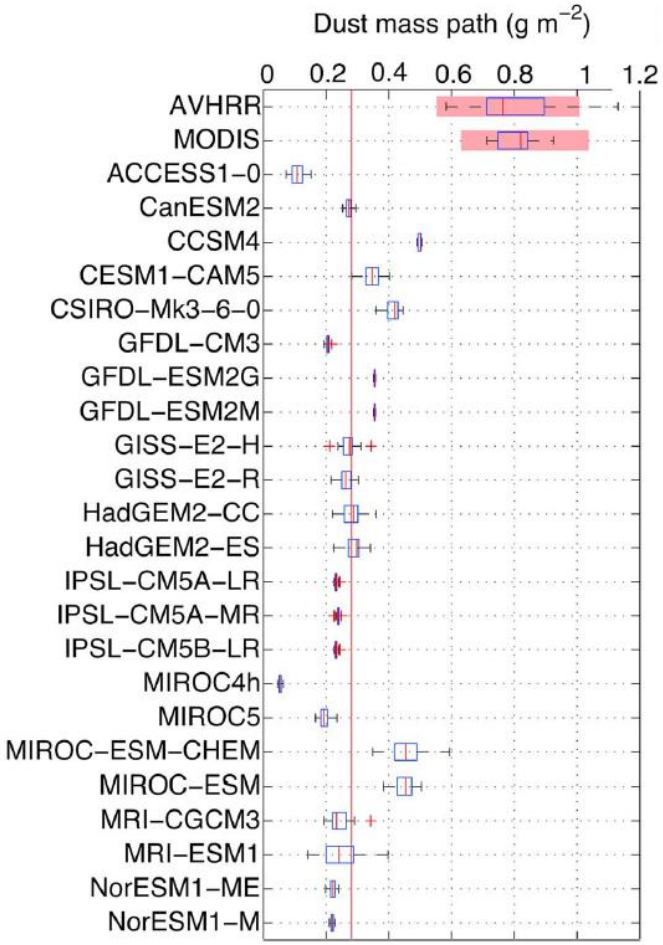

Figure 2-3: Long-term mean dust mass path (vertically integrated mass of atmospheric dust per unit area, 10°–20°N and 20°–30°W) from the advanced very high resolution radiometer (AVHRR) and MODIS, compared with CMIP5 model simulations. Box plots show medians (red lines), interquartile range (blue boxes), the interquartile value ± 1.25 times the interquartile range (black "whiskers") and outliers (red crosses). The red shaded regions indicate the uncertainty in the satellite estimates of long-term median dust mass path. Source: Figure 1a, Evan, A. T., C. Flamant, S. Fiedler, and O. Doherty (2014), An analysis of aeolian dust in climate models, Geophysical Research Letters, 41(16), 2014GL060545, doi: 10.1002/2014gl060545. ©2014. American Geophysical Union. All Rights Reserved. Reproduced with permission of John Wiley & Sons.

2.3. Global dust sources

The most significant dust sources globally are desiccated lake beds, alluvial fans and playas, which act as deposits of eroded and readily deflatable fine material [e.g. *Prospero et al.*, 2002; *Washington et al.*, 2003; *Bullard et al.*, 2011]. Vegetation cover

is typically low or non-existent, moisture content is negligible (although inundation may have been common in the past) and wind speeds are high and/or gusty [e.g. *Engelstaedter and Washington*, 2007a; *Washington and Wiggs*, 2011]. Dust sources are thus mostly found in arid or semi-arid regions. Satellite data has proved invaluable for mapping dust sources on a global scale. For example, the absorbing properties of mineral aerosol in the ultraviolet have been exploited to generate an aerosol index [*Herman et al.*, 1997], which has then been used to map the distribution of dust according to the Total Ozone Mapping Spectrometer (TOMS) instrument carried by the Nimbus 7 polar-orbiting satellite. Such an approach was taken by *Prospero et al.* [2002] and *Washington et al.* [2003]. These authors found that most dust sources were located in the northern hemisphere subtropics, in particular the Sahara, the Arabian Peninsula, south-west Asia, the Taklamakan and the Great Basin of the United States. Other important sources were found to be central Australia, the Etosha and Mkgadikgadi basins of southern Africa, Patagonia and the Salar de Uyuni in Bolivia. The TOMS aerosol index shows the most important source region globally to be the Sahara [*Washington et al.*, 2003] (Figure 2-4).

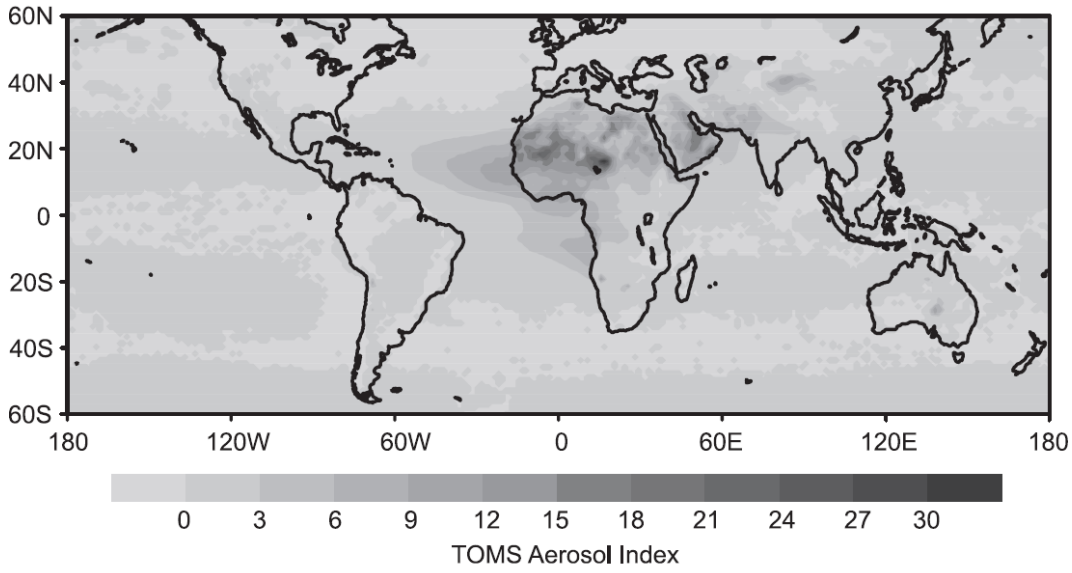

Figure 2-4: TOMS Aerosol Index (1978-1993). Source: Figure 1, Washington, R., M. C. Todd, N. J. Middleton, and A. S. Goudie (2003), Dust-Storm Source Areas Determined by the Total Ozone Monitoring Spectrometer and Surface Observations, Annals of the Association of American Geographers, 93(2), 297-313, doi: 10.1111/1467-8306.9302003. Reprinted by permission of the Association of American Geographers (http://www.aag.org).

An important finding of the TOMS studies was that the persistent dust source regions were not sand dunes or sand seas (ergs) but rather areas of extensive alluvial deposits, provided they are now in an arid setting [*Prospero et al.*, 2002]. However, this has more recently been debated. Using manual back-tracking of dust plumes with 15-minute temporal resolution Spinning Enhanced Visible and Infra-Red Imager (SEVIRI) geostationary satellite imagery, *Crouvi et al.* [2012] find that active sand dunes are the most frequent dust sources in the Sahara. *Crouvi et al.* [2012] propose that aeolian abrasion (sandblasting) removes sharp corners and clay coatings from sand grains, producing fine dust within the sand dunes themselves. *Rosenberg et al.* [2014] hypothesise that sand dunes may play an important role by 'injecting' large particles into the atmosphere from their crests: they argue that flow separation over dune crests may be what allows dust particles of sizes 30-100μm (usually seen as large, but in fact the mode in dust mass flux during Fennec research flights) to be entrained into the

atmosphere. Automated objective back-tracking of dust plumes with 15-minute temporal resolution SEVIRI imagery has not identified sand dunes as important dust source areas however, except occasionally at their margins, where sand seas provide material for saltation onto palaeolakes, leading to deflation by saltation bombardment [*Ashpole and Washington*, 2013a].

Debate about the source geomorphology notwithstanding, studies since *Prospero et al.* [2002] and *Washington et al.* [2003] are in agreement that North Africa is the most important global source of dust. Estimates vary, but authors have suggested that North Africa is responsible for 40-70% of the global annual dust emission total [*Engelstaedter et al.*, 2006]. Both model-based [e.g. *Tanaka and Chiba*, 2006] and satellite-based [e.g. *Ginoux et al.*, 2012] work has demonstrated the primacy of North Africa as the most important global source of dust. Research tends to suggest that the Sahara Desert is the most important source region in North Africa [e.g. *Engelstaedter et al.*, 2006; *Tanaka and Chiba*, 2006; *Laurent et al.*, 2008] but some arguments have been made that the importance of the Sahel as a source region has been underestimated [e.g. *Bou Karam et al.*, 2009a; *Ginoux et al.*, 2012]. This may be because of limitations of satellite retrieval, for example sensitivity of TOMS aerosol index to boundary layer height [e.g. *Mahowald and Dufresne*, 2004] and sensitivity of SEVIRI dust detection to column moisture [*Brindley et al.*, 2012]. It is also difficult to distinguish mineral dust from biomass burning in the Sahel [e.g. *Engelstaedter et al.*, 2006]. A possible resolution is proposed by *Klose et al.* [2010], who use observation stations in the Sahel to analyse the synoptic patterns associated with dust between 1983-2008 and find that, whilst dust loadings in the Sahel can be very high (especially between December and April), the dust tends to originate from the Sahara and be in suspension over the Sahel.

2.4. Saharan dust sources

2.4.1. The Bodélé Depression

In the annual mean, dust is present across a wide swath of the Sahara, but one source region stands out in particular, the Bodélé Depression in Chad (Figure 2-5). This topographic depression, situated in the Lake Chad Basin between the Tibesti Mountains and the Ennedi Massif, was identified as the most intense dust source in the world by *Prospero et al.* [2002] and *Washington et al.* [2003]. It is estimated by *Evan et al.* [2015] to be responsible for 64±16% total North African emission. Dust emission from the Bodélé peaks in March, although it occurs year-round [*Washington and Todd*, 2005].

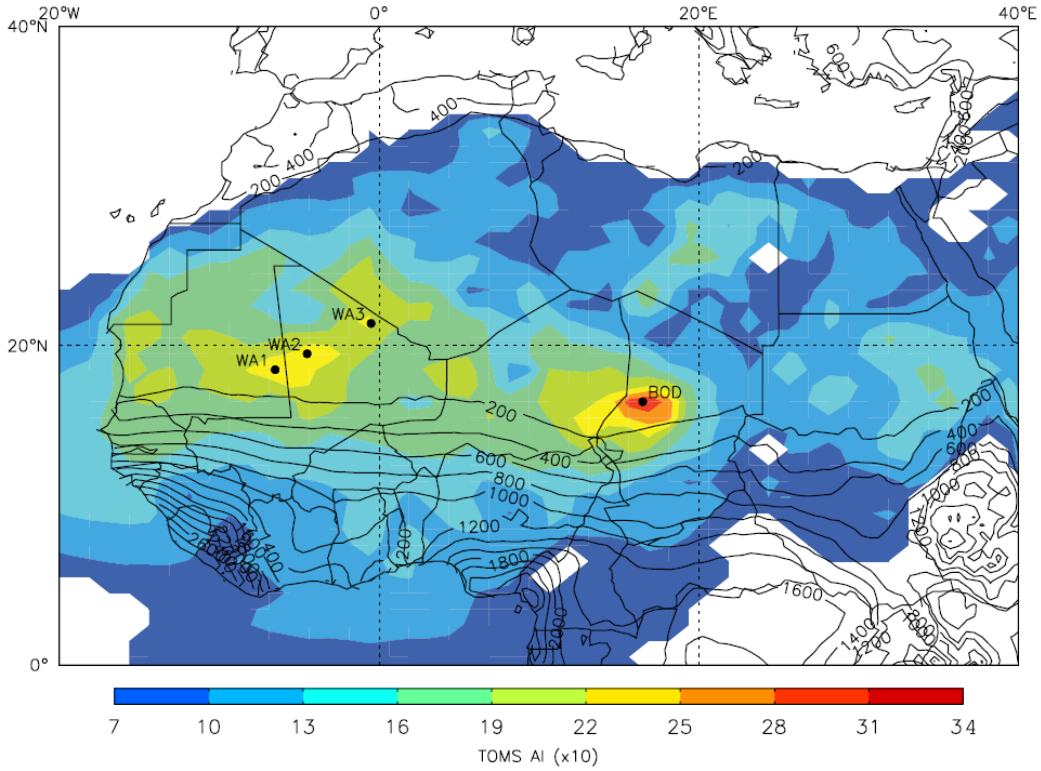

Figure 2-5: Mean (1980-1992) TOMS Aerosol Index (AI) over North Africa (colour contours). Mean (1961-1990) precipitation (black isohyets). The Bodélé Depression is identified as 'BOD'; three West African dust maxima are also identified. Source: Figure 1 of Engelstaedter, S., and R. Washington (2007b), Atmospheric controls on the annual cycle of North African dust, J. Geophys. Res., 112(D3), D03103, doi: 10.1029/2006jd007195. Copyright 2007 by the American Geophysical Union. Reproduced by permission of John Wiley & Sons.

The Bodélé Field Experiment in February-March 2005 provided the first surface-based measurements of the atmospheric circulation over the depression. Pilot balloon and automatic weather station (AWS) data confirmed the presence of the north-easterly Bodélé Low Level Jet (LLJ), previously identified by *Washington and Todd* [2005] from NCEP reanalysis data, and allowed a thorough investigation of its dynamics [*Washington et al.*, 2006a]. The core of the LLJ is focused around 500m above ground level, with the strongest wind speeds (>20 m s^{-1}) developing between midnight and sunrise. At the surface, wind speeds lag behind those in the jet core, peaking several hours after sunrise as turbulence, generated by radiative heating, mixes the momentum from the jet down to the surface. The diurnal cycle is evident on both dusty and dust-free days. On dusty days, however, composite winds at the surface are maintained above 10 m s^{-1} for five hours from 0600 to 1300, whereas on dust-free days composite wind speeds peak at 9 m s^{-1} for only an hour, around 0900.

The Bodélé LLJ partly owes its existence to the Tibesti Mountains and Ennedi Massif, which channel the north-easterly Harmattan flow between them and accelerate it downslope. It is likely that a relationship between the jet and the basin has developed over millennial timescales. During dry phases such as the Last Glacial Maximum (~22,000 cal. year BP) the jet eroded out the basin. During pluvials, the basin was filled with water and provided a habitat for diatoms; with subsequent desiccation a deposit of fine diatomite sediment became available for transport [*Washington et al.*, 2006b]. The strength of the jet follows a seasonal cycle together with the Harmattan: it is strongest in boreal winter and weakest in summer. It also appears to be influenced by the strength of the Libyan High: positive 925hPa geopotential height anomalies over northern Libya accelerate the easterlies and north-easterlies around the system, and lead to an ageostrophic flow which 'pulses' the LLJ [*Washington and Todd*, 2005].

2.4.2. Central Saharan dust sources

Whilst the Bodélé Depression is a clearly identifiable dust 'hotspot', dust sources in other parts of the Sahara have, until recently, been harder to pinpoint. Relative to the Bodélé, dust activity is moderate or low in other parts of the desert except in summer, when dust loadings are very high over an extensive region of the central and central-western Sahara [e.g. *Engelstaedter and Washington*, 2007b; *Ashpole and Washington*, 2012; *Ginoux et al.*, 2012]. However, this large region (roughly 15-30°N, 10°W-10°E) is not one single dust source. The 15-minute temporal resolution of SEVIRI has enabled individual 'dust sources' to be identified by backtracking dust plumes to their point of first detection, both manually/subjectively [*Schepanski et al.*, 2007] and automatically/objectively [*Ashpole and Washington*, 2013a]. These results are in good agreement, although the automated technique of *Ashpole and Washington* [2013a] has the advantage of being able to exploit the native high resolution of SEVIRI (0.03° compared to 1° in *Schepanski et al.* [2007]). In both studies, summertime (June, July, August) dust sources are concentrated in north-east Mali, north-west Niger and southern Algeria. *Ashpole and Washington* [2013a] identify 15 individual clusters of particularly active dust sources, of which 10 are associated with palaeolakes (Figure 2-6).

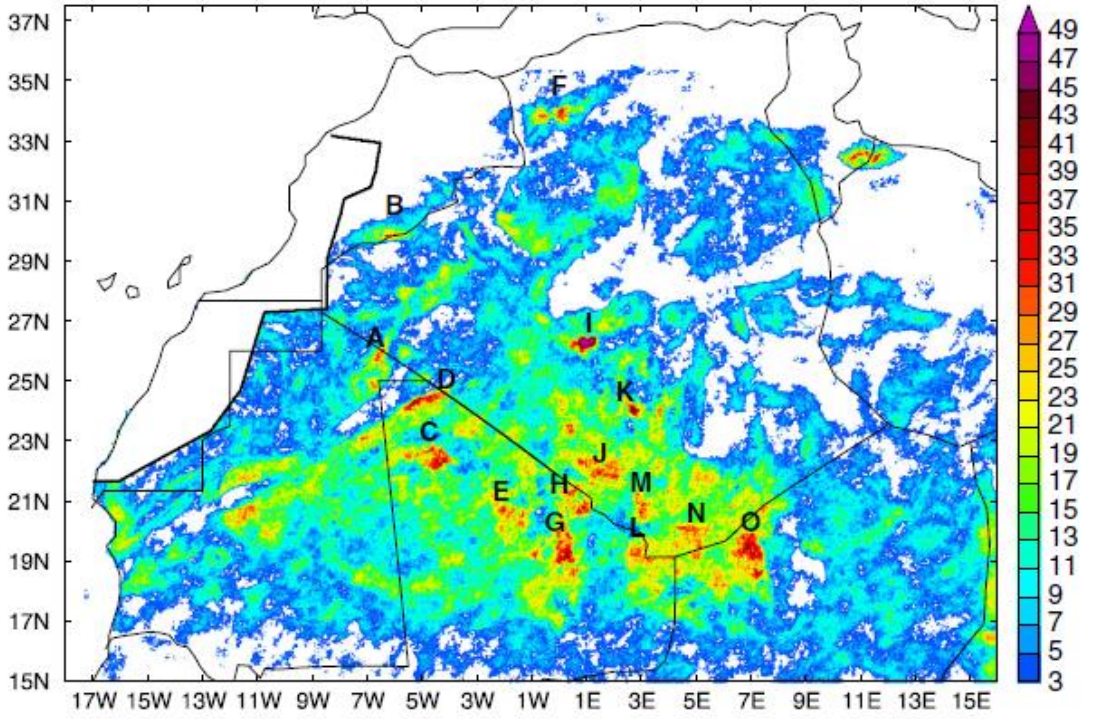

Figure 2-6: Frequency of occurrence of dust sources detected by automated back-tracking of dust in SEVIRI imagery, 2004-2010 June-August. Individual dust sources labelled. Black contour bounds a region where stratus cloud is commonly mistaken for dust in the algorithm, so here the count is set to zero. Source: Figure 5, Ashpole, I., and R. Washington (2013), A new high-resolution central and western Saharan summertime dust source map from automated satellite dust plume tracking, J. Geophys. Res. Atmos., 118, doi:10.1002/jgrd.50554. ©2013 American Geophysical Union. Reproduced with permission of John Wiley & Sons.

2.5. Climatology of West African dust emission

The controls of dust emission from the Bodélé Depression, the world's largest single dust source [e.g. *Prospero et al.*, 2002] are relatively well understood [e.g. *Washington and Todd*, 2005; *Washington et al.*, 2006a; *Todd et al.*, 2008] (and see Section 2.4.1). However, the controls on emission from the central Saharan sources are more complicated and have been more difficult to study [e.g. *Engelstaedter and Washington*, 2007b]. Since these sources collectively make the central Sahara the dustiest place in the world in summer [*Engelstaedter et al.*, 2006] and, as has been discussed in Section

2.2, dust has wide ranging and significant impacts on the climate system, understanding the mechanisms that generate the dust in the central Sahara has been identified as a priority for research [*Knippertz and Todd*, 2012]. The starting point is the climatological setting of West Africa.

In boreal winter, the inter-tropical convergence zone (ITCZ) is centred south of the equator and West Africa is dominated by dry, north-easterly trade winds. There is little dust emission from the central Saharan sources but over Chad, where the north-easterly flow is particularly strong, the Bodélé LLJ is at its strongest and emission from this source is at its maximum [*Engelstaedter et al.*, 2006]. Dust is transported south-westwards towards the Gulf of Guinea where it mixes with black carbon aerosol from biomass burning and is transported onwards below the trade wind inversion (<2km asl) across the Atlantic Ocean towards the Amazon Rainforest [*Kaufman et al.*, 2005; *Schepanski et al.*, 2009a] (Figure 2-7).

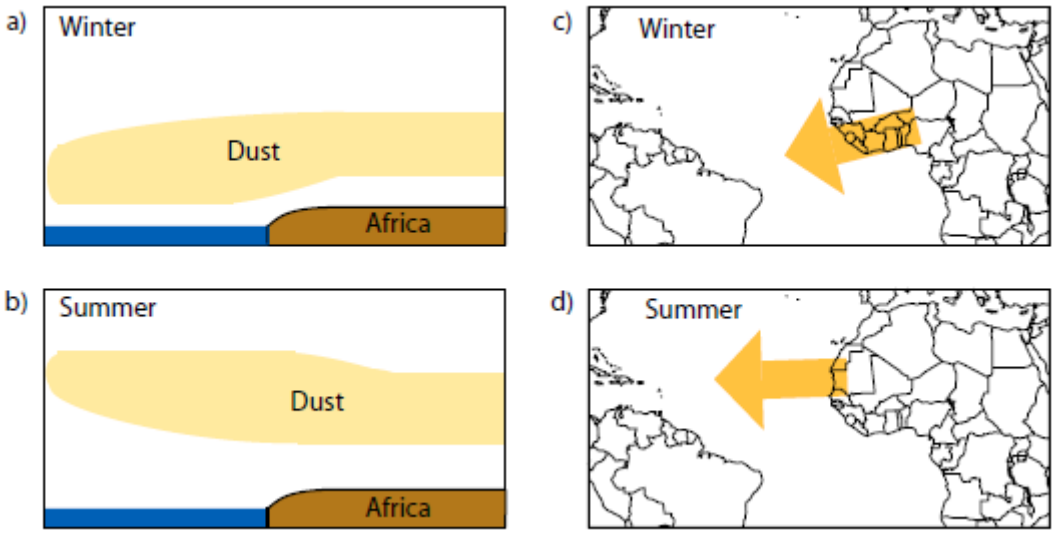

Figure 2-7: Cartoon showing dust transport out of North Africa in winter (top) and summer (bottom). In winter, dust is predominantly transported south-westwards below the trade wind inversion; in summer it is predominantly transported westwards within the Saharan Air Layer. Source: Figure 1, Schepanski, K., I. Tegen, and A. Macke (2009a), Saharan dust transport and deposition towards the tropical northern Atlantic, Atmos. Chem. Phys., 9(4), 1173-1189, doi: 10.5194/acp-9-1173-2009. Reproduced under Creative Commons Attribution 3.0 CC BY license.

Spring and autumn can be seen as seasons of transition in West Africa. They are, respectively, the seasons of the development and decline of the West African Monsoon (WAM[4]). An important ingredient for the development of the WAM is the position and intensity of the Saharan Heat Low (SHL) [e.g. *Sultan and Janicot*, 2003], a regional-scale cyclonic centre of high temperature and low pressure extending from the surface to about 700hPa. In spring, the SHL shifts from northern Cameroon north-westwards towards its summer position over northern Mali [*Lavaysse et al.*, 2009] (Figure 2-8). Dust emission from the central Saharan sources also begins to increase in spring [*Engelstaedter and Washington*, 2007b]. In autumn, the SHL returns back from northern Mali to northern Cameroon [*Lavaysse et al.*, 2009] (Figure 2-8) and dust

[4] Note that WAM is used in this thesis only to refer to the moist monsoon circulation

emission from the central Saharan sources decreases [*Engelstaedter and Washington*, 2007b].

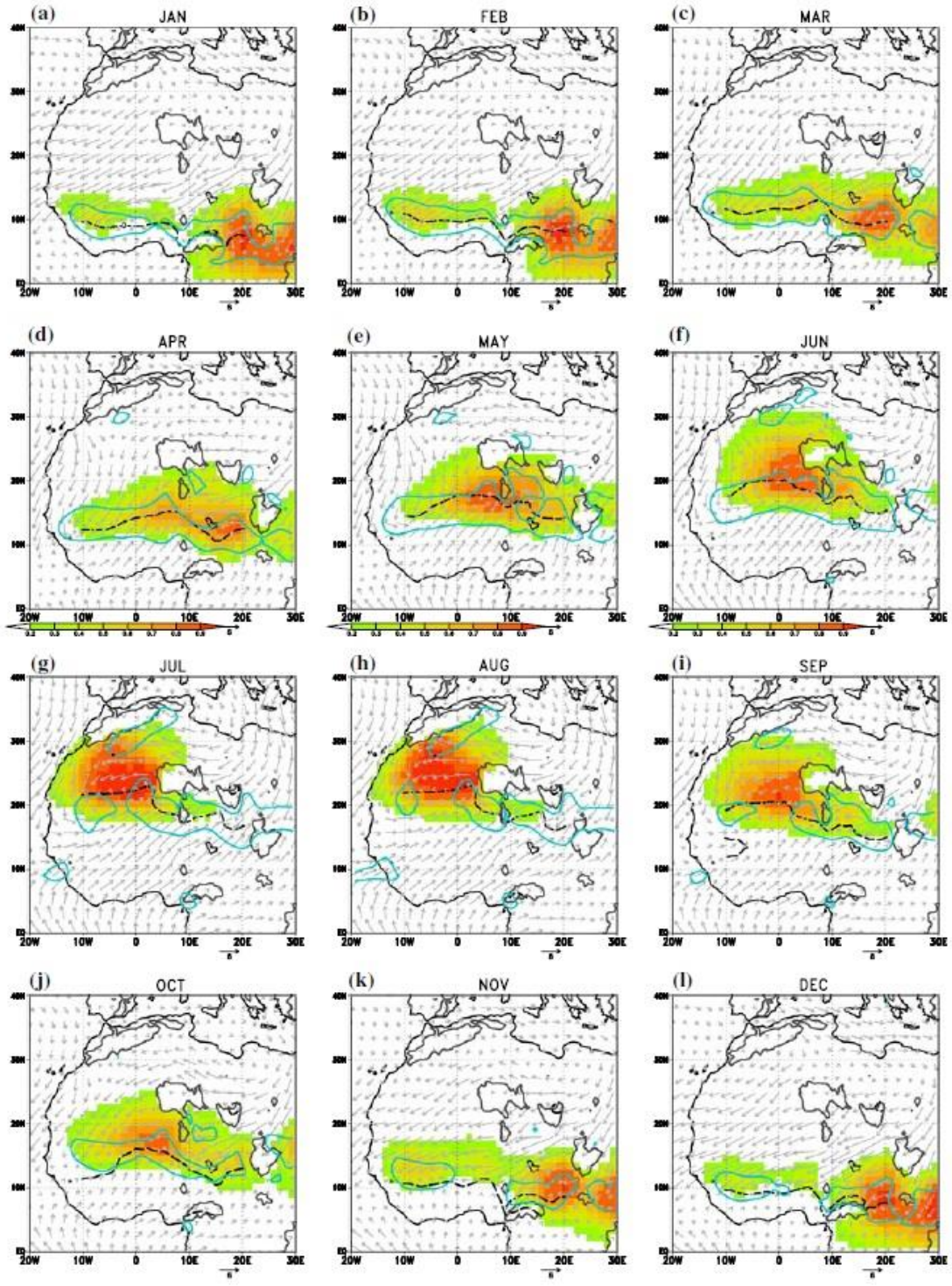

Figure 2-8: Monthly mean (1979-2001) heat low occurrence frequency (colours) and 925 hPa wind field (vectors, m s^{-1}). Blue contours indicate the 8 x 10^{-6} s^{-1} level of horizontal convergence and black lines display the position of the lowest 925 hPa geopotential height between the Equator and 28°N. Grey lines display the contour of orography above 925 hPa. Source: Figure 4, Lavaysse, C., C. Flamant, S. Janicot, D. J. Parker, J. P. Lafore, B. Sultan, and J. Pelon (2009), Seasonal evolution of the West African heat low: a climatological perspective, Climate Dynamics, 33(2), 313-330, doi: 10.1007/s00382-009-0553-4. With permission of Springer Science+Business Media.

In summer the SHL is located over the central Sahara and dust emission from the central Saharan dust sources peaks [e.g. *Knippertz and Todd*, 2012]. The reasons behind the colocation of the SHL with the summer global dust maximum are not fully understood. It appears, however, that the WAM plays a key role.

2.6. The search for atmospheric dust emission mechanisms in the SHL

The exceptionally high temperatures in the SHL are caused primarily by the intense solar radiation at the surface, although adiabatic processes also contribute [*Lavaysse et al.*, 2009]. The air rises in convection currents, lowering the pressure at the surface and resulting in a cyclonic circulation at low levels. The resulting horizontal pressure gradient between the SHL and the Santa Helena anticyclone sets up the moist onshore monsoon winds [e.g. *Sultan and Janicot*, 2003]. Because the SHL is a cyclonic feature, the near-surface monsoon winds in the Sahel and southern Sahara are typically south-westerly [e.g. *Lothon et al.*, 2008; *Engelstaedter et al.*, 2015] (Figure 2-9). The anticyclonic circulation at the top of the SHL (about 700hPa) results in a southward 'return' flow which contributes to maintaining the AEJ [*Thorncroft and Blackburn*, 1999], which is a fundamental feature of the momentum balance of the WAM [*Parker et al.*, 2005]. By providing easterly wind shear with height, which separates the updraft and downdraft regions, the AEJ additionally allows strong and long-lasting cumulonimbus systems to develop [e.g. *Thorpe et al.*, 1982], fundamental features of monsoonal weather. The SHL thus contributes to generating and maintaining the WAM at the near surface and aloft. A schematic of the West African Monsoon system is provided in Figure 2-10.

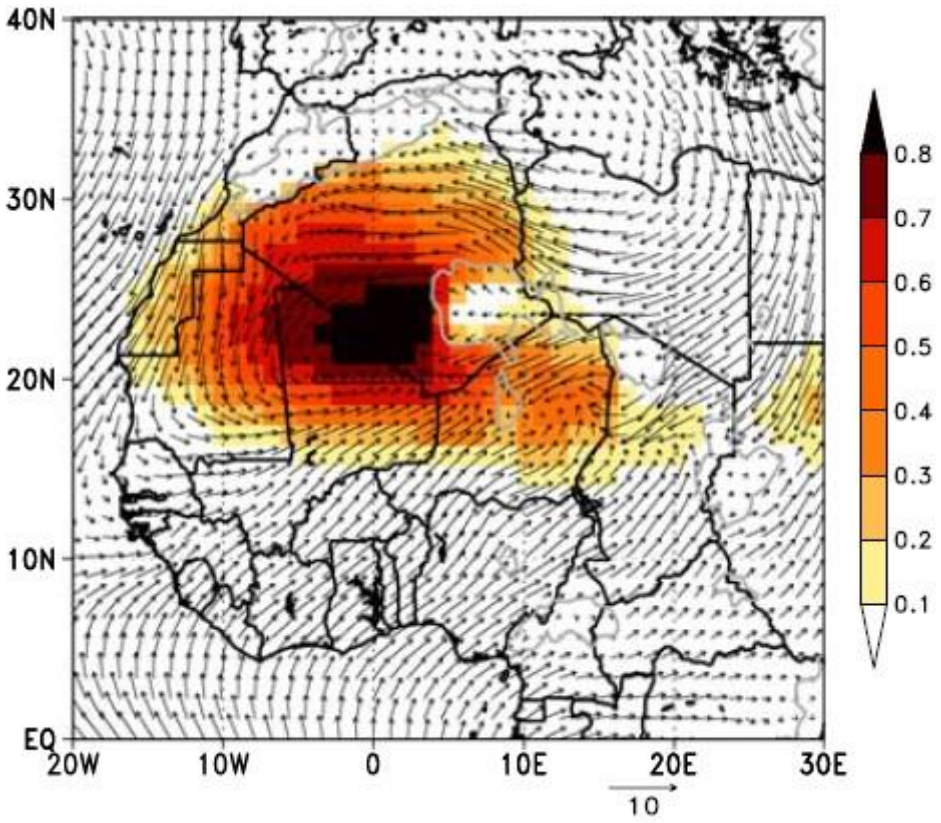

Figure 2-9: Mean heat low occurrence frequency for June-October 1971-2001 at 0600 UTC (shaded). 925hPa wind vectors are overlain. Source: Figure 9a, Lavaysse, C., C. Flamant, S. Janicot, D. J. Parker, J. P. Lafore, B. Sultan, and J. Pelon (2009), Seasonal evolution of the West African heat low: a climatological perspective, Climate Dynamics, 33(2), 313-330, doi: 10.1007/s00382-009-0553-4. With permission of Springer Science+Business Media.

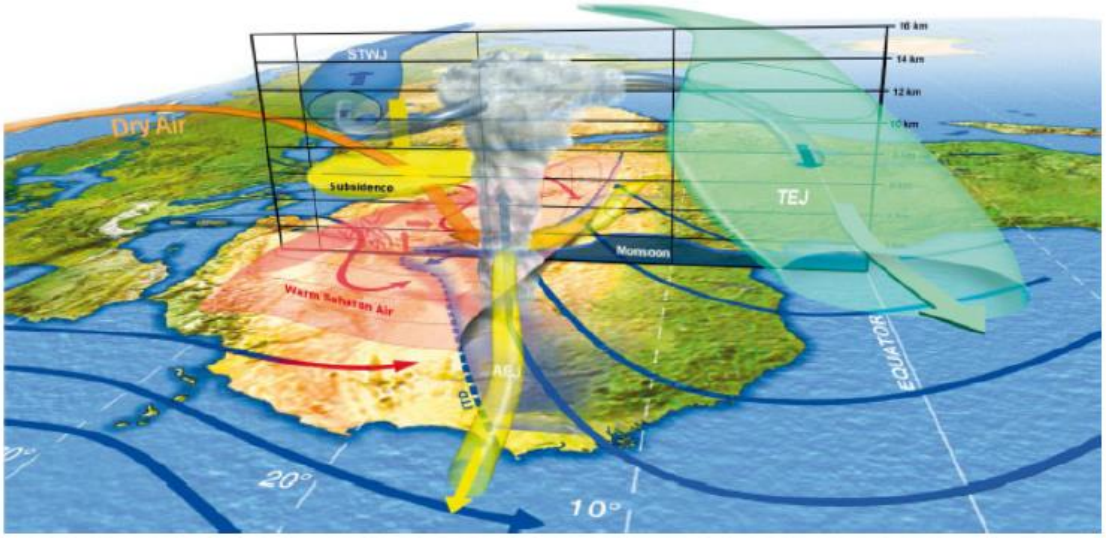

Figure 2-10: Schematic of the WAM in context. STWJ = sub-tropical westerly jet, TEJ = tropical easterly jet, AEJ = African easterly jet, ITD = inter-tropical discontinuity. Source: Figure 1, Lafore, J.-P., Flamant, C., Giraud, V., Guichard, F., Knippertz, P., Mahfouf, J.-F., Mascart, P. and Williams, E.R. (2010), Introduction to the AMMA Special Issue on 'Advances in understanding atmospheric processes over West Africa through the AMMA field campaign'. Q.J.R. Meteorol. Soc., 136: 2–7. doi: 10.1002/qj.583. Copyright 2010 Royal Meteorological Society. Reproduced with permission of John Wiley & Sons.

A link between WAM and summer dust emission from West Africa was proposed by *Engelstaedter and Washington* [2007b]. Using TOMS and ECMWF ERA-40 reanalysis data, they found that the highest dust levels coincided with the northward progression of the ITCZ over the dust sources. The authors argued that it was the high wind gusts caused by dry convection in the convergence zone, rather than the mean wind speeds, that resulted in dust emission. *Williams* [2008] challenged *Engelstaedter and Washington* [2007b] on the basis that TOMS cannot see beneath cirrus (common at the ITCZ), and therefore cannot detect cold pool outflows from deep convection. *Williams* [2008] argued that as a consequence, *Engelstaedter and Washington* [2007b] had neglected the contribution of cold pool outflows to dust emission in summertime West Africa and overestimated the importance of dry convection.

Subsequent studies, using aircraft and model data, searched for the atmospheric mechanisms which could be responsible for the maximum in dustiness in the summer SHL region. *Knippertz* [2008] performed a detailed study using ECMWF operational analyses for the period 29 May to 3 June 2006, and concluded that there were two main mechanisms of dust mobilisation in the vicinity of the SHL: (i) downward mixing of momentum from LLJs in the morning (ii) cold pool outflows associated with the northward shifting inter-tropical discontinuity (ITD). Using aircraft observations over Niger from 7 July 2006, *Bou Karam et al.* [2008] found that the monsoon flow into the Sahara was itself causing dust emission, as near-surface winds and turbulence were particularly strong at its leading edge. *Marsham et al.* [2008] described similar results from an aircraft transect over southern Mali and southern Mauritania and, as also recorded by *Bou Karam et al.* [2008] and *Flamant et al.* [2007], found evidence for cold pool outflow dust emission within the monsoon flow. *Marsham et al.* [2008] also proposed an explanation for why dust loadings were higher during monsoon onset than monsoon retreat (as described by [*Engelstaedter and Washington*, 2007b]): downdraft convective available potential energy from convective storms was higher during monsoon onset, leading to more intense cold pools.

In the following years, a number of atmospheric mechanisms have been identified that may collectively explain why dust emission is so intense in the Sahara in summer. Understanding how these individual mechanisms operate is essential for detecting and attributing Saharan dust loadings, and for diagnosing why model winds are simulated well or simulated poorly.

2.6.1. Cold pool outflows

Cold pool outflows form from downdrafts of deep moist convection, when evaporating or sublimating precipitation cools the air at mid-levels (800-500hPa), allowing it to sink to the surface, particularly if the environment is dry adiabatic and/or there is sufficient drag by falling precipitation [e.g. *S D Miller et al.*, 2008]. As the sinking air approaches the surface it spreads away from the parent storm along a density gradient [*Simpson*, 1997]. Turbulence and high winds at the leading edge of the outflow (the gust front) can raise substantial 'walls' of dust, especially where the threshold shear velocity is low [*Flamant et al.*, 2007; *Knippertz et al.*, 2007; *S D Miller et al.*, 2008; *Williams et al.*, 2009; *Emmel et al.*, 2010; *Solomos et al.*, 2012; *Bou Karam et al.*, 2014] (Figure 2-11). Such dust storms are frequently called 'haboobs' in the Sahara and Arabian Peninsula and can be observed in satellite imagery, for instance in false colour SEVIRI 'pink dust' images, where moist cold pools are usually visually discernible from the hot and dry surrounding air [e.g. *Bou Karam et al.*, 2014; *Roberts and Knippertz*, 2014]. Cold pools are frequently associated with abrupt changes in meteorological variables as they pass, e.g. switch in wind direction, rapid increase in wind speed, increase in water vapour mixing ratio or a change in temperature [e.g. *Emmel et al.*, 2010]. Because of their formation from thunderstorm downdrafts, cold pools are simulated very poorly or not at all in numerical models which do not explicitly resolve convection [*Reinfried et al.*, 2009; *Marsham et al.*, 2011; *Solomos et al.*, 2012]. However, when models can be run with explicit convection, cold pools are shown to account for roughly half the dust emission in the Saharan region in summer [*Marsham et al.*, 2011; *Heinold et al.*, 2013].

Figure 2-11: A cold pool outflow photographed near Phoenix, Arizona. CEBImagery. Used under Creative Commons Attribution non-commercial license CC BY-NC 2.0.

Due to their association with moist convection, cold pools are not ubiquitous across the Sahara. One region where they are observed relatively frequently is the Atlas Mountains [*Knippertz et al.*, 2007; *Emmel et al.*, 2010]. *Emmel et al.* [2010] report that, for the southern foothills of the Moroccan Atlas, 11±4 cold pool are usually observed per year, primarily between April and September. Cold pools are common in the region because the mountains both promote convection, especially when there is a trough at upper levels, and also accelerate sinking air down the lee slopes [*Knippertz et al.*, 2007] (Figure 2-12). These currents frequently lead to dust storms since fine eroded materials at the foot of the slopes are a ready source of entrainable sediment [*Knippertz et al.*, 2007].

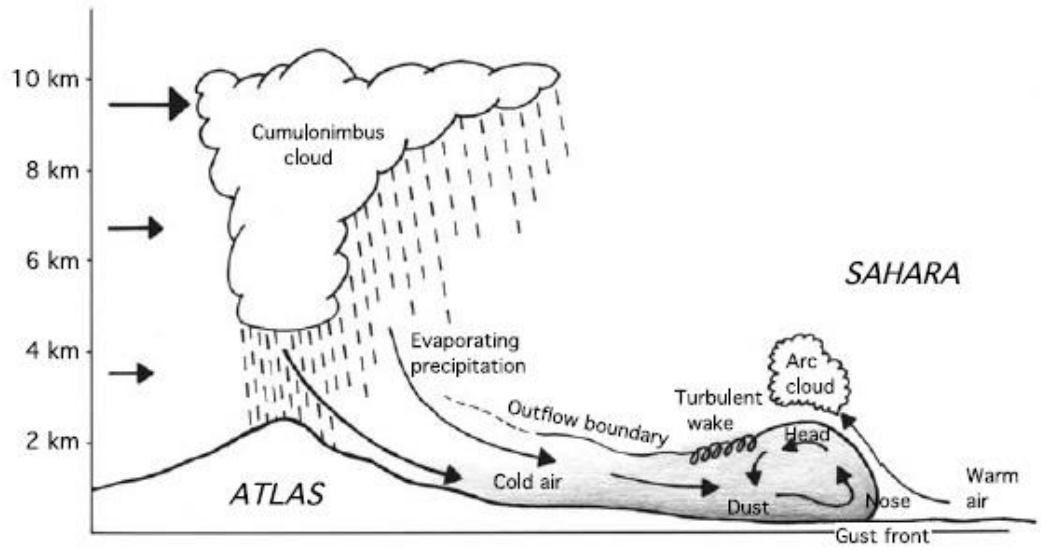

Figure 2-12: Schematic of cold pool generation on the lee side of the Atlas Mountains. Generation of cold pools in other regions (e.g. the southern Sahara) is similar, except that cumulonimbus generation is not orographic. Source: Figure 2, Knippertz, P., C. Deutscher, K. Kandler, T. Müller, O. Schulz, and L. Schütz (2007), Dust mobilization due to density currents in the Atlas region: Observations from the Saharan Mineral Dust Experiment 2006 field campaign, J. Geophys. Res., 112, D21109, doi:10.1029/2007JD008774. Copyright 2007 by the American Geophysical Union. Reproduced with permission of John Wiley & Sons.

As the ITD progresses northwards in boreal summer, the moist air brought in from the Gulf of Guinea by the monsoon fuels deep convection and cold pools become more common in the Sahel and in the central Sahara [e.g. *Cuesta et al.*, 2008; *Cuesta et al.*, 2009; *Marticorena et al.*, 2010; *Cavazos-Guerra and Todd*, 2012], particularly in the afternoon and at night [e.g. *Schepanski et al.*, 2009b; *Marsham et al.*, 2011]. *Knippertz and Todd* [2010] argue that AEWs promote cold pool dust emission by advecting moist air northwards into the central Sahara. Using an automated objective satellite dust detection product, the SEVIRI dust flag (SDF) [*Ashpole and Washington*, 2012], *Ashpole and Washington* [2013a] find that summertime dust events originating from the central Saharan dust sources around the Mali-Algeria-Niger triple point are typically associated with deep convection and have no dominant transport direction. The authors

argue that this points to the important role of cold pools in this region, in contrast to dust sources further north, where dust events are not usually associated with deep convection and have a dominant south-westward transport direction, pointing to the importance of LLJs (Figure 2-13).

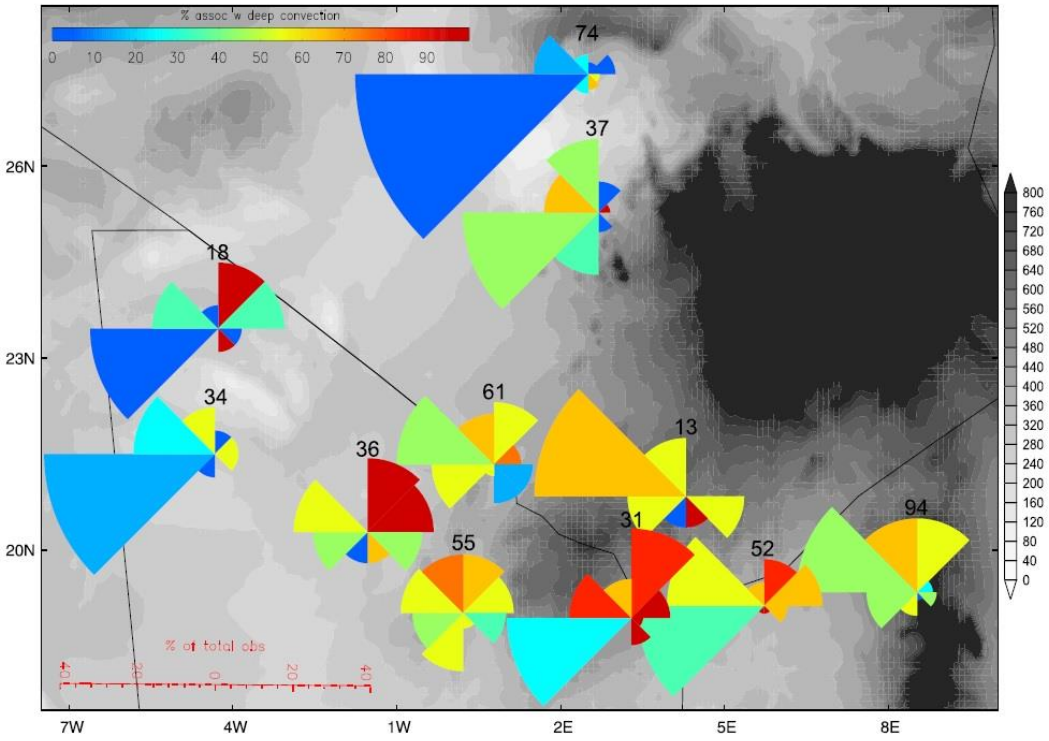

Figure 2-13: Characteristics of dust events to originate from the dominant central Saharan dust sources. Each dust source shows transport direction of dust events in their first 6 h following first detection (i.e., away from the centre of the wind rose) and proportion of events to originate at that source area traveling in each segment direction (length of segments). Colours of each segment indicate % of events traveling in that direction associated with deep convection. Number above each source area corresponds to number of events included in the analysis. Grayscale shading on background map represents topography in m. Source: Figure 10 of Ashpole, I., and R. Washington (2013), A new high-resolution central and western Saharan summertime dust source map from automated satellite dust plume tracking, J. Geophys. Res. Atmos., 118, doi:10.1002/jgrd.50554. ©2013. American Geophysical Union. Reproduced with permission of John Wiley & Sons.

2.6.2. Low level jets

LLJs can form in desert regions after sunset when turbulent heating dies down and winds aloft become decoupled from surface frictional damping [e.g. *Blackadar*, 1957; *Stensrud*, 1996; *Mahrt*, 1999]. In conditions of a moderate or strong pressure gradient the flow can then become super-geostrophic above the nocturnal inversion [*Blackadar*, 1957]. Other recorded mechanisms for LLJ formation are shallow baroclinicity (e.g. at the land/sea interface), terrain effects (diurnal heating contrasts on slopes), synoptic forcing, and rapid air parcel displacement increasing the local pressure gradient force [*Stensrud*, 1996]. The core of the LLJ (i.e. the altitude of peak wind speeds) is usually found a few hundred metres above the surface [e.g. *May*, 1995; *Washington et al.*, 2006a; *Bain et al.*, 2010; *van de Wiel et al.*, 2010; *Madougou et al.*, 2012]. After sunrise, turbulent mixing begins to increase and momentum from the LLJ core can be mixed down to the surface [*Washington et al.*, 2006a; *Lothon et al.*, 2008; *Todd et al.*, 2008] (Figure 2-14). This results in high winds at the surface in the mid-morning/early afternoon and potentially dust emission [e.g. *Washington et al.*, 2006a]. This process has been examined in detail for the Bodélé LLJ (see Section 2.4.1). However, research with numerical models and satellite retrieval suggests that LLJs also play an important role in dust emission across other parts of the Sahara [*Schepanski et al.*, 2009b; *Fiedler et al.*, 2013; *Heinold et al.*, 2013].

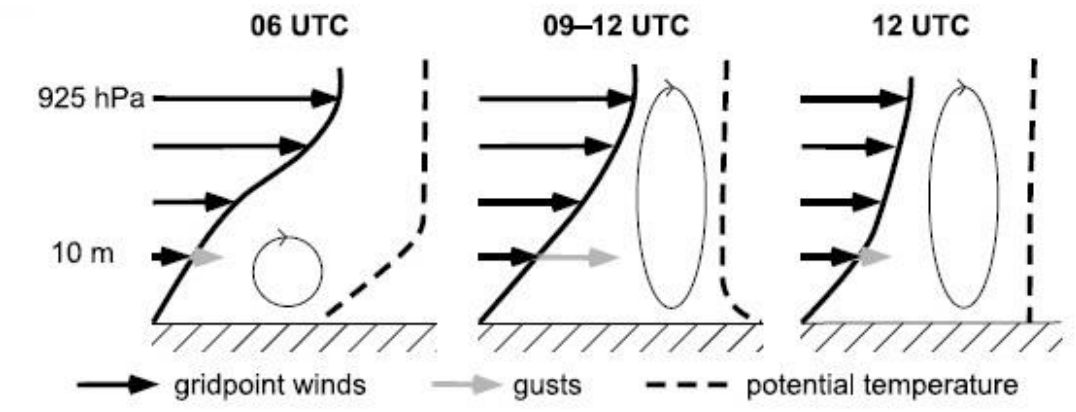

Figure 2-14: Schematic depiction of typical changes in the vertical profile of low-level wind, gusts, potential temperature, and turbulence over the Sahara during morning hours, showing the breakdown of a LLJ due to turbulent mixing. Source: Figure 1, Knippertz, P. (2008), Dust emissions in the West African heat trough the role of the diurnal cycle and of extratropical disturbances, Meteorologische Zeitschrift, 17(5), 553-563, doi: 10.1127/0941-2948/2008/0315. Reproduced with permission of Schweizerbart Science Publishers www.schweizerbart.de.

Schepanski et al. [2007] manually back-track dust plumes in SEVIRI satellite imagery and compile a dataset of the location and time of day dust first appears. This is used to produce a map of Saharan dust source activation frequency. Between March 2006 and February 2008, 65% of dust source activation occurs during the period 0600-0900 UTC, which *Schepanski et al.* [2009a] argue demonstrates the importance of LLJ breakdown in causing dust emission. The authors then use an empirically established criterion to identify LLJs in 1990-99 ERA-40 reanalysis data (wind shear greater than 5 m/s between 770hPa and 925hPa). They find that the spatial extent of LLJ frequency is largest in January, when the Harmattan flow extends furthest south, with >50% LLJ occurrence encompassing a wide belt between 12 and 21°N across North Africa. In July the spatial extent of >50% occurrence is reduced, more patchy and shifted further north together with the ITD. At this time the highest LLJ occurrence frequencies are over

southern Mauritania and central Mali, central and eastern Algeria, western Libya, the Bodélé and northern Sudan (Figure 2-15).

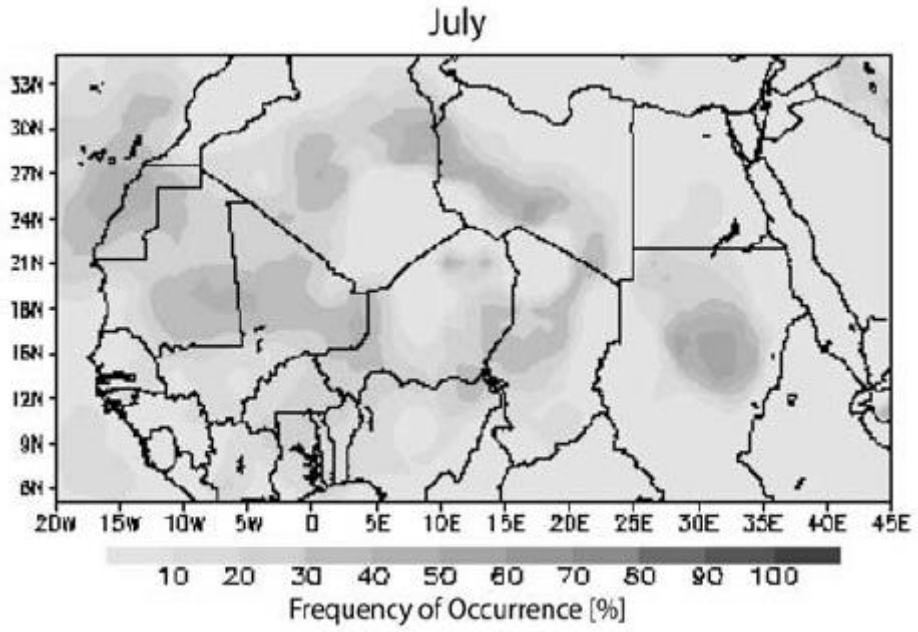

Figure 2-15: Frequency of July LLJ occurrence at 0600 in ERA-40 (1990-1999). LLJs as defined by *Schepanski et al.* [2009a] (see text above). Source: Figure 3c, Schepanski, K., I. Tegen, M. C. Todd, B. Heinold, G. Bönisch, B. Laurent, and A. Macke (2009), Meteorological processes forcing Saharan dust emission inferred from MSG-SEVIRI observations of subdaily dust source activation and numerical models, J. Geophys. Res., 114, D10201, doi:10.1029/2008JD010325. Copyright 2009 by the American Geophysical Union. Reproduced with permission of John Wiley & Sons.

Tegen et al. [2013] compare the dust source activation record of *Schepanski et al.* [2007] with a dust emission scheme [*Tegen et al.*, 2002] driven by regional model COSMO-MUSCAT (model described in detail by *Heinold et al.* [2007]). *Tegen et al.* [2013] find that, in the model, LLJs lead to dust emission later in the day and less frequently than in the dust source activation record. The authors propose that the model may have an inadequate boundary layer scheme, or that the grid size (28km) is too coarse to resolve strong gradients in topography – regions where dust source activation frequently occurs. However, *Tegen et al.* [2013] also point out that the dust source activation satellite

approach of *Schepanski et al.* [2007] has limitations, for example that dust emission that occurs beneath existing dust clouds will be missed. They also highlight discrepancies between dust source activation results and AERONET aerosol optical thickness (AOT), suggesting that frequency of events may not be a good indicator for emission fluxes.

An alternative approach is presented by *Fiedler et al.* [2013]. LLJs are identified in ECMWF ERA-Interim reanalysis (ERAI) over North Africa using a set of objective detection criteria: wind speed maximum between 30 m and 1500 m above the surface, vertical wind shear in the 500 m deep layer above the jet core <-0.5 m s^{-1} per 100 m and vertical gradient in virtual potential temperature from surface to 100 m >0.1°C. *Fiedler et al.* [2013] find that LLJs occur in 29% nights in the annual and spatial mean, with particular summer hotspots within the moist south-westerly WAM flow, onshore along the coast of Mauritania and Western Sahara and onshore along the coast of Libya. The authors use ERAI to drive the dust emission model of *Tegen et al.* [2002] and calculate that downward mixing of LLJ momentum is associated with 15% North African dust emission in the annual and spatial mean. Summer appears as the least active season for LLJ emission overall, although in parts of Algeria, Mali and Mauritania the percentage of LLJ-induced emission still reaches 35% [*Fiedler et al.*, 2013]. Driving the same *Tegen et al.* [2002] dust emission scheme with a much higher resolution (4km) convection-permitting NWP model, *Heinold et al.* [2013] found that from 25 July to 2 September 2006, 40% dust emission in West Africa was caused by LLJs, arguing that they are still a significant dust mechanism in the summer.

Studies of LLJs in West Africa using observational data are usually restricted by data availability to the Sahel [e.g. *Parker et al.*, 2005; *Lothon et al.*, 2008; *Bain et al.*, 2010]. An important exception is *Cowie et al.* [2014], who use records from surface synoptic

observation (SYNOP) stations and infer the presence of LLJs from 10m-winds and dust observations across broader regions of North Africa where stations exist. However, the authors are unable to make a statement about the overall contribution of LLJs to the dust burden, presumably because the SYNOP measurements are not comprehensive enough.

2.6.3. Dry convective plumes and dust devils

Local observations are particularly important for recording the smallest-scale dust emission mechanisms, dry convective plumes and dust devils. Under dry conditions with intense surface heating, localized turbulent circulations develop producing short-lived updrafts or vortices which lead to dust uplift if the surface is erodible [e.g. *Sinclair*, 1969; *Kaimal and Bussinger*, 1970; *Renno et al.*, 1998; *Balme and Greeley*, 2006] (Figure 2-16). Dust devils are rotating vortices, with a mean diameter of 7m and heights from a few metres to over 1km [*Balme and Greeley*, 2006]. Dry convective plumes are dusty non-rotating updrafts, with diameter ~100m [*Ansmann et al.*, 2009]. Lidar observations from Ouarzazate, Morocco and Tamanrasset in the Hoggar Mountains of Algeria have recorded dry convective plume heights from <1km to 2km [*Cuesta et al.*, 2008; *Ansmann et al.*, 2009].

Figure 2-16: Dust devil in Arizona, USA. It is a few metres in diameter. Note the house in the background for scale. Source: Figure 1c, Balme, M., and R. Greeley (2006), Dust devils on Earth and Mars, Rev. Geophys., 44, RG3003, doi:10.1029/2005RG000188. Copyright 2006 by the American Geophysical Union. Reproduced by permission of John Wiley & Sons.

Dry convective plumes and dust devils are relatively short-lived, on the order of a few minutes for dust devils and an hour or so for dusty dry convective plumes [*Ansmann et al.*, 2009]. They are usually associated with a pressure drop at the surface, known as a 'pressure well' [*Balme and Greeley*, 2006; *Lorenz*, 2012]. Light winds (<7 m s^{-1}) are required to allow dry convective plumes and dust devils to develop [*Oke et al.*, 2007]. If the wind speed within the plumes and vortices themselves remains low, dust emission does not occur by saltation bombardment but by direct aerodynamic lifting caused by convective turbulence [*Klose and Shao*, 2012]. However, wind speeds within the plumes and vortices can often exceed 7-10 m s^{-1}, resulting in dust emission from saltation bombardment [*Ansmann et al.*, 2009].

Koch and Renno [2005] use a semi-empirical approach to conclude that dry convective plumes and vortices are responsible for 35% global dust burden. A very different value is given by *Jemmett-Smith et al.* [2015], who apply detection criteria to ECMWF operational analyses coupled with the dust source mask of [*Ginoux et al.*, 2001] and suggest a best estimate of 3.4%. Whether observations give a similar estimate of the contribution of dry convective plumes and vortices in the Sahara is unknown and has been identified as an important avenue for research [*Knippertz and Todd*, 2012]. *Cakmur et al.* [2004] found that including subgrid-scale wind variability from dry convection in an AGCM significantly improved model AOT compared to observations, especially during summer in the Sahara. Its inclusion also resulted in improved modelling of dust transport over the Atlantic from the Sahara [*R L Miller et al.*, 2006].

It is important to recognise that dry convection occurs throughout daylight hours in the Sahara, as heating of the ground surface generates turbulent eddies which can have a range of scales up to the boundary layer height. It is these turbulent eddies that result in momentum mix-down from LLJs. In this thesis however, the term 'dry convective plume' is restricted to afternoon gustiness which raises dust in discrete updrafts. The role of dry convection - which includes momentum mix-down from aloft – is therefore broader than what here are described as 'dry convective plumes'.

2.6.4. Monsoon surges

Monsoon surges are large scale incursions of the summer moist monsoon inflow into the northern Sahel and southern reaches of the Sahara. *Couvreux et al.* [2010] present a detailed characterisation of the phenomena, summarised below. Monsoon surges have a timescale of 3-5 days which appears to be driven primarily by SHL dynamics. A strengthening of the SHL surface cyclonic circulation promotes southerly and south-

westerly winds at the south-east flank of the SHL. These winds transport cold and moist air northward in a surge which can have a horizontal length of ~1000 km. This air serves to weaken the SHL, providing a negative feedback on monsoon surge development[5]. After a few days, the SHL recovers and the cycle repeats. Some surges are stationary, others appear to propagate westward in association with AEWs. Under conditions of a mature WAM (late July 2006), monsoon surges were shown to bring rainfall as far north as the Hoggar Mountains [*Cuesta et al.*, 2010]. These surges were promoted by a strong SHL cyclonic circulation (possibly reinforced by strong Harmattan winds to the north-east) and an AEW trough at the northern Mali-Mauritania border [*Cuesta et al.*, 2010]. A similar trough leading to a strong monsoon surge over north-east Mali and southern Algeria in August 2006 was documented by [*Knippertz and Todd*, 2010].

Aircraft measurements have shown that monsoon surges raise dust at their leading edge, where wind speeds and turbulence are high [*Bou Karam et al.*, 2008; *Flamant et al.*, 2009]. But since they also transport moisture into very hot regions they can promote deep moist convection and subsequent cold pool dust emission within the monsoon flow itself [*Bou Karam et al.*, 2008; *Marsham et al.*, 2008]. Such situations were also found in a numerical simulation of dust emission over West Africa in June 2006 at 10 km resolution using the Weather Research and Forecasting model and the Goddard Global Ozone Chemistry Aerosol Radiation and Transport dust scheme [*Cavazos-Guerra and Todd*, 2012]. Using self-organising maps (SOMs) of SDF for June–August 2004–2010,

[5] *Bou Karam et al.* [2014] have shown that a large cold pool can also cause a weakening of the SHL. The authors attribute the reduction in surface temperatures to cold air advection or dust reducing incident shortwave radiation.

Ashpole and Washington [2013b] find that states with high dust loadings are associated with extensive penetration of the south-westerly monsoon flow into the Sahara.

2.6.5. Dry cyclones and depressions

Saharan cyclones (also known as Sharav or Khamsin cyclones) are most common in spring [*Alpert and Ziv*, 1989; *Fiedler et al.*, 2014], although they do also occur in the summer [e.g. *Bou Karam et al.*, 2009b; *Schepanski and Knippertz*, 2011]. High winds within the cyclones can raise dust directly [e.g. *Bou Karam et al.*, 2009b; *Fiedler et al.*, 2014], but frequently the dust emission is likely caused by smaller-scale embedded mechanisms such as LLJs or cold pool outflows [*Knippertz and Fink*, 2006; *Fiedler et al.*, 2014]. Stationary depressions are common in summer as heat lows [*Fiedler et al.*, 2014]. Using ERAI to drive the emission scheme of *Tegen et al.* [2002], *Fiedler et al.* [2014] argue that up to 90% of dust emission in North Africa in summer is associated with atmospheric depressions. These very large values are perhaps unsurprising given that the authors attribute any dust emission in a circle of radius 10° (radius ~1000 km) from the geopotential height minimum to the depression. *Fiedler et al.* [2014] acknowledge that smaller-scale mechanisms such as cold pool outflows and LLJs will contribute to these totals.

2.6.6. Advected dust

Advected dust is dust that is not being locally emitted but is being transported above the surface. It still of course contributes to radiative interactions so its detection is important. However, its contribution is ignored in studies that only calculate dust emission, or use an ‘uplift potential’ approach [e.g. *Marsham et al.*, 2011]. Using SOMs applied to the SDF dataset, *Ashpole and Washington* [2013b] find that the most common of the twelve SOM states is one of low dust presence over the Sahara (21% frequency of occurrence

JJA 2004-2010), and by extension, low emission. The relative importance of advection against emission for dust totals in the Saharan atmosphere has not been quantified (although care should be taken generalising from results at an individual point to a larger domain, since advection is a transient and geographically specific process which moves dust from a source to a sink.) The Fennec aircraft campaign has shown that transported dust particles are frequently much larger than previously thought (coarse mode volume median diameter from 5.8 to 45.3 μm), causing much greater absorption and atmospheric heating [*Ryder et al.*, 2013b].

Many of the processes that can lead to dust emission, including cold pools, LLJs and monsoon surges can also advect dust [e.g. *Kalu*, 1979; *Flamant et al.*, 2007; *Bou Karam et al.*, 2008; *S D Miller et al.*, 2008]. Whilst immediately following dust emission dust will be confined near the surface, there are several processes which redistribute the dust vertically through the Saharan boundary layer. *Cuesta et al.* [2009] provide a summary. One such process is isentropic upgliding (lifting of dust upwards along a slanted surface of constant potential temperature). Dust can be transported upwards in this way when cold pools or the monsoon flow undercut the convective boundary layer [e.g. *Parker et al.*, 2005; *Flamant et al.*, 2007; *Bou Karam et al.*, 2008]. Other processes of vertical lifting include orographic effects and surface albedo hot spots [*Cuesta et al.*, 2009]. The deep convective boundary layer will also lift dust as it grows upwards during the daytime – reaching up to 6km in summer [*Gamo*, 1996]. If dust is lifted into the residual layer or the free troposphere (i.e. above the convective boundary layer) then it can be advected much longer distances. In summer, dust in this elevated layer – termed the Saharan Air Layer by *Karyampudi and Carlson* [1988] – crosses the Atlantic westward towards the Caribbean, frequently under the influence of a mid-tropospheric easterly jet

or AEWs [e.g. *Jones et al.*, 2003; *Prospero and Lamb*, 2003; *Kaufman et al.*, 2005; *Goudie and Middleton*, 2006; *Schepanski et al.*, 2009a].

2.7. Current understanding of summertime dust production in the central Sahara

As documented in Section 2.6 above, there has been an effort by researchers to identify and understand the different atmospheric mechanisms responsible for dust production (i.e. dust emission and transport) in the central Sahara in summer. The atmospheric mechanisms are thought to include cold pools, low level jets, dry convective plumes and monsoon surges. However, studies have tended to focus on one particular atmospheric mechanism or a case study of a particular event. With the exception of some recent model studies [*Marsham et al.*, 2011; *Fiedler et al.*, 2013; *Heinold et al.*, 2013], the relative importance of the different atmospheric mechanisms for dust production has not been addressed. Moreover, with very few exceptions [*Cuesta et al.*, 2008; *Cowie et al.*, 2014] all of the studies so far have been from observations outside of the central Sahara (i.e. on the fringes of the SHL), have been based on satellite retrieval, or have been performed using numerical models or reanalyses. Prior to the Fennec Project, of which this thesis is a part, there were no detailed observational studies of dust storms in the remote central Sahara, simply because the measurements did not exist. With these considerations in mind, the next chapter provides a formal motivation for the DPhil and a list of its research aims.

2.8. References

Alpert, P., and B. Ziv (1989), The Sharav Cyclone: Observations and some theoretical considerations, *Journal of Geophysical Research: Atmospheres*, *94*(D15), 18495-18514, doi: 10.1029/JD094iD15p18495.

Ansmann, A., M. Tesche, P. Knippertz, E. Bierwirth, D. Althausen, D. Müller, and O. Schulz (2009), Vertical profiling of convective dust plumes in southern Morocco during SAMUM, *Tellus B*, *61*(1), 340-353, doi: 10.1111/j.1600-0889.2008.00384.x.

Ashpole, I., and R. Washington (2012), An automated dust detection using SEVIRI: A multiyear climatology of summertime dustiness in the central and western Sahara, *J. Geophys. Res.*, *117*(D8), D08202, doi: 10.1029/2011jd016845.

Ashpole, I., and R. Washington (2013a), A new high-resolution central and western Saharan summertime dust source map from automated satellite dust plume tracking, *Journal of Geophysical Research D: Atmospheres*, *118*(13), 6981-6995, doi: 10.1002/jgrd.50554.

Ashpole, I., and R. Washington (2013b), Intraseasonal variability and atmospheric controls on daily dust occurrence frequency over the central and western Sahara during the boreal summer, *Journal of Geophysical Research: Atmospheres*, *118*(23), 2013JD020267, doi: 10.1002/2013jd020267.

Atkinson, J. D., B. J. Murray, M. T. Woodhouse, T. F. Whale, K. J. Baustian, K. S. Carslaw, S. Dobbie, D. O/'Sullivan, and T. L. Malkin (2013), The importance of feldspar for ice nucleation by mineral dust in mixed-phase clouds, *Nature*, *498*(7454), 355-358, doi: 10.1038/nature12278.

Bagnold, R. A. (1941), *The Physics of Blown Sand and Desert Dunes*, Methuen, London.

Bain, C. L., D. J. Parker, C. M. Taylor, L. Kergoat, and F. Guichard (2010), Observations of the Nocturnal Boundary Layer Associated with the West African Monsoon, *Monthly Weather Review*, *138*(8), 3142-3156, doi: 10.1175/2010mwr3287.1.

Balme, M., and R. Greeley (2006), Dust devils on Earth and Mars, *Reviews of Geophysics*, *44*(3), doi: 10.1029/2005RG000188.

Biasutti, M., A. H. Sobel, and S. J. Camargo (2009), The Role of the Sahara Low in Summertime Sahel Rainfall Variability and Change in the CMIP3 Models, *Journal of Climate*, *22*(21), 5755-5771, doi: 10.1175/2009jcli2969.1.

Blackadar, A. K. (1957), Boundary layer wind maxima and their significance for the growth of nocturnal inversion, *Bull. Am. Meteorol. Soc*, *38*(5), 283-290.

Bou Karam, D., C. Flamant, P. Tulet, J.-P. Chaboureau, A. Dabas, and M. C. Todd (2009a), Estimate of Sahelian dust emissions in the intertropical discontinuity region of the West African Monsoon, *Journal of Geophysical Research-Atmospheres*, *114*, doi: 10.1029/2008jd011444.

Bou Karam, D., C. Flamant, P. Tulet, M. C. Todd, J. Pelon, and E. Williams (2009b), Dry cyclogenesis and dust mobilization in the intertropical discontinuity of the West African Monsoon: A case study, *Journal of Geophysical Research-Atmospheres*, *114*, doi: 10.1029/2008jd010952.

Bou Karam, D., C. Flamant, P. Knippertz, O. Reitebuch, J. Pelon, M. Chong, and A. Dabas (2008), Dust emissions over the Sahel associated with the West African monsoon intertropical discontinuity region: A representative case-study, *Quarterly Journal of the Royal Meteorological Society*, *134*(632), 621-634, doi: 10.1002/qj.244.

Bou Karam, D., E. Williams, M. Janiga, C. Flamant, M. McGraw-Herdeg, J. Cuesta, A. Auby, and C. Thorncroft (2014), Synoptic-scale dust emissions over the Sahara Desert initiated by a moist convective cold pool in early August 2006, *Quarterly Journal of the Royal Meteorological Society*, *140*(685), 2591-2607, doi: 10.1002/qj.2326.

Boucher, O., D. Randall, P. Artaxo, C. Bretherton, G. Feingold, P. Forster, V.-M. Kerminen, Y. Kondo, H. Liao, U. Lohmann, P. Rasch, S. K. Satheesh, S. Sherwood, S. B., and Z. X. Y. (2013), Clouds and Aerosols, in *Climate Change 2013: The Physical Science Basis. Contribution of Working Group I to the Fifth Assessment Report of the Intergovernmental Panel on Climate Change*, edited, pp. 571-658, Cambridge University Press, Cambridge.

Bretl, S., P. Reutter, C. C. Raible, S. Ferrachat, C. S. Poberaj, L. E. Revell, and U. Lohmann (2015), The influence of absorbed solar radiation by Saharan dust on hurricane genesis, *Journal of Geophysical Research: Atmospheres*, *120*(5), 1902-1917, doi: 10.1002/2014jd022441.

Brindley, H., P. Knippertz, C. Ryder, and I. Ashpole (2012), A critical evaluation of the ability of the Spinning Enhanced Visible and Infrared Imager (SEVIRI) thermal infrared red-green-blue rendering to identify dust events: Theoretical analysis, *Journal of Geophysical Research D: Atmospheres*, *117*(7), doi: 10.1029/2011JD017326.

Bullard, J. E., S. P. Harrison, M. C. Baddock, N. Drake, T. E. Gill, G. McTainsh, and Y. Sun (2011), Preferential dust sources: A geomorphological classification designed for use in global dust-cycle models, *Journal of Geophysical Research: Earth Surface*, *116*(F4), F04034, doi: 10.1029/2011jf002061.

Cakmur, R. V., R. L. Miller, and O. Torres (2004), Incorporating the effect of small-scale circulations upon dust emission in an atmospheric general circulation model, *Journal of Geophysical Research: Atmospheres*, *109*(D7), D07201, doi: 10.1029/2003jd004067.

Cavazos-Guerra, C., and M. C. Todd (2012), Model Simulations of Complex Dust Emissions over the Sahara during the West African Monsoon Onset, *Advances in Meteorology*, *2012*, 17, doi: 10.1155/2012/351731.

Chepil, W. S. (1945), Dynamics of wind erosion, *Soil Science*, *60*, 305-320.

Choobari, O. A., P. Zawar-Reza, and A. Sturman (2014), The global distribution of mineral dust and its impacts on the climate system: A review, *Atmospheric Research*, *138*(0), 152-165, doi: 10.1016/j.atmosres.2013.11.007.

Couvreux, F., F. Guichard, O. Bock, B. Campistron, J. P. Lafore, and J. L. Redelsperger (2010), Synoptic variability of the monsoon flux over West Africa prior to the onset, *Quarterly Journal of the Royal Meteorological Society*, *136*(S1), 159-173, doi: 10.1002/qj.473.

Cowie, S. M., P. Knippertz, and J. H. Marsham (2014), A climatology of dust emission events from northern Africa using long-term surface observations, *Atmos. Chem. Phys.*, *14*(16), 8579-8597, doi: 10.5194/acp-14-8579-2014.

Crouvi, O., K. Schepanski, R. Amit, A. R. Gillespie, and Y. Enzel (2012), Multiple dust sources in the Sahara Desert: The importance of sand dunes, *Geophysical Research Letters*, *39*(13), L13401, doi: 10.1029/2012gl052145.

Cuesta, J., J. H. Marsham, D. J. Parker, and C. Flamant (2009), Dynamical mechanisms controlling the vertical redistribution of dust and the thermodynamic structure of the West Saharan atmospheric boundary layer during summer, *Atmospheric Science Letters*, *10*(1), 34-42, doi: 10.1002/asl.207.

Cuesta, J., C. Lavaysse, C. Flamant, M. Mimouni, and P. Knippertz (2010), Northward bursts of the West African monsoon leading to rainfall over the Hoggar Massif, Algeria, *Quarterly Journal of the Royal Meteorological Society*, *136*, 174-189, doi: 10.1002/qj.439.

Cuesta, J., D. Edouart, M. Mimouni, P. H. Flamant, C. Loth, F. Gibert, F. Marnas, A. Bouklila, M. Kharef, B. Ouchene, M. Kadi, and C. Flamant (2008), Multiplatform observations of the seasonal evolution of the Saharan atmospheric boundary layer in Tamanrasset, Algeria, in the framework of the African Monsoon Multidisciplinary Analysis field campaign conducted in 2006, *Journal of Geophysical Research-Atmospheres*, *113*, doi: 10.1029/2007jd009417.

DeMott, P. J., K. Sassen, M. R. Poellot, D. Baumgardner, D. C. Rogers, S. D. Brooks, A. J. Prenni, and S. M. Kreidenweis (2003), African dust aerosols as atmospheric ice nuclei, *Geophysical Research Letters*, *30*(14), 1732, doi: 10.1029/2003gl017410.

di Sarra, A., D. Fuà, and D. Meloni (2013), Estimate of surface direct radiative forcing of desert dust from atmospheric modulation of the aerosol optical depth, *Atmos. Chem. Phys.*, *13*(11), 5647-5654, doi: 10.5194/acp-13-5647-2013.

Druyan, L. M. (2011), Studies of 21st-century precipitation trends over West Africa, *International Journal of Climatology*, *31*(10), 1415-1424, doi: 10.1002/joc.2180.

Dunion, J. P., and C. S. Velden (2004), The Impact of the Saharan Air Layer on Atlantic Tropical Cyclone Activity, *Bulletin of the American Meteorological Society*, *85*(3), 353-365, doi: 10.1175/bams-85-3-353.

Emmel, C., P. Knippertz, and O. Schulz (2010), Climatology of convective density currents in the southern foothills of the Atlas Mountains, *J. Geophys. Res.*, *115*(D11), D11115, doi: 10.1029/2009jd012863.
Engelstaedter, S., and R. Washington (2007a), Temporal controls on global dust emissions: The role of surface gustiness, *Geophys. Res. Lett.*, *34*(15), L15805, doi: 10.1029/2007gl029971.
Engelstaedter, S., and R. Washington (2007b), Atmospheric controls on the annual cycle of North African dust, *J. Geophys. Res.*, *112*(D3), D03103, doi: 10.1029/2006jd007195.
Engelstaedter, S., I. Tegen, and R. Washington (2006), North African dust emissions and transport, *Earth-Science Reviews*, *79*(1–2), 73-100, doi: 10.1016/j.earscirev.2006.06.004.
Engelstaedter, S., R. Washington, C. Flamant, D. Parker, C. J. T. Allen, and M. C. Todd (2015), The Saharan heat low and moisture transport pathways in the central Sahara – multi-aircraft observations and Africa-LAM evaluation, *Journal of Geophysical Research-Atmospheres 120*, doi:10.1002/2015JD023123.
Evan, A. T., G. R. Foltz, D. Zhang, and D. J. Vimont (2011), Influence of African dust on ocean-atmosphere variability in the tropical Atlantic, *Nature Geoscience*, *4*(11), 762-765, doi: 10.1038/ngeo1276.
Evan, A. T., C. Flamant, S. Fiedler, and O. Doherty (2014), An analysis of aeolian dust in climate models, *Geophysical Research Letters*, *41*(16), 2014GL060545, doi: 10.1002/2014gl060545.
Evan, A. T., J. Dunion, J. A. Foley, A. K. Heidinger, and C. S. Velden (2006), New evidence for a relationship between Atlantic tropical cyclone activity and African dust outbreaks, *Geophysical Research Letters*, *33*(19), L19813, doi: 10.1029/2006gl026408.
Evan, A. T., D. J. Vimont, A. K. Heidinger, J. P. Kossin, and R. Bennartz (2009), The Role of Aerosols in the Evolution of Tropical North Atlantic Ocean Temperature Anomalies, *Science*, *324*(5928), 778-781.
Evan, A. T., S. Fiedler, C. Zhao, L. Menut, K. Schepanski, C. Flamant, and O. Doherty (2015), Derivation of an observation-based map of North African dust emission, *Aeolian Research*, *16*(0), 153-162, doi: 10.1016/j.aeolia.2015.01.001.
Fiedler, S., K. Schepanski, B. Heinold, P. Knippertz, and I. Tegen (2013), Climatology of Nocturnal Low-Level Jets over North Africa and Implications for Modeling Mineral Dust Emission, *Journal of Geophysical Research: Atmospheres*, *118*, 6100–6121, doi: 10.1002/jgrd.50394.
Fiedler, S., K. Schepanski, P. Knippertz, B. Heinold, and I. Tegen (2014), How important are atmospheric depressions and mobile cyclones for emitting mineral dust aerosol in North Africa?, *Atmos. Chem. Phys.*, *14*(17), 8983-9000, doi: 10.5194/acp-14-8983-2014.
Flamant, C., P. Knippertz, D. J. Parker, J. P. Chaboureau, C. Lavaysse, A. Agusti-Panareda, and L. Kergoat (2009), The impact of a mesoscale convective system cold pool on the northward propagation of the intertropical discontinuity over West Africa, *Quarterly Journal of the Royal Meteorological Society*, *135*(638), 139-159, doi: 10.1002/qj.357.
Flamant, C., J. P. Chaboureau, D. J. Parker, C. M. Taylor, J. P. Cammas, O. Bock, F. Timouk, and J. Pelon (2007), Airborne observations of the impact of a convective system on the planetary boundary layer thermodynamics and aerosol distribution in the inter-tropical discontinuity region of the West African Monsoon, *Quarterly Journal of the Royal Meteorological Society*, *133*(626), 1175-1189, doi: 10.1002/qj.97.
Formenti, P., J. L. Rajot, K. Desboeufs, F. Saïd, N. Grand, S. Chevaillier, and C. Schmechtig (2011), Airborne observations of mineral dust over western Africa in the summer Monsoon season: Spatial and vertical variability of physico-chemical and optical properties, *Atmospheric Chemistry and Physics*, *11*(13), 6387-6410.
Gamo, M. (1996), Thickness of the dry convection and large-scale subsidence above deserts, *Boundary-Layer Meteorology*, *79*(3), 265-278, doi: 10.1007/bf00119441.
Gillette, D. A. (1981), Production of dust that may be carried great distances, *Geol. Soc. Am.*, *186*, 11-26.
Ginoux, P., J. M. Prospero, T. E. Gill, N. C. Hsu, and M. Zhao (2012), Global-scale attribution of anthropogenic and natural dust sources and their emission rates based on MODIS Deep Blue aerosol products, *Reviews of Geophysics*, *50*(3), doi: 10.1029/2012RG000388.

Ginoux, P., M. Chin, I. Tegen, J. M. Prospero, B. Holben, O. Dubovik, and S.-J. Lin (2001), Sources and distributions of dust aerosols simulated with the GOCART model, *Journal of Geophysical Research: Atmospheres*, *106*(D17), 20255-20273, doi: 10.1029/2000jd000053.

Goudie, A. S., and N. J. Middleton (2006), *Desert Dust in the Global System*, 287 pp., Springer, Berlin.

Gu, Y., K. N. Liou, J. H. Jiang, H. Su, and X. Liu (2012), Dust aerosol impact on North Africa climate: a GCM investigation of aerosol-cloud-radiation interactions using A-Train satellite data, *Atmos. Chem. Phys.*, *12*(4), 1667-1679, doi: 10.5194/acp-12-1667-2012.

Haywood, J. M., R. P. Allan, I. Culverwell, T. Slingo, S. Milton, J. Edwards, and N. Clerbaux (2005), Can desert dust explain the outgoing longwave radiation anomaly over the Sahara during July 2003?, *J. Geophys. Res.*, *110*(D5), D05105, doi: 10.1029/2004jd005232.

Heinold, B., I. Tegen, S. Bauer, and M. Wendisch (2011), Regional modelling of Saharan dust and biomass-burning smoke Part 2: Direct radiative forcing and atmospheric dynamic response, *63*(4).

Heinold, B., J. Helmert, O. Hellmuth, R. Wolke, A. Ansmann, B. Marticorena, B. Laurent, and I. Tegen (2007), Regional modeling of Saharan dust events using LM-MUSCAT: Model description and case studies, *Journal of Geophysical Research: Atmospheres*, *112*(D11), D11204, doi: 10.1029/2006jd007443.

Heinold, B., P. Knippertz, J. H. Marsham, S. Fiedler, N. S. Dixon, K. Schepanski, B. Laurent, and I. Tegen (2013), The role of deep convection and nocturnal low-level jets for dust emission in summertime West Africa: Estimates from convection-permitting simulations, *Journal of Geophysical Research: Atmospheres*, *118*, 4385–4400, doi: 10.1002/jgrd.50402.

Herman, J. R., P. K. Bhartia, O. Torres, C. Hsu, C. Seftor, and E. Celarier (1997), Global distribution of UV-absorbing aerosols from Nimbus 7/TOMS data, *J. Geophys. Res.*, *102*(D14), 16911-16922, doi: 10.1029/96jd03680.

Huneeus, N., M. Schulz, Y. Balkanski, J. Griesfeller, J. Prospero, S. Kinne, S. Bauer, O. Boucher, M. Chin, F. Dentener, T. Diehl, R. Easter, D. Fillmore, S. Ghan, P. Ginoux, A. Grini, L. Horowitz, D. Koch, M. C. Krol, W. Landing, X. Liu, N. Mahowald, R. Miller, J. J. Morcrette, G. Myhre, J. Penner, J. Perlwitz, P. Stier, T. Takemura, and C. S. Zender (2011), Global dust model intercomparison in AeroCom phase I, *Atmos. Chem. Phys.*, *11*(15), 7781-7816, doi: 10.5194/acp-11-7781-2011.

Iverson, J. D., and B. R. White (1982), Saltation threshold on Earth, Mars and Venus, *Sedimentology*, *29*, 111-119, doi: 10.1111/j.1365-3091.1982.tb01713.x.

Jemmett-Smith, B. C., J. H. Marsham, P. Knippertz, and C. A. Gilkeson (2015), Quantifying global dust devil occurrence from meteorological analyses, *Geophysical Research Letters*, 2015GL063078, doi: 10.1002/2015gl063078.

Jickells, T. D., Z. S. An, K. K. Andersen, A. R. Baker, G. Bergametti, N. Brooks, J. J. Cao, P. W. Boyd, R. A. Duce, K. A. Hunter, H. Kawahata, N. Kubilay, J. laRoche, P. S. Liss, N. Mahowald, J. M. Prospero, A. J. Ridgwell, I. Tegen, and R. Torres (2005), Global Iron Connections Between Desert Dust, Ocean Biogeochemistry, and Climate, *Science*, *308*(5718), 67-71, doi: 10.1126/science.1105959.

Jones, C., N. Mahowald, and C. Luo (2003), The Role of Easterly Waves on African Desert Dust Transport, *Journal of Climate*, *16*(22), 3617-3628, doi: 10.1175/1520-0442(2003)016<3617:troewo>2.0.co;2.

Kaimal, J. C., and J. A. Bussinger (1970), Case studies of a convective plume and a dust devil, *J. Appl. Meteorol.*, *9*, 612-620.

Kalu, A. (1979), The African dust plume: its characteristics and propagation across West Africa in winter, in *Saharan Dust*, edited by C. Morales, pp. 95-118, John Wiley & Sons, Chichester.

Kandji, S. T., L. Verchot, and J. Mackensen (2006), Climate Change and Variability in the Sahel Region: Impacts and Adaptation Strategies in the Agricultural Sector*Rep.*, United Nations Environment Programme & World Agroforestry Centre.

Karyampudi, V. M., and T. N. Carlson (1988), Analysis and Numerical Simulations of the Saharan Air Layer and Its Effect on Easterly Wave Disturbances, *Journal of the Atmospheric Sciences*, *45*(21), 3102-3136, doi: 10.1175/1520-0469(1988)045<3102:aansot>2.0.co;2.

Kaufman, Y. J., I. Koren, L. A. Remer, D. Tanré, P. Ginoux, and S. Fan (2005), Dust transport and deposition observed from the Terra-Moderate Resolution Imaging Spectroradiometer (MODIS) spacecraft over the Atlantic Ocean, *J. Geophys. Res.*, *110*(D10), D10S12, doi: 10.1029/2003jd004436.

Klose, M., and Y. Shao (2012), Stochastic parameterization of dust emission and application to convective atmospheric conditions, *Atmos. Chem. Phys.*, *12*(16), 7309-7320, doi: 10.5194/acp-12-7309-2012.

Klose, M., Y. Shao, M. K. Karremann, and A. H. Fink (2010), Sahel dust zone and synoptic background, *Geophysical Research Letters*, *37*(9), L09802, doi: 10.1029/2010gl042816.

Knippertz, P. (2008), Dust emissions in the West African heat trough the role of the diurnal cycle and of extratropical disturbances, *Meteorologische Zeitschrift*, *17*(5), 553-563, doi: 10.1127/0941-2948/2008/0315.

Knippertz, P., and A. H. Fink (2006), Synoptic and dynamic aspects of an extreme springtime Saharan dust outbreak, *Quarterly Journal of the Royal Meteorological Society*, *132*(617), 1153-1177, doi: 10.1256/qj.05.109.

Knippertz, P., and M. C. Todd (2010), The central west Saharan dust hot spot and its relation to African easterly waves and extratropical disturbances, *J. Geophys. Res.*, *115*(D12), D12117, doi: 10.1029/2009jd012819.

Knippertz, P., and M. C. Todd (2012), Mineral dust aerosols over the Sahara: Meteorological controls on emission and transport and implications for modeling, *Reviews of Geophysics*, *50*(1), doi: 10.1029/2011RG000362.

Knippertz, P., C. Deutscher, K. Kandler, T. Müller, O. Schulz, and L. Schütz (2007), Dust mobilization due to density currents in the Atlas region: Observations from the Saharan Mineral Dust Experiment 2006 field campaign, *J. Geophys. Res.*, *112*(D21), D21109, doi: 10.1029/2007jd008774.

Koch, J., and N. O. Renno (2005), The role of convective plumes and vortices on the global aerosol budget, *Geophys. Res. Lett.*, *32*(18), L18806, doi: 10.1029/2005gl023420.

Kocha, C., J. P. Lafore, P. Tulet, and Y. Seity (2012), High-resolution simulation of a major West African dust-storm: Comparison with observations and investigation of dust impact, *Quarterly Journal of the Royal Meteorological Society*, *138*(663), 455-470.

Kok, J. F. (2011), A scaling theory for the size distribution of emitted dust aerosols suggests climate models underestimate the size of the global dust cycle, *Proceedings of the National Academy of Sciences*, doi: 10.1073/pnas.1014798108.

Lafore, J. P., C. Flamant, V. Giraud, F. Guichard, P. Knippertz, J. F. Mahfouf, P. Mascart, and E. R. Williams (2010), Introduction to the AMMA Special Issue on 'Advances in understanding atmospheric processes over West Africa through the AMMA field campaign', *Quarterly Journal of the Royal Meteorological Society*, *136*(S1), 2-7, doi: 10.1002/qj.583.

Laurent, B., B. Marticorena, G. Bergametti, J. F. Le´on, and N. M. Mahowald (2008), Modeling mineral dust emissions from the Sahara desert using new surface properties and soil database, J. Geophys. Res., 113, D14218, doi:10.1029/2007JD009484.

Lavaysse, C., J.-P. Chaboureau, and C. Flamant (2011), Dust impact on the West African heat low in summertime, *Quarterly Journal of the Royal Meteorological Society*, *137*(658), 1227-1240, doi: 10.1002/qj.844.

Lavaysse, C., C. Flamant, S. Janicot, D. J. Parker, J. P. Lafore, B. Sultan, and J. Pelon (2009), Seasonal evolution of the West African heat low: a climatological perspective, *Climate Dynamics*, *33*(2), 313-330, doi: 10.1007/s00382-009-0553-4.

Lorenz, R. D. (2012), Power law distribution of pressure drops in dust devils: Observation techniques and Earth–Mars comparison, *Planetary and Space Science*, *60*(1), 370-375, doi: 10.1016/j.pss.2011.11.003.

Lothon, M., F. Saïd, F. Lohou, and B. Campistron (2008), Observation of the Diurnal Cycle in the Low Troposphere of West Africa, *Monthly Weather Review*, *136*(9), 3477-3500, doi: 10.1175/2008mwr2427.1.

Loveland, T. R., and A. S. Belward (1997), The IGBP-DIS global 1km land cover data set, DISCover: First results, *International Journal of Remote Sensing*, *18*(15), 3289-3295, doi: 10.1080/014311697217099.

Madougou, S., F. Saïd, B. Campistron, M. Lothon, and C. Kebe (2012), Results of UHF radar observation of the nocturnal low-level jet for wind energy applications, *Acta Geophys.*, *60*(5), 1413-1453, doi: 10.2478/s11600-012-0062-4.

Mahowald, N., and L. M. Kiehl (2003), Mineral aerosol and cloud interactions, *Geophysical Research Letters*, *30*(9), 1475, doi: 10.1029/2002gl016762.

Mahowald, N., and J.-L. Dufresne (2004), Sensitivity of TOMS aerosol index to boundary layer height: Implications for detection of mineral aerosol sources, *Geophysical Research Letters*, *31*(3), L03103, doi: 10.1029/2003gl018865.

Mahowald, N., S. Albani, J. F. Kok, S. Engelstaeder, R. Scanza, D. S. Ward, and M. G. Flanner (2013), The size distribution of desert dust aerosols and its impact on the Earth system, *Aeolian Research*(0), doi: 10.1016/j.aeolia.2013.09.002.

Mahowald, N., S. Kloster, S. Engelstaedter, J. K. Moore, S. Mukhopadhyay, J. R. McConnell, S. Albani, S. C. Doney, A. Bhattacharya, M. A. J. Curran, M. G. Flanner, F. M. Hoffman, D. M. Lawrence, K. Lindsay, P. A. Mayewski, J. Neff, D. Rothenberg, E. Thomas, P. E. Thornton, and C. S. Zender (2010), Observed 20th century desert dust variability: impact on climate and biogeochemistry, *Atmos. Chem. Phys.*, *10*(22), 10875-10893, doi: 10.5194/acp-10-10875-2010.

Mahrt, L. (1999), Stratified Atmospheric Boundary Layers, *Boundary-Layer Meteorology*, *90*(3), 375-396, doi: 10.1023/a:1001765727956.

Marsham, J. H., D. J. Parker, C. M. Grams, C. M. Taylor, and J. M. Haywood (2008), Uplift of Saharan dust south of the intertropical discontinuity, *J. Geophys. Res.*, *113*(D21), D21102, doi: 10.1029/2008jd009844.

Marsham, J. H., P. Knippertz, N. S. Dixon, D. J. Parker, and G. M. S. Lister (2011), The importance of the representation of deep convection for modeled dust-generating winds over West Africa during summer, *Geophys. Res. Lett.*, *38*(16), L16803, doi: 10.1029/2011gl048368.

Marticorena, B., and G. Bergametti (1995), Modeling the atmospheric dust cycle: 1. Design of a soil-derived dust emission scheme, *J. Geophys. Res.*, *100*(D8), 16415-16430, doi: 10.1029/95jd00690.

Marticorena, B., B. Chatenet, J. L. Rajot, S. Traoré, M. Coulibaly, A. Diallo, I. Koné, A. Maman, T. Ndiaye, and A. Zakou (2010), Temporal variability of mineral dust concentrations over West Africa: analyses of a pluriannual monitoring from the AMMA Sahelian Dust Transect, *Atmos. Chem. Phys.*, *10*(18), 8899-8915, doi: 10.5194/acp-10-8899-2010.

Martin, J. H., R. M. Gordon, and S. E. Fitzwater (1990), Iron in Antarctic waters, *Nature*, *345*(6271), 156-158.

Martínez Avellaneda, N., N. Serra, P. J. Minnett, and D. Stammer (2010), Response of the eastern subtropical Atlantic SST to Saharan dust: A modeling and observational study, *J. Geophys. Res.*, *115*(C8), C08015, doi: 10.1029/2009jc005692.

May, P. T. (1995), The Australian nocturnal jet and diurnal variations of boundary-layer winds over Mt. Isa in North-eastern Australia, *Quarterly Journal of the Royal Meteorological Society*, *121*(525), 987-1003, doi: 10.1002/qj.49712152503.

Miller, R. L., I. Tegen, and J. Perlwitz (2004a), Surface radiative forcing by soil dust aerosols and the hydrologic cycle, *J. Geophys. Res.*, *109*(D4), D04203, doi: 10.1029/2003jd004085.

Miller, R. L., J. Perlwitz, and I. Tegen (2004b), Feedback upon dust emission by dust radiative forcing through the planetary boundary layer, *Journal of Geophysical Research: Atmospheres*, *109*(D24), D24209, doi: 10.1029/2004jd004912.

Miller, R. L., R. V. Cakmur, J. Perlwitz, I. V. Geogdzhayev, P. Ginoux, D. Koch, K. E. Kohfeld, C. Prigent, R. Ruedy, G. A. Schmidt, and I. Tegen (2006), Mineral dust aerosols in the NASA Goddard Institute for Space Sciences ModelE atmospheric general circulation model, *Journal of Geophysical Research: Atmospheres*, *111*(D6), D06208, doi: 10.1029/2005jd005796.

Miller, S. D., A. P. Kuciauskas, M. Liu, Q. Ji, J. S. Reid, D. W. Breed, A. L. Walker, and A. A. Mandoos (2008), Haboob dust storms of the southern Arabian Peninsula, *Journal of Geophysical Research D: Atmospheres*, *113*(1), doi: 10.1029/2007JD008550.

Mohalfi, S., H. S. Bedi, T. N. Krishnamurti, and S. D. Cocke (1998), Impact of Shortwave Radiative Effects of Dust Aerosols on the Summer Season Heat Low over Saudi Arabia, *Monthly Weather Review*, *126*(12), 3153-3168, doi: 10.1175/1520-0493(1998)126<3153:iosreo>2.0.co;2.

Moosmüller, H., J. P. Engelbrecht, M. Skiba, G. Frey, R. K. Chakrabarty, and W. P. Arnott (2012), Single scattering albedo of fine mineral dust aerosols controlled by iron concentration, *Journal of Geophysical Research: Atmospheres*, *117*(D11), D11210, doi: 10.1029/2011jd016909.

Naeger, A. R., S. A. Christopher, and B. T. Johnson (2013), Multiplatform analysis of the radiative effects and heating rates for an intense dust storm on 21 June 2007, *Journal of Geophysical Research: Atmospheres*, *118*(16), 9316-9329, doi: 10.1002/jgrd.50713.

Oke, A. M. C., N. J. Tapper, and D. Dunkerley (2007), Willy-willies in the Australian landscape: The role of key meteorological variables and surface conditions in defining frequency and spatial characteristics, *Journal of Arid Environments*, *71*(2), 201-215, doi: 10.1016/j.jaridenv.2007.03.008.

Parker, D. J., R. R. Burton, A. Diongue-Niang, R. J. Ellis, M. Felton, C. M. Taylor, C. D. Thorncroft, P. Bessemoulin, and A. M. Tompkins (2005), The diurnal cycle of the West African monsoon circulation, *Quarterly Journal of the Royal Meteorological Society*, *131*(611), 2839-2860, doi: 10.1256/qj.04.52.

Pérez, C., S. Nickovic, G. Pejanovic, J. M. Baldasano, and E. Özsoy (2006), Interactive dust-radiation modeling: A step to improve weather forecasts, *Journal of Geophysical Research: Atmospheres*, *111*(D16), D16206, doi: 10.1029/2005jd006717.

Perrone, M. R., A. M. Tafuro, and S. Kinne (2012), Dust layer effects on the atmospheric radiative budget and heating rate profiles, *Atmospheric Environment*, *59*(0), 344-354, doi: 10.1016/j.atmosenv.2012.06.012.

Prospero, J. M., and P. J. Lamb (2003), African Droughts and Dust Transport to the Caribbean: Climate Change Implications, *Science*, *302*(5647), 1024-1027, doi: 10.1126/science.1089915.

Prospero, J. M., P. Ginoux, O. Torres, S. E. Nicholson, and T. E. Gill (2002), Environmental characterization of global sources of atmospheric soil dust identified with the NIMBUS 7 Total Ozone Mapping Spectrometer (TOMS) absorbing aerosol product, *Rev. Geophys.*, *40*(1), 1002, doi: 10.1029/2000rg000095.

Ravi, S., P. D'Odorico, D. D. Breshears, J. P. Field, A. S. Goudie, T. E. Huxman, J. Li, G. S. Okin, R. J. Swap, A. D. Thomas, S. Van Pelt, J. J. Whicker, and T. M. Zobeck (2011), Aeolian processes and the biosphere, *Rev. Geophys.*, *49*(3), RG3001, doi: 10.1029/2010rg000328.

Redmond, H. E., K. D. Dial, and J. E. Thompson (2010), Light scattering and absorption by wind blown dust: Theory, measurement, and recent data, *Aeolian Research*, *2*(1), 5-26, doi: 10.1016/j.aeolia.2009.09.002.

Reinfried, F., I. Tegen, B. Heinold, O. Hellmuth, K. Schepanski, U. Cubasch, H. Huebener, and P. Knippertz (2009), Simulations of convectively-driven density currents in the Atlas region using a regional model: Impacts on dust emission and sensitivity to horizontal resolution and convection schemes, *Journal of Geophysical Research: Atmospheres*, *114*(D8), D08127, doi: 10.1029/2008jd010844.

Renno, N. O., M. L. Burkett, and M. P. Larkin (1998), A Simple Thermodynamical Theory for Dust Devils, *Journal of the Atmospheric Sciences*, *55*(21), 3244-3252, doi: 10.1175/1520-0469(1998)055<3244:asttfd>2.0.co;2.

Roberts, A. J., and P. Knippertz (2014), The formation of a large summertime Saharan dust plume: Convective and synoptic-scale analysis, *Journal of Geophysical Research: Atmospheres*, *119*(4), 1766-1785, doi: 10.1002/2013jd020667.

Rodwell, M. J., and T. Jung (2008), Understanding the local and global impacts of model physics changes: an aerosol example, *Quarterly Journal of the Royal Meteorological Society*, *134*(635), 1479-1497, doi: 10.1002/qj.298.

Rosenberg, P. D., D. J. Parker, C. L. Ryder, J. H. Marsham, L. Garcia-Carreras, J. R. Dorsey, I. M. Brooks, A. R. Dean, J. Crosier, J. B. McQuaid, and R. Washington (2014), Quantifying particle size and turbulent scale dependence of dust flux in the Sahara using aircraft

measurements, *Journal of Geophysical Research: Atmospheres*, *119*(12), 2013JD021255, doi: 10.1002/2013jd021255.
Rosenfeld, D., W. L. Woodley, A. Khain, W. R. Cotton, G. Carrió, I. Ginis, and J. H. Golden (2012), Aerosol Effects on Microstructure and Intensity of Tropical Cyclones, *Bulletin of the American Meteorological Society*, *93*(7), 987-1001, doi: 10.1175/bams-d-11-00147.1.
Ryder, C. L., E. J. Highwood, T. M. Lai, H. Sodemann, and J. H. Marsham (2013a), Impact of atmospheric transport on the evolution of microphysical and optical properties of Saharan dust, *Geophysical Research Letters*, *40*(10), 2433-2438, doi: 10.1002/grl.50482.
Ryder, C. L., E. J. Highwood, P. D. Rosenberg, J. Trembath, J. K. Brooke, M. Bart, A. Dean, J. Crosier, J. Dorsey, H. Brindley, J. Banks, J. H. Marsham, J. B. McQuaid, H. Sodemann, and R. Washington (2013b), Optical properties of Saharan dust aerosol and contribution from the coarse mode as measured during the Fennec 2011 aircraft campaign, *Atmos. Chem. Phys.*, *13*(1), 303-325, doi: 10.5194/acp-13-303-2013.
Santos, D., M. J. Costa, A. M. Silva, and R. Salgado (2013), Modeling Saharan desert dust radiative effects on clouds, *Atmospheric Research*, *127*(0), 178-194, doi: 10.1016/j.atmosres.2012.09.024.
Schepanski, K., and P. Knippertz (2011), Soudano-Saharan depressions and their importance for precipitation and dust: a new perspective on a classical synoptic concept, *Quarterly Journal of the Royal Meteorological Society*, *137*(659), 1431-1445, doi: 10.1002/qj.850.
Schepanski, K., I. Tegen, and A. Macke (2009a), Saharan dust transport and deposition towards the tropical northern Atlantic, *Atmos. Chem. Phys.*, *9*(4), 1173-1189, doi: 10.5194/acp-9-1173-2009.
Schepanski, K., I. Tegen, B. Laurent, B. Heinold, and A. Macke (2007), A new Saharan dust source activation frequency map derived from MSG-SEVIRI IR-channels, *Geophys. Res. Lett.*, *34*(18), L18803, doi: 10.1029/2007gl030168.
Schepanski, K., I. Tegen, M. C. Todd, B. Heinold, G. Bönisch, B. Laurent, and A. Macke (2009b), Meteorological processes forcing Saharan dust emission inferred from MSG-SEVIRI observations of subdaily dust source activation and numerical models, *J. Geophys. Res.*, *114*(D10), D10201, doi: 10.1029/2008jd010325.
Shao, Y. (2001), A model for mineral dust emission, *Journal of Geophysical Research: Atmospheres*, *106*(D17), 20239-20254, doi: 10.1029/2001jd900171.
Shao, Y. (2004), Simplification of a dust emission scheme and comparison with data, *Journal of Geophysical Research: Atmospheres*, *109*(D10), D10202, doi: 10.1029/2003jd004372.
Shao, Y. (2008), *Physics and Modelling of Wind Erosion*, 2 ed., 452 pp., Springer Netherlands.
Shao, Y., M. R. Raupach, and P. A. Findlater (1993), Effect of saltation bombardment on the entrainment of dust by wind, *Journal of Geophysical Research: Atmospheres*, *98*(D7), 12719-12726, doi: 10.1029/93jd00396.
Simpson, J. E. (1997), *Gravity currents in the environment and the laboratory*, 2nd ed., 244 pp., Cambridge University Press, Cambridge.
Sinclair, P. C. (1969), General characteristics of dust devils, *J. Appl. Meteorol.*, *8*, 32-45, doi: 10.1175/1520-0450(1969)008<0032:GCODD>2.0.CO;2.
Smoydzin, L., A. Teller, H. Tost, M. Fnais, and J. Lelieveld (2012), Impact of mineral dust on cloud formation in a Saharan outflow region, *Atmos. Chem. Phys.*, *12*(23), 11383-11393, doi: 10.5194/acp-12-11383-2012.
Solomos, S., G. Kallos, E. Mavromatidis, and J. Kushta (2012), Density currents as a desert dust mobilization mechanism, *Atmospheric Chemistry and Physics*, *12*(22), 11199-11211, doi: 10.5194/acp-12-11199-2012.
Stanelle, T., B. Vogel, H. Vogel, D. Bäumer, and C. Kottmeier (2010), Feedback between dust particles and atmospheric processes over West Africa during dust episodes in March 2006 and June 2007, *Atmos. Chem. Phys.*, *10*(22), 10771-10788, doi: 10.5194/acp-10-10771-2010.
Stensrud, D. J. (1996), Importance of low-level jets to climate: A review, *Journal of Climate*, *9*(8), 1698-1711, doi: 10.1175/1520-0442(1996)009<1698:IOLLJT>2.0.CO;2.
Sultan, B., and S. Janicot (2003), The West African monsoon dynamics. Part II: The "preonset" and "onset" of the summer monsoon, *Journal of Climate*, *16*(21), 3407-3427, doi: 10.1175/1520-0442(2003)016<3407:TWAMDP>2.0.CO;2.

Swap, R., M. Garstang, S. Greco, R. Talbot, and P. KÅLlberg (1992), Saharan dust in the Amazon Basin, *Tellus B*, *44*(2), 133-149, doi: 10.1034/j.1600-0889.1992.t01-1-00005.x.

Tanaka, T. Y., and M. Chiba (2006), A numerical study of the contributions of dust source regions to the global dust budget, *Global and Planetary Change*, *52*(1–4), 88-104, doi: 10.1016/j.gloplacha.2006.02.002.

Tegen, I., and A. A. Lacis (1996), Modeling of particle size distribution and its influence on the radiative properties of mineral dust aerosol, *Journal of Geophysical Research: Atmospheres*, *101*(D14), 19237-19244, doi: 10.1029/95jd03610.

Tegen, I., K. Schepanski, and B. Heinold (2013), Comparing two years of Saharan dust source activation obtained by regional modelling and satellite observations, *Atmos. Chem. Phys.*, *13*(5), 2381-2390, doi: 10.5194/acp-13-2381-2013.

Tegen, I., P. Hollrig, M. Chin, I. Fung, D. Jacob, and J. Penner (1997), Contribution of different aerosol species to the global aerosol extinction optical thickness: Estimates from model results, *Journal of Geophysical Research: Atmospheres*, *102*(D20), 23895-23915, doi: 10.1029/97jd01864.

Tegen, I., S. P. Harrison, K. Kohfeld, I. C. Prentice, M. Coe, and M. Heimann (2002), Impact of vegetation and preferential source areas on global dust aerosol: Results from a model study, *Journal of Geophysical Research: Atmospheres*, *107*(D21), 4576, doi: 10.1029/2001jd000963.

Thorncroft, C. D., and M. Blackburn (1999), Maintenance of the African easterly jet, *Quarterly Journal of the Royal Meteorological Society*, *125*(555), 763-786, doi: 10.1002/qj.49712555502.

Thorpe, A. J., M. J. Miller, and M. W. Moncrieff (1982), Two-dimensional convection in non-constant shear: A model of mid-latitude squall lines, *Quarterly Journal of the Royal Meteorological Society*, *108*(458), 739-762, doi: 10.1002/qj.49710845802.

Todd, M. C., R. Washington, S. Raghavan, G. Lizcano, and P. Knippertz (2008), Regional model simulations of the Bodélé low-level jet of Northern Chad during the Bodélé dust experiment (BoDEx 2005), *Journal of Climate*, *21*(5), 995-1012, doi: 10.1175/2007JCLI1766.1.

Tompkins, A. M., C. Cardinali, J. J. Morcrette, and M. Rodwell (2005), Influence of aerosol climatology on forecasts of the African Easterly Jet, *Geophys. Res. Lett.*, *32*(10), L10801, doi: 10.1029/2004gl022189.

Twomey, S. (1977), The influence of pollution on the shortwave albedo of clouds, *Journal of the Atmospheric Sciences*, *34*, 1149-1152.

van de Wiel, B. J. H., A. F. Moene, G. J. Steeneveld, P. Baas, F. C. Bosveld, and A. A. M. Holtslag (2010), A conceptual view on inertial oscillations and nocturnal low-level jets, *Journal of the Atmospheric Sciences*, *67*(8), 2679-2689, doi: 10.1175/2010JAS3289.1.

Wang, C., S. Dong, A. T. Evan, G. R. Foltz, and S.-K. Lee (2012), Multidecadal Covariability of North Atlantic Sea Surface Temperature, African Dust, Sahel Rainfall, and Atlantic Hurricanes, *Journal of Climate*, *25*(15), 5404-5415, doi: 10.1175/jcli-d-11-00413.1.

Wang, Z., H. Zhang, X. Jing, and X. Wei (2013), Effect of non-spherical dust aerosol on its direct radiative forcing, *Atmospheric Research*, *120–121*(0), 112-126, doi: 10.1016/j.atmosres.2012.08.006.

Washington, R., and M. C. Todd (2005), Atmospheric controls on mineral dust emission from the Bodélé Depression, Chad: The role of the low level jet, *Geophys. Res. Lett.*, *32*(17), L17701, doi: 10.1029/2005gl023597.

Washington, R., and G. F. S. Wiggs (2011), Desert Dust, in *Arid Zone Geomorphology*, edited by D. S. G. Thomas, pp. 517-537, John Wiley & Sons, Chichester.

Washington, R., M. C. Todd, N. J. Middleton, and A. S. Goudie (2003), Dust-Storm Source Areas Determined by the Total Ozone Monitoring Spectrometer and Surface Observations, *Annals of the Association of American Geographers*, *93*(2), 297-313, doi: 10.1111/1467-8306.9302003.

Washington, R., M. C. Todd, S. Engelstaedter, S. Mbainayel, and F. Mitchell (2006a), Dust and the low-level circulation over the Bodélé Depression, Chad: Observations from BoDEx 2005, *J. Geophys. Res.*, *111*(D3), D03201, doi: 10.1029/2005jd006502.

Washington, R., M. C. Todd, G. Lizcano, I. Tegen, C. Flamant, I. Koren, P. Ginoux, S. Engelstaedter, C. S. Bristow, C. S. Zender, A. S. Goudie, A. Warren, and J. M. Prospero (2006b), Links between topography, wind, deflation, lakes and dust: The case of the Bodélé Depression, Chad, *Geophys. Res. Lett.*, *33*(9), L09401, doi: 10.1029/2006gl025827.

Wiggs, G. F. S. (2011), Sediment mobilisation by the wind, in *Arid Zone Geomorphology*, edited by D. S. G. Thomas, pp. 455-486, John Wiley & Sons, Chichester.

Williams, E. (2008), Comment on "Atmospheric controls on the annual cycle of North African dust" by S. Engelstaedter and R. Washington, *J. Geophys. Res.*, *113*(D23), D23109, doi: 10.1029/2008jd009930.

Williams, E., N. Nathou, E. Hicks, C. Pontikis, B. Russell, M. Miller, and M. J. Bartholomew (2009), The electrification of dust-lofting gust fronts ('haboobs') in the Sahel, *Atmospheric Research*, *91*(2-4), 292-298, doi: doi:10.1016/j.atmosres.2008.05.017.

3. Thesis motivation

3.1. The importance of observations for understanding the climate of remote regions

As has been seen in the Literature Review (Chapter 2), the vast majority of research on dust in the central Sahara has drawn its conclusions from modelling or satellite retrieval. Models and satellite retrieval are, unsurprisingly, the primary tools that inform our understanding of the climate of remote regions. Whilst this is hugely useful from a practical perspective, the results often implicitly or explicitly assume that the models or satellite algorithms are correct, or at least fit for purpose. This assumption is untestable without observations.

Suppose we start with the most extreme (and hopefully unrealistic) scenario that a given model is simulating dust processes fundamentally incorrectly. The only way we can know this, and indeed do something about it, is by comparing the model with good observations. In the above scenario, the good observations show that the model is simulating the processes fundamentally incorrectly, or perhaps missing them entirely. This may be an extreme case. But unfortunately it is not completely unrealistic. In a recent study, *Evan et al.* [2014: 5] conclude starkly that "CMIP5 models are unable to capture any of the salient features of northern African dust emission and transport"[6].

Evan et al. [2014] compared the CMIP5 models with satellite estimates of dust emission and transport. Of course, these satellite estimates will have their own errors too[7]. As will ground or airborne or any other observations. But this is not a reason not to make

[6] CMIP5 'simulations' is probably more correct than CMIP5 'models'. What counts as 'salient features' is admittedly somewhat subjective; the authors' claim is only relevant for the criteria examined. For a fuller discussion see Section 2.2.3.

[7] See also Section 2.2.3 above for a fuller discussion of *Evan et al.* [2014].

validation a major goal of climate science. It is important to test whether a model (or satellite algorithm, or even observational dataset) is fit for purpose. Statements that a model is 'state of the art' are not equivalent to saying that a model is accurate. With regard to the errors in observations, these should be identified and addressed as far as possible, for example by using a variety of independent instrumentation, to make sure that the observations – and any validation undertaken using them – is robust.

A great asset that numerical models and satellites provide is their spatial and temporal coverage. This is very difficult to replicate with observations, which is a major reason that, particularly in remote and hostile regions such as the Sahara, models and satellites make an important contribution. The problem is that when they disagree with each other, it is difficult to justify believing one product over another when there are no (or very few) observations. This problem has been illustrated over the Congo Basin by *Washington et al.* [2013]. The authors show that satellite-derived precipitation estimates over the basin differ by a factor of at least two, and up to 2000 mm yr^{-1} in absolute terms. In the DJF dry season, individual CMIP5 model members simulate rainfall amounts with a spread that spans an order of magnitude [*Washington et al.*, 2013]. With only three meteorological stations from the Democratic Republic of Congo reporting to the Global Telecommunication System in 2013, there is a pressing need for field observations in order to establish which models and satellite products are reliable [*Washington et al.*, 2013]. Similarly, *Huneeus et al.* [2011] compare 15 global aerosol models and suggest that dust emission from North Africa ranges from 400 to 2200 Tg yr^{-1}, whilst also pointing out that there are no datasets of measured dust emission that can be used to constrain this estimate. It is also possible that the true emission rate is outside of this range. Following the terminology of *Smith and Stern*

[2011], the emission range is uncertain not simply because it is imprecise, it is also ambiguous – the values cannot be assigned a probability.

There is an important distinction that should be made between model development and model improvement. Models (and satellite algorithms) develop all the time – new versions are constantly being released. But to know whether the developments have resulted in an improvement we need observations with which to validate them. (Strictly, we need to know the truth, but since we cannot know the truth it is important that our observations are as good as possible.) In remote regions, where satellite retrieval and model forecasts are relied upon most heavily, validation with observations should be a paramount objective.

Finally, observations are fundamental in themselves to making discoveries in climate science. Since they typically make fewer *a priori* assumptions than many of the other technologies available to climate scientists, we can expect them to help us discover some of nature's surprises.

3.2. The importance of understanding dust in the central Sahara

As has been reviewed, dust is an important constituent of the climate because it can lead to pronounced changes in the radiation budget [e.g. *Haywood et al.*, 2005; *Ryder et al.*, 2013], atmospheric dynamics [e.g. *Rodwell and Jung*, 2008; *Stanelle et al.*, 2010] and biogeochemistry [e.g. *Jickells et al.*, 2005; *Mahowald et al.*, 2010]. In boreal summer, the central Sahara is the dustiest place in the world [*Prospero et al.*, 2002; *Engelstaedter et al.*, 2006]. It follows therefore that to understand the effect of dust on climate it is important to understand dust emission from the central Sahara in boreal summer.

Our understanding of why it is so dusty in the remote central Sahara has been based on satellite retrievals and numerical modelling [e.g. *Marticorena et al.*, 1997; *Schepanski et al.*, 2009; *Marsham et al.*, 2011]. However, whilst significant progress has been made using these tools, they have their limitations. Polar-orbiting satellites will only pass the Sahara once or twice a day, and usually near noon, which introduces a significant sampling bias. Geostationary satellite instruments such as SEVIRI (with a temporal resolution of 15 min) can be exploited to much greater effect [e.g. *Ashpole and Washington*, 2012; *Banks et al.*, 2013] but no high temporal resolution satellite product has the capability to detect dust under cloud [*Ashpole and Washington*, 2013]. This is a major problem in boreal summer for satellite retrieval since the influence of the West African Monsoon extends to the southern regions of the Sahara at this time [e.g. *Sultan and Janicot*, 2003]. Furthermore, satellite studies of dust emission can usually provide only indirect evidence of emission mechanisms. For example, in the *Schepanski et al.* [2009] SEVIRI study, the conclusions were based heavily on the inference that dust detection at a particular time of day would be due to a particular emission mechanism. For numerical weather prediction models, simulation of dust emission mechanisms remains a challenge: without explicit convection, cold pool outflow dust emission is poorly represented if at all [*Marsham et al.*, 2011], and dry convective plumes occur on a spatial scale that is far too small (<100m) to be captured even in high resolution NWP. As for climate models, there is huge (> 7.5 orders of magnitude) disagreement in dust emission totals over North Africa between individual CMIP5 models [*Washington et al.*, in prep.].

As a result, there has been a pressing need for field observations in the remote central Sahara to understand why it is so dusty. (Indeed, in the case of dust devils, more systematic observations have been made on Mars than on Earth [*Lorenz*, 2012].) Prior

to the Fennec Project, there were no ground observations across vast tracts of the central Sahara, including most of eastern Mauritania, northern Mali and south-west Algeria (Figure 3-1). The Fennec Project targeted these regions in particular, and this thesis makes use of these unique new ground-based measurements to explore – in some cases for the first time – the atmospheric processes which make the central Sahara the summer global dust hotspot.

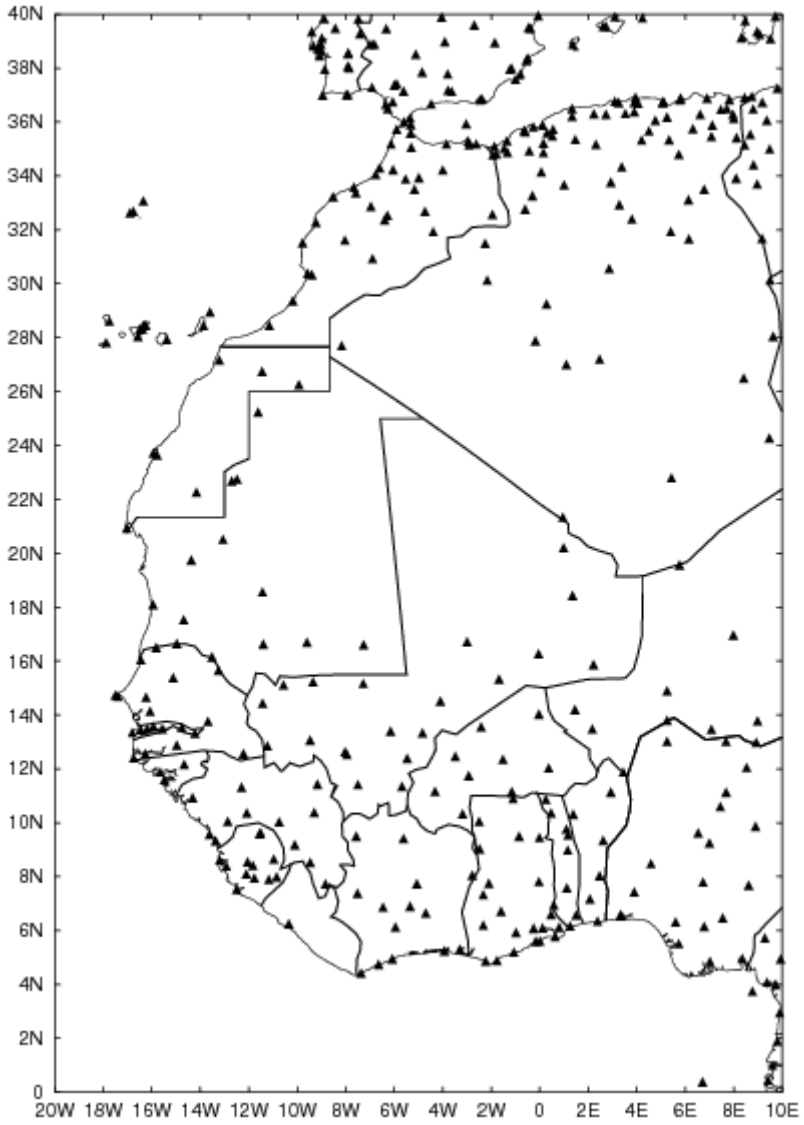

Figure 3-1: Map of West Africa showing the distribution of weather stations (from the Met Office Global Weather Observation Archive; Fennec weather stations not included). Figure courtesy of Sebastian Engelstaedter.

A particular challenge for Saharan dust research is the quantification of the different atmospheric mechanisms of dust emission. Until now, with some exceptions, work has focused on individual dust mechanisms [e.g. *Ansmann et al.*, 2009; *Emmel et al.*, 2010] or individual case study events [e.g. *Knippertz and Fink*, 2006; *Kocha et al.*, 2012; *Roberts and Knippertz*, 2014]. The relative importance of the different atmospheric emission mechanisms is slowly beginning to be addressed, but prior to the Fennec Project [*Washington et al.*, 2012] the approach has had to be restricted to modelling [*Heinold et al.*, 2013].

Understanding the relative importance of atmospheric emission mechanisms from observations is important to ascertain which mechanisms are primarily responsible for the boreal summer dust maximum, to focus research on the important atmospheric processes, to make projections about future dust loadings (especially if the important mechanisms have links to the synoptic scale) and to evaluate and develop dust processes in models and satellite products. For this last purpose, it is particularly important that quantitative estimates can be obtained from observations.

Evaluation and development of models is crucial for the central Sahara. Since we have not had any systematic field observations from the central Sahara, it is hard to know how well models perform over this region. As *Engelstaedter and Washington* [2007:1] state: 'If dust emission is not well simulated, all subsequent processes involving dust in the atmosphere will not be realistic either.' And if dust from the world's largest source in boreal summer is simulated poorly, as is certainly the case for CMIP5 [*Evan et al.*, 2014], then the implications are profound. Several authors have already shown how improved representation of Saharan dust results in model circulation improvements on the continent and beyond [e.g. *Tompkins et al.*, 2005; *Rodwell and Jung*, 2008]. More

pragmatically, we need good models because extensive field campaigns are very expensive and, particularly in an area as hostile as the Sahara, come with significant logistical challenges.

Significant improvements are being made to the dust cycle in numerical models. However, this work has tended to either be in the parameterization of deflation processes at the surface [e.g. *Marticorena and Bergametti*, 1995; *Klose and Shao*, 2012; *Haustein et al.*, 2014; *Kok et al.*, 2014] or in the improvement of dust radiative parameterizations [e.g. *Kok*, 2011; *Wang et al.*, 2013]. Arguably what is missing is an assessment of the atmospheric mechanisms that create the winds that cause deflation. Although it makes no difference to the dust itself whether the high winds have been caused by a cold pool outflow or a LLJ, knowing which it is allows for a much more meaningful diagnosis of model error. Knowing that the modelled friction velocity is incorrect is good, but knowing why the model gets it wrong (i.e. what atmospheric mechanisms the model is missing or simulating poorly) is better. If the atmospheric mechanisms leading to high winds are not simulated, then even perfect deflation and radiative parameterization schemes are redundant.

This aims of the DPhil are therefore:

1. To use Fennec ground-based observations to identify the atmospheric mechanisms that cause dust emission and transport in the Sahara in summer; first at the dust maximum, then across the Fennec instrument network.
2. To ascertain the relative importance of the different atmospheric dust mechanisms.
3. To examine in detail the operation of the LLJ as a dust emission mechanism.
4. To document the variability of the atmospheric dust mechanisms from one summer to another.
5. To evaluate the fidelity of different measurement approaches to detect dust under central Saharan atmospheric conditions.
6. To assess the ability of numerical models to capture the characteristics of LLJs and surface winds in the central Sahara.

The following chapter describes the Fennec Project and the geographical scope of the thesis in more detail.

3.3. References

Ansmann, A., M. Tesche, P. Knippertz, E. Bierwirth, D. Althausen, D. Müller, and O. Schulz (2009), Vertical profiling of convective dust plumes in southern Morocco during SAMUM, *Tellus B*, *61*(1), 340-353, doi: 10.1111/j.1600-0889.2008.00384.x.

Ashpole, I., and R. Washington (2012), An automated dust detection using SEVIRI: A multiyear climatology of summertime dustiness in the central and western Sahara, *J. Geophys. Res.*, *117*(D8), D08202, doi: 10.1029/2011jd016845.

Ashpole, I., and R. Washington (2013), A new high-resolution central and western Saharan summertime dust source map from automated satellite dust plume tracking, *Journal of Geophysical Research D: Atmospheres*, *118*(13), 6981-6995, doi: 10.1002/jgrd.50554.

Banks, J. R., H. E. Brindley, C. Flamant, M. J. Garay, N. C. Hsu, O. V. Kalashnikova, L. Klüser, and A. M. Sayer (2013), Intercomparison of satellite dust retrieval products over the west African Sahara during the Fennec campaign in June 2011, *Remote Sensing of Environment*, *136*(0), 99-116, doi: 10.1016/j.rse.2013.05.003.

Emmel, C., P. Knippertz, and O. Schulz (2010), Climatology of convective density currents in the southern foothills of the Atlas Mountains, *J. Geophys. Res.*, *115*(D11), D11115, doi: 10.1029/2009jd012863.

Engelstaedter, S., and R. Washington (2007), Temporal controls on global dust emissions: The role of surface gustiness, *Geophys. Res. Lett.*, *34*(15), L15805, doi: 10.1029/2007gl029971.

Engelstaedter, S., I. Tegen, and R. Washington (2006), North African dust emissions and transport, *Earth-Science Reviews*, *79*(1–2), 73-100, doi: 10.1016/j.earscirev.2006.06.004.

Evan, A. T., C. Flamant, S. Fiedler, and O. Doherty (2014), An analysis of aeolian dust in climate models, *Geophysical Research Letters*, *41*(16), 2014GL060545, doi: 10.1002/2014gl060545.

Haustein, K., R. Washington, J. King, G. Wiggs, D. Thomas, and L. Menut (2014), Testing the performance of state-of-the-art dust emission schemes using DO4Models field data, *Geosci. Model Dev. Discuss.*, *7*(5), 5739-5789, doi: 10.5194/gmdd-7-5739-2014.

Haywood, J. M., R. P. Allan, I. Culverwell, T. Slingo, S. Milton, J. Edwards, and N. Clerbaux (2005), Can desert dust explain the outgoing longwave radiation anomaly over the Sahara during July 2003?, *J. Geophys. Res.*, *110*(D5), D05105, doi: 10.1029/2004jd005232.

Heinold, B., P. Knippertz, J. H. Marsham, S. Fiedler, N. S. Dixon, K. Schepanski, B. Laurent, and I. Tegen (2013), The role of deep convection and nocturnal low-level jets for dust emission in summertime West Africa: Estimates from convection-permitting simulations, *Journal of Geophysical Research: Atmospheres*, *118*, 4385–4400, doi: 10.1002/jgrd.50402.

Huneeus, N., M. Schulz, Y. Balkanski, J. Griesfeller, J. Prospero, S. Kinne, S. Bauer, O. Boucher, M. Chin, F. Dentener, T. Diehl, R. Easter, D. Fillmore, S. Ghan, P. Ginoux, A. Grini, L. Horowitz, D. Koch, M. C. Krol, W. Landing, X. Liu, N. Mahowald, R. Miller, J. J. Morcrette, G. Myhre, J. Penner, J. Perlwitz, P. Stier, T. Takemura, and C. S. Zender (2011), Global dust model intercomparison in AeroCom phase I, *Atmos. Chem. Phys.*, *11*(15), 7781-7816, doi: 10.5194/acp-11-7781-2011.

Jickells, T. D., Z. S. An, K. K. Andersen, A. R. Baker, G. Bergametti, N. Brooks, J. J. Cao, P. W. Boyd, R. A. Duce, K. A. Hunter, H. Kawahata, N. Kubilay, J. laRoche, P. S. Liss, N. Mahowald, J. M. Prospero, A. J. Ridgwell, I. Tegen, and R. Torres (2005), Global Iron Connections Between Desert Dust, Ocean Biogeochemistry, and Climate, *Science*, *308*(5718), 67-71, doi: 10.1126/science.1105959.

Klose, M., and Y. Shao (2012), Stochastic parameterization of dust emission and application to convective atmospheric conditions, *Atmos. Chem. Phys.*, *12*(16), 7309-7320, doi: 10.5194/acp-12-7309-2012.

Knippertz, P., and A. H. Fink (2006), Synoptic and dynamic aspects of an extreme springtime Saharan dust outbreak, *Quarterly Journal of the Royal Meteorological Society*, *132*(617), 1153-1177, doi: 10.1256/qj.05.109.

Kocha, C., J. P. Lafore, P. Tulet, and Y. Seity (2012), High-resolution simulation of a major West African dust-storm: Comparison with observations and investigation of dust impact, *Quarterly Journal of the Royal Meteorological Society*, *138*(663), 455-470.

Kok, J. F. (2011), A scaling theory for the size distribution of emitted dust aerosols suggests climate models underestimate the size of the global dust cycle, *Proceedings of the National Academy of Sciences*, doi: 10.1073/pnas.1014798108.

Kok, J. F., S. Albani, N. M. Mahowald, and D. S. Ward (2014), An improved dust emission model – Part 2: Evaluation in the Community Earth System Model, with implications for the use of dust source functions, *Atmos. Chem. Phys.*, *14*(23), 13043-13061, doi: 10.5194/acp-14-13043-2014.

Lorenz, R. D. (2012), Power law distribution of pressure drops in dust devils: Observation techniques and Earth–Mars comparison, *Planetary and Space Science*, *60*(1), 370-375, doi: 10.1016/j.pss.2011.11.003.

Mahowald, N., S. Kloster, S. Engelstaedter, J. K. Moore, S. Mukhopadhyay, J. R. McConnell, S. Albani, S. C. Doney, A. Bhattacharya, M. A. J. Curran, M. G. Flanner, F. M. Hoffman, D. M. Lawrence, K. Lindsay, P. A. Mayewski, J. Neff, D. Rothenberg, E. Thomas, P. E. Thornton, and C. S. Zender (2010), Observed 20th century desert dust variability: impact on climate and biogeochemistry, *Atmos. Chem. Phys.*, *10*(22), 10875-10893, doi: 10.5194/acp-10-10875-2010.

Marsham, J. H., P. Knippertz, N. S. Dixon, D. J. Parker, and G. M. S. Lister (2011), The importance of the representation of deep convection for modeled dust-generating winds over West Africa during summer, *Geophys. Res. Lett.*, *38*(16), L16803, doi: 10.1029/2011gl048368.

Marticorena, B., and G. Bergametti (1995), Modeling the atmospheric dust cycle: 1. Design of a soil-derived dust emission scheme, *J. Geophys. Res.*, *100*(D8), 16415-16430, doi: 10.1029/95jd00690.

Marticorena, B., G. Bergametti, B. Aumont, Y. Callot, C. N'Doumé, and M. Legrand (1997), Modeling the atmospheric dust cycle 2. Simulation of Saharan dust sources, *Journal of Geophysical Research D: Atmospheres*, *102*(4), 4387-4404, doi: 10.1029/96JD02964.

Prospero, J. M., P. Ginoux, O. Torres, S. E. Nicholson, and T. E. Gill (2002), Environmental characterization of global sources of atmospheric soil dust identified with the NIMBUS 7 Total Ozone Mapping Spectrometer (TOMS) absorbing aerosol product, *Rev. Geophys.*, *40*(1), 1002, doi: 10.1029/2000rg000095.

Roberts, A. J., and P. Knippertz (2014), The formation of a large summertime Saharan dust plume: Convective and synoptic-scale analysis, *Journal of Geophysical Research: Atmospheres*, *119*(4), 1766-1785, doi: 10.1002/2013jd020667.

Rodwell, M. J., and T. Jung (2008), Understanding the local and global impacts of model physics changes: an aerosol example, *Quarterly Journal of the Royal Meteorological Society*, *134*(635), 1479-1497, doi: 10.1002/qj.298.

Ryder, C. L., E. J. Highwood, P. D. Rosenberg, J. Trembath, J. K. Brooke, M. Bart, A. Dean, J. Crosier, J. Dorsey, H. Brindley, J. Banks, J. H. Marsham, J. B. McQuaid, H. Sodemann, and R. Washington (2013), Optical properties of Saharan dust aerosol and contribution from the coarse mode as measured during the Fennec 2011 aircraft campaign, *Atmos. Chem. Phys.*, *13*(1), 303-325, doi: 10.5194/acp-13-303-2013.

Schepanski, K., I. Tegen, M. C. Todd, B. Heinold, G. Bönisch, B. Laurent, and A. Macke (2009), Meteorological processes forcing Saharan dust emission inferred from MSG-SEVIRI observations of subdaily dust source activation and numerical models, *J. Geophys. Res.*, *114*(D10), D10201, doi: 10.1029/2008jd010325.

Smith, L. A., and N. Stern (2011), Uncertainty in science and its role in climate policy, *Philosophical Transactions of the Royal Society of London A: Mathematical, Physical and Engineering Sciences*, *369*(1956), 4818-4841, doi: 10.1098/rsta.2011.0149.

Stanelle, T., B. Vogel, H. Vogel, D. Bäumer, and C. Kottmeier (2010), Feedback between dust particles and atmospheric processes over West Africa during dust episodes in March 2006 and June 2007, *Atmos. Chem. Phys.*, *10*(22), 10771-10788, doi: 10.5194/acp-10-10771-2010.

Sultan, B., and S. Janicot (2003), The West African monsoon dynamics. Part II: The "preonset" and "onset" of the summer monsoon, *Journal of Climate*, *16*(21), 3407-3427, doi: 10.1175/1520-0442(2003)016<3407:TWAMDP>2.0.CO;2.

Tompkins, A. M., C. Cardinali, J. J. Morcrette, and M. Rodwell (2005), Influence of aerosol climatology on forecasts of the African Easterly Jet, *Geophys. Res. Lett.*, *32*(10), L10801, doi: 10.1029/2004gl022189.

Wang, Z., H. Zhang, X. Jing, and X. Wei (2013), Effect of non-spherical dust aerosol on its direct radiative forcing, *Atmospheric Research*, *120–121*(0), 112-126, doi: 10.1016/j.atmosres.2012.08.006.

Washington, R., I. Ashpole, and C. Duckworth (in prep.), An Assessment of Coupled Climate Model Dust Emission Simulations over North Africa.

Washington, R., R. James, H. Pearce, W. M. Pokam, and W. Moufouma-Okia (2013), Congo Basin rainfall climatology: can we believe the climate models?, *Philosophical Transactions of the Royal Society of London B: Biological Sciences*, *368*(1625), doi: 10.1098/rstb.2012.0296.

Washington, R., C. Flamant, D. J. Parker, J. H. Marsham, J. B. McQuaid, H. Brindley, M. C. Todd, E. Highwood, C. Ryder, J. P. Chaboureau, C. Kocha, M. Bechir, and A. Saci (2012), Fennec - The Saharan Climate System, *CLIVAR Exchanges*, *17*(3), 31-33.

4. Datasets and scope

This short chapter describes the datasets that will be used in this thesis (including a description of the Fennec Project) and defines its geographical and temporal scope.

4.1. Datasets: The Fennec Project

This thesis has been undertaken under the auspices of the international scientific consortium project Fennec (full name *Fennec: The Saharan Climate System*). The aims of Fennec are to improve understanding of the climate of the central Sahara and surrounding regions, with a particular emphasis on developing, deploying and exploiting new field observations (ground-based and aircraft). Deliverables of the Fennec Project include new observational datasets; a characterisation of Saharan dynamics, thermodynamics and atmospheric composition; an assessment of dust emission mechanisms and dust radiative forcing, and an evaluation of numerical model performance over the region. Further details of the project can be found in *Washington et al.* [2012] and at http://fennec.ouce.ox.ac.uk/.

The Fennec Project has, for the first time, systematically instrumented the remote Sahara Heat Low region in the central Sahara Desert [*Washington et al.*, 2012; *Hobby et al.*, 2013; *Marsham et al.*, 2013; *Todd et al.*, 2013] (fieldwork in which I was heavily involved). The resulting measurements provide an unprecedented chance to research central Saharan dust emission from observations, where work has been and is mainly restricted to model simulations [e.g. *Marticorena et al.*, 1997; *Laurent et al.*, 2010; *Marsham et al.*, 2011; *Kocha et al.*, 2012; *Heinold et al.*, 2013], satellite retrieval [e.g. *Engelstaedter and Washington*, 2007; *Schepanski et al.*, 2009; *Ashpole and Washington*, 2013a] or observational campaigns on the fringes of the Heat Low [*Redelsperger et al.*,

2006; *Haywood et al.*, 2008; *Ansmann et al.*, 2011; *Haywood et al.*, 2011]. To take advantage of the opportunity provided by the new measurements, Fennec ground-based observations form the principal dataset behind the thesis. Since research flights are by nature highly variable in time and space, ground-based observations are more suitable for addressing the aims of the thesis. Moreover, logistical constraints meant that the research flights could only be undertaken in the western portions of the Sahara [*Ryder et al.*, 2015], rather than in the dustier central Saharan interior.

The Fennec ground-based observations can be split into three components: the supersites, the automatic weather stations (AWSs), and additional radiosonde launches. There are two Fennec supersites, Bordj-Badji Mokhtar (BBM), Algeria (21.38°N, 0.92°E; elevation 420m; WMO ID 60686) and Zouerat, Mauritania (22.75°N, 12.48°W; elevation 343 m; WMO ID 61404). The supersites were manned and comprised a suite of sophisticated meteorological instrumentation, including radiosondes. Eight AWSs were deployed across remote northern Mauritania and western Algeria by the meteorological services of Mauritania and Algeria. The AWSs were left unmanned and transmitted data back to the UK by satellite. Finally, additional radiosonde launches were made from the existing Algerian weather stations of Tindouf, In Salah and Tamanrasset. The location of the Fennec ground-based observations is shown in Figure 4-1.

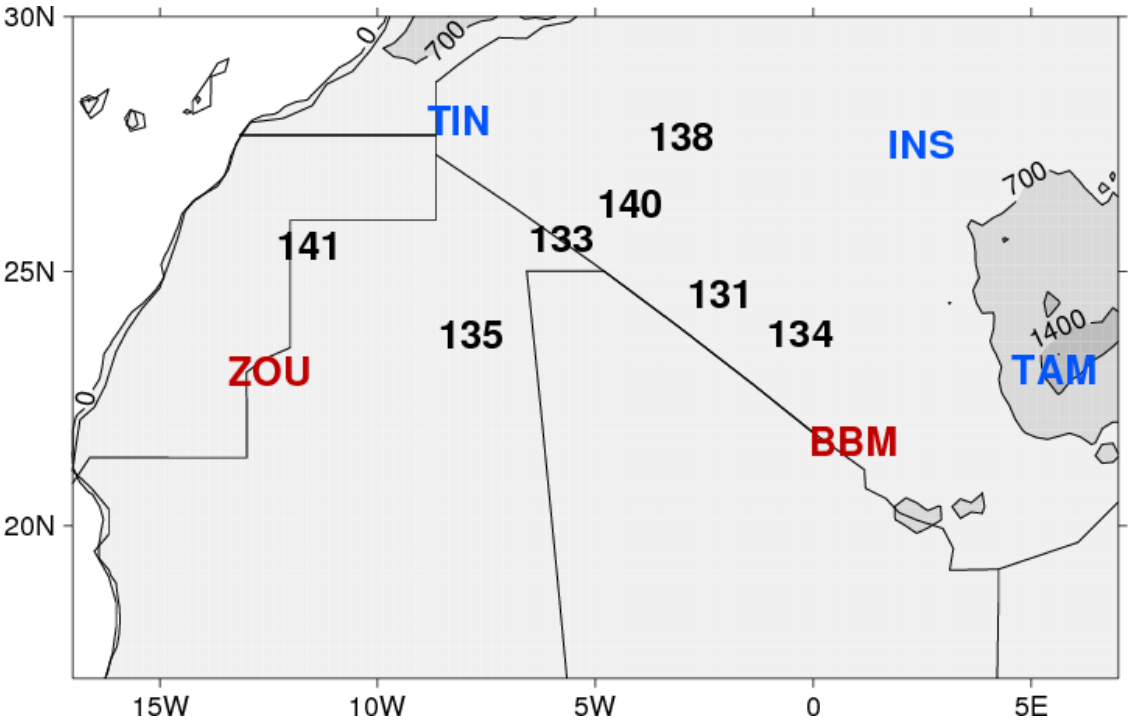

Figure 4-1: Map of the central-western Sahara showing location of Fennec AWSs (black numbers), supersites (red) and radiosonde stations (blue). Note that radiosondes were also launched from ZOU and BBM. ZOU=Zouerat, BBM=Bordj Badji Mokhtar, TIN=Tindouf, INS=In Salah, TAM=Tamanrasset. Greyscale background is elevation (700m contour step).

Fennec consisted of two intensive observation periods (IOPs): June 2011 and June 2012. In June 2011, BBM and Zouerat were most heavily instrumented; in June 2012 most but not all instruments were available at the supersites. In addition to the IOPs, an Extended Observation Period ran from May 2011 until November 2013, when limited instrumentation was present at the supersites and the AWSs were transmitting[8]. The thesis focuses on the June IOPs, since (i) summer is the dustiest period (ii) instrument availability is highest. The instruments at each of the supersites and on the AWSs are described in later chapters when their measurements are employed; full details can also be found in *Hobby et al.* [2013], *Marsham et al.* [2013], and *Todd et al.* [2013].

[8] Component failure meant that there were initially several months with no data at some AWSs.

4.2. Geographic scope of the research

Much of the research focuses on results from BBM. It was chosen because it is in the heart of the central Saharan – and therefore global – dust maximum in June [*Ashpole and Washington*, 2012] (Figure 4-2). BBM is in a major dust source region itself and within 300km of four other major dust sources [*Ashpole and Washington*, 2013b] (see also Figure 2-6). It was also the most heavily instrumented Fennec site, with a wealth of sophisticated instrumentation deployed during the IOPs. BBM can be either north or south of the ITD in summer which means that it is an excellent site at which to sample different dust emission mechanisms, including cold pool outflows, dry convective plumes and low level jets. In Chapter 8 the focus will be expanded to include the AWSs and Zouerat, in order to establish whether the dust processes which dominate at BBM are the same as those present across the other instrumented Fennec sites (Figure 4-1), and to establish whether model performance varies across the region. Since the stations are by nature only 'points', model and satellite data will be called upon where appropriate to provide spatial context. Care will be taken to distinguish such use of model and satellite data from validation of model simulations and satellite retrieval algorithms so as to avoid circular arguments.

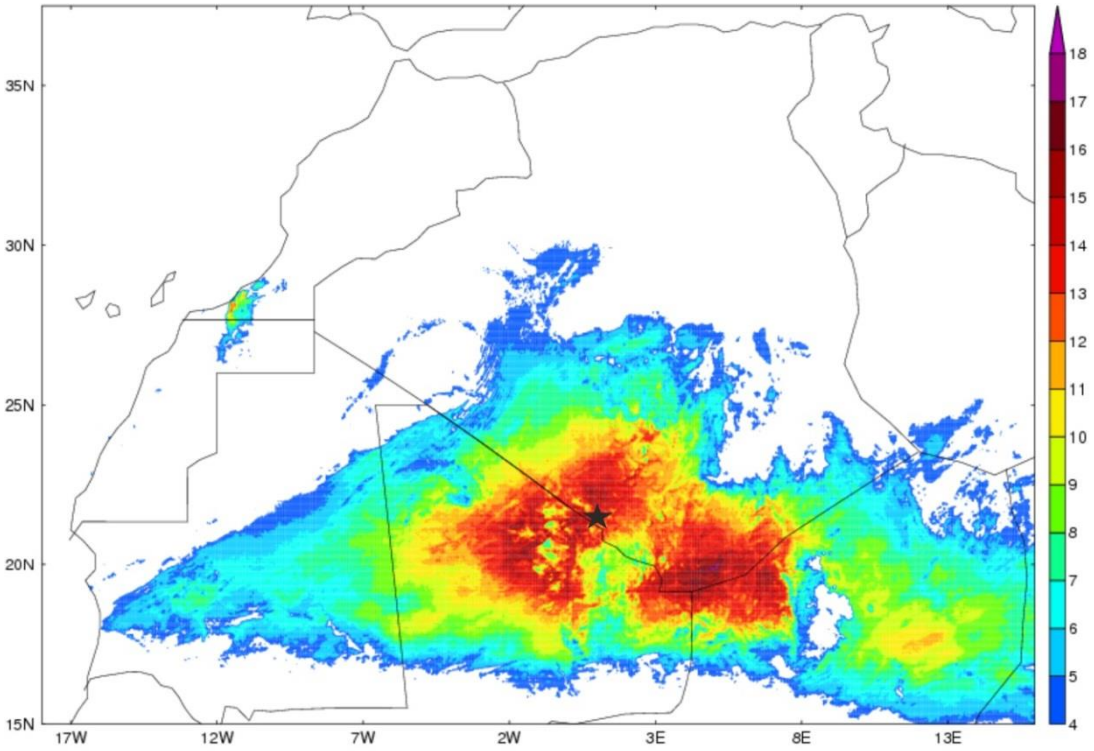

Figure 4-2: Mean frequency of SDF satellite dust detection, June 2004-2010. Expressed as the percentage of available timesteps when dust is detected by SDF. The location of BBM is shown with a star. Figure courtesy of Ian Ashpole.

4.3. References

Ansmann, A., A. Petzold, K. Kandler, I. N. A. Tegen, M. Wendisch, D. Müller, B. Weinzierl, T. Müller, and J. Heintzenberg (2011), Saharan Mineral Dust Experiments SAMUM–1 and SAMUM–2: what have we learned?, *Tellus B*, *63*(4), 403-429, doi: 10.1111/j.1600-0889.2011.00555.x.

Ashpole, I., and R. Washington (2012), An automated dust detection using SEVIRI: A multiyear climatology of summertime dustiness in the central and western Sahara, *J. Geophys. Res.*, *117*(D8), D08202, doi: 10.1029/2011jd016845.

Ashpole, I., and R. Washington (2013a), Intraseasonal variability and atmospheric controls on daily dust occurrence frequency over the central and western Sahara during the boreal summer, *Journal of Geophysical Research: Atmospheres*, *118*(23), 2013JD020267, doi: 10.1002/2013jd020267.

Ashpole, I., and R. Washington (2013b), A new high-resolution central and western Saharan summertime dust source map from automated satellite dust plume tracking, *Journal of Geophysical Research D: Atmospheres*, *118*(13), 6981-6995, doi: 10.1002/jgrd.50554.

Engelstaedter, S., and R. Washington (2007), Atmospheric controls on the annual cycle of North African dust, *J. Geophys. Res.*, *112*(D3), D03103, doi: 10.1029/2006jd007195.

Haywood, J. M., B. T. Johnson, S. R. Osborne, A. J. Baran, M. Brooks, S. F. Milton, J. Mulcahy, D. Walters, R. P. Allan, A. Klaver, P. Formenti, H. E. Brindley, S. Christopher, and P. Gupta (2011), Motivation, rationale and key results from the GERBILS Saharan dust measurement campaign, *Quarterly Journal of the Royal Meteorological Society*, *137*(658), 1106-1116, doi: 10.1002/qj.797.

Haywood, J. M., J. Pelon, P. Formenti, N. Bharmal, M. Brooks, G. Capes, P. Chazette, C. Chou, S. Christopher, H. Coe, J. Cuesta, Y. Derimian, K. Desboeufs, G. Greed, M. Harrison, B. Heese, E. J. Highwood, B. Johnson, M. Mallet, B. Marticorena, J. Marsham, S. Milton, G. Myhre, S. R. Osborne, D. J. Parker, J. L. Rajot, M. Schulz, A. Slingo, D. Tanré, and P. Tulet (2008), Overview of the Dust and Biomass-burning Experiment and African Monsoon Multidisciplinary Analysis Special Observing Period-0, *Journal of Geophysical Research: Atmospheres*, *113*(D23), D00C17, doi: 10.1029/2008jd010077.

Heinold, B., P. Knippertz, J. H. Marsham, S. Fiedler, N. S. Dixon, K. Schepanski, B. Laurent, and I. Tegen (2013), The role of deep convection and nocturnal low-level jets for dust emission in summertime West Africa: Estimates from convection-permitting simulations, *Journal of Geophysical Research: Atmospheres*, *118*, 4385–4400, doi: 10.1002/jgrd.50402.

Hobby, M., M. Gascoyne, J. H. Marsham, M. Bart, C. J. T. Allen, S. Engelstaedter, D. M. Fadel, A. Gandega, R. Lane, J. B. McQuaid, B. Ouchene, A. Ouladichir, D. J. Parker, P. Rosenberg, M. S. Ferroudj, A. Saci, F. Seddik, M. Todd, D. Walker, and R. Washington (2013), The Fennec Automatic Weather Station (AWS) Network: Monitoring the Saharan Climate System, *Journal of Atmospheric and Oceanic Technology*, *30*(4), 709-724, doi: 10.1175/jtech-d-12-00037.1.

Kocha, C., J. P. Lafore, P. Tulet, and Y. Seity (2012), High-resolution simulation of a major West African dust-storm: Comparison with observations and investigation of dust impact, *Quarterly Journal of the Royal Meteorological Society*, *138*(663), 455-470.

Laurent, B., I. Tegen, B. Heinold, K. Schepanski, B. Weinzierl, and M. Esselborn (2010), A model study of Saharan dust emissions and distributions during the SAMUM-1 campaign, *J. Geophys. Res.*, *115*(D21), D21210, doi: 10.1029/2009jd012995.

Marsham, J. H., P. Knippertz, N. S. Dixon, D. J. Parker, and G. M. S. Lister (2011), The importance of the representation of deep convection for modeled dust-generating winds over West Africa during summer, *Geophys. Res. Lett.*, *38*(16), L16803, doi: 10.1029/2011gl048368.

Marsham, J. H., M. Hobby, C. J. T. Allen, J. R. Banks, M. Bart, B. J. Brooks, C. Cavazos-Guerra, S. Engelstaedter, M. Gascoyne, A. R. Lima, J. V. Martins, J. B. McQuaid, A. O'Leary, B. Ouchene, A. Ouladichir, D. J. Parker, A. Saci, M. Salah-Ferroudj, M. C. Todd, and R. Washington (2013), Meteorology and dust in the central Sahara: Observations from

Fennec supersite-1 during the June 2011 Intensive Observation Period, *Journal of Geophysical Research: Atmospheres*, *118*, 4069–4089, doi: 10.1002/jgrd.50211.

Marticorena, B., G. Bergametti, B. Aumont, Y. Callot, C. N'Doumé, and M. Legrand (1997), Modeling the atmospheric dust cycle 2. Simulation of Saharan dust sources, *Journal of Geophysical Research D: Atmospheres*, *102*(4), 4387-4404, doi: 10.1029/96JD02964.

Redelsperger, J.-L., C. D. Thorncroft, A. Diedhiou, T. Lebel, D. J. Parker, and J. Polcher (2006), African Monsoon Multidisciplinary Analysis: An International Research Project and Field Campaign, *Bulletin of the American Meteorological Society*, *87*(12), 1739-1746, doi: 10.1175/bams-87-12-1739.

Ryder, C. L., J. B. McQuaid, C. Flamant, R. Washington, H. E. Brindley, E. J. Highwood, J. H. Marsham, D. J. Parker, M. C. Todd, J. R. Banks, J. K. Brooke, S. Engelstaedter, V. Estellés, P. Formenti, L. Garcia-Carreras, C. Kocha, F. Marenco, P. Rosenberg, H. Sodemann, C. J. T. Allen, A. Bourdon, M. Bart, C. Cavazos-Guerra, S. Chevaillier, J. Crosier, E. Darbyshire, A. R. Dean, J. R. Dorsey, J. Kent, D. O'Sullivan, K. Schepanski, K. Szpek, and A. Woolley (2015), Advances in understanding mineral dust and boundary layer processes over the Sahara from Fennec aircraft observations, *Atmos. Chem. Phys. Discuss.*, *15*(1), 199-290, doi: 10.5194/acpd-15-199-2015.

Schepanski, K., I. Tegen, M. C. Todd, B. Heinold, G. Bönisch, B. Laurent, and A. Macke (2009), Meteorological processes forcing Saharan dust emission inferred from MSG-SEVIRI observations of subdaily dust source activation and numerical models, *J. Geophys. Res.*, *114*(D10), D10201, doi: 10.1029/2008jd010325.

Todd, M. C., C. J. T. Allen, M. Bart, M. Bechir, J. Bentefouet, B. J. Brooks, C. Cavazos-Guerra, T. Clovis, S. Deyane, M. Dieh, S. Engelstaedter, C. Flamant, L. Garcia-Carreras, A. Gandega, M. Gascoyne, M. Hobby, C. Kocha, C. Lavaysse, J. H. Marsham, J. V. Martins, J. B. McQuaid, J. B. Ngamini, D. J. Parker, T. Podvin, A. Rocha-Lima, S. Traore, Y. Wang, and R. Washington (2013), Meteorological and dust aerosol conditions over the Western Saharan region observed at Fennec supersite-2 during the Intensive Observation Period in June 2011, *Journal of Geophysical Research: Atmospheres*, *118*, 8426–8447, doi: 10.1002/jgrd.50470.

Washington, R., C. Flamant, D. J. Parker, J. H. Marsham, J. B. McQuaid, H. Brindley, M. C. Todd, E. Highwood, C. Ryder, J. P. Chaboureau, C. Kocha, M. Bechir, and A. Saci (2012), Fennec - The Saharan Climate System, *CLIVAR Exchanges*, *17*(3), 31-33.

5. Dust emission and transport mechanisms in the central Sahara: Fennec ground-based observations from Bordj Badji Mokhtar, June 2011

Christopher J.T. Allen, Richard Washington and Sebastian Engelstaedter

Published in Journal of Geophysical Research Atmospheres 24 June 2013

doi: 10.1002/jgrd.50534[9] *(CC BY 4.0 license)*

Abstract

A detailed analysis of the first ever high resolution ground-based dust observations in the remote central Sahara is presented from observations at Bordj Badji Mokhtar (BBM), taken during the Fennec project in June 2011. Detailed case studies are presented for three dust producing mechanisms (cold pool outflows, low level jets (LLJs) and dry convective plumes). The results confirm the importance of cold pools in dust emission and transport in the region. 45% of the dust over BBM is generated by local emission in cold pool outflows. 27% of the dust is advected rather than locally emitted dust; on three occasions it is advected over 500km to BBM by cold pool outflows. Dust that has been in long range transport to the area within such cold pool outflows is found to carry larger particles and be responsible for higher dust loadings than fresh uplift. LLJs are of tertiary importance in the partitioning, responsible for 14% dust over BBM. Dry convective plumes are identifiable in the data but produce much less significant quantities of dust, approximately 2% of the June total. The cube of wind speed has a stronger correlation with dust emission than wind speed. The correlation is strongest (at

[9] Note that following Minor Corrections required by the DPhil examiners (requested after this chapter was published) the content of this chapter is not identical to the published version.

95% confidence) for LLJ-induced emission (0.88), followed by locally emitting cold pools (0.78).

5.1. Introduction

The Sahara desert is the dustiest place on Earth [*Prospero et al.*, 2002; *Washington et al.*, 2003]. Atmospheric dust has an important effect on the radiation budget [e.g. *Haywood et al.*, 2005], global biogeochemical cycles [e.g. *Mahowald et al.*, 2010], atmospheric circulation [e.g. *Stanelle et al.*, 2010] and ocean circulation [e.g. *Evan et al.*, 2011], as well as being a hazard to transportation and human health. The atmospheric mechanism responsible for dust emission in the Bodélé depression in Chad, a largely winter and spring time source, has been shown to be a strong low level jet (LLJ) identifiable even in long-term mean wind fields [*Washington and Todd*, 2005; *Washington et al.*, 2006]. By contrast, boreal summer central Saharan dust emission, which dominates the global atmospheric dust burden [*Engelstaedter et al.*, 2006] is thought to be the result of several atmospheric mechanisms acting over multiple dust sources. Mechanisms include (i) the mixing down of momentum from low level jets towards the surface after sunrise [e.g. *Schepanski et al.*, 2009]; (ii) high winds and turbulence at the leading edge of cold pool outflows [e.g. *Emmel et al.*, 2010]; (iii) dust devils and dry convective plumes [e.g. *Ansmann et al.*, 2009]. However, although there has been ground-based work in Tamanrasset, Hoggar Mountains, Algeria [*Cuesta et al.*, 2008], much of what we know about the mechanisms of dust emission in the central Sahara has been inferred from satellite analysis [e.g. *Schepanski et al.*, 2009] and numerical model simulations [e.g. *Marsham et al.*, 2011]. Progress in understanding summer central Saharan dust emission has been hampered by a paucity of high-quality ground-based observations.

5.1.1. The Fennec Project

The Fennec programme [*Washington et al.*, 2012] was designed to gain observations from the data sparse region of the central Sahara. Fennec includes three observational components: airborne [*Ryder et al.*, 2015], satellite [*Banks et al.*, 2013] and ground-based. The ground-based component comprises a network of remote automatic weather stations [*Hobby et al.*, 2013] and two supersites: Zouerate, Mauritania [*Todd et al.*, 2013] and Bordj Badji Mokhtar (BBM) on the Algerian-Mali border [*Marsham et al.*, 2013]. BBM is within a few kilometres of the mean centre of summertime dust loadings as estimated from the Spinning Enhanced Visible & Infrared Imager (SEVIRI) data [*Ashpole and Washington*, 2012]. Key aims of the Fennec programme include the identification of mechanisms associated with dust emission and determining the contribution of these mechanisms to the total dust burden in the central Sahara.

5.1.2. Atmospheric dust emission mechanisms

There are several different atmospheric dust emission mechanisms that operate in the Sahara, ranging from the scale of tens of metres to thousands of kilometres. The operation of those pertinent to this study are briefly summarised below.

5.1.2.1. Cold pool outflows

Cold pool outflows form from downdrafts of moist convection, when evaporating or sublimating precipitation cools the air in the subcloud layer, allowing it to sink to the surface, particularly if the environment is dry adiabatic [e.g. *Miller et al.*, 2008]. As the sinking air approaches the surface it spreads away from the parent storm in a density current or outflow. Turbulence and high winds at the leading edge of the outflow (the gust front) can raise substantial ‘walls’ of dust [*Flamant et al.*, 2007; *Knippertz et al.*, 2007; *Miller et al.*, 2008; *Williams et al.*, 2009; *Emmel et al.*, 2010; *Solomos et al.*,

2012], especially where the threshold velocity for sediment entrainment is low. Dust storms caused by cold pool outflows are frequently called ‘haboobs’. If a density current propagates into a zone of strong static stability such as a nocturnal inversion it can initiate a bore ahead of the current [e.g. *Smith*, 1988; *Fulton et al.*, 1990; *S E Koch et al.*, 1991]. The typical signature of a passing bore is a short-lived pressure rise, increase in wind speed and shift in wind direction. Unlike during a density current, there is no decrease in surface temperature: pure bores do not transport mass [*Simpson*, 1997; *Kingsmill and Crook*, 2003].

5.1.2.2. Low level jets

LLJs frequently form in desert regions after sunset when turbulent heating dies down and winds aloft become decoupled from the surface. In conditions of a moderate or strong pressure gradient the flow can then become super-geostrophic above the nocturnal inversion [e.g. *Blackadar*, 1957; *Knippertz and Todd*, 2012]. After sunrise, turbulent mixing begins to increase and momentum from the LLJ can be mixed down to the surface [e.g. *Washington et al.*, 2006; *Todd et al.*, 2008]. LLJs can be found in the Harmattan [*Washington and Todd*, 2005] and monsoon flow [*Parker et al.*, 2005]. Satellite-based work suggests that they play a dominant role in dust emission across the Sahara [*Schepanski et al.*, 2009].

5.1.2.3. Dry convective plumes and dust devils

On the smallest spatial scale, dry convective plumes and dust devils lead to dust emission. Under dry conditions with intense surface heating, localized turbulent circulations can develop producing short-lived plumes or vortices associated with dust lofting [*Sinclair*, 1969; *Kaimal and Bussinger*, 1970; *J Koch and Renno*, 2005; *Balme and Greeley*, 2006; *Ansmann et al.*, 2009]. Dust devils are rotating vortices, with a mean

diameter of 7m and heights from a few metres to over 1km [*Balme and Greeley,* 2006]. Dry convective plumes are non-rotating updrafts, with diameter ~100m [*Ansmann et al.*, 2009]. Dry convective plumes observed in the Saharan summer reach heights of 1-2km in Tamanrasset, Algeria [*Cuesta et al.*, 2008] and<1km in Ouarzazate, Morocco [*Ansmann et al.*, 2009].

It is important to recognise that dry convection occurs throughout daylight hours in the Sahara, as heating of the ground surface generates turbulent eddies which can have a range of scales up to the boundary layer height. It is these turbulent eddies that result in momentum mix-down from LLJs. Here however, the term 'dry convective plume' is restricted to afternoon gustiness which raises dust in discrete updrafts. The role of dry convection - which includes momentum mix-down from aloft – is therefore broader than what here are described as 'dry convective plumes'.

5.1.2.4. Monsoon surges

Penetration of the West African Monsoon (WAM) into the Sahara can raise dust emission as it acts as an intrusive surge, with strong wind speeds occurring at the leading edge of the monsoon flow [*Bou Karam et al.*, 2008]. WAM surges behave like large-scale density currents, but since they also transport moisture into very hot regions they can promote deep moist convection and subsequent density currents within the monsoon flow itself [*Bou Karam et al.*, 2008]. Indeed, it is not always easy to separate the two [*Marsham et al.*, 2013].

This paper presents a detailed analysis of summer dust production from observational data in the heart of the central Sahara during the Fennec Intensive Observation Period (IOP) of June 2011. June was chosen since the satellite-derived absorbing aerosol index from the Total Ozone Mapping Spectrometer and Ozone Monitoring Instrument

demonstrates that June is the dustiest month in the central Sahara [e.g. *Engelstaedter et al.*, 2006]. The aims of this paper are to 1) document the main dust outbreaks during the 2011 Fennec IOP at Bordj Badji Mokhtar 2) identify the mechanisms associated with dust production and establish their relative importance 3) document the characteristics of the key dust producing mechanisms and their relationship with wind speed for dust emission. The paper is structured as follows. Section 5.2 describes the location of the observations, the instrumentation and additional data employed. Sections 5.3 to 5.6 describe the detection and attribution of dust events and their characteristics. Section 5.7 presents a selection of detailed case studies. Sections 5.8-5.10 provide interpretation of the dust mechanisms in relation to aims 2 and 3. The conclusions are presented in Section 5.11.

5.2. Data

This section describes observational data analysed in this paper, notably from the Fennec supersite at BBM, and supporting satellite and numerical model products.

5.2.1. The Bordj-Badji Mokhtar supersite during the Fennec 2011 IOP

The existing synoptic station of Bordj-Badji Mokhtar (21.38N, 0.92E; WMO ID: 60686; altitude 420m asl) was chosen as the location for Fennec supersite 1. It is located in south-western Algeria, near the border with Mali. BBM was heavily instrumented for almost the entire duration of June 2011, the first Fennec (IOP). *Marsham et al.* [2013] provide an overview of the meteorology over BBM for the period. The instrumentation consisted of a HALO Photonics Streamline 1.55μm Doppler lidar; a Scintec MFAS phased array sodar; a Cimel sun photometer; a vacuum pump aerosol sampler; an inverse nephelometer (670nm) and a real-time absorption reflectometer (both at 2m);

Vaisala RS92 GPS radiosondes (launched at three hourly to six hourly intervals) and a 15m mast (the 'flux tower') instrumented with 20-Hz sonic anemometers at 10m and 15m. At 2m on the mast pressure measurements and passively ventilated measurements of temperature and humidity were taken. A separate 2m mast was used to support a Kipp and Zonen CNR4 radiometer. Filters from the aerosol sampler are still being analysed and the data are not presented in this paper. There are individual periods when observations are missing: these are mentioned in the text and in the captions, where possible including the most likely explanation for the data gaps.

Instrument measurement accuracy is as follows: nephelometer scattering $\pm 10^{-7} m^{-1}$; relative humidity ±2%; temperature ±0.3°C; pressure ±0.5hPa; anemometer wind speed ±0.1m/s. Wind speeds are reported at 10m agl unless otherwise stated. The Doppler measurement precision of the lidar is $\leq 10 cm^{-1}$ in the boundary layer [*Pearson et al.*, 2009]; its minimum range is 75m above ground level (agl). A standard lidar inversion technique, the Klett-Fernald method, is employed to obtain the aerosol backscatter coefficient profile [*Fernald et al.*, 1972; *Klett*, 1981; *Fernald*, 1984]. Lidar horizontal wind speed and direction measurements are derived using a using a modified velocity-azimuth display algorithm [*Browning and Wexler*, 1968; *Banta et al.*, 2002] and have an accuracy of ±0.1m/s and ≤0.9° respectively[10]. Aerosol Optical Thickness (AOT) is reported at 500nm and the Ångstrom exponent (α) is calculated from 440 and 675nm. Both AOT and α are level 1.5 (cloud-screened). AOT is accurate to ±0.01. The sun photometer formed part of the AERONET project [*Holben et al.*, 1998] during its deployment. Unless otherwise stated, times are all in UTC.

[10] Information on the accuracy of the lidar-derived wind direction retrieval is not readily available. In a study using an identical Doppler lidar, *Newsom et al*. [2013] found that the difference between the wind direction measured by sonic anemometer and wind direction retrieved by lidar was up to 0.9°.

5.2.2. Satellite and numerical model data

False colour imagery from SEVIRI on board the Meteosat Second Generation satellite at 0N, 0E [*Lensky and Rosenfeld*, 2008] is used to help identify deep cloud and dust. Colours map onto features as follows - deep cumulonimbus: dark red; thick water clouds: gold; clouds with small particles: green; thin cirrus: black; desert dust: pink; surface quartz sand: light blue/grey. The Cloud-Aerosol Lidar with Orthogonal Polarization [*Winker et al.*, 2003] on board the CALIPSO satellite is used to provide information on aerosol profiles. Operational fields (18h UTC initialisation) from the UK Met Office Africa Limited Area Model (LAM), 12km resolution, are used to provide a regional context for interpretation of the supersite data.

5.3. Detection and attribution of dust events at BBM

The time series of nephelometer scattering (Figure 5-1a) during June 2011 was used to identify dust event periods. Since this is the sampling base, from now onwards the IOP will be defined as the period when nephelometer scattering data are available (i.e. from 2020 on 5 June to the end of 30 June). Nephelometer scattering at 670nm can be used as a proxy for dustiness since (i) dust scatters visible light [e.g. *Redmond et al.*, 2010] (ii) mineral dust is the dominant aerosol in the region, especially in summer [*Herman et al.*, 1997; *Engelstaedter et al.*, 2006]. Ground-based nephelometer scattering has also been used previously as a criterion for dust event identification [*Andreae et al.*, 2002]. At 2m height, the nephelometer scattering will identify both local emission and also advection [*Marsham et al.*, 2013]. Any period where nephelometer scattering $>2x10^{-4}m^{-1}$ was designated a ‘dust event’; below this threshold it proved very difficult to unambiguously determine any individual events. 32 individual events were identified in this way. The peak nephelometer scattering of each event was then used to rank them by strength. Ranking was not performed using the lidar data since in situations when the lidar beam

is strongly attenuated, column-integrated lidar measurements will not give a true representation of the strength of an event. The sun photometer was not used to create a ranking since it provides no nocturnal data and therefore misses many dust events (10/32 events started between sunset and sunrise).

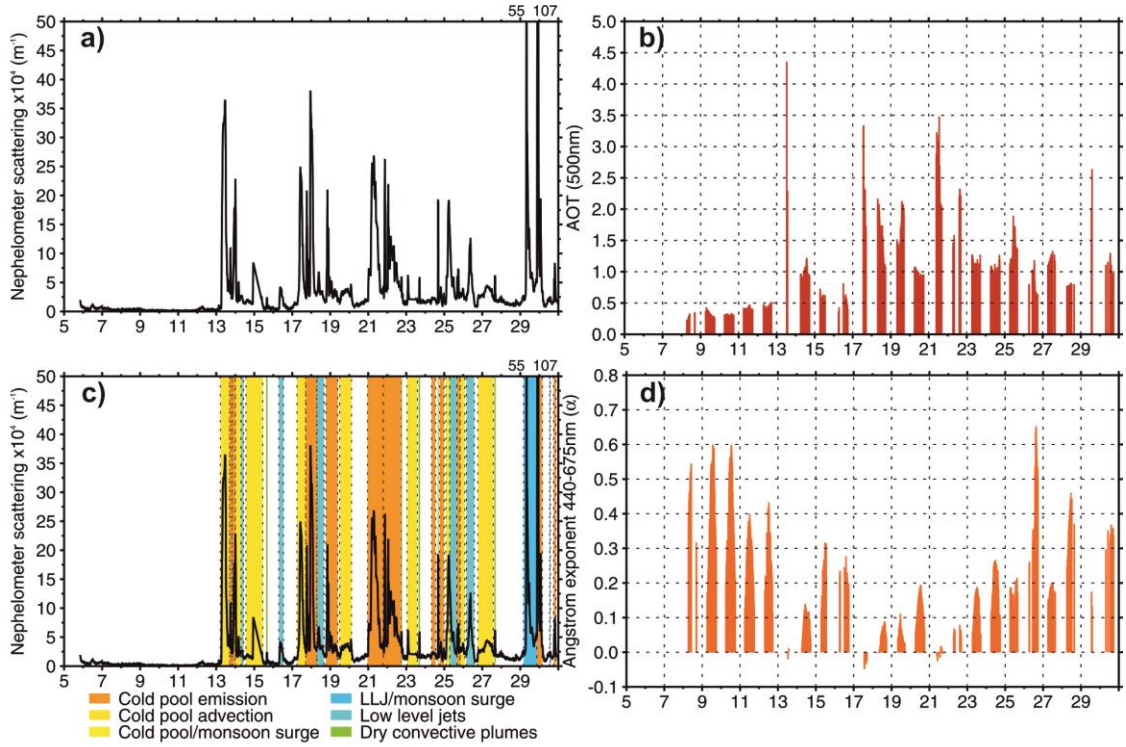

Figure 5-1. Time series, BBM, June 2011. Date is along x-axes. (a) 670nm nephelometer scattering (x10^{4}m^{-1}). Nephelometer not deployed until 5 June. The numbers at the top right are nephelometer scattering (x10^{4}m^{-1}) for two peaks which are off the scale. (b) 500nm aerosol optical thickness (measurements prior to 8 June contain calibration errors and are not shown) (c) nephelometer scattering as (a) but showing event classification in colours (see Section 5.3). Event classed as advection if wind speed ≤6m/s (Section 5.4). (d) 440-675nm Ångstrom exponent (measurements prior to 8 June contain calibration errors and are not shown).

Each of the 32 dust events were attributed to their most likely causal mechanism (Figure 5-1c). This was done using all available observations made at BBM, SEVIRI false colour composites and Africa LAM fields, using existing literature as a guide for attribution. Lines of ground-based evidence to help attribution include: (i) sudden changes in humidity, temperature and pressure to identify cold pool outflows [e.g. *Miller et al.*, 2008; *Emmel et al.*, 2010] (ii) timing of events: LLJs likely to lead to dust emission in the mid-late morning, dry convective plumes most likely to occur in the afternoon when surface temperatures are highest (iii) structure in lidar backscatter

profile: a raised ‘nose’ is likely to be the leading edge of a haboob [e.g. *Solomos et al.*, 2012], a narrow spire of raised backscatter is likely to be from a dry convective plume [e.g. *Cuesta et al.*, 2008] (iv) timing of wind speed changes: a progressive change is likely to be associated with momentum mix-down from a LLJ [e.g. *Washington et al.*, 2006] whereas a sudden spike is likely due to the passing of a cold pool gust front [e.g. *Miller et al.*, 2008] or dry convective plume if the prior winds are <7m/s [*Ansmann et al.*, 2009].

Lines of satellite evidence for attribution include presence of deep convection and possibly arcus clouds for cold pool outflows [*Knippertz et al.*, 2007] and identification of dust storm origin by backtracking 15-minute SEVIRI timesteps. Additionally, Africa LAM fields provide important continental-scale context, although cold pools will not be represented since the resolution (12km) is too low and convection is parameterized [*Marsham et al.*, 2011; *Solomos et al.*, 2012]. An ‘automated’ approach to determine the dust production mechanism in each case was considered but not used since most time series (especially the flux tower measurements) have several gaps (explained in the captions e.g. on 13, 17, 21, 29 June). Key observations for the strongest dust events during the IOP including wind speeds, Ångstrom exponents, AOT, SEVIRI, event duration and nephelometer scattering are given in Table 5-1.

Table 5-1 (overleaf): Diagnostics of the strongest dust events for each atmospheric dust production mechanism observed at BBM during the IOP. The ranking/identification process is discussed in Section 5.3. For discussion of categorization of dust as advected/emitted/mixed and thresholds see Section 5.4. Ångstrom exponents presented are averaged over the course of each event. Both event peak AOTs and event-averaged AOTs are shown. Dust layer thickness statistics are based on the height of the 10^{-5} $m^{-1}sr^{-1}$ lidar backscatter contour and are likely to be conservative, especially in cases of attenuation. For discussion of dust layer heights see Section 5.5. CBL=convective boundary layer, top height is diagnosed from radiosondes (defined as height at which potential temperature begins to increase with height). N/A=not available, N/I=not identifiable.

DATE (June 2011) & START TIME	OVERALL NEPHELOMETER RANK	NEPHELOMETER RANK BY MECHANISM	ADVECTION/ EMISSION/ MIXTURE?	DUST IDENTIFIED ON SEVIRI?	440-675 nm ÅNGSTROM [α] event average	500nm AOT peak (event average)	DURATION [h]	PEAK NEPH. SCATTERING [x10^{4} m^{-1}]	WIND SPEED [m/s] at peak neph. scattering	MINIMUM DUST LAYER THICKNESS [m] (time observed)	CBL HEIGHT [m] (time observed)
Cold pool outflows											
29th 22h	1	1	Emis	Y	N/A	N/A	6.8	107	17.5	300 (21h)	N/A (21h)
17th 17h	3	2	Emis	Y	N/A	N/A	9.8	38	11	800 (21h)	N/I (21h)
13th 0530h	4	3	Adv	Y	-0.01	4.4 (3.3)	11.7	36.5	6	300 (9h)	400 (9h)
20th 23h	5	4	Mix	Y	0.00	3.5 (2.5)	20	27	7	500 (12h on 21st)	800 (12h on 21st)
21st 19h	6	5	Mix	Under cloud	0.06	2.3 (1.8)	22.7	26.5	7	600 (18h)	3200 (18h)
17th 06h	7	6	Adv	Y	-0.03	3.3 (2.2)	11	25	2.5	500 (12h)	800 (12h)
Low level jets											
29th 0730h	2	1	Emis	3h late and not that pink	0.15	2.6 (2.3)	13.4	55	19	700 (12h)	900 (12h)
26th 06h	12	2	Emis	N	0.33	1.2 (0.9)	8.2	13	15.5	400 (9h)	400 (9h)
18th 07h	17	3	Emis	no signal in background dust	0.05	2.2 (1.7)	9.1	7	8.5	500 (12h)	1000 (12h)
25th 07h	22	4	Emis	N	0.19	1.9 (1.4)	8.8	6	11	600 (12h)	1600 (12h)
16th 07h	25	5	Emis	3h late and not that pink	0.25	0.8 (0.8)	6	4.5	15	400 (9h)	N/I (9h)
Dry convective plumes											
24th 16h	11	1	Emis	N/A	0.11	1.2 (1.2)	1.2	19	11	1300 (16h)	3600 (15h)
27th 15h	19	2	Emis	N/A	0.17	1.2 (1.2)	2	6.5	11.5	800 (16h)	4400 (15h)
23rd 16h	20	3	Emis	N/A	0.08	1.3 (1.2)	2.2	6	11	1000 (17h)	4600 (15h)
22nd 18h	21	4	Emis	N/A	N/A	N/A	1.1	6	10	1000 (18h)	4600 (18h)

5.4. Distinguishing local emission from dust advection

Distinguishing local dust emission from dust advection over the site is difficult to do with the instrumental setup available (Section 5.2.1). AOT, lidar backscatter and nephelometer scattering at 2m provide measurements of dustiness, as distinct from dust emission. Ångstrom exponents are sometimes used to help distinguish emission from advection [e.g. *Knippertz et al.*, 2009] but here it is difficult since (i) so many events occur at night when the sun photometer is not operational (Section 5.3) (ii) it is not clear that at BBM low Ångstrom exponents imply local emission (discussed in Section 5.9). *Marsham et al.* [2013] use uplift potential, the wind dependent component of the *Marticorena and Bergametti* [1995] dust uplift parameterisation, to separate emission from advection at BBM. However, they still report uncertainty regarding the wind speed threshold for emission.

Here, we propose a local emission threshold based on a dust event which, of all the events during the IOP, shows the strongest evidence for local dust emission. This evidence is (i) changes in wind speed correspond closely to changes in 2m nephelometer scattering (Figure 5-2a) (ii) the increases in 2m nephelometer scattering lead lidar backscatter (which only measures above 75m) by up to two hours (Figure 5-2b) (iii) the mid-morning timing of the wind speed increase suggests that it represents local LLJ momentum mixing down to the surface. During this event (ranked 12th dustiest of the IOP), the relationship between wind speed and nephelometer scattering shows a clear threshold at 8m/s. Below 8m/s, nephelometer scattering is low and has a narrow range between $3x10^{-4}m^{-1}$ and $4.5x10^{-4}m^{-1}$. Above 8m/s, although there is some variability, the general trend is a substantial increase in nephelometer scattering up to $13x10^{-4}m^{-1}$ (Figure 5-2c).

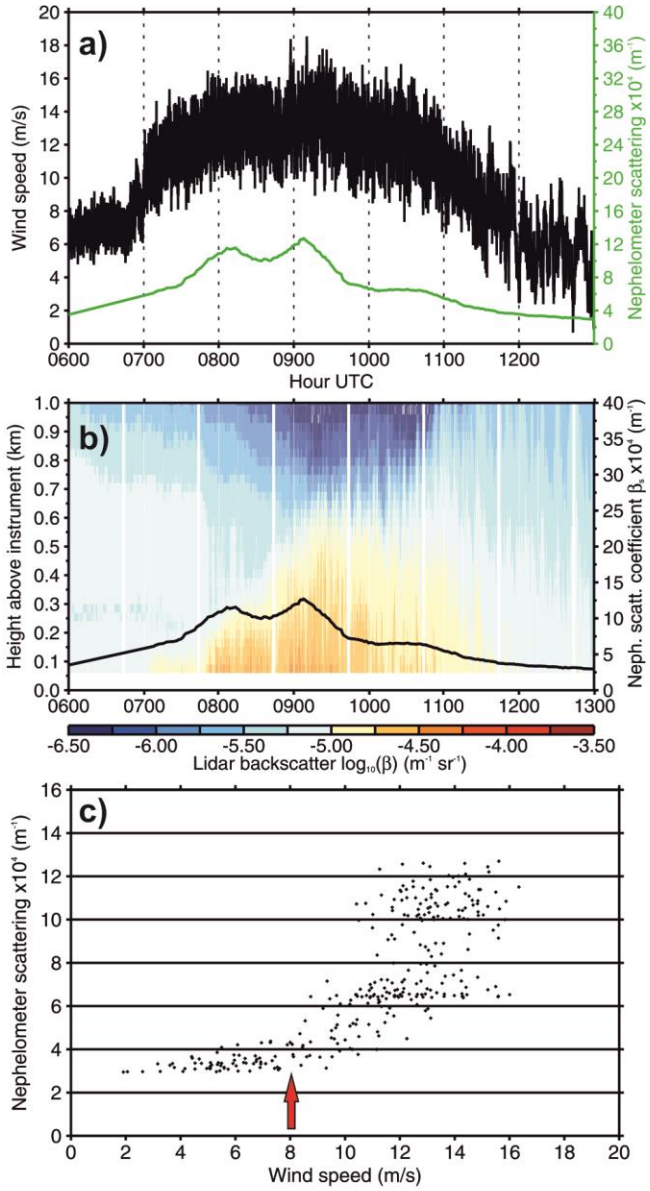

Figure 5-2: The local LLJ-induced emission event of 26 June 2011: (a) timeseries of 10m wind speed (m/s, black) and 670nm nephelometer scattering (x10^{4}m^{-1}, green) (b) timeseries of 1.55µm lidar backscatter, β, (colour contours show log(β), m^{-1} sr^{-1}) and nephelometer scattering (black) (c) scatter plot of 10m wind speed against nephelometer scattering for the same period as (a) and (b) i.e. 0600-1300. The red arrow shows the identified emission threshold at 8m/s. Full details in Section 5.4.

The choice of an 8m/s threshold for emission is similar to other work: *Marticorena et al.* [1997] and *Callot et al.* [2000] suggest a 7.5m/s threshold for the 1° box containing BBM (also for winds at 10m height). In order to take into account related studies and

the fact that some dust events may contain a mixture of advected and locally emitted dust, we propose a range as follows. Advected dust: wind speed ≤6m/s (the lowest threshold in the range chosen by *Marsham et al.* [2013]). Mixture of advected and emitted dust: 6<wind speed<8m/s. Locally emitted dust: wind speed ≥8m/s (Table 5-2). The classification of an event as advected dust/emitted dust/mixed is done once based on the average wind speed of the dust event.[11]

Table 5-2 (below): Wind thresholds used to discriminate between local dust emission and dust advection. Wind speed is at 10m height. See Section 5.4 for full details.

Type	Threshold
Local emission	Wind speed ≥ 8m/s
Advected dust	Wind speed ≤ 6m/s
Mixture of advected and emitted dust	6<Wind speed<8m/s

5.5. Estimating dust storm heights

Estimating the height of dust storms at BBM during the IOP proved problematic since on many occasions (particularly during cold pool outflows) the lidar signal was strongly attenuated. Since AOT values were so high there was little the inversion procedure could do about this. *Williams et al.* [2009] report haboob dust top heights in Niamey, Niger, for 12 late summer cases to vary from 2000 to 5000m with a mean of 3500m, substantially higher than suggested by the lidar data at BBM. This may be partly because Niamey is further away from the main summer dust source regions than BBM [*Schepanski et al*, 2007; *Ashpole and Washington*, 2012]. But as the attenuation of the lidar backscatter makes determination of the heights from this dataset difficult, we

[11] In Chapter 7 (Section 7.4) this is refined and assessed at 15 min intervals.

suggest the depth of the convective boundary layer (CBL) as a guide for maximum dust plume height. Within the CBL, dust will be mixed fairly rapidly. The top of the CBL is defined as the height at which potential temperature (derived from the radiosondes) begins to increase with height. However, this proxy is only strictly valid for events which are caused by local emission, when the dust will for a short time at least not be elevated/penetrate into the Saharan residual layer [*Cuesta et al.*, 2009; *Messager et al.*, 2010]. This proxy is not valid for dust some way behind the leading edge of cold pools which can be lifted above the CBL [*Flamant et al.*, 2007; *Bou Karam et al.*, 2008]. However, attenuation limitations notwithstanding, this particular scenario does not appear to have occurred at BBM during the IOP. CBL heights, where identifiable, are included in Table 5-1, together with a gauge for the absolute minimum dust layer thickness, the height of the 10^{-5} $m^{-1}sr^{-1}$ lidar backscatter contour. This will be particularly conservative in cases of strong attenuation, as discussed.

The CALIPSO space-borne lidar can be used to gauge dust plume heights. However, CALIPSO data are not available on 4 June or 6-14 June 2011. Of the remaining days, there is only one case (early morning of 18 June) for which the satellite passes close enough to BBM and at the right time to gauge dust plume height. On this case, thick dust is detected to 2000m above the surface (not shown). Wind speeds of between 4 and 8m/s at the time of the overpass suggest that it is dust remaining from the strong emission event of the previous night (see Section 5.7.2.2).

5.6. Dust detection by SEVIRI

The false colour SEVIRI satellite dust detection algorithm [*Lensky and Rosenfeld*, 2008], is used frequently to identify dust over the North African region, both for nowcasting and for research [*Schepanski et al.*, 2007; *Knippertz*, 2008; *Marsham et al.*,

2008; *Bou Karam et al.*, 2010; *Knippertz and Todd*, 2010; *Ashpole and Washington*, 2012; *Marsham et al.*, 2013]. Central to the appeal of SEVIRI is the very high temporal resolution of the data (15 minutes), which allows qualitative inspection of emission sources and inference of mechanisms. In the case of the central Sahara, the performance of SEVIRI has been difficult to assess owing to the paucity of comparatively high quality ground-based observations. In the case of data from BBM, SEVIRI is more reliable in identifying cold pools than LLJs (Table 5-1). With sufficient moisture, cold pool outflows can generate a line of arc clouds along the leading edge [e.g. *Knippertz et al.*, 2007]. Five of the six haboobs listed are detectable in SEVIRI but one event is not as the area is covered by cloud. Of the five strongest LLJ events at BBM in June 2011, none is clearly detectable using SEVIRI (Table 5-1). Two are not identifiable at all, one is not detectable against the background dust, and two are detected three hours after the lidar on the ground detects them, and do not show up strongly as the cold pool events. One possible reason for the missed SEVIRI detection of the LLJs is that the dust generated by the breakdown of the LLJ does not penetrate deep enough into the atmosphere to be identified by the algorithm, although precise dust heights are difficult to establish (Section 5.5; Table 5-1).

As demonstrated by *Brindley et al.* [2012], SEVIRI detection can also fail if a surface temperature inversion is present in the early hours of the morning. This is the case at 0600 on the LLJ days of 16 and 29 June for example. This would also explain why, during the 13 and 17 June cold pool events which arrive at BBM at roughly 0600, the SEVIRI images do not appear bright pink until the late morning, 2-3 hours after the dust maximum in the lidar backscatter and after the inversion has been broken. On 13 June, the 0600 surface inversion is about 2°C (Figure 5-7h); on 17 June it is about 5°C (Figure 5-5h). Since many cold pool outflows arrive at BBM in the late afternoon or

early evening (Figure 5-1c), when a temperature inversion is not present or only beginning to develop, they tend to be detected more easily by the algorithm.

If the SEVIRI algorithm has difficulty detecting LLJ-induced emission in other regions of the Sahara, analyses based on SEVIRI may be under-representing the importance of LLJs for Saharan dust uplift. There is therefore a possibility that results such as those of *Schepanski et al.* [2009], which already point to the importance of low level jet breakdown as a dust emission mechanism, are conservative.

5.7. Analysis of dust mechanisms at BBM during the IOP

In this section, the three principal dust mechanisms in operation at BBM (cold pool outflows, low level jets and dry convective plumes) are analysed in turn. Each subsection contains a selection of case studies, followed by a discussion of notable characteristics.

5.7.1. Cold pool outflows

A total of 20 cold pool outflow events were identified over BBM during the IOP; 9 containing mostly advected dust and 11 generating local emission or at least containing a mixture of local and advected dust (see Section 5.4/Table 5-2 for how the distinction is defined). This is a high number of such events: for comparison, *Todd et al.* [2013] report only 4 cold pools reaching Fennec supersite 2 at Zouerate, western Mauritania, during the June 2011 IOP and *Cuesta et al.* [2008] report only 8 cold pools between May and September 2006 at Tamanrasset, southern Algeria. In the former case this small number is probably mainly due to the long distance between Zouerate and both monsoon and Atlas convection; in the latter case it is likely because the rock/gravel soil at Tamanrasset is too coarse to permit much local emission [*Callot et al.* 2000; *Cuesta et al.* 2008] therefore for the most part only advected dust contributes.

The dustiest four cold pool outflow events during the Fennec IOP (as ranked by the nephelometer timeseries, Table 5-1 and Figure 5-1) are presented here.

5.7.1.1. 29 June 2011 21h

By far the largest peak in the nephelometer scattering time series (107×10^{-4} m^{-1}, almost twice as high as the next highest peak at 0730 the same day; Table 5-1) is the haboob event beginning at 21h on 29 June. On the evening of 29 June, BBM is just to the south of the centre of the Saharan Heat Low (SHL). The centre is very well defined, with the highest 925hPa temperatures (>39.5°C) and lowest geopotential heights (<730hPa) almost exactly co-located (Figure 5-3c). The SHL location is between the June and July mean presented by *Lavaysse et al.* [2009], as expected for a date so late in June. SEVIRI shows deep convection developing to the SW of the Hoggar Mountains in southern Algeria from midday on 29 June. The moisture for this convection is provided by a monsoon surge which arrives in the morning (Figure 5-4h and see also *Marsham et al.* [2013]); the surge is likely promoted by the strong SHL centre to the north of BBM. At 1830 a density current/dust front begins to propagate westwards away from the convective system, with its leading edge marked by a thin band of cloud. These may be arc clouds, which have been observed at the leading edge of density currents propagating downslope from the Atlas Mountains [*Knippertz et al.*, 2007]. The arc cloud/haboob front passes over BBM at 2130 (Figure 5-4f), in excellent agreement with the lidar and nephelometer observations (Figure 5-4a).

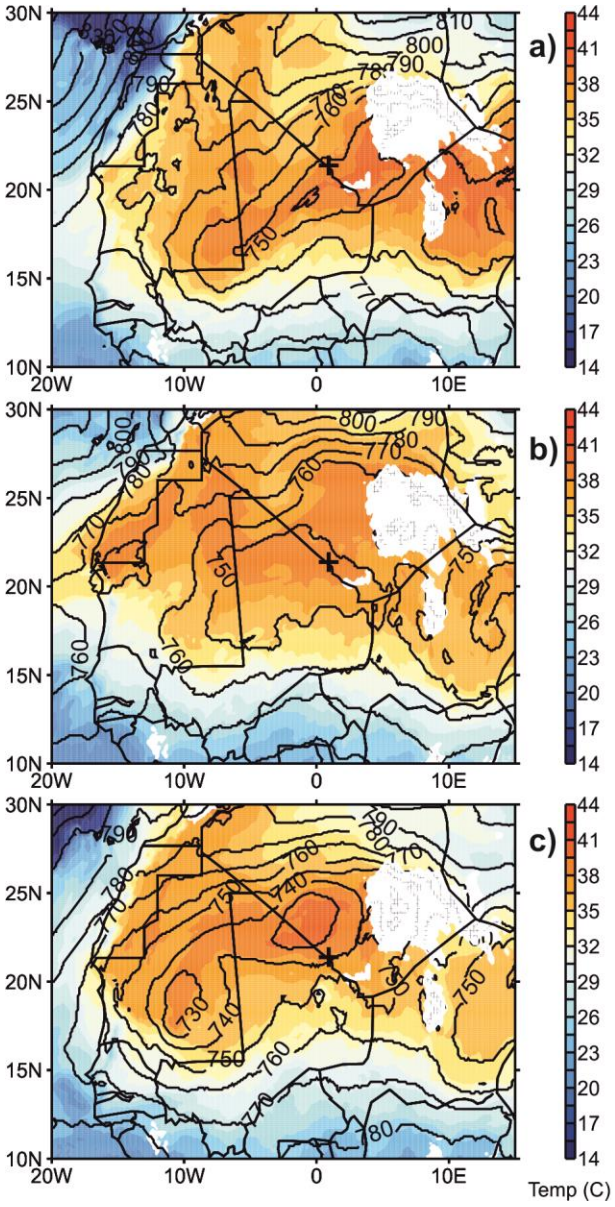

Figure 5-3. The evolution of the Saharan heat low (a) 17 June 2011, 1800 (b) 24 June, 1800 (c) 29 June, 1800. Colour contours show 925hPa temperature (°C) and lines show 925hPa geopotential height. Transparent white regions denote orography above the 925hPa level. Cross shows location of BBM.

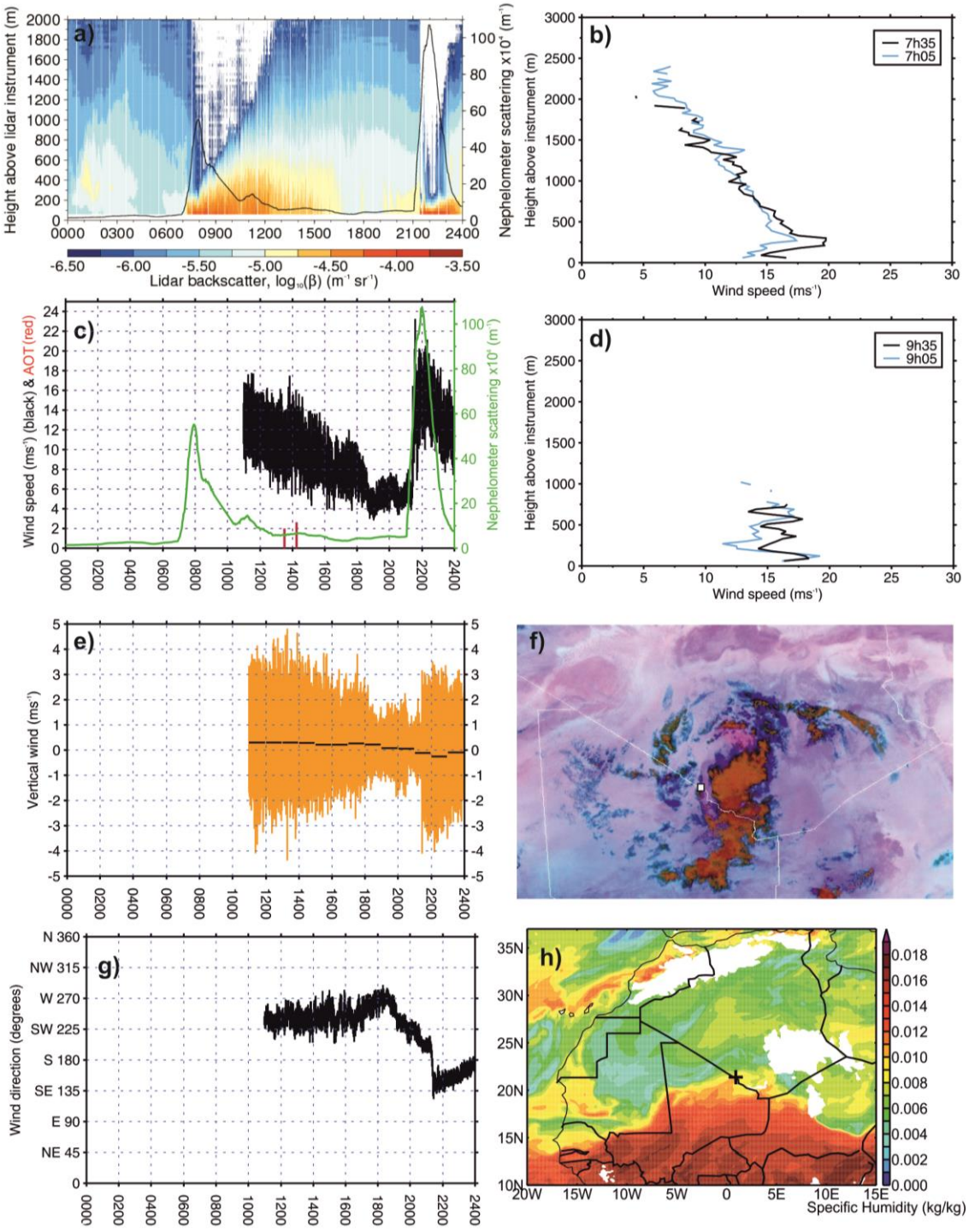

Figure 5-4. Dust events of 29 June 2011 at BBM: a monsoon surge/LLJ (from 07h) and cold pool (from 21h). (a) lidar backscatter (contours) and nephelometer scattering (line). Note the scattering axis spans a range almost 3x greater than plots for other days. (b) and (d) lidar wind speed profiles (c) 10m wind speed (black), nephelometer scattering (green) and 500nm AOT (red bars, same axis as wind speed) (e) 10m vertical wind (+ve upward, lines show hourly mean) (f) SEVIRI dust detection algorithm image centred on BBM (square) at 2130, see colour key in Section 5.2.2 (g) 10m wind direction (h) 0900 Africa LAM specific humidity (925hPa. Cross marks BBM location). Flux tower data (i.e 10m wind speed, direction and vertical component) are missing prior to 1030, in the late morning possibly due to the strong winds mixed down by the LLJ.

At 2130 10m winds show a sharp surge from 6m/s to almost 22m/s, then steadily decrease until midnight with fluctuations between 9m/s and 20m/s (Figure 5-4c). These wind speeds are more than strong enough for local dust emission. Vertical winds (w) also show a strong jump at 2130, from roughly ±1m/s to ±3m/s (Figure 5-4e). The hourly mean vertical winds during the event are all negative (net downward component). With the passing of the front, relative humidity shows a rapid drop and rise of 2%, corresponding to a fluctuation in dew point temperature of 2.9°C (from 18.6°C to 15.7°C). This is followed by a slightly more gradual decrease to a plateau at 32% (not shown). Recorded temperatures show the same structure: a rapid drop and rise of 2.5°C, followed by a slightly more gradual decrease to plateau at 32°C. At 2130 there is also a sharp decrease in pressure of 1hPa, and wind direction rapidly changes by 50° from roughly 200° (SSW) to roughly 150° (SSE) (Figure 5-4g). There are no Cimel sun photometer measurements of the cold pool since it passes at night.

5.7.1.2. 17 June 2011 06h

The haboob that occurs on the morning of 17 June has the 7th highest peak in nephelometer scattering of the IOP (Table 5-1), 25x10^{-4} m^{-1} at 1020. SEVIRI shows that the dust arrives at BBM as part of a cold pool outflow, which is spawned from a mesoscale convective complex (MCC) over western Niger. The density current begins to propagate northwestwards from the MCC at 1800 on 16 June and the front arrives at BBM at 0600 on 17 June (Figure 5-5a,g), covering 500km in 12 hours with an average speed of 11.6m/s. SEVIRI-based estimates of propagation indicate that the current slows down as expected as it progresses: between 1800 and 2100 the leading edge average speed is 18.1m/s; between 0300 and 0600 this reduces to 10.5m/s.

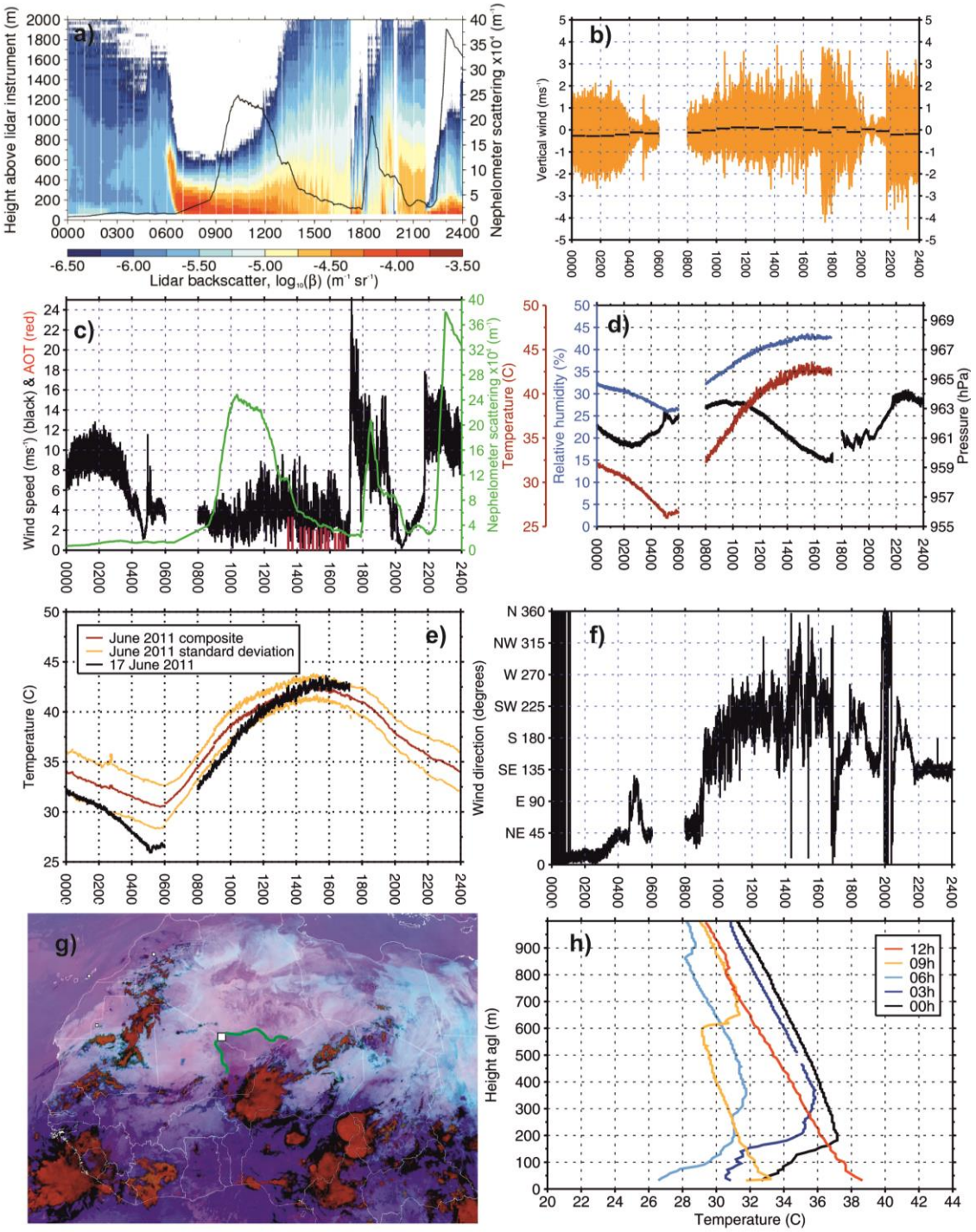

Figure 5-5. Dust events of 17 June 2011 at BBM: three cold pools starting 06h, 17h, 22h. (a) lidar backscatter (colour contours) and nephelometer scattering (line) (b) 10m vertical wind (+ve upward; lines show hourly mean) (c) 10m wind speed (black), nephelometer scattering (green) and 500nm aerosol optical thickness (red bars) (d) 2m temperature, relative humidity and pressure (e) 2m temperature comparison with June 2011 composite and standard deviation (f) 10m wind direction (g) SEVIRI dust detection algorithm image at 0600. BBM is shown as a white square on the Algeria/Mali border. The dust front is outlined in green. (h) radiosonde temperature profiles. Flux tower data (i.e. 2m temperature, relative humidity and pressure; 10m wind speed, direction and vertical component) are missing from 0600-0800. For the winds, this may be due to the anticipated strong winds and turbulence at the gust front. Temperature and relative humidity data are unrecorded from 1715.

Near 0500, one hour before the dust arrival at BBM, there are two spikes in 10m wind speed (11.5 and 8.2 m/s, Figure 5-5c) accompanied by two jumps in pressure with a sudden 0.8hPa drop in between (Figure 5-5d). 10m wind direction (Figure 5-5f) at 0500 is south easterly (the direction from which SEVIRI shows the density current to propagate), in contrast to the northerlies and north-easterlies that occur before and after. The mentioned changes are short-lived (wind speed subsides after 15 minutes) and are not followed by a near-surface temperature decrease (Figure 5-5). As such they fulfil the typical criteria used to define a bore (Section 5.1.2.1), suggesting that one precedes the density current which brings the dust to BBM.

At 0600 at BBM there is a clear jump in lidar backscatter values from $10^{-5.5}$ $m^{-1}sr^{-1}$ to $10^{-4.25}$ $m^{-1}sr^{-1}$ above 400m agl (Figure 5-5a). Flux tower data was not recorded from 0600 to 0800, possibly due to strong winds in the gust front damaging the instrumentation, but this cannot be verified since the only other wind observations are from the local station at 0600 (before dust is detected at the surface) which record a speed of only 4.1m/s. The haboob arrives at BBM with a raised nose, the structure of the lidar backscatter suggesting it is tilted towards the direction of the propagation (Figure 5-5a). The nephelometer scattering data supports this hypothesis, as nephelometer scattering values (at 2m agl, Figure 5-5a) only begin to increase half an hour after the dust is seen in the lidar backscatter, once the main body of the current arrives. Combined with SEVIRI-based estimates of the leading edge propagation between 0600 and 0630, this suggests that the nose has a horizontal extent of 9.9km.

The increase in scattering from 0800 onwards is coincident with a steady increase in the magnitude of the 10m vertical wind (not shown). The minimum dust layer thickness is 500m at 1200, 300m below the CBL height of 800m (Figure 5-5a, Table 5-1). The dust

storm is also represented in the AOT (peak of 3.3 at 1330, Figure 5-5c). There are no AOT data before 1330 on 17 June, and since the lidar and nephelometer peak several hours before 1330, it is likely that at its thickest, the AOT was greater than 3.3, making it a very major dust storm.

Throughout the passage of the density current over BBM (i.e. until roughly 1700), 10m horizontal wind speeds are low, fluctuating mainly between 1 and 7 m/s (Figure 5-5c) . At the time of peak nephelometer scattering, wind speed is only 2.5m/s (Table 5-1). This suggests that the dust is mostly advected (Section 5.4; Table 5-2). Ångstrom exponents for this event are all below 0 where recorded and as low as -0.04 (Figure 5-1d) which implies large particle sizes. These Ångstrom exponents are the lowest over the 2011 IOP. This is somewhat surprising since large particle sizes are usually more dominant in freshly emitted rather than transported dust (in this case, transported some 500km; discussed further in Section 5.9).

5.7.1.3. 17 June 2011 17h

The third largest peak in the nephelometer time series for June 2011 (Table 5-1) was associated with a cold pool outflow that reached BBM at approximately 2140 on 17 June (Figure 5-5a). Nephelometer scattering peaks at $38x10^{-4}m^{-1}$ at 2300. This density current was proceeded by two others, at 0600 (discussed in Section 5.7.1.2) and at 1700 (Figure 5-5a). The 1700 and 2140 haboobs are described together since SEVIRI imagery suggests that both originate from the same convective cell, and unlike the 0600 event, wind speeds in both cases are suggestive of local emission (Figure 5-5c). The arrival of the 1700 cold pool outflow appears to disrupt the boundary layer structure: at 1500 the CBL height is 3200m, but at 1800 (still before sunset) a fluctuating stable layer is present up to 2000m, possibly caused by the cold pool (Figure 5-6). Above

2000m the air is well-mixed to 4000m, still growing into the residual layer, later in the afternoon than commonly observed in the Sahara [*Cuesta et al.* 2009]. At 2140 lidar backscatter shows a sharp transition from a dusty column up to at least 900m agl, caused by the 1700 haboob, to a much shallower but thicker dust layer (Figure 5-5c), which suggests that the backscatter after 2140 is high enough to attenuate the lidar signal.

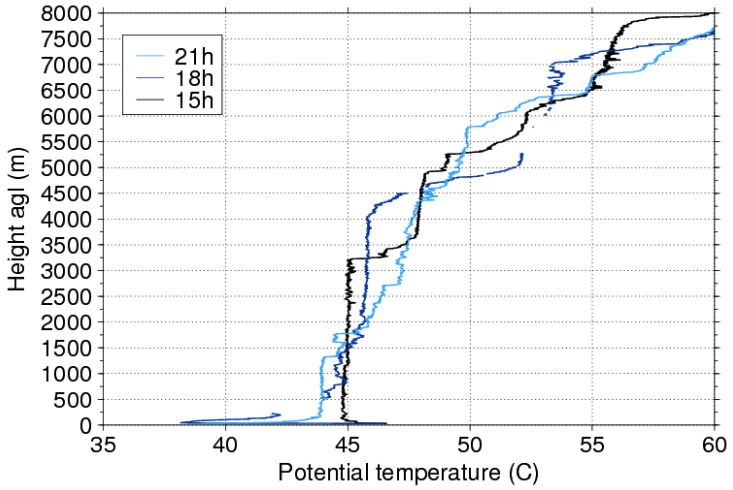

Figure 5-6: Radiosonde-derived potential temperature profiles from BBM, afternoon of 17 June 2011. Some points were removed from the 18h profile in the quality control process (pressures<0).

SEVIRI shows that the density current emanates from an MCC that evolves to the south west of the Hoggar, in a similar way to the 29 June evening cold pool (Section 5.7.1.1). The convection is evident from 1500 onwards, where it develops over an extensive dust layer. The convection is likely promoted by the very high temperatures to the south west of the Hoggar, over 39.5°C at 925hPa (Figure 5-3a). Geopotential heights over the region show that the SHL is not as intense as later in the month however (compare Figure 5-3c). Cloud is present over BBM from 1700 onwards. A haboob front emerges

from the MCC at 2015, and propagates south-westward. The satellite imagery shows the front crossing BBM at approximately 2130 (not shown), in very good agreement with the ground-based data. The density current then propagates radially out from BBM over a distance of approximately 300km during the following eight hours.

At 2140, 10m wind speeds jump from 6m/s to over 17m/s (Figure 5-5c), and vertical winds from ±0.5m/s to ±3.5m/s (Figure 5-5b). This is likely to be the signature of the gust front. Wind speeds then fluctuate between 8 and 16m/s until midnight. These speeds are high enough for local dust emission (Table 5-2). As on the evening of 29 June, hourly mean vertical winds during the event are all downward. The sodar (not shown) measured wind speeds >15m/s for all but the lowest 50m of the atmosphere after 2200. On 18 June, 10m wind speeds decrease from 10m/s at midnight to 3.5m/s at 0300 (Figure 5-8c). The nephelometer scattering follows this decreasing trend very closely, which is further evidence that the emission was local.

Wind direction at 10m during the passing of the density current was steady and southeasterly (Figure 5-5f). Between 2130 and 2200, the period within which the current front passed BBM, wind direction changed from southerly to southeasterly**.** There are no sharp changes in pressure in this period (Figure 5-5d); no coincident temperature or relative humidity data are available from the flux tower.

It is interesting that this cold pool event, the third strongest dust event over BBM in June 2011, followed another very strong haboob earlier the same day (see Section 5.7.1.1 above). Density currents are known to initiate convection under certain conditions, even far away from their origin [e.g. *Thorpe et al.*, 1982; *Carbone et al.*, 1990; *Moncrieff and Liu*, 1999] and convection can then issue new density currents. It is possible that the density current which arrived at BBM at 0600 helped promote the

convection that began at 1500 by enhancing lifting of air: the morning density current propagated from the south-east and prevailing winds were northeasterly. This positive feedback will be discussed further in section 5.7.1.5.

5.7.1.4. 13 June 2011 0530h

The cold pool outflow that arrived at BBM on 13 June at 0530 was the fourth largest event in the nephelometer timeseries (Table 5-1). It is similar to the 17 June event (Section 5.7.1.2). Nephelometer scattering peaks at $37x10^{-4}m^{-1}$ at 1120 (Figure 5-7a). The earliest Cimel AOT available on the day, at 1240, is 4.4 (Figure 5-7c), a remarkably high value (although it may be cloud contaminated: the lidar detects no clouds but a dust/cloud mix is present over the BBM region in SEVIRI, not shown). The cold pool was spawned from deep convection to the east of the Algeria-Niger-Mali triple point. It is visible in the SEVIRI imagery from about 1930 on 12 June. The dust/arc cloud front is most clearly visible at 2130 (Figure 5-7e). The front propagates westward towards the triple point and then veers north-westward. Its arrival is very clear in the BBM lidar backscatter (Figure 5-7a). The LAM 925hPa wind vectors (Figure 5-7g) suggest that the current propagates against a headwind and, as on 17 June, the elevated 'nose' (reaching at least 700m agl) arrives first and the nephelometer scattering only begins to increase an hour later, at 0630. At 0900, the minimum dust layer thickness is 300m, slightly below the CBL height of 400m (Figure 5-7a, Table 5-1). The average (SEVIRI-derived) propagation speed of the current from 1900 to 0530 is 16.2 m/s, 4.6m/s faster than the current on 17 June.

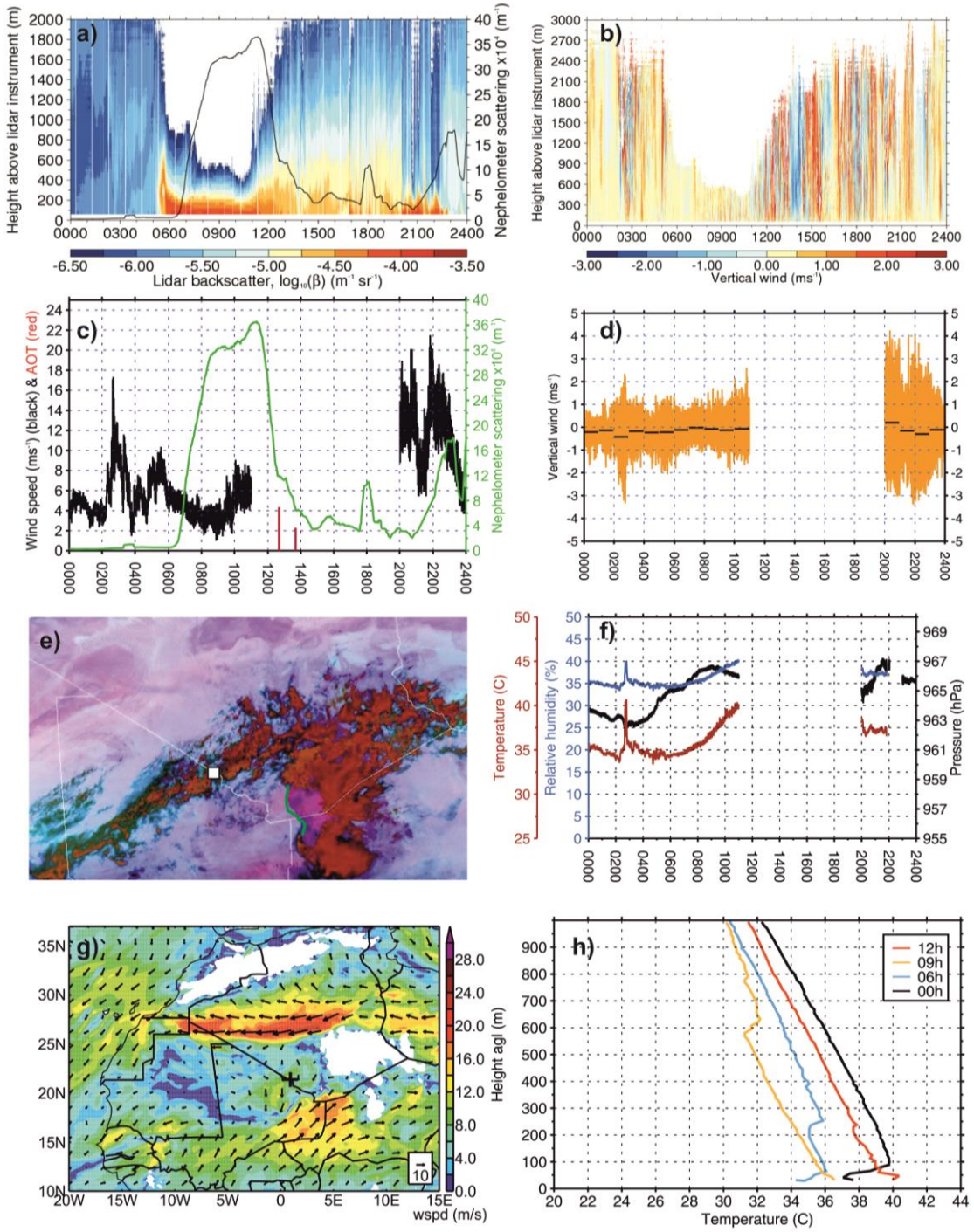

Figure 5-7. Dust events of 13 June 2011 at BBM: two cold pools: from 05h and from 20h. (a) lidar backscatter (contours) and nephelometer scattering (line) (b) lidar vertical wind (+ve upward) (c) 10m wind speed (black), nephelometer scattering (green) and 500nm AOT (red bars) (d) 10m vertical wind (+ve upward, lines show hourly mean) (e) 12 June 2130 SEVIRI dust detection algorithm image centred on BBM, with the dust front marked in green (f) 2m temperature, relative humidity and pressure (g) 0600 Africa LAM wind vectors (925hPa) (h) radiosonde temperature profiles. Flux tower data (i.e. 10m wind speed, vertical component; 2m temperature, pressure and relative humidity) are missing from 1030 to 2000. This is likely due to the voltage regulators of the tower overheating. Humidity and temperature are missing from 2200 to 2400.

At 0220, 3h10 minutes before the arrival of the haboob at BBM, surface pressure increases by 0.5hPa followed by a marked spike in 10m wind speed, up to over 17m/s (Figure 5-7). At the same time, the 10m vertical wind component shows an increase from roughly ±1m/s to -3.5<w<2.5m/s (Figure 5-7d). Similar values are seen in the lidar-derived vertical wind, up to 2800m agl (Figure 5-7b). This suggests that, as on the morning of 17 June, the density current may be preceded by a bore. Twenty minutes after the initial pressure increase, coincident sudden spikes in temperature (increase of 5.5°C) and relative humidity (increase of 5%) are observed (Figure 5-7f), the latter corresponding to a change in dew point temperature of 7.2°C (from 17.4°C to 24.6°C). The hourly mean w component at 10m is strongly downward at the time (Figure 7d). Radiosondes show that the temperature inversion below 100m agl is stronger at 0000 than at 0600 (Figure 5-7h). These findings all suggest mixing down of warm air at 0240, possibly caused by a bore, as can happen when one breaks a temperature inversion [*Clarke et al.*, 1981].

After the passing of the nose of the density current, 10m wind speeds are low. Between 0600 and 0800 they decrease from 5.5m/s to 3m/s, then from 0800 to 1100 increase to 6m/s (Figure 5-7c). This suggests, as on 17 June, that the dust passing over BBM behind the leading edge is transported, not emitted. Again like 17 June, Ångstrom exponents (measured at 1240 and 1340) are very low (-0.01, Table 5-1), suggesting that the dust particles are very large (see Section 5.9). No measurements are available from the flux tower from 1100-2000, probably due to the voltage regulators overheating. At 1800, the time of a nephelometer scattering spike to $11 \times 10^{-4} m^{-1}$, local station wind speed is 11.3m/s and dew point 8°C.

5.7.1.5. Notable cold pool outflow characteristics

In several cold pool outflow cases, the lidar backscatter (which is only available above 75m agl) leads the 2m agl nephelometer observations by up to several hours. A simple explanation for this is the elevated leading edge (or nose) of the cold pool outflows. A raised density current nose has been observed in other studies [e.g. *Sun et al.*, 2002]: as a density current propagates, surface drag slows down propagation speeds near the surface and an elevated nose develops. In the case of some events (e.g. 13 June, Section 5.7.1.4) the ambient winds may also have contributed to the elevation of the nose. *Liu and Moncrieff* [1996] have shown using a numerical model that flow against the propagation direction of density currents, as in this case, raises the nose. However, on the morning of 17 June, this raised nose is estimated to have a horizontal extent of 9.9km (Section 5.7.1.1), which seems rather extensive.

An alternative explanation for such an extensive apparent 'nose' is that the density current propagated above a stable nocturnal layer. This may have been the case on 17 June. However, since an elevated density current cannot produce dust uplift, the density current must have propagated along the surface before arriving at BBM and before a nocturnal temperature inversion began to develop. At some later time, the current (now with dust mixed within it) was raised above a strengthening surface inversion, possibly by isentropic upgliding, as it propagated northward. At levels above the surface, wind speeds are likely to be higher: this may explain why the current could carry such large particles within it (Ångstrom exponents all below 0, Table 5-1 and Figure 5-1d). There are no observational data to intercept these features between western Niger and BBM, but the propagation of a moist and dusty feature, with a clear leading edge, from NW Niger towards BBM is evident in SEVIRI (see Figure 5-5g).

Between 0600 and 0900, as the surface temperature inversion at BBM was eroded, the density current and the dust within it mixed down to the surface. There is some evidence to support this. Between 0000 and 0600, the three-hourly radiosonde launches show a strong (~5°C) temperature inversion between the surface and 200m agl (Figure 5-5h). A comparison of the 2m temperatures on 17 June with the June 2011 composite temperatures (Figure 5-5e) shows that before 0230 BBM 2m temperatures are colder than usual, at 1 standard deviation below the June mean, and after 0230 cool even more rapidly, becoming 5°C colder than the June mean at 0500. Under these conditions it is possible that the 'cold pool' could in fact be less dense than the surface, and therefore propagate towards BBM above the cold nocturnal surface layer [Marsham et al., pers. comm.]. Indeed, at 0600 the temperature of the dusty elevated density current (the layer between 400-800m agl, Figure 5-5a) is 28.5-31.5°C (Figure 5-5h) and the 2m temperature under the inversion is colder, 26.5°C (Figure 5-5e). As solar heating warms the surface, 2m temperatures begin to increase, the temperature inversion begins to erode and from 0600 onwards the dusty current mixes down to the surface.

Elevated cold pools have been shown in both theoretical and laboratory measurements, where such currents are known as intrusions [*Simpson*, 1997], occurring when a layer of intermediate density flows along the interface between a more and less dense layer of fluid; in this case, the nocturnal surface layer and the residual layer. Fluctuations evident in temperature, wind and pressure (e.g. near 0500 on 17 June, Figure 5-5) match the kind of features documented by *Liu and Moncrieff* [1996] in their 2D numerical model.

Several of the case studies describe events where cold pools follow each other in succession. On 9/12 occasions cold pools that occur in the morning, or persist through

the night into the morning, are followed by another in the afternoon. Additionally, on 3/3 occasions, cold pools that start in the evening are followed by a new cold pool in the morning. It is plausible that there is a 'positive feedback' of cold pool formation: cold pools which propagate into an area initiate convergence, which leads to an increase in convection and, potentially, the issuing of a new density current from the system. There are plenty of studies which deal with the role of density currents for initiating new convection [e.g. *Weckwerth and Wakimoto*, 1992; *Tompkins*, 2001]; *Miller et al.* [2008] also observed outflows in the Arabian Peninsula intensifying existing convective cells.

5.7.2. Low level jets

Dust emission from LLJs was identified on seven occasions from the nephelometer scattering timeseries (Section 5.3; Figure 5-1c), with an additional two such events identifiable in the lidar backscatter and synops station winds (not shown) prior to the activation of the nephelometer at 2020 on 5 June. The diurnal cycle at BBM during the IOP shows a period of increased nephelometer scattering coincident with increased wind speed between 0600 and 1200 (*Marsham et al*. [2013], their Figure 8). However, LLJ-induced dust emission does not occur every day. On several occasions the increases in wind speed and scattering could be at least in part caused by cold pool outflows (e.g. mornings of 13, 21, 22, 25 June; see also Section 5.8). Additionally, a LLJ is not present on every day of June 2011, and even when it is, momentum may not always be mixed down to the surface. LLJ-induced emission at BBM is higher than observed in Tamanrasset by *Cuesta et al.* [2008], who record only six events over the entire of 2006, probably due to the lower erodibility and possibly also the complex topography, but LLJs are not the dominant mechanism at BBM, as in the northwestern SHL region [*Todd et al.* 2013].

Two of the dustiest events at BBM associated with LLJs in June 2011 are presented next.

5.7.2.1. 29 June 2011

The morning of 29 June saw the second highest peak in the nephelometer scattering data, $55x10^{-4}m^{-1}$ at 0800 (Figure 5-4a, Table 5-1). Lidar backscatter values are high from 0700 to 1700 (Figure 5-4a). Two sun photometer measurements are available between 1300 and 1500 (Figure 5-1): AOTs of 2 and 2.6 and Ångstrom exponents of 0.175 and 0.13. (There may be some cloud contamination as SEVIRI detects cloud and dust in close proximity over BBM in this period.) The cause of the dust emission is a strong LLJ (clear in the LAM fields; not shown) which mixes down to the surface. Lidar wind profiles show a LLJ developing from midnight onwards. At 0735, wind speeds in the core of the jet (250m above the lidar instrument) reach just under 20m/s (Figure 5-4b). The lidar profiles then show the highest wind speeds propagate down towards the surface (Figure 5-4d; the lidar cannot measure below 75m however). Sunrise on 29 June was at 0516; in the following hours it is likely the surface was heated enough to mix the momentum from the LLJ down to the surface and lead to dust emission. No radiosonde was launched at 0900 but by 1200, the CBL had grown to a height of 900m and the minimum dust layer thickness was 700m (Figure 5-4a, Table 5-1).

Wind speeds from the flux tower are not available until 1100, after which they fluctuate between 9 and 17m/s (Figure 5-4c). The 10m vertical wind component from 1100 to 1700 is also very high, with peaks reaching <-4m/s and >+4m/s, highly turbulent conditions (Figure 5-4e). The 0900 reading from the local meteorological station reports a wind speed of 19m/s and ‘light sandstorm’ conditions. Wind directions are

southwesterly in the local station data at 0900 and 1200, in the flux tower data from 1100 to 1700 (Figure 5-4g), and in the Africa LAM model over the course of the entire morning (not shown). Observed dewpoint temperatures are 15°C at 0900 and 1200. This suggests that the LLJ is embedded in a monsoon feed, which is supported by the LAM 925hPa specific humidity which shows a tongue of relatively moist (0.01kg/kg) air over southern Algeria over the course of the morning (Figure 5-4h). Indeed, the event shows some similar characteristics to a monsoon surge, especially in this large-scale northward penetration of moisture. However, the timing of the dust emission, mainly from 0700-1300 (Figure 5-4a), and of the wind speed propagation to the surface (Figure 5-4b and d) conforms more to a LLJ-breakdown scenario than a monsoon surge. In monsoon surges, dust emission can be observed before dawn (not the case here) since the surge acts as a density current [*Bou Karam et al.*, 2008]; see also discussion in *Marsham et al.* [2013]. It is nonetheless possible that the monsoon incursion promoted the strong winds in the LLJ core.

Dust from the LLJ is not readily identifiable from the SEVIRI imagery. This is likely because the relatively high moisture levels around BBM at the time are causing the algorithm to fail (*Brindley et al*. [2012]; see also Section 5.6)

5.7.2.2. 18 June 2011

The morning of 18 June has high dust concentrations recorded in both the nephelometer scattering and lidar backscatter (Figure 5-8a). In the early morning this is due to a strong haboob that occurred the prior evening (see Section 5.7.1.3 above); however there is also evidence of a weak low level jet breakdown contribution to the dust loading later in the morning. The event is the 3rd dustiest LLJ of the IOP but only 17th overall (Table 5-1).

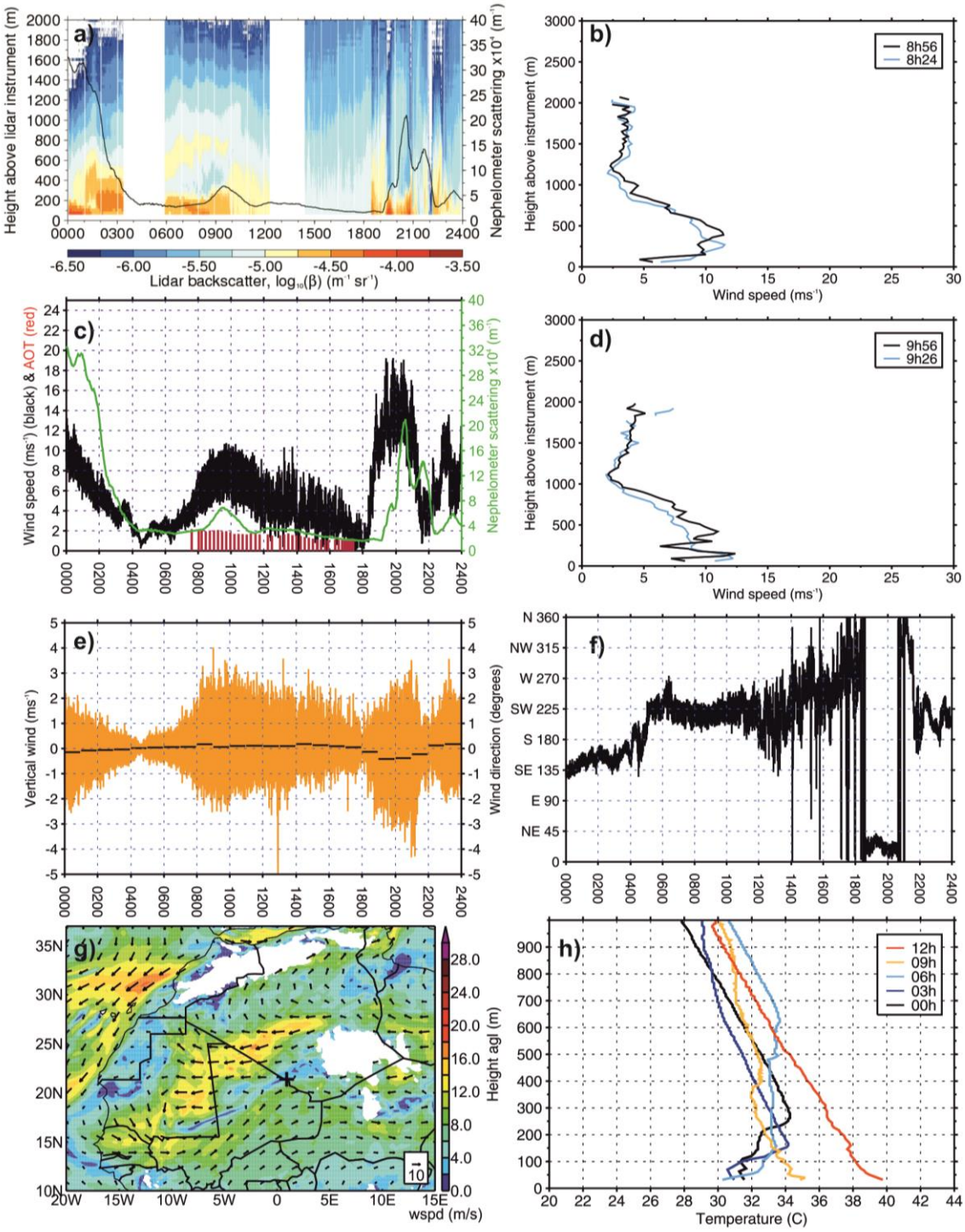

Figure 5-8. Dust events of 18 June 2011 at BBM: morning remnants of the last cold pool from 17 June (see also Figure 5-5), a LLJ (from 07h) and a cold pool (from 18h). (a) lidar backscatter (contours) and nephelometer scattering (line) (b) and (d) lidar wind speed profiles (c) 10m wind speed (black), nephelometer scattering (green) and 500nm AOT (red bars) (e) 10m vertical wind (+ve upward, lines show hourly mean) (f) 10m wind direction (g) 0900 Africa LAM wind vectors (925hPa) (h) radiosonde temperature profiles. Lidar data is unavailable from 0330 to 0600 and 1230 to 1430, in the latter period probably because the instrument overheated.

At 0800, nephelometer scattering increases very closely in line with the 10m wind speeds (Figure 5-8c), peaking at 0930 at a modest $7x10^{-4}m^{-1}$, unsurprising given that the wind speeds only just reach 10m/s. As wind speeds begin to decline so does the scattering: the match between the wind speeds and the scattering also suggesting that this is almost certainly local emission. The vertical wind component shows a gradual increase from 0700 (averaging about ±1m/s) to 0900 (averaging +2.7 and -2.2m/s); in this period and for the rest of the morning the hourly mean vertical wind is upward (Figure 5-8e). AOTs during the event are high but not extreme for BBM: averaging 1.7. Ångstrom exponents average 0.05 (Table 5-1).

Arrival of mixed-down LLJ winds are clear in the lidar data between 0856 and 0926 (Figure 5-8b and Figure 5-8d), coincident with the increase in 10m wind speeds. Degeneration of the nocturnal inversion is apparent when the 0600 and 0900 radiosonde temperature profiles are compared (Figure 5-8h). The reason dust emission is modest is likely because the LLJ is itself weak; lidar profiles (not shown) show that wind speed in the core declines from 18m/s at midnight to 12m/s by 0700.

As on 29 June, the LLJ is embedded in the monsoon flow: observed wind directions at 10m height are southwesterly from 0500 to 1200 (Figure 5-8f); Africa LAM 925hPa wind directions are southwesterly over BBM during the morning (Figure 5-8g) and a moist monsoon tongue is apparent in the model specific humidity field over southern Algeria (not shown). Consistent with these features, the model shows that BBM is very close to the inter-tropical discontinuity (ITD) on the morning of 18 June.

5.7.2.3. The monsoon and low level jets

The nephelometer scattering time series (Figure 5-1) shows that prior to 13 June there is little dust at BBM. *Marsham et al.* [2013] demonstrate that the dusty period from 13

June is coincident with monsoon influence at BBM. The WAM can promote dust emission in the region directly or indirectly. Indirectly, the WAM promotes dust emission by encouraging deep convection, promoting cold pool outflows and haboobs [*Flamant et al.*, 2007; *Marsham et al.*, 2008]. Directly, the monsoon flow can lead to dust emission as it acts as an intrusive surge [*Bou Karam et al.*, 2008], or when LLJs are embedded within the flow [*Parker et al.*, 2005].

Of the 12 strongest LLJs to occur over BBM, the Africa LAM suggests that 9 were embedded in the monsoon flow. Only two of the 12 strongest jets were embedded in the Harmattan flow. The remaining LLJ was an extension of a strong Atlantic inflow. Coupled with the importance of cold pool outflows, this clearly shows the primacy of the monsoon in promoting dust emission in the region.

5.7.3. Dry convective plumes

A case study of the dustiest dry convective plume is presented here. The others (Figure 5-1c) developed in a very similar fashion. All of the dry convective plumes detected occurred in the second half of June 2011. This is consistent with the higher surface temperatures and deeper boundary layer heights found at BBM after 13 June 2011, 600-450hPa compared to 700hPa prior to 13 June [*Marsham et al.* 2013], linked on the synoptic scale to the westward displacement of the SHL [*Marsham et al.* 2013; *Todd et al.* 2013].

5.7.3.1. 24 June 2011 16h

On 24 June BBM is within the centre of the SHL (Figure 5-3b). 925hPa temperatures exceed 38°C at 1800, although the heat maximum and pressure minimum are not as strongly co-located or as intense as on 29 June (compare Figure 5-3c). Nonetheless, the CBL is deep, 3.6km at 1500 and 4km at 1800 (Figure 5-9). At 1600 there is a very

sudden spike in the nephelometer scattering, lidar backscatter and 10m wind speed (Figure 5-10a and Figure 5-10c). This dust event is ranked 11th in the nephelometer time series, at 19x10^{-4}m^{-1} (Table 5-1). There are several features which suggest that this event is a dry convective plume. These are: (i) wind speed rise from 1m/s to 21m/s in just 20 minutes (Figure 5-10c) (ii) vertical wind component reaches over +4m/s (Figure 5-10b) (iii) drop in pressure of 1hPa (a 'pressure well', Figure 5-10d) (iv) concurrent timing of wind speed, lidar and nephelometer changes. The plume lasts just over an hour and is at least 1.3km in height (Figure 5-10a, Table 5-1), although the CBL height at 1500 is 3.6km. This is similar to observations by *Cuesta et al.* [2008] from Tamanrasset in June/July 2006, who record dry convective dust plume heights of 1-2km, despite an average CBL height of 4.7km at 1800. Although a detailed near-surface temperature profile is unavailable, in its first 55m of ascent the 1500 radiosonde recorded a decrease in temperature of 3°C, a strong super-adiabatic temperature profile. Super-adiabatic temperature profiles near the surface promote dust plumes since hot air from the surface can rise very fast. Lidar backscatter and SEVIRI show clouds at 5000m agl present over BBM during the dry convective plume period (not shown), as also observed for a case in Tamanrasset [*Cuesta et al*., 2008]. Clouds may reduce surface temperatures, but the related convective updrafts could also promote dust uplift.

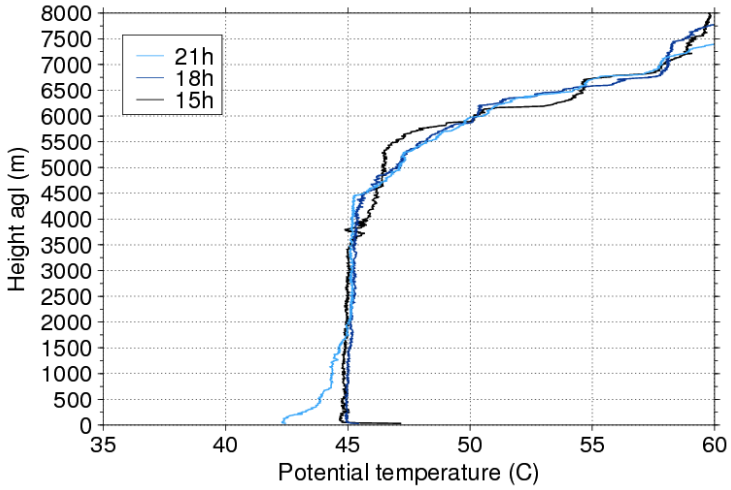

Figure 5-9 (above): Radiosonde-derived potential temperature profiles from BBM, afternoon of 24 June 2011

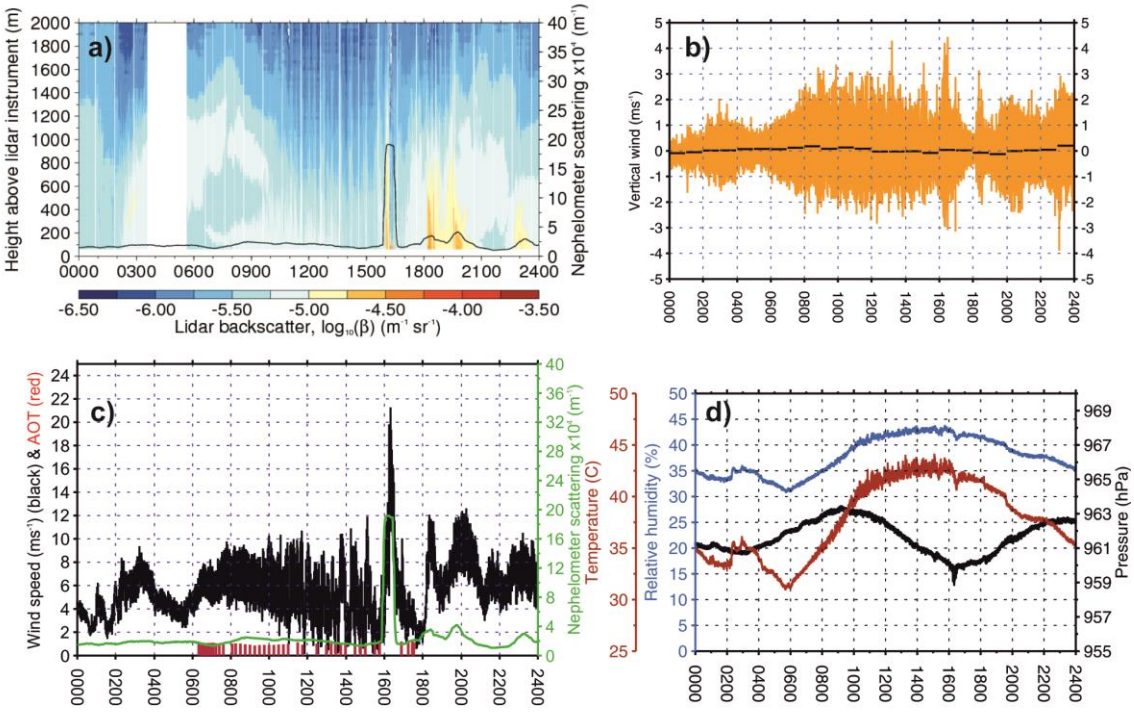

Figure 5-10 (above). Dust events of 24 June 2011 at BBM: a dry convective plume (16h) and cold pool (from 18h). (a) lidar backscatter (contours) and nephelometer scattering (line) (b) 10m vertical wind (+ve upward, lines show hourly mean) (c) 10m wind speed (black), nephelometer scattering (green) and 500nm AOT (red bars) (d) 2m temperature, relative humidity and pressure. Lidar data is unavailable from 0330-0530.

Coincident with the plume are drops in temperature and relative humidity of 2°C and 2% respectively (Figure 5-10d), corresponding to a drop in dew point of 2.3°C from 27.3 to 25°C. This suggests there is subsidence surrounding the plume.

5.7.3.2. Dry convective plume characteristics

BBM dry convective plume evolution is broadly consistent with previous studies. Height estimates are similar to lidar observations of dust plumes from Ouarzazate, Morocco, where most convective plumes reached <1km [*Ansmann et al.*, 2009]. Also consistent with theory and with the measurements of *Ansmann et al.* [2009] are (i) the low (2-7m/s) prior wind speeds necessary for the plumes to develop (these were 1-7m/s in the hour preceding the plume on 24 June) (ii) the high wind speeds within the plumes (up to 21m/s on 24 June).

The formation of a dry convective plume on 22 June following a dusty cold pool (Figure 5-1c) suggests that a prior optical depth <0.3 is not necessary for plume development, as suggested by *Ansmann et al.* [2009]. This may be because temperatures were still hot enough for the plume to form (~42°C at 2m), despite the high background dust loadings (AOT>2 at 1600, Figure 5-1b).

Although no dust devils were explicitly identified in the BBM data, this is not to say that they do not occur in the region. Because of their narrow diameter (~7m) and duration of only a few minutes (e.g. Balme and Greeley, 2006), it is possible that several passed nearby the site but not over the lidar or past the flux tower. A network of instrumentation over a grid (rather than just one instance of each instrument) is more likely to have detected them.

5.8. Relative importance of dust mechanisms (partitioning)

Fennec data provide the first opportunity to quantify the characteristics of the dust layer during the central Saharan summer. The data also provide the opportunity to partition the dust burden between the different generating mechanisms (Figure 5-11). The Figure considers all 32 dust events of the IOP and also the background dust, i.e. periods when nephelometer scattering is less than $2x10^{-4}m^{-1}$ (see Section 5.3). Four dust producing mechanisms are distinguished: local cold pool emission; cold pool dust advection (i.e. cold pools with wind speeds ≤6m/s, Section 5.4); LLJ-induced emission and dry convective plumes.

Partitioning is done in two different ways which provide complementary information. The first method (red bars of Figure 5-11) considers the duration of dust events. The duration of each dust event is distinguished (Section 5.3), and for each mechanism separately (i.e. LLJs, dry convective plumes etc.) the summation of the dust event durations is calculated. Since the duration of the IOP, representing 100%, is known, the percentage of time that any mechanism is in operation can be calculated. The red residual represents the percentage of time that nephelometer scattering is below $2x10^{-4}m^{-1}$, which is the threshold value chosen between background dust and dust events (Section 5.4). The second way partitioning is done is by nephelometer scattering (blue bars of Figure 5-11). The sum of the nephelometer scattering during each dust event is calculated (one 'sum' for each event). For each dust mechanism separately, the total of the sums of the nephelometer scattering is calculated. Since the total nephelometer scattering during the IOP, representing 100%, is known, the percentage of scattering that occurs during the operation of any mechanism can be calculated. The blue residual represents the total nephelometer scattering during periods which are not

designated as dust events (Section 5.3). Since the whole duration of the IOP is represented, the values of the blue and red columns each add up to 100.

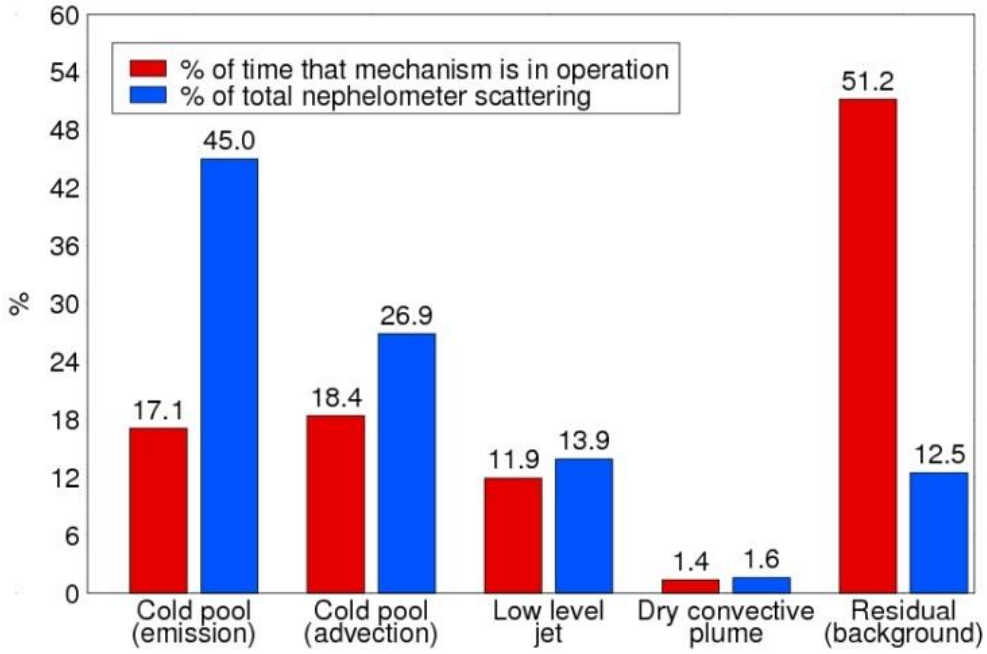

Figure 5-11. Partitioning of dust events during the IOP at BBM by mechanism. Red bars represent the percentage of time during which each mechanism is in operation (see Section 5.3 for discussion of how the mechanisms were identified from the data). Blue bars represent the percentage of the total nephelometer scattering each mechanism is responsible for. The residual is defined as the background dust loading, i.e. periods when nephelometer scattering is less than $2x10^{-4}m^{-1}$ and when no dust events are identified (Section 5.3). There is no overlap between any of the categories. The numbers above the bars are the percentage each bar represents, included for clarity. Since the whole duration of the IOP is represented, the values of the blue and red columns each add up to 100. See Section 5.8 for full details and discussion of the contribution of monsoon surges.

Locally emitting cold pool outflows are the most important dust emission mechanism during the IOP, responsible for 45.0% nephelometer scattering. Advected dust in cold pools occurs marginally more frequently (18.4% of the time compared to 17.1% of the time) but dust in these cold pools is responsible for less nephelometer scattering, 26.9%.

Nonetheless, cold pool dust advection is the second largest contributor to the dust burden. Together, both types of cold pool are responsible for 71.9% of the nephelometer scattering at BBM. LLJ-induced emission is responsible for just 13.9% nephelometer scattering and dry convective plumes only 1.6%. This is an order of magnitude less than the global estimate of 35% by *Koch and Renno* [2005]. We note again that the definition of 'dry convective plumes' is not equivalent to 'dry convection' (see also Section 5.1.2.3). The former are dusty updrafts caused by afternoon gustiness, the latter occurs throughout the day and is additionally responsible for the mixdown of momentum from aloft. This momentum mixdown work done by dry convection is implicitly included in the LLJ category.

Dust events are actually not present over BBM 51.2% of the time, but the percentage of nephelometer scattering that occurs in this period is only 12.5%: this is the contribution of the 'background' dust loading. Nonetheless, this is close to the LLJ contribution of 13.9%.

Marsham et al. [2013] also present a partitioning of dust events at BBM, primarily based on uplift potential (see Section 5.4). These uplift potential results also show the dominance of cold pool outflows and the secondary importance of LLJs. Their results with regard to nephelometer scattering are slightly different to those presented here however. *Marsham et al.* [2013] suggest that both cold pool outflows and LLJs are responsible for 33% nephelometer scattering (compare Figure 5-11). However, the authors define LLJ periods simply as those between 6-12 UTC. This is likely to overestimate their contribution: frequently LLJs do not lead to dust uplift at BBM (e.g. 28 June, Figure 5-1c) and on several occasions between 6-12 UTC cold pool outflows are responsible for dust (e.g. 13 June, Section 5.7.1.4; see also Figure 5-1c). Cold pool

contributions between 6-12 UTC not only explain why the LLJ contributions to nephelometer scattering in the present paper are lower than *Marsham et al.* [2013] but also why cold pool contributions presented here are higher. Additionally, since *Marsham et al.* [2013] use uplift potential as a sampling base, they do not explicitly consider scattering due to dust advected in low wind conditions, which is significant (26.9%, Figure 5-11). This paper also builds upon the initial partitioning results of *Marsham et al.* [2013] by including a dry convective plume category.

Monsoon surges are not identified explicitly in Figure 5-11. This is because they are difficult to unambiguously identify [*Marsham et al.*, 2013]: they can share characteristics of both LLJs and cold pool outflows [see also *Bou Karam et al.*, 2008]. However, *Marsham et al.* [2013] do suggest that monsoon surges produce or at least contribute to dust at BBM on two particular occasions: the early morning of 25 June and the late morning to mid-afternoon of 29 June. In Figure 5-11, the former event is included as advected cold pool dust and the latter as a LLJ (see also discussion in Section 5.7.2.1 above). However, if they are treated separately, the early morning event of 25 June is responsible for 2.7% of IOP nephelometer scattering and the afternoon event of 29 June is responsible for 7.2%, a significant fraction. Thus monsoon surges could be responsible for 9.9% nephelometer scattering during the IOP.

The high relative importance of cold pools during the IOP at BBM is unsurprising given its location: monsoon-related deep convection frequently reaches the southern fringes of the Sahara in summer [*Sultan and Janicot*, 2003; *Cuesta et al.*, 2010]. Although the meteorological processes at BBM are not representative of the Sahara as a whole (particularly further north, away from monsoon influence), it is important to recall that BBM is very close to the global dust maximum in summer [e.g. *Ashpole and*

Washington, 2012], therefore it remains likely that cold pool outflows are a significant contributor to the dust maximum.

5.9. Ångstrom Exponent and dust advection

The Ångstrom exponent is the exponent used when calculating the dependence of extinction on wavelength. It has the useful property of varying with particle size: α is typically larger for smaller particles, and usually <0.5 for coarse windblown dust [*Redmond et al.*, 2010]. The α time series from BBM is shown in Figure 5-1d. Ångstrom exponents for all the events listed in Table 5-1 are below 0.4, a criterion used by *Huneeus et al.* [2010] in the definition of a station as 'dusty' (the other criterion is that monthly average of AOT is over 0.2, which is certainly the case). What is intriguing, however, is that the lowest α (as low as -0.04, Figure 1d), indicating the presence of very coarse particles in the atmospheric column, occur on days when the dust is transported over BBM, rather than emitted. This is somewhat counter-intuitive, as it is expected that transported large particles will fall out of the column early due to gravitational settling, whilst fresh emission under high wind speeds should lead to a greater number of larger particles in the column. However, this is similar to the results of *Cuesta et al*. [2008] who found that the lowest Ångstrom Exponent values (α=0.17, standard deviation ±0.08) in Tamanrasset in 2006 occurred during the late May-mid June period when long-range dust transport was most frequent. The three events of June 2011 with the lowest α values are density currents spawned by mesoscale convective complexes over western Niger (Table 5-1; Sections 5.7.1.2 and 5.7.1.4). It is therefore possible that (i) the sedimentology over the western Niger region provides much larger particles for emission than over the BBM region (ii) the density currents over western Niger have much stronger gust fronts than those spawned near BBM, allowing much

larger particles to be uplifted (iii) transport of the dust could be above a stable nocturnal boundary layer, as discussed for 17 June (Section 5.7.1.5).

Values from the Cimel sun photometer are not available for many of the cold pool events, which occur at night. This highlights the importance of 24 hour monitoring capacity to observe dust in this region, and the usefulness of the lidar and nephelometer instruments, especially as observers cannot rely on a predictable dust diurnal cycle due to the influence of distant convective events.

5.10. Relationship between wind speed and dust production

To further examine the relationship between wind speed and dust production, the peak nephelometer scattering for each of the dust events during the IOP is plotted as a function of the wind speed at the time of the scattering peak, $wspd_p$ (Figure 5-12). 31 events are plotted, including those defined as advected dust ($wspd_p \leq 6m/s$), local emission ($wspd_p \geq 8m/s$) and mixed emission and advection ($6m/s < wspd_p < 8m/s$). See Section 5.4 for discussion of emission thresholds. $wspd_p$ is chosen as the independent variable so that the independent and dependent variables are coincident in time. It can be seen from Figure 5-12 that dust that is not locally emitted (i.e. $wspd_p < 8m/s$) is responsible for relatively high nephelometer scattering values. Indeed, in four of these cases peak nephelometer scattering is over $20x10^{-4}m^{-1}$, which is never the case for dry convective plumes and only the case for one LLJ.

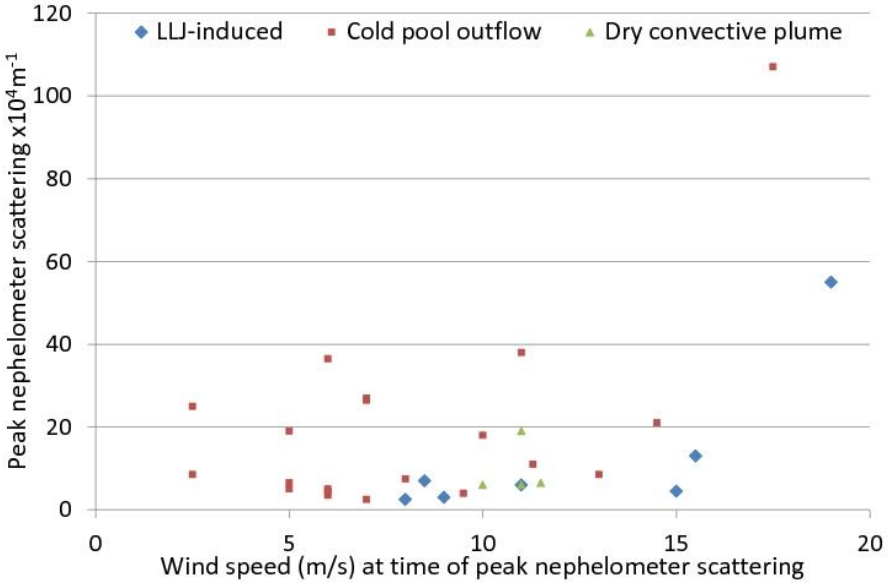

Figure 5-12: Scatter plot showing peak nephelometer scattering (x10^{4}m^{-1}) for individual dust events as a function of wind speed at the time of the peak scattering (wspd$_p$). (Associated correlation coefficients are presented in Table 5-3.) Three different symbols are used to differentiate between the different atmospheric mechanisms (top). Wind speed is measured at 10m height, nephelometer scattering at 2m height and 670nm wavelength. 31 events are presented; wind measurements were unavailable for one dry convective plume.

The correlation between wspd$_p$ and peak nephelometer scattering for all events is not particularly strong, r=0.44 ($p<0.05$; Table 5-3). This is unsurprising given that 12 of the events are not considered to represent purely locally emitted dust. More telling are the correlation coefficients obtained when the calculations are done separately for each dust mechanism. The correlation is highest for LLJs, r=0.77 ($p<0.05$; Table 5-3). Cold pool outflows with wspd$_p$>6m/s (i.e excluding purely advected dust) come second, r=0.64 ($p<0.05$; Table 5-3). Unsurprisingly, the correlation for advected dust is low and statistically insignificant, r=-0.16 ($p>0.05$). The correlation for dry convective plumes is surprisingly low, r=0.16, but caution should be taken in interpreting this result since the sample size, four events, is low and r is statistically insignificant ($p>0.05$).

Table 5-3: Correlation coefficients between $wspd_p$ (wind speed observed at the time of peak nephelometer scattering) and peak nephelometer scattering, for all dust events observed during the IOP except one dry convective plume (15 June) when no wind speed measurements were available. Correlation coefficients are calculated for all events (left column) and also separately for each category of dust mechanism (other columns). Correlations are similarly calculated for $wpsd_p^3$. Italicised correlations are significant at 95% confidence. For full details see Section 5.10. Figure 5-12 presents a visual representation of $wspd_p$ relationship with peak nephelometer scattering.

	All events	Cold pool outflow			LLJ-induced	Dry convective plume
		All	$wspd_p$>6m/s	$wspd_p$≤6m/s		
number of events	31	20	11	9	7	4
r ($wspd_p$, peak nephelometer scattering)	*0.44*	*0.55*	*0.64*	-0.16	*0.77*	0.16
r ($wspd_p^3$, peak nephelometer scattering)	*0.60*	*0.74*	*0.78*	-0.13	*0.88*	0.14

Research dating back to [*Bagnold*, 1941] suggests that in many cases the relationship between emission and the cube of wind speed is stronger than that with wind speed alone. This also appears to be the case with these results (Table 5-3). Taking $wspd_p^3$ results in stronger correlations with peak nephelometer scattering for all cases, except those where a relationship is not expected anyway (purely advected dust) or where the correlation with $wspd_p$ is not statistically significant either (purely advected dust and dry convective plumes). The correlation with $wspd_p^3$ is highest for LLJ-induced emission ($r=0.88$, $p<0.05$) followed by cold pool outflows with $wspd_p$>6m/s ($r=0.78$, $p<0.05$).

5.11. Summary and discussion

This paper has presented the first detailed descriptions of dust production mechanisms from observations near the centre of the Saharan heat low, in the June dust maximum region. Three aims were outlined in the introduction: 1) document the main dust outbreaks in June 2011 at Bordj Badji Mokhtar 2) identify the mechanisms associated with dust production and establish their relative importance 3) document the characteristics of the key dust producing mechanisms and their relationship with wind speed for dust emission.

A total of 32 individual dust events were identified during the June 2011 IOP (Figure 5-1c). Three main mechanisms led to dust over BBM: cold pool outflows, low level jets and dry convective plumes. They have been identified and documented primarily from the ground-based observations, but also with the aid of satellite products where necessary. Monsoon surges are also potentially important but since they can share cold pool or LLJ characteristics their contribution is difficult to isolate unambiguously.

Cold pool outflows are the most important mechanism for dust over BBM (Figure 5-11). Their contribution can be split between locally emitting outflows (44% nephelometer scattering) and advected dust (28%). LLJs come third (14% nephelometer scattering) followed by dry convective plumes (2%). Using a partitioning based on uplift potential (see Section 5.4) *Marsham et al.* [2013] also found that cold pool outflows were the most important dust production mechanism at BBM during the IOP. Their partitioning based on nephelometer scattering however assigned equal importance to LLJs and cold pool outflows (33% each); this difference with the present findings can likely be explained by the decision of *Marsham et al.* [2013] to take scattering between 0600-1200 to be caused by LLJ emission, whereas frequently in this period cold pool

outflows produced dust (Figure 5-1c). This study extends the partitioning work of *Marsham et al.* [2013] by including advected dust and dry convective plumes.

Of the top 15 dustiest events as ranked by nephelometer scattering at BBM in June 2011, 12 are cold pool outflows and 2 are LLJs embedded in the monsoon feed. The remaining event (ranked 11th) is a dust plume. This is consistent with the AOT measurements: the dustiest LLJ-induced emission events have peak AOTs between 0.8 and 2.6, whilst for the dustiest cold pools AOTs are between 2.3 and 4.4 (Table 5-1; AOTs are not available for the frequent night-time outflows). The AOT of the dustiest convective plume is 1.25.

The meteorological observations during the dust events are broadly consistent with modelling work and observations from other parts of the Sahara, but with some interesting differences. Cold pool outflows at BBM are typically associated with sudden air temperature changes of the order 2-2.5°C (usually increases in the early morning and decreases at other times); fluctuations in pressure of between 0.4 and 1hPa; sudden increases in wind speeds of 9-16m/s; rapid increases of the vertical wind component of between 1.3 and 2.5m/s; changes in relative humidity of around 2%; changes (positive and negative) in dew point from 2.8-7.2°C and rapid switches in wind direction. In their climatology of density currents in the Atlas foothills, *Emmel et al.* [2010] note, for example, a mean temperature decrease of 2.3°C, dew point temperature increase of 5.4°C and wind speed increase of 8.2m/s, in good agreement with these results. Many of these rapid changes as the gust front passes also match modelling work, even in two dimensions [e.g. *Liu and Moncrieff,* 1996]. The changes are not as extreme as those at the outflow fronts observed by *Miller et al.* [2008] in the Arabian Peninsula, who report

an idealized ‘ensemble’ pressure rise of 2hPa, air temperature drop of 7°C and relative humidity increase of 15%.

It appears that density currents promote further convection and new outflows, as reported by several authors [e.g. *Weckwerth and Wakimoto*, 1992; *Moncrieff and Liu*, 1999; *Tompkins*, 2001]. Several also appear to be preceded by bore-like phenomena as has been shown in laboratory experiments [e.g. *Simpson*, 1997] and recorded in observations [e.g. *S E Koch et al.*, 1991]. Where reasonable estimates of the average propagation speed of density currents can be made (based on SEVIRI), these are faster than their counterparts in the Atlas foothills: 12m/s and 16m/s compared with 6m/s [*Knippertz et al.*, 2007], 3-11m/s [*Emmel et al.*, 2010] and 11m/s [*Solomos et al.*, 2012]. The average propagation speed is however within the range of that computed for the three case studies reported by *Miller et al.* [2008] in the Arabian Peninsula (10.5-18m/s).

Low level jet-induced emission appears to conform to the classic ‘jet breakdown’ theory and observations from other parts of the Sahara [*Blackadar*, 1957; *Washington et al.*, 2006]. The degeneration of the surface temperature inversion and the propagation of wind speeds towards the surface after sunrise are clear in the lidar wind profiles and radiosonde measurements. There is frequently a strong correspondence between the wind speed curve on these mornings and the nephelometer scattering and lidar backscatter (e.g Figure 5-2 and Figure 5-8c).

The intensive measurements at BBM in June 2011 detected 5 dry convective plumes. Similar to other observational studies, a superadiabatic temperature gradient at low levels is often present, there is a 1hPa pressure well during the strongest plumes, and very large and rapid increases in wind speed are observed after a period of very low wind (an increase of 21m/s on one occasion). In contrast to the work of *Ansmann et al.*

[2009], low AOT prior to the plume does not appear to be a prerequisite for formation, possibly because temperatures at BBM are still very high at the time of formation (~42°C at 2m). Dry convective plumes are only responsible for 2% of the dustiness during the IOP. Note however that the definition of dry convective plumes only extends to dust raised by afternoon gustiness (Section 5.1.2.3): dry convection is additionally responsible for mixing LLJ momentum down to the surface and this is implicitly included in the LLJ partitioning category.

The current work presents some unexpected results when it comes to long-range dust advection and particle size. Cold pool outflows advected from Niger had very large AOTs, with peaks from 3.3-4.4 (Table 5-1). These density currents also carried very large particles, with Ångstrom exponents as low as -0.04 (Figure 5-1d and Table 5-1). Indeed, the largest particles found over BBM were associated with advected dust behind the leading edge rather than local emission. *Cuesta et al.* [2008] also report the lowest Ångstrom exponents at Tamanrasset to be in advected dust, and the long-range advection potential of density currents is highlighted in *Miller et al*. [2008]. Advected dust in cold pool outflows was responsible for 28% nephelometer scattering during the IOP.

For locally-emitting dust events, the cube of wind speed has a closer relationship with nephelometer scattering than wind speed alone. The correlation with the cube of wind speed is 0.88 for LLJ-induced emission and 0.77 for emission caused by cold pool outflows (both at 95% confidence, Table 5-3). This is in agreement with long-held ideas regarding the cube of wind speed as an important control on emission (dating from *Bagnold* [1941]), reflected in commonly used parameterization schemes such as *Marticorena and Bergametti* [1995].

North Africa is of global importance for dust emission in boreal summer [e.g. *Ginoux et al.*, 2012]. Given the primacy of cold pool outflows and monsoon-embedded LLJs observed over BBM, there is strong incentive for research to improve model representation of moist processes and to use explicit convection where possible, as this appears to significantly improve representation of dust storms in the region [e.g. *Marsham et al.*, 2011; *Kocha et al.*, 2012].

5.12. Acknowledgements

Fennec was funded by a NERC consortium grant (NE/G017166/1). The authors wish to thank the following individuals and institutions. For establishing and instrumenting the supersite and/or data processing: B Abderrahmane, M Bart, BJ Brooks, F Davies, M Gascoyne, M Hobby, A Lima, M Limam, JH Marsham, V Martins, JB McQuaid, A O'Leary, B Ouchene, A Ouladichir, DJ Parker, A Saci, M Salah-Ferroudj, D Sidali, MC Todd, ONM Algérie, the AERONET PHOTONS team, the University of Leeds and the University of Sussex. For providing the SEVIRI imagery at http://www.fennec.imperial.ac.uk: H Brindley and J Banks. For the Africa-LAM dataset: UK Met Office. For frequent suggestions and support: I Ashpole and J King. For helpful discussion of some of the case studies: P Knippertz, A O'Leary, JH Marsham, A Roberts. We thank FGAM (Facility for Ground-based Atmospheric Measurement) and NCAS (National Centre for Atmospheric Science) for the use of the sodar, lidar and radiosonde units. We would also like to thank E Williams and two anonymous reviewers for their comments which significantly improved the manuscript.

5.13. References

Andreae, T. W., M. O. Andreae, C. Ichoku, W. Maenhaut, J. Cafmeyer, A. Karnieli, and L. Orlovsky (2002), Light scattering by dust and anthropogenic aerosol at a remote site in the Negev desert, Israel, *Journal of Geophysical Research D: Atmospheres*, *107*(1-2), doi: 10.1029/2001JD900252.

Ansmann, A., M. Tesche, P. Knippertz, E. Bierwirth, D. Althausen, D. Müller, and O. Schulz (2009), Vertical profiling of convective dust plumes in southern Morocco during SAMUM, *Tellus B*, *61*(1), 340-353, doi: 10.1111/j.1600-0889.2008.00384.x.

Ashpole, I., and R. Washington (2012), An automated dust detection using SEVIRI: A multiyear climatology of summertime dustiness in the central and western Sahara, *J. Geophys. Res.*, *117*(D8), D08202, doi: 10.1029/2011jd016845.

Bagnold, R. A. (1941), *The Physics of Blown Sand and Desert Dunes*, Methuen, London.

Balme, M., and R. Greeley (2006), Dust devils on Earth and Mars, *Reviews of Geophysics*, *44*(3), doi: 10.1029/2005RG000188.

Banks, J. R., H. E. Brindley, C. Flamant, M. J. Garay, N. C. Hsu, O. V. Kalashnikova, L. Klüser, and A. M. Sayer (2013), Intercomparison of satellite dust retrieval products over the west African Sahara during the Fennec campaign in June 2011, *Remote Sensing of Environment*, *136*(0), 99-116, doi: http://dx.doi.org/10.1016/j.rse.2013.05.003.

Banta, R. M., R. K. Newsom, J. K. Lundquist, Y. L. Pichugina, R. L. Coulter, and L. Mahrt (2002), Nocturnal Low-Level Jet Characteristics Over Kansas During Cases-99, *Boundary-Layer Meteorology*, *105*(2), 221-252, doi: 10.1023/a:1019992330866.

Blackadar, A. K. (1957), Boundary layer wind maxima and their significance for the growth of nocturnal inversion, *Bull. Am. Meteorol. Soc*, *38*(5), 283-290.

Bou Karam, D., C. Flamant, J. Cuesta, J. Pelon, and E. Williams (2010), Dust emission and transport associated with a Saharan depression: February 2007 case, *Journal of Geophysical Research-Atmospheres*, *115*, doi: 10.1029/2009jd012390.

Bou Karam, D., C. Flamant, P. Knippertz, O. Reitebuch, J. Pelon, M. Chong, and A. Dabas (2008), Dust emissions over the Sahel associated with the West African monsoon intertropical discontinuity region: A representative case-study, *Quarterly Journal of the Royal Meteorological Society*, *134*(632), 621-634, doi: 10.1002/qj.244.

Brindley, H., P. Knippertz, C. Ryder, and I. Ashpole (2012), A critical evaluation of the ability of the Spinning Enhanced Visible and Infrared Imager (SEVIRI) thermal infrared red-green-blue rendering to identify dust events: Theoretical analysis, *Journal of Geophysical Research D: Atmospheres*, *117*(7), doi: 10.1029/2011JD017326.

Browning, K., and R. Wexler (1968), The determination of kinematic properties of a wind field using Doppler radar, *J. Appl. Meteorol.*, *7*, 105-113, doi: 10.1175/1520-0450(1968)007<0105:TDOKPO>2.0.CO;2.

Callot, Y., B. Marticorena, and G. Bergametti (2000), Geomorphologic approach for modelling the surface features of arid environments in a model of dust emissions: Application to the Sahara desert, *Geodinamica Acta*, *13*(5), 245-270, doi: 10.1016/S0985-3111(00)01044-5.

Carbone, R. E., J. W. Conway, N. A. Crook, and M. W. Moncrieff (1990), The Generation and Propagation of a Nocturnal Squall Line. Part I: Observations and Implications for Mesoscale Predictability, *Monthly Weather Review*, *118*(1), 26-49, doi: 10.1175/1520-0493(1990)118<0026:tgapoa>2.0.co;2.

Clarke, R. H., R. K. Smith, and D. G. Reid (1981), The morning glory of the Gulf of Carpentaria: an atmospheric undular bore, *Monthly Weather Review*, *109*, 1726-1750, doi: 10.1175/1520-0493(1981)109<1726:TMGOTG>2.0.CO;2.

Cuesta, J., J. H. Marsham, D. J. Parker, and C. Flamant (2009), Dynamical mechanisms controlling the vertical redistribution of dust and the thermodynamic structure of the West Saharan atmospheric boundary layer during summer, *Atmospheric Science Letters*, *10*(1), 34-42, doi: 10.1002/asl.207.

Cuesta, J., C. Lavaysse, C. Flamant, M. Mimouni, and P. Knippertz (2010), Northward bursts of the West African monsoon leading to rainfall over the Hoggar Massif, Algeria, *Quarterly Journal of the Royal Meteorological Society*, *136*, 174-189, doi: 10.1002/qj.439.

Cuesta, J., D. Edouart, M. Mimouni, P. H. Flamant, C. Loth, F. Gibert, F. Marnas, A. Bouklila, M. Kharef, B. Ouchene, M. Kadi, and C. Flamant (2008), Multiplatform observations of the seasonal evolution of the Saharan atmospheric boundary layer in Tamanrasset, Algeria, in the framework of the African Monsoon Multidisciplinary Analysis field campaign conducted in 2006, *Journal of Geophysical Research-Atmospheres*, *113*, doi: 10.1029/2007jd009417.

Emmel, C., P. Knippertz, and O. Schulz (2010), Climatology of convective density currents in the southern foothills of the Atlas Mountains, *J. Geophys. Res.*, *115*(D11), D11115, doi: 10.1029/2009jd012863.

Engelstaedter, S., I. Tegen, and R. Washington (2006), North African dust emissions and transport, *Earth-Science Reviews*, *79*(1–2), 73-100, doi: 10.1016/j.earscirev.2006.06.004.

Evan, A. T., G. R. Foltz, D. Zhang, and D. J. Vimont (2011), Influence of African dust on ocean-atmosphere variability in the tropical Atlantic, *Nature Geoscience*, *4*(11), 762-765, doi: 10.1038/ngeo1276.

Fernald, F. (1984), Analysis of atmospheric lidar observations: some comments, *Applied Optics*, *23*(5), 652-653, doi: 10.1364/AO.23.000652.

Fernald, F., B. Herman, and J. Reagan (1972), Determination of aerosol height distributions by Lidar, *J. Appl. Meteorol.*, *11*, 482-489, doi: 10.1175/1520-0450(1972)011<0482:DOAHDB>2.0.CO;2.

Flamant, C., J. P. Chaboureau, D. J. Parker, C. M. Taylor, J. P. Cammas, O. Bock, F. Timouk, and J. Pelon (2007), Airborne observations of the impact of a convective system on the planetary boundary layer thermodynamics and aerosol distribution in the inter-tropical discontinuity region of the West African Monsoon, *Quarterly Journal of the Royal Meteorological Society*, *133*(626), 1175-1189, doi: 10.1002/qj.97.

Fulton, R., D. S. Zrnic, and R. J. Doviak (1990), Initiation of a solitary wave family in the demise of a nocturnal thunderstorm density current, *Journal of the Atmospheric Sciences*, *47*(3), 319-337, doi: 10.1175/1520-0469(1990)047<0319:IOASWF>2.0.CO;2.

Haywood, J. M., R. P. Allan, I. Culverwell, T. Slingo, S. Milton, J. Edwards, and N. Clerbaux (2005), Can desert dust explain the outgoing longwave radiation anomaly over the Sahara during July 2003?, *J. Geophys. Res.*, *110*(D5), D05105, doi: 10.1029/2004jd005232.

Herman, J. R., P. K. Bhartia, O. Torres, C. Hsu, C. Seftor, and E. Celarier (1997), Global distribution of UV-absorbing aerosols from Nimbus 7/TOMS data, *J. Geophys. Res.*, *102*(D14), 16911-16922, doi: 10.1029/96jd03680.

Hobby, M., M. Gascoyne, J. H. Marsham, M. Bart, C. J. T. Allen, S. Engelstaedter, D. M. Fadel, A. Gandega, R. Lane, J. B. McQuaid, B. Ouchene, A. Ouladichir, D. J. Parker, P. Rosenberg, M. S. Ferroudj, A. Saci, F. Seddik, M. Todd, D. Walker, and R. Washington (2013), The Fennec Automatic Weather Station (AWS) Network: Monitoring the Saharan Climate System, *Journal of Atmospheric and Oceanic Technology*, *30*(4), 709-724, doi: 10.1175/jtech-d-12-00037.1.

Holben, B. N., T. F. Eck, I. Slutsker, D. Tanré, J. P. Buis, A. Setzer, E. Vermote, J. A. Reagan, Y. J. Kaufman, T. Nakajima, F. Lavenu, I. Jankowiak, and A. Smirnov (1998), AERONET - A federated instrument network and data archive for aerosol characterization, *Remote Sensing of Environment*, *66*(1), 1-16, doi: 10.1016/s0034-4257(98)00031-5.

Huneeus, N., M. Schulz, Y. Balkanski, J. Griesfeller, S. Kinne, J. Prospero, S. Bauer, O. Boucher, M. Chin, F. Dentener, T. Diehl, R. Easter, D. Fillmore, S. Ghan, P. Ginoux, A. Grini, L. Horowitz, D. Koch, M. C. Krol, W. Landing, X. Liu, N. Mahowald, R. Miller, J. J. Morcrette, G. Myhre, J. E. Penner, J. Perlwitz, P. Stier, T. Takemura, and C. Zender (2011), Global dust model intercomparison in AeroCom phase I, *Atmos. Chem. Phys. Discuss.*, *10*(10), 23781-23864, doi: 10.5194/acpd-10-23781-2010.

Kaimal, J. C., and J. A. Bussinger (1970), Case studies of a convective plume and a dust devil, *J. Appl. Meteorol.*, *9*, 612-620.

Kingsmill, D. E., and N. A. Crook (2003), An observational study of atmospheric bore formation from colliding density currents, *Monthly Weather Review*, *131*(12), 2985-3002.

Klett, J. D. (1981), Stable analytical inversion solution for processing lidar returns, *Applied Optics*, *20*(2), 211-220, doi: 10.1364/AO.20.000211.
Knippertz, P. (2008), Dust emissions in the West African heat trough the role of the diurnal cycle and of extratropical disturbances, *Meteorologische Zeitschrift*, *17*(5), 553-563, doi: 10.1127/0941-2948/2008/0315.
Knippertz, P., and M. C. Todd (2010), The central west Saharan dust hot spot and its relation to African easterly waves and extratropical disturbances, *J. Geophys. Res.*, *115*(D12), D12117, doi: 10.1029/2009jd012819.
Knippertz, P., and M. C. Todd (2012), Mineral dust aerosols over the Sahara: Meteorological controls on emission and transport and implications for modeling, *Reviews of Geophysics*, *50*(1), doi: 10.1029/2011RG000362.
Knippertz, P., C. Deutscher, K. Kandler, T. Müller, O. Schulz, and L. Schütz (2007), Dust mobilization due to density currents in the Atlas region: Observations from the Saharan Mineral Dust Experiment 2006 field campaign, *J. Geophys. Res.*, *112*(D21), D21109, doi: 10.1029/2007jd008774.
Knippertz, P., A. Ansmann, D. Althausen, D. Müller, M. Tesche, E. Bierwirth, T. Dinter, T. Müller, W. Von Hoyningen-Huene, K. Schepanski, M. Wendisch, B. Heinold, K. Kandler, A. Petzold, L. Schütz, and I. N. A. Tegen (2009), Dust mobilization and transport in the northern Sahara during SAMUM 2006 – a meteorological overview, *Tellus B*, *61*(1), 12-31, doi: 10.1111/j.1600-0889.2008.00380.x.
Koch, J., and N. O. Renno (2005), The role of convective plumes and vortices on the global aerosol budget, *Geophys. Res. Lett.*, *32*(18), L18806, doi: 10.1029/2005gl023420.
Koch, S. E., P. B. Dorian, R. Ferrare, S. H. Melfi, W. C. Skillman, and D. Whiteman (1991), Structure of an Internal Bore and Dissipating Gravity Current as Revealed by Raman Lidar, *Monthly Weather Review*, *119*(4), 857-887, doi: 10.1175/1520-0493(1991)119<0857:soaiba>2.0.co;2.
Kocha, C., J. P. Lafore, P. Tulet, and Y. Seity (2012), High-resolution simulation of a major West African dust-storm: Comparison with observations and investigation of dust impact, *Quarterly Journal of the Royal Meteorological Society*, *138*(663), 455-470.
Lavaysse, C., C. Flamant, S. Janicot, D. J. Parker, J. P. Lafore, B. Sultan, and J. Pelon (2009), Seasonal evolution of the West African heat low: a climatological perspective, *Climate Dynamics*, *33*(2), 313-330, doi: 10.1007/s00382-009-0553-4.
Lensky, I. M., and D. Rosenfeld (2008), Clouds-Aerosols-Precipitation Satellite Analysis Tool (CAPSAT), *Atmos. Chem. Phys.*, *8*(22), 6739-6753, doi: 10.5194/acp-8-6739-2008.
Liu, C., and M. W. Moncrieff (1996), A numerical study of the effects of ambient flow and shear on density currents, *Monthly Weather Review*, *124*(10), 2282-2303, doi: 10.1175/1520-0493(1996)124<2282:ANSOTE>2.0.CO;2.
Mahowald, N. M., S. Kloster, S. Engelstaedter, J. K. Moore, S. Mukhopadhyay, J. R. McConnell, S. Albani, S. C. Doney, A. Bhattacharya, M. A. J. Curran, M. G. Flanner, F. M. Hoffman, D. M. Lawrence, K. Lindsay, P. A. Mayewski, J. Neff, D. Rothenberg, E. Thomas, P. E. Thornton, and C. S. Zender (2010), Observed 20th century desert dust variability: impact on climate and biogeochemistry, *Atmos. Chem. Phys.*, *10*(22), 10875-10893, doi: 10.5194/acp-10-10875-2010.
Marsham, J. H., D. J. Parker, C. M. Grams, C. M. Taylor, and J. M. Haywood (2008), Uplift of Saharan dust south of the intertropical discontinuity, *J. Geophys. Res.*, *113*(D21), D21102, doi: 10.1029/2008jd009844.
Marsham, J. H., P. Knippertz, N. S. Dixon, D. J. Parker, and G. M. S. Lister (2011), The importance of the representation of deep convection for modeled dust-generating winds over West Africa during summer, *Geophys. Res. Lett.*, *38*(16), L16803, doi: 10.1029/2011gl048368.
Marsham, J. H., M. Hobby, C. J. T. Allen, J. R. Banks, M. Bart, B. J. Brooks, C. Cavazos-Guerra, S. Engelstaedter, M. Gascoyne, A. R. Lima, J. V. Martins, J. B. McQuaid, A. O'Leary, B. Ouchene, A. Ouladichir, D. J. Parker, A. Saci, M. Salah-Ferroudj, M. C. Todd, and R. Washington (2013), Meteorology and dust in the central Sahara: Observations from

Fennec supersite-1 during the June 2011 Intensive Observation Period, *Journal of Geophysical Research: Atmospheres*, *118*, 4069–4089, doi: 10.1002/jgrd.50211.
Marticorena, B., and G. Bergametti (1995), Modeling the atmospheric dust cycle: 1. Design of a soil-derived dust emission scheme, *J. Geophys. Res.*, *100*(D8), 16415-16430, doi: 10.1029/95jd00690.
Marticorena, B., G. Bergametti, B. Aumont, Y. Callot, C. N'Doumé, and M. Legrand (1997), Modeling the atmospheric dust cycle 2. Simulation of Saharan dust sources, *Journal of Geophysical Research D: Atmospheres*, *102*(4), 4387-4404, doi: 10.1029/96JD02964.
Messager, C., D. J. Parker, O. Reitebuch, A. Agusti-Panareda, C. M. Taylor, and J. Cuesta (2010), Structure and dynamics of the Saharan atmospheric boundary layer during the West African monsoon onset: observations and analyses from the research flights of 14 and 17 July 2006, *Quarterly Journal of the Royal Meteorological Society*, *136*(S1), 107-124, doi: 10.1002/qj.469.
Miller, S. D., A. P. Kuciauskas, M. Liu, Q. Ji, J. S. Reid, D. W. Breed, A. L. Walker, and A. A. Mandoos (2008), Haboob dust storms of the southern Arabian Peninsula, *Journal of Geophysical Research D: Atmospheres*, *113*(1), doi: 10.1029/2007JD008550.
Moncrieff, M. W., and C. Liu (1999), Convection initiation by density currents: Role of convergence, shear, and dynamical organization, *Monthly Weather Review*, *127*(10), 2455-2464.
Newsom R. K., Berg L. K., Shaw W. J. and Fischer M. L. (2015), Turbine-scale wind field measurements using dual-Doppler lidar, Wind Energ., 18, 219–235, doi: 10.1002/we.1691.
Parker, D. J., R. R. Burton, A. Diongue-Niang, R. J. Ellis, M. Felton, C. M. Taylor, C. D. Thorncroft, P. Bessemoulin, and A. M. Tompkins (2005), The diurnal cycle of the West African monsoon circulation, *Quarterly Journal of the Royal Meteorological Society*, *131*(611), 2839-2860, doi: 10.1256/qj.04.52.
Pearson, G., F. Davies, and C. Collier (2009), An analysis of the performance of the UFAM pulsed Doppler lidar for observing the boundary layer, *Journal of Atmospheric and Oceanic Technology*, *26*(2), 240-250, doi: 10.1175/2008JTECHA1128.1.
Prospero, J. M., P. Ginoux, O. Torres, S. E. Nicholson, and T. E. Gill (2002), Environmental characterization of global sources of atmospheric soil dust identified with the NIMBUS 7 Total Ozone Mapping Spectrometer (TOMS) absorbing aerosol product, *Rev. Geophys.*, *40*(1), 1002, doi: 10.1029/2000rg000095.
Redmond, H. E., K. D. Dial, and J. E. Thompson (2010), Light scattering and absorption by wind blown dust: Theory, measurement, and recent data, *Aeolian Research*, *2*(1), 5-26, doi: 10.1016/j.aeolia.2009.09.002.
Ryder, C. L., J. B. McQuaid, C. Flamant, R. Washington, H. E. Brindley, E. J. Highwood, J. H. Marsham, D. J. Parker, M. C. Todd, J. R. Banks, J. K. Brooke, S. Engelstaedter, V. Estellés, P. Formenti, L. Garcia-Carreras, C. Kocha, F. Marenco, P. Rosenberg, H. Sodemann, C. J. T. Allen, A. Bourdon, M. Bart, C. Cavazos-Guerra, S. Chevaillier, J. Crosier, E. Darbyshire, A. R. Dean, J. R. Dorsey, J. Kent, D. O'Sullivan, K. Schepanski, K. Szpek, and A. Woolley (2015), Advances in understanding mineral dust and boundary layer processes over the Sahara from Fennec aircraft observations, *Atmos. Chem. Phys. Discuss.*, *15*(1), 199-290, doi: 10.5194/acpd-15-199-2015.
Schepanski, K., I. Tegen, B. Laurent, B. Heinold, and A. Macke (2007), A new Saharan dust source activation frequency map derived from MSG-SEVIRI IR-channels, *Geophys. Res. Lett.*, *34*(18), L18803, doi: 10.1029/2007gl030168.
Schepanski, K., I. Tegen, M. C. Todd, B. Heinold, G. Bönisch, B. Laurent, and A. Macke (2009), Meteorological processes forcing Saharan dust emission inferred from MSG-SEVIRI observations of subdaily dust source activation and numerical models, *J. Geophys. Res.*, *114*(D10), D10201, doi: 10.1029/2008jd010325.
Simpson, J. E. (1997), *Gravity currents in the environment and the laboratory*, 2nd ed., 244 pp., Cambridge University Press, Cambridge.
Sinclair, P. C. (1969), General characteristics of dust devils, *J. Appl. Meteorol.*, *8*, 32-45, doi: 10.1175/1520-0450(1969)008<0032:GCODD>2.0.CO;2.

Smith, R. K. (1988), Travelling waves and bores in the lower atmosphere: the 'morning glory' and related phenomena, *Earth Science Reviews*, *25*(4), 267-290, doi: 10.1016/0012-8252(88)90069-4.

Solomos, S., G. Kallos, E. Mavromatidis, and J. Kushta (2012), Density currents as a desert dust mobilization mechanism, *Atmospheric Chemistry and Physics*, *12*(22), 11199-11211, doi: 10.5194/acp-12-11199-2012.

Stanelle, T., B. Vogel, H. Vogel, D. Bäumer, and C. Kottmeier (2010), Feedback between dust particles and atmospheric processes over West Africa during dust episodes in March 2006 and June 2007, *Atmos. Chem. Phys.*, *10*(22), 10771-10788, doi: 10.5194/acp-10-10771-2010.

Sultan, B., and S. Janicot (2003), The West African monsoon dynamics. Part II: The "preonset" and "onset" of the summer monsoon, *Journal of Climate*, *16*(21), 3407-3427, doi: 10.1175/1520-0442(2003)016<3407:TWAMDP>2.0.CO;2.

Sun, J., S. P. Burns, D. H. Lenschow, R. Banta, R. Newsom, R. Coulter, S. Frasier, T. Ince, C. Nappo, J. Cuxart, W. Blumen, X. Lee, and X.-Z. Hu (2002), Intermittent Turbulence Associated with a Density Current Passage in the Stable Boundary Layer, *Boundary-Layer Meteorology*, *105*(2), 199-219, doi: 10.1023/a:1019969131774.

Thorpe, A. J., M. J. Miller, and M. W. Moncrieff (1982), Two-dimensional convection in non-constant shear: A model of mid-latitude squall lines, *Quarterly Journal of the Royal Meteorological Society*, *108*(458), 739-762, doi: 10.1002/qj.49710845802.

Todd, M. C., R. Washington, S. Raghavan, G. Lizcano, and P. Knippertz (2008), Regional model simulations of the Bodélé low-level jet of Northern Chad during the Bodélé dust experiment (BoDEx 2005), *Journal of Climate*, *21*(5), 995-1012, doi: 10.1175/2007JCLI1766.1.

Todd, M. C., C. J. T. Allen, M. Bart, M. Bechir, J. Bentefouet, B. J. Brooks, C. Cavazos-Guerra, T. Clovis, S. Deyane, M. Dieh, S. Engelstaedter, C. Flamant, L. Garcia-Carreras, A. Gandega, M. Gascoyne, M. Hobby, C. Kocha, C. Lavaysse, J. H. Marsham, J. V. Martins, J. B. McQuaid, J. B. Ngamini, D. J. Parker, T. Podvin, A. Rocha-Lima, S. Traore, Y. Wang, and R. Washington (2013), Meteorological and dust aerosol conditions over the Western Saharan region observed at Fennec supersite-2 during the Intensive Observation Period in June 2011, *Journal of Geophysical Research: Atmospheres*, *118*, 8426–8447, doi: 10.1002/jgrd.50470.

Tompkins, A. M. (2001), Organization of Tropical Convection in Low Vertical Wind Shears: The Role of Cold Pools, *Journal of the Atmospheric Sciences*, *58*(13), 1650-1672, doi: 10.1175/1520-0469(2001)058<1650:ootcil>2.0.co;2.

Washington, R., and M. C. Todd (2005), Atmospheric controls on mineral dust emission from the Bodélé Depression, Chad: The role of the low level jet, *Geophys. Res. Lett.*, *32*(17), L17701, doi: 10.1029/2005gl023597.

Washington, R., M. C. Todd, N. J. Middleton, and A. S. Goudie (2003), Dust-Storm Source Areas Determined by the Total Ozone Monitoring Spectrometer and Surface Observations, *Annals of the Association of American Geographers*, *93*(2), 297-313, doi: 10.1111/1467-8306.9302003.

Washington, R., M. C. Todd, S. Engelstaedter, S. Mbainayel, and F. Mitchell (2006), Dust and the low-level circulation over the Bodélé Depression, Chad: Observations from BoDEx 2005, *J. Geophys. Res.*, *111*(D3), D03201, doi: 10.1029/2005jd006502.

Washington, R., C. Flamant, D. J. Parker, J. H. Marsham, J. B. McQuaid, H. Brindley, M. C. Todd, E. Highwood, C. Ryder, J. P. Chaboureau, C. Kocha, M. Bechir, and A. Saci (2012), Fennec - The Saharan Climate System, *CLIVAR Exchanges*, *17*(3), 31-33.

Weckwerth, T. M., and R. M. Wakimoto (1992), The Initiation and Organization of Convective Cells atop a Cold-Air Outflow Boundary, *Monthly Weather Review*, *120*(10), 2169-2187, doi: 10.1175/1520-0493(1992)120<2169:tiaooc>2.0.co;2.

Williams, E., N. Nathou, E. Hicks, C. Pontikis, B. Russell, M. Miller, and M. J. Bartholomew (2009), The electrification of dust-lofting gust fronts ('haboobs') in the Sahel, *Atmospheric Research*, *91*(2-4), 292-298, doi: doi:10.1016/j.atmosres.2008.05.017.

Winker, D. M., J. Pelon, and M. P. McCormick (2003), The CALIPSO mission: Spaceborne lidar for observation of aerosols and clouds, paper presented at Lidar Remote Sensing for Industry and Environment Monitoring III, March 24, 2003.

6. The low level jet dust emission mechanism in the central Sahara: observations from Bordj-Badji Mokhtar during the June 2011 Fennec IOP

Christopher J.T. Allen and Richard Washington

Published in Journal of Geophysical Research Atmospheres 21 March 2014[12]

doi: 10.1002/2013JD020594[13] *(CC BY 3.0 license)*

Abstract

This paper presents the first detailed analysis of low level jets (LLJs) in the central Sahara from ground-based observations at Bordj-Badji Mokhtar, Algeria (BBM) and addresses their operation as a dust emission mechanism. On LLJ mornings, composite wind speeds in the core (300m agl, ≈935hPa) reach 13.5ms^{-1} between 0400-0500. 2m temperatures increase from 0545 (30 min. after sunrise), and jet decay begins around 0600. 10m wind speeds lag those in the core by five hours; peak 10m wind speed, 7.5ms^{-1}, occurs between 0900-1000. Only the deepest and strongest LLJs lead to dust emission. At 0600, these five LLJs have core wind speeds ≥16ms^{-1}, below-core wind shear ≥0.6ms^{-1}/30m, and wind shear between the core and 500m above the core ≤-1.8 ms^{-1}. On these occasions momentum mixes down from the LLJ after the onset of surface heating, leading to emission. On non-dusty LLJ mornings, the convective

[12] The Editor of JGR-Atmospheres highlighted this paper as 'a contribution of special significance' with the following description: "Using observations collected from a field campaign and numerical model output, this study documents in detail the low-level jet in central Sahara, including its diurnal cycle, three-dimensional structure, connection to the monsoon flow and the Harmattan, and vertical momentum transport as a mechanism for dust emission. The results are significant contributions to our understanding of the low-level jet and its role in Saharan climate". A description of the article was featured as a Research Spotlight in *Eos* (Vol. 95 No. 33 19 August 2014).

[13] Note that following Minor Corrections required by the DPhil examiners (requested after this chapter was published) the content of this chapter is not identical to the published version.

boundary layer is 100m shallower than on dusty mornings, and the LLJ is too weak to provide enough momentum to be mixed-down to the surface for emission. LLJs are most frequently embedded in the monsoon flow or in the Harmattan; there is clear association between the Saharan Heat Low and LLJ strength and orientation. ERA-Interim reanalysis underestimates winds in the core of both Harmattan and monsoon LLJs (by 4ms^{-1} and 6ms^{-1} respectively). The Met Office Africa Limited Area Model underestimates Harmattan LLJ core winds by only 0.2ms^{-1}. Winds in the core of monsoon LLJs however are underestimated by 8.5ms^{-1}. Surface winds at 0900 are underestimated in both cases, by up to 6ms^{-1}.

6.1. Introduction

Mineral aerosol, or dust, is being increasingly studied because of its effects on the atmospheric radiation budget [e.g. *Haywood et al.*, 2005; *García et al.*, 2012], subsequent changes in atmospheric and ocean circulation [e.g. *Tompkins et al.*, 2005; *Stanelle et al.*, 2010; *Evan et al.*, 2011; *Solmon et al.*, 2012], modification of biogeochemical processes [e.g. *Mahowald et al.*, 2010] and impacts on human health [e.g. *de Longueville et al.*, 2012; *Dukić et al.*, 2012]. In the Sahara Desert mechanisms which are known to lead to dust emission include cold pool outflows [e.g. *Marsham et al.*, 2008; *Emmel et al.*, 2010; *Allen et al.*, 2013]; dry convective plumes [e.g. *Ansmann et al.*, 2009]; monsoon surges [e.g. *Bou Karam et al.*, 2008; *Cuesta et al.*, 2010] and low level jets (LLJs) [e.g. *Washington and Todd*, 2005; *Washington et al.*, 2006a].

Dust emission from the Bodélé Depression, the dustiest place on Earth, is caused by the strong (20ms^{-1}) and persistent Bodélé low level jet (LLJ) [*Washington and Todd*, 2005; *Washington et al.*, 2006a]. LLJs are thought to lead to dust emission over much wider areas of the Sahara [e.g. *Schepanski et al.*, 2009; *Fiedler et al.*, 2013], but the lack of

observational data in the region, particularly before the Fennec project [*Washington et al.*, 2012] has meant that there is a need for more direct evidence to examine the link between LLJs and dust emission. This paper uses high resolution Fennec observations from the remote central Sahara to examine current LLJ dust emission understanding, and draws upon high resolution numerical model data to investigate the wider spatial context.

Much of the current work on LLJs stems from the ideas of *Blackadar* [1957] who proposed that LLJs can form over flat terrain after sunset, when the frictional force caused by turbulent mixing in the boundary layer is removed and the flow near the top of the boundary layer effectively becomes decoupled from the surface. If the background pressure gradient is strong enough, the flow accelerates and undergoes an inertial oscillation, with a period of $2\pi/f$, where f is the Coriolis parameter. In cloud-free desert regions, where nocturnal radiative cooling is intense, the conditions for the development of such jets are particularly favourable. Some numerical (large eddy simulation) modelling has successfully generated LLJs due to inertial oscillations [e.g. *Basu et al.*, 2008], and an exact analytical solution to the Blackadar model has also been demonstrated [*Shapiro and Fedorovich*, 2010]. The model has been extended to include frictional effects within the nocturnal boundary layer [*van de Wiel et al.*, 2010]. In many model simulations and observations, at locations as wide-ranging as Chad [*Washington et al.*, 2006a], the Netherlands [*van de Wiel et al.*, 2010], Niger [*Madougou et al.*, 2012], Mali [*Bain et al.*, 2010] and the Weddell Sea [*Andreas et al.*, 2000], the core of the jet is found a few hundred metres above the ground, although LLJs with core heights of ~100m or less have also been documented [*Banta et al.*, 2002]. *Marsham et al.* [2013] show that a nocturnal LLJ was a common feature at Fennec supersite 1 in the central

Sahara in June 2011, detectable in the mean diurnal cycle of near-surface and boundary layer winds, with peak winds at around 300m.

The mix-down of momentum from a LLJ to the surface is the process that leads to dust emission. This has been documented in detail for the Bodélé LLJ from observations [*Washington et al.,* 2006a] and regional climate model (RCM) simulations [*Todd et al.,* 2008]. After sunrise, turbulent mixing induced by surface heating increases and momentum from the jet is mixed down towards the surface [e.g. *Lothon et al.,* 2008]. Surface wind speeds begin to increase, and if they surpass the local emission threshold, dust uplift takes place. There is a lag of several hours between the peak wind speed in the LLJ (just before sunrise) and peak wind speed at the surface. On dusty days during the Bodélé Dust Experiment (BoDEx) in spring 2005, composite wind speeds (i.e. wind speeds averaged for dusty days) at the surface were maintained above $10ms^{-1}$ from 0600 to 1300 UTC [*Washington et al.,* 2006a]. At Fennec supersite 2 in the western Sahara, this lagged relationship is complicated by the Atlantic inflow, resulting in a much slower LLJ breakdown [*Todd et al.* 2013]. LLJs have also been documented to raise dust in other parts of the central and western Sahara [e.g. *Cuesta et al.,* 2008; *Knippertz,* 2008; *Schepanski et al.,* 2009]. Using ERA-Interim reanalysis [*Dee et al.,* 2011] and an offline dust model, *Fiedler et al.* [2013] estimate that 15% dust in the North African annual and spatial mean is caused by mix-down of LLJ momentum to the surface. In the Bodélé Depression, this figure is up to 60%. One reason the Bodélé LLJ is particularly strong and persistent is that the north-easterly Harmattan flow is channelled between two mountain chains, the Tibesti and Ennedi. RCM sensitivity experiments show that without this topography, 925hPa winds during a strong deflation event are 30% slower than with topography [*Washington et al.,* 2006b]. However, it has been argued that LLJs occur frequently in areas of the Sahara with little orography [*Schepanski et al.,* 2009],

and can occur in the monsoon flow [*Parker et al.,* 2005] as well as north of the inter-tropical discontinuity (ITD) [*Bou Karam et al.,* 2009].

Given the potential importance of LLJs as a dust mechanism in the central Sahara and given the observational data available for the first time from Fennec, the key questions posed by this paper are: (i) What are the observed characteristics of the LLJ in the central Sahara at Bordj-Badji Mokhtar (BBM) in summer? (ii) How well are LLJs at BBM represented by the Met Office Africa Limited Area Model and ERA-Interim reanalysis? (iii) Under what synoptic and local conditions is LLJ development favourable? (iv) What are the characteristics of LLJs associated with dust emission? (v) Is dust emission consistent with the mix-down of momentum from the jet core?

Section 6.2 describes the location of the observations, the instrumentation and additional data and methods employed. Section 6.3 presents the June 2011 composite LLJ, surface wind speeds and temperature from the Fennec supersite 1. Section 6.4 develops a LLJ detection scheme and an index of LLJ strength. Section 6.5 explains the spatial orientation of the LLJs and assesses model performance at simulating LLJ profiles. Section 6.6 addresses the synoptic and local conditions for LLJ development. Section 6.7 attends to the relationship between LLJs and dust emission. Section 6.8 discusses evidence for low-level oscillations and a discussion and conclusions are presented in Section 6.9.

6.2. Data and methods

6.2.1. The Bordj-Badji Mokhtar supersite during the Fennec project

The Fennec project [*Washington et al.,* 2012] is the first project to instrument the remote central Sahara and provide detailed airborne and ground-based observations of central Saharan atmospheric dynamics, dust and radiation. Fennec supersite 1 is located

in south-west Algeria at the existing synoptic station of BBM on the border with Mali (21.38N, 0.92E; altitude 420m asl; WMO ID: 60686). It is very close to the boreal summer global climatological dust maximum [e.g. *Ashpole and Washington*, 2012] which makes it an unparalleled location to study central Saharan dust emission. *Ashpole and Washington* [2013] identify 15 major source regions of dust in the central Sahara. BBM is within one of these. Additionally, they identify major sources ≈100km to the NW, ≈300km to the WSW, ≈200km to the SSW and ≈200km to the ESE. The ITD frequently lies over BBM in summer, making it an excellent site from which to sample LLJs in both the south-westerly monsoon flow and the north-easterly Harmattan.

During the first Fennec Intensive Observation Period (IOP) in June 2011, BBM was heavily instrumented. June was chosen since the satellite-derived absorbing aerosol index from the Total Ozone Mapping Spectrometer shows that June is the dustiest month in the central Sahara [e.g. *Engelstaedter et al.*, 2006]. The instrumentation included a HALO Photonics Streamline 1.55μm Doppler lidar; a Scintec MFAS phased array sodar; a Cimel sun photometer; an inverse nephelometer (670nm, fixed at 2m height); Vaisala RS92 GPS radisosondes (launched at three-hourly to six-hourly intervals) and a 15m mast (the 'flux tower') instrumented with 20-Hz sonic anemometers at 10m and 15m. Pressure, visibility and passively ventilated measurements of temperature and humidity were taken at 2m. Unless otherwise stated, all times reported are in UTC. *Marsham et al.* [2013] provide a comprehensive overview of the meteorology and *Allen et al.* [2013] provide a detailed analysis of the dust events during the IOP. There was no rain at BBM during the IOP.

Instrument measurement accuracy is as follows: nephelometer scattering $\pm 10^{-7} m^{-1}$; relative humidity ±2%; temperature ±0.3°C; pressure ±0.5hPa; anemometer wind speed

$\pm 0.1 ms^{-1}$. The Doppler measurement precision of the lidar is $\leq 10 cm^{-1}$ in the boundary layer [*Pearson et al.*, 2009]. A standard lidar inversion technique is employed to obtain the aerosol backscatter coefficient profile [*Fernald et al.*, 1972; *Klett*, 1981; *Fernald*, 1984]. Lidar horizontal wind speed and direction measurements are derived using a modified velocity-azimuth display algorithm [*Browning and Wexler*, 1968; *Banta et al.*, 2002] and have an accuracy of $\pm 0.1 ms^{-1}$ and $\leq 0.9°$ respectively[14]. Minimum lidar range is 75m above ground level (agl) although the lowest lidar wind measurements are taken at 90m agl. The vertical resolution of the measurements is 30m. Lidar horizontal wind speed profiles were taken twice an hour; unless otherwise stated these two profiles are averaged to obtain hourly resolution. Lidar data were obtained from 3 June 2011 to the end of the month.

Aerosol Optical Thickness is reported at 500nm (AOT_{500}) and is level 1.5 (cloud-screened). AOT is accurate to ±0.01. The sun photometer formed part of the AERONET project [*Holben et al.*, 1998] during deployment. AOT availability is not continuous: where there are gaps this is not because AOT_{500} is zero but because either (i) no AOT measurements were taken (e.g. night) or (ii) AOT measurements were removed as part of the level 1.5 cloud screening process. Radiosondes were launched at three- or six-hourly intervals, from 8 June 2011 to the end of the month. Reproducibility (standard deviation of differences in twin soundings) of radiosonde measurements is as follows: temperature 0.2°C, humidity 2% RH, pressure 0.5hPa. The positioning uncertainty of the radiosonde GPS in the horizontal is 10m. There are some periods with missing data; where relevant these are highlighted in the text and in the captions with an explanation given where possible.

[14] Information on the accuracy of the lidar-derived wind direction retrieval is not readily available. In a study using an identical Doppler lidar, *Newsom et al*. [2013] found that the difference between the wind direction measured by sonic anemometer and wind direction retrieved by lidar was up to 0.9°.

6.2.2. Satellite and numerical model data

The presence of deep cloud and dust over the wider Saharan region is identified using false colour imagery from the Spinning Enhanced Visible & Infrared Imager (SEVIRI) on board the Meteosat Second Generation satellite at 0N, 0E [*Lensky and Rosenfeld*, 2008]. Additionally, a SEVIRI cloud mask product (available from the EUMETSAT website) is also used.

A configuration of the UK Met Office Unified Model [*Walters et al.*, 2011], the Africa Limited Area Model (LAM), is used to provide a regional context and for comparison with observations. Africa LAM horizontal resolution is 12km. There are 70 levels in the vertical. The lowest level is at 10m; levels are terrain following in the lower troposphere. The boundary layer scheme is described by *Lock et al.* [2000] with modifications as in *Lock* [2001] and *Brown et al.* [2008]. It is a first-order turbulence closure which mixes adiabatically conserved variables. In stable boundary layers and in the free troposphere a local Richardson number scheme [*Smith*, 1990] is used with the stable stability dependence given over land by the 'long tail' function. In unstable boundary layers, diffusion coefficients (K-profiles) are specified functions of height through the boundary layer, related to the strength of the turbulence forcing. Two K-profiles are used, one for surface sources of turbulence (surface heating and wind shear) and one for cloudtop sources (radiative and evaporative cooling) [*Walters et al.*, 2011]. The LAM is driven by the Met Office Global Model (the Unified Model in its numerical weather prediction configuration), which assimilates data globally using Hybrid Incremental 4D-Var. Boundary conditions are applied in a ten-point rim around the edge of the LAM domain. Sea surface temperatures are held constant during runs. The LAM simulations ran to T+54h. There were two forecast runs per day (at 06z and 18z), but only data from

the 18z forecast are available. The LAM fields presented here are T+12 (18z initialisation, valid at 0600).

European Centre for Medium Range Weather Forecasts ERA-Interim reanalysis (ERAI) [*Dee et al.*, 2011] is presented for comparison with the LAM in Section 6.5.2. ERAI has a six-hourly temporal resolution, horizontal resolution of 0.75 degrees (roughly 83km in the central Sahara) and 60 levels in the vertical, which are terrain following in the lower troposphere. A K-diffusion scheme is used to parameterize turbulent transport in the stable boundary layer [*Bechtold et al.*, 2008].

The LAM was chosen as the primary model tool for several reasons. (i) Automatic weather station (AWS) measurements from Fennec AWS across remote Mauritania and Algeria were assimilated [*Hobby et al.*, 2012]. (ii) 12km is very high spatial resolution. (iii) LAM simulation of Harmattan LLJs at BBM is excellent, and substantially better than ERAI (see Section 6.5.2). (iv) An objective of the Fennec project is to better understand and improve Met Office numerical weather prediction tools in the Sahara.

6.2.3. Momentum calculations

Most studies of LLJs in the Sahara use wind speed as a proxy for momentum. The Fennec instrumentation at BBM, however, allowed direct calculations of momentum to be made for the atmospheric column above the supersite. Wind velocity at 30m intervals through the atmosphere was obtained from the lidar, at hourly timesteps. The mass of each 30x1x1m column of air was derived from its density, which was calculated from radiosonde observations at every 30m height interval. With the velocity and mass of each 30m column known, momentum could be calculated. When sonde launches were three-hourly, the hourly lidar velocity profiles were used together with mass calculations from the (temporally) closest sonde launch to obtain hourly

momentum profiles. When sonde launches were six-hourly, momentum profiles were not estimated for intermediate hours. For the 0600 radiosonde launches (the launch time when the LLJ was strongest), balloon horizontal deviations from the launch point were never more than 9km (by 2000m agl) and only 1.0km by 300m agl (the mean height of the wind speed maximum). Momentum at 10m agl was calculated using measurements taken on the flux tower.

On mornings when LLJs were detected (see Section 6.4), the lidar-derived wind direction in the lowest ~1km of the troposphere (i.e. containing the LLJ) was roughly constant. With a constant wind direction with height, its effect on vertical momentum mixing will be small. The constant wind direction in the bottom ~1km also made it possible to determine whether the LLJ was embedded in the Harmattan or the monsoon flow.

6.2.4. Assessment of dust producing mechanisms

Assessment of the dust conditions (Section 6.7) was accomplished following the approach of *Allen et al.* [2013]. This is a multi-platform approach which includes the SEVIRI dust detection algorithm; lidar backscatter and wind speed profiles; nephelometer scattering; 2m temperature, pressure and relative humidity; 10m wind direction and speed; sodar wind speed and Africa LAM simulations. The approach is able to separate different dust production mechanisms and distinguish between advected and locally emitted dust. See Sections 3 and 4 of *Allen et al.* [2013] for full details.

6.3. Composite LLJ, near-surface wind speeds and temperature

The following two sections address key question 1: What are the observed characteristics of the LLJ in the central Sahara at BBM in summer?

6.3.1. Composite LLJ wind profile and daily variability

The composite wind speed profile for 3-30 June 2011 clearly shows that the LLJ is detectable in the mean diurnal cycle over BBM (lidar wind data, Figure 6-1). From 0000 to 0700, the core of the jet is found close to 300m agl (Figure 6-1; 300m≈935hPa). (Henceforth 'core' will be used to refer to the height of the LLJ wind speed maximum.) The LLJ begins to develop after sunset (1839h on 15 June). Peak mean LLJ wind speed, 12 ms^{-1} in the composite, occurs from 0300 to 0500 (Table 6-1). After sunrise (0513h on 15 June) the jet decays and the height of the wind speed maximum increases (Figure 6-1, Table 6-1).

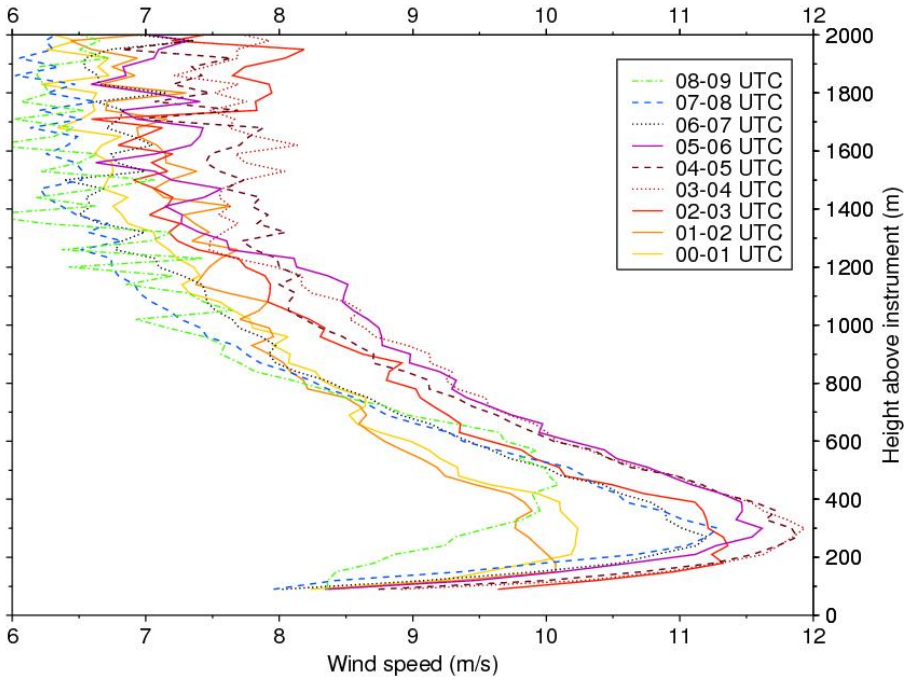

Figure 6-1: Composite wind speed-height profiles for 3-30 June 2011 (ms^{-1}). Measurements are from the lidar instrument. Measurement times (boxed) refer to the average of the two wind profiles taken by the lidar within the given hour interval.

Table 6-1: June 2011 composite wind statistics for morning hours at BBM.†

Time (UTC)	Peak wind speed (m/s) (composite)	Height agl of peak wind speed	Wind speed at 10m height (composite)
00-01	10.2	300m	5.6
01-02	10.2	190m	5.6
02-03	11.4	250m	6.3
03-04	12.0	300m	6.0
04-05	12.0	300m	5.5
05-06	11.6	300m	5.3
06-07	11.3	290m	5.1
07-08	11.4	300m	6.0
08-09	10.2	480m	6.8
09-10	9.0	600m	7.0

† Wind speeds shown are from the lidar instrument except for those at 10m height which are measured on the flux tower. All available measurements are averaged across the indicated time intervals. The time period for the composite is 3-30 June 2011. 10m wind speeds for hours after 1000 are shown in Figure 6-3a.

Although the composite shows a clear LLJ structure (Figure 6-1), there is significant day-to-day variability in the wind speed profiles in the nocturnal and morning hours over the course of the month. Between 0400 and 0500, when the composite LLJ is at its peak wind speed, wind speed maxima on different days of June 2011 range from 4.7ms^{-1} to 23ms^{-1} (Figure 6-2). Several of the profiles do not display the characteristic LLJ shape, with the height of the wind speed maxima below 2000m agl ranging from 90m to 1680m (Figure 6-2). There is similarly large variability in the wind speed profiles at other nocturnal and morning hours (not shown). In Section 6.4, it will be shown that not all of these profiles are LLJs.

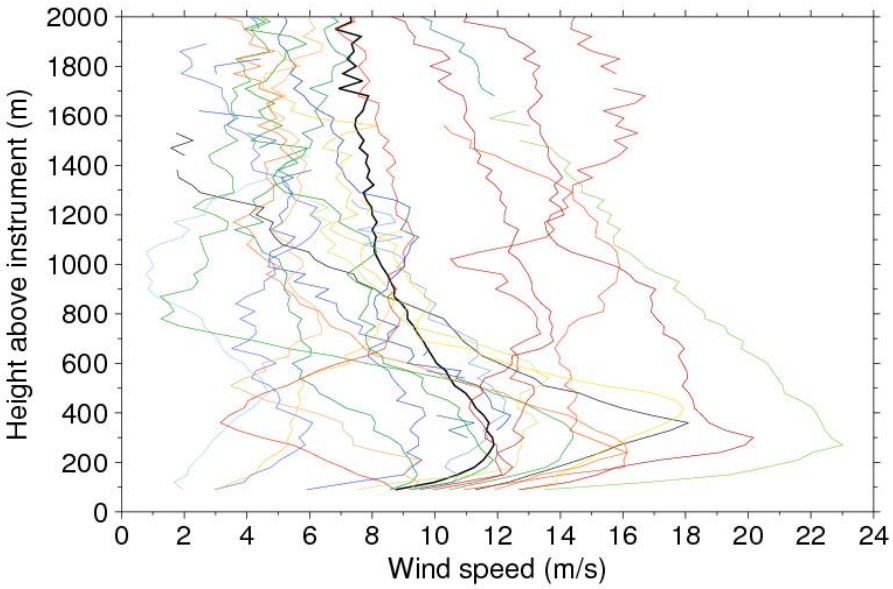

Figure 6-2: 3-30 June 2011 lidar wind speed-height profiles for 04-05h, the peak LLJ time interval. The different colours represent different days; on each day the two profiles taken by the lidar between 0400 and 0500 were averaged to produce one profile. The thicker black line is the mean of all the profiles.

6.3.2. Composite 10m wind speed

Composite wind speeds (6-30 June, 10m agl) decline gradually from 02-03h to 06-07h (Figure 6-3a, Table 6-1). Between 06-07h and 07-08h there is a relatively large jump in 10m wind speed, from 5.1ms^{-1} to 6.0ms^{-1}. Composite wind speeds continue to increase until 09-10h, when they peak at 7ms^{-1}. This peak is five hours behind the composite LLJ peak (Table 6-1). Such a lagged relationship was also found in the Bodélé, where composite surface wind speeds for the BoDEx period also peaked from 09-10h, but were higher (9ms^{-1}; Washington et al, 2006a). The composite 10m wind has large standard deviations (always larger than any change in mean wind speed from one hour to the next). The peak composite wind speed of the diurnal cycle at 09-10h is only

7.0ms^{-1}, but has a standard deviation of 3.0 ms^{-1}. It is likely that the large variability of the LLJ contributes to the large variability of the 10m wind speed in the late morning.

6.3.3. Composite 2m temperature

Composite 2m temperature (6-30 June) follows the expected diurnal cycle, peaking at 42.5°C at 1500 (Figure 6-3b). The standard deviations are larger in the evening and early morning than at other times. This is likely due in part to the effect of cold pool outflows, which are most frequent at these times (see *Allen et al.* [2013] and *Marsham et al.* [2013] for details of these events), and to the influence of the monsoon flow, which intrudes furthest north at night but displays significant daily variability [*Parker et al.*, 2005; *Marsham et al.*, 2013]. Temperatures begin to increase again at 0545. The LLJ begins to decay from this point onward (Figure 6-1) and 10m wind speeds start to increase from 0700 onward (Figure 6-3a). Taken together, the timings of these three features (2m temperature, LLJ speed, 10m wind speed) are consistent with the theory that turbulent mixing soon after sunrise mixes down momentum from the LLJ towards the surface.

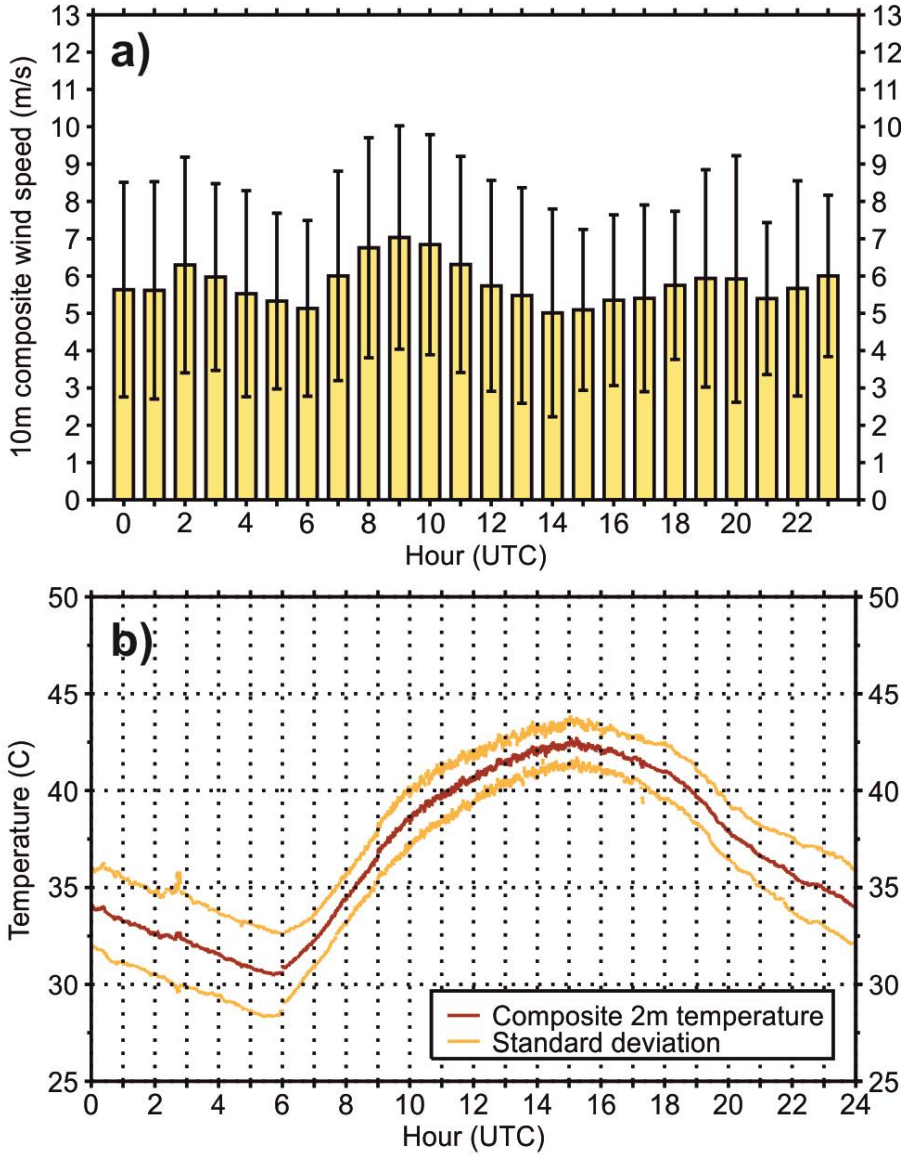

Figure 6-3: 6-30 June 2011 (a:) composite 10m wind speed (ms^{-1}, yellow bars) and ±1 standard deviation (lines). (b:) composite 2m temperature (°C) and ±1 standard deviation. Wind speed measurements are shown averaged for hourly periods (i.e. 00h-01h, 01h-02h etc). Flux tower winds speed and temperature measurements are not available prior to 6 June.

6.4. LLJ detection criteria

Given the large daily variability in wind profiles discussed in Section 6.3.1, it is important to be able to objectively identify mornings on which LLJs occurred. There are no universally accepted criteria for identifying LLJs [*Kallistratova and Kouznetsov*,

2012; *Nunalee and Basu*, 2013]. *Schepanski et al.* [2009] and *Fiedler et al.* [2013] have developed LLJ detection schemes for the Sahara, from ERA-40 and ERAI reanalysis data respectively. Although ERAI is the newer version of the product, it still likely underestimates the morning LLJ strength [*Fiedler et al.*, 2013] and, in the nocturnal boundary layer, simulates artificially smooth changes in meteorological variables with height [*Sandu et al.*, 2013]. Given these problems, and given the existence of the high quality Fennec observational dataset for BBM, we optimize the *Fiedler et al.* [2013] detection method to LLJ values based on thresholds from observations at BBM rather than those which are appropriate for reanalysis data. We later show that application of the original *Fiedler et al.* [2013] criteria to the observational data would be unsuitable given the differences between ERAI reanalysis and the observed (Section 6.5.2), and that adoption of the *Fiedler et al.* [2013] detection criteria would miss 3/5 of the LLJs which lead to dust emission at BBM (Section 6.7.1).

The LLJ identification criteria were developed and applied to the 06-07h lidar wind speed profiles. This period was chosen for three reasons (i) it is a period when shear is still present in the LLJ profile (Figure 6-1) but the jet is close to breakdown: the strength of the LLJ from 06-07h is expected to have a close relationship with dust emission, which is a key focus of this paper (ii) it is an hour commonly used for model outputs, allowing for easy model-observation comparison (iii) it opens the possibility of future comparison with 0600 radiosoundings across West Africa.

LLJ detection is executed in four steps. First, the wind speed maximum below 600m agl is identified. This is much lower than 1500m which is used by [*Fiedler et al.*, 2013]. It is chosen based on the composite wind profiles (Figure 6-1) and in order to avoid detecting elevated wind speed maxima which occur on some mornings. These elevated

maxima can occur together with or without LLJs, and are likely caused by processes other than frictional decoupling from the surface since they are found several hundred metres above the nocturnal temperature inversion. (Indeed, *Fiedler et al.* [2013] acknowledge that a 1500m window is a generous allowance for LLJ heights.) Second, the wind shear between the LLJ core and 500m above the core must be $\leq$ -1.8 ms^{-1}. Tests for wind shear over multiple, shallower layers above the core were considered but rejected since several events subjectively identified as LLJs have periods when the above-core wind shear reverses and becomes positive. Third, the wind speed under the core must decrease to the lowest measurement (90m agl). Finally, the core wind speed must be > 8 ms^{-1}. LLJs were found to occur on 21/28 mornings of June 2011 (lidar measurements unavailable prior to 3 June). The values for each of these criteria, along with the classification of the LLJs, are listed in a case by case basis in Table 6-2.

Date	Wind speed max (ms^{-1})	Height of wind speed max (m agl)	Above core wind shear (ms^{-1})	Below core wind shear (ms^{-1}/30m)	LLJ?	Low level jet index (LLJi, m^2s^{-1})	Cold pool present in the morning?	LLJ leads to dust emission?
Not LLJs								
4	4.3	90	-1.4	N/A¶	N	N/A	N	N/A
7	6.4	300	-1.8	0.5	N	N/A	N	N/A
19	5.5	90	-4	N/A¶	N	N/A	Y	N/A
27	10.6	180	-1.1	0.5	N	N/A	N	N/A
6	7.3	270	+2.2	0.2	N	N/A	N	N/A
24	12	150	-0.8	0.5	N	N/A	N	N/A
17	10.8	210	-1.7	0.5	N	N/A	Y	N/A
Non dust producing LLJs/LLJs combined with cold pools	*all > 8m/s*		*all ≤ -1.8*					
11	10.6	280	-3.6	1.0	Y	1410	N	N
12	10.9	180	-3.7	0.9	Y	3160	N	N
22	9.8	150	-2.6	0.7	Y	3610	Y	N
20	9.7	180	-4	1.5	Y	4650	N	N
8	8.9	270	-2.6	0.5	Y	5060	N	N
23	11.1	180	-6	0.7	Y	6170	Y	N
13	11.1	120	-3.9	0.9	Y	7010	Y	N
10	9.8	210	-3	1.0	Y	7380	N	N
15	14.3	240	-7.4	1.2	Y	7930	N	N
14	13.1	240	-11.4	0.5	Y	10860	N	N
9	13.4	120	-5.2	1.4	Y	14350	N	N
18	10.4	300	-7	0.6	Y	14710	Y	N
25	15.3	390	-7.5	0.7	Y	24180	Y	N
28	13.2	210	-3.4	0.8	Y	29700	N	N
21	14.8	450	-4.7	0.6	Y	31240	Y	N
30	17.2	540	-3	0.4	Y	73480	Y	N
Dust producing LLJs	*all > 16m/s*		*all ≤ -1.8*	*all ≥0.6/30m*				
5	17.2*	300*	-7*	0.7*	Y	23120	N	Y
3	18	330	-9	1.1	Y	24750	N	Y
29	16.2	360	-2.2	0.6	Y	44130	N	Y
26	19.2	270	-3.2	1.6	Y	53580	N	Y
16	22.7	270	-1.8	1.3	Y	94550	N	Y

Table 6-2 (above): Day-to-day variability in 06-07h wind profiles at BBM, June 2011.

Measurements are from the lidar instrument, averaged between 06-07h. Wind speed maxima are reported for observations below 600m agl. 'Above core wind shear' is the wind shear between the LLJ core (i.e. the height of the wind speed maximum) and 500m above the core. Below core wind shear is calculated between the LLJ core and 90m agl (the lowest available measurement) and is shown /30m height interval to be comparable. ¶ When the wind speed maxima themselves are at 90m agl (the lowest measurement), below-core wind shear cannot be calculated (4 and 19 June). Only 19 June could be a missed detection however since 4 June fails the above-core shear criterion. *indicates that measurements between 06-07h are unavailable and the average is calculated for the 07-08h period. No measurements are available prior to 3 June. For details on how events are classified as LLJs, see Section 6.4. Within each subsection, events are ranked by low level jet index (LLJi, low to high). For the definition of the LLJi see Section 6.4.1. Figure 6-6 summarises the LLJ detection scheme graphically. For further details on the distinction between LLJs that lead to dust emission and those that do not, see Section 6.7.

A surface temperature inversion criterion was considered but not included for two reasons: i) radiosonde soundings were not made at 0600 on 7/28 mornings ii) on 2/7 mornings when cold pool outflows occur together with LLJs, a surface temperature inversion is not present at 0600. However, a temperature inversion criterion alone is not sufficient to detect cold pools which is why we restrict the LLJ detection criteria to wind metrics and use the multi-platform detection approach of *Allen et al.* [2013] for cold pools (see Sections 6.2.4, 6.4.2 and 6.7.2.4).

The thresholds used for LLJ detection were developed from subjective analysis of individual wind speed profiles. Discriminant Analysis was subsequently used to demonstrate that the subjectively derived thresholds were objectively reproducible. Discriminant Analysis is a statistical technique that objectively classifies categories on the basis of a set of variables. Comparison with the objective classification derived from the linear combination of a set of variables reveals the extent to which an *a priori* classification scheme which might have been subjectively derived is reproducible [e.g. *Diab et al.*, 1991; *Michailidou et al.*, 2009; *Garrity et al.*, 2010]. Using the below-600m agl wind speed maximum, above-core wind shear and below-core wind shear as the discriminating variables (the same as those presented in the LLJ detection scheme, Table 6-2), the technique was used to objectively reclassify the profiles into the two classes. On 19/21 occasions, profiles which were classified *a priori* as LLJs by the original detection scheme remained in the same class, and on 7/7 occasions profiles which were classified *a priori* as not being LLJs remained in the same class. Since 93% of the observations are well-classified according to Discriminant Analysis the detection scheme is considered to be apposite.

There is a clear distinction between composite lidar wind profiles for LLJ mornings and mornings without LLJs (Figure 6-4). On LLJ mornings, there is a well-defined LLJ structure, similar to the all-June composite (Figure 6-1) but the core wind speeds (300m agl) reach a maximum of 13.5 ms^{-1} at 04-05h, 1.5 ms^{-1} faster than the all-June composite. Core wind speeds stay above 12.5 ms^{-1} until 08-09h. At 10m agl, flux tower wind speeds follow a similar structure to the all-June composite (Table 6-1), also peaking at 09-10h but at 7.5 ms^{-1} (Table 6-3), 0.5ms^{-1} faster than the all-June composite. On non-LLJ mornings, there is a weak and shallow LLJ-like structure from 00-03h (the LLJ criteria are applied at 06-07h for the reasons given above) but the low-level winds decay rather than develop from 03-04h onwards (Figure 6-4b). This shows that LLJ-like development in the nocturnal hours does not necessarily result in fully fledged LLJs by the morning.

Table 6-3: Flux tower composite 10m winds for mornings when LLJs are detected†

Time (UTC)	00-01	01-02	02-03	03-04	04-05	05-06	06-07	07-08	08-09	09-10	10-11	11-12	12-13
Composite wind speed (ms^{-1})	5.8	5.7	6.4	6.1	5.9	5.6	5.4	6.5	7.2	7.5	7.1	6.2	5.6

†All available measurements are averaged across the indicated time intervals. Mornings included in the composite (i.e. LLJ mornings) are shown in Table 6-2.

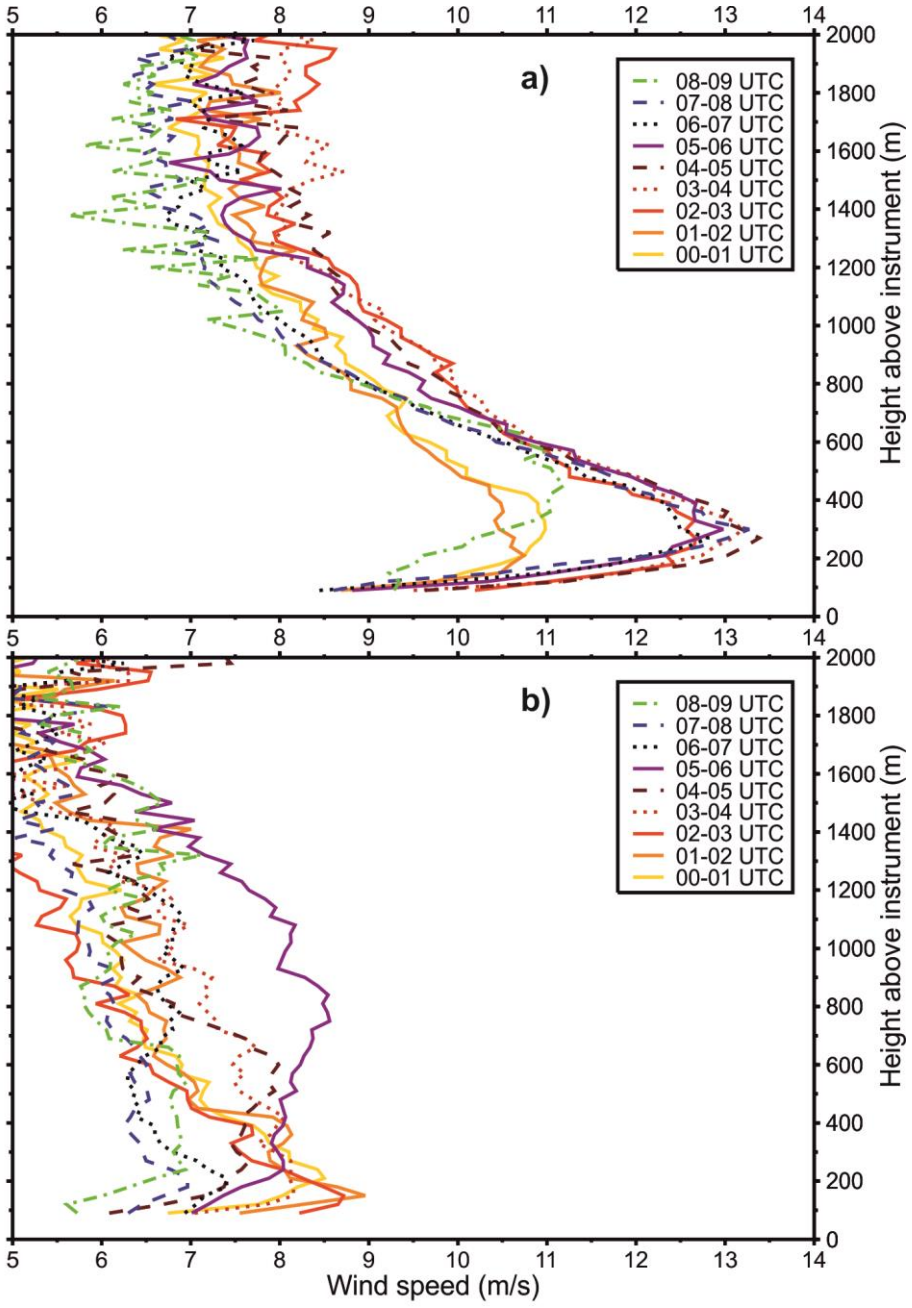

Figure 6-4: Lidar composite hourly-mean wind speed-height profiles (ms^{-1}, key in box). (a:) mornings which pass the LLJ detection criteria (Section 6.4). (b:) mornings which fail the LLJ detection criteria.

6.4.1. An index of LLJ strength

Having classified the LLJs over BBM during June 2011, it is useful to have a measure of their strength. Whilst peak wind speed is one metric, it does not take into account the

depth of the atmosphere through which the LLJ exists, or for how many hours high winds persist. Next we develop a more comprehensive index that can be used to compare the strength of different LLJs. The LLJ index (LLJi), which is only applied on mornings when LLJs are detected (Section 6.4), is defined as the summation of wind speed exceeding a threshold in lower troposphere over a chosen time period (Equation 1).

$$LLJi = \sum_{h=1}^{n} \int_{z_1}^{z_2} f_h(z)\, dz \qquad (1)$$

n is the number of hours in the time period, z_1 and z_2 are the chosen lower and upper height bounds and $f_h(z)$ is the wind profile over the chosen threshold wind speed at hour h. Units are m^2s^{-1}. The time period chosen is from 0000-0900 in order to capture LLJs that persist after sunrise. We use a threshold wind speed of 8 ms^{-1} and height bounds 90-1100m. These are chosen to correspond with the LLJ detection scheme (Section 6.4). Below-core wind shear is calculated down to the lowest lidar measurement, 90m agl, so this is used as the LLJi lower height bound. The detection scheme searches under 600m agl for wind speed maxima over 8 ms^{-1} and then checks the wind shear between the height of the maximum and 500m above this, making a logical LLJi upper height bound 1100m (i.e. 600m+500m). Since the LLJi integrates over any areas within the height bounds where wind speeds are greater than 8 ms^{-1}, on mornings when the LLJ is shallow the LLJi will also capture elevated areas of high wind speed if these are present. However, reducing z_2 to 900m agl or 600m agl to combat this does not change the LLJi rankings significantly: in all three cases the strongest 5 LLJs retain identical rankings and the strongest 14 LLJs remain the strongest

14 LLJs. Reducing z_2 also has the undesirable consequence of underestimating the strength of the strongest, deepest LLJs so z_2 is kept at 1100m agl.

The LLJi time series is shown in Figure 6-5 (numerical values in Table 6-2). Although LLJi is only applied to mornings when LLJs are detected, there is considerable variability in the strength of the 21 LLJs over the course of the month. The strongest LLJ is on 16 June, followed by 30 and 26 June. A cartoon summarising the LLJ detection process and LLJi calculation is shown in Figure 6-6.

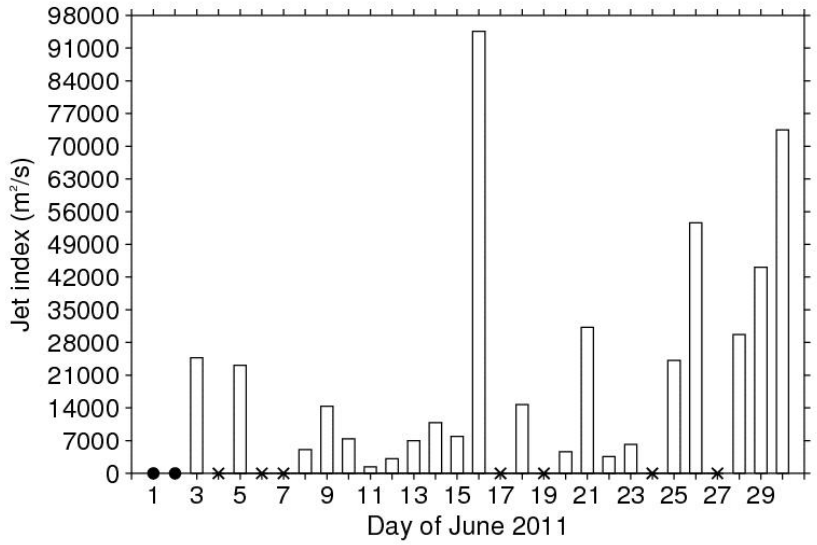

Figure 6-5: Time series of BBM low level jet index (LLJi, m^2s^{-1}) for June 2011. LLJi is defined by Equation 1 (see Section 6.4.1 for full details). Chosen parameters are: threshold wind speed 8 ms^{-1}; core height bounds 90-1100m agl; time interval 0000 to 0900. Solid circles indicate mornings when the lidar did not take any wind speed profiles (1 and 2 June). Crosses indicate mornings which do not pass the LLJ detection criteria (Section 6.4, Table 6-2).

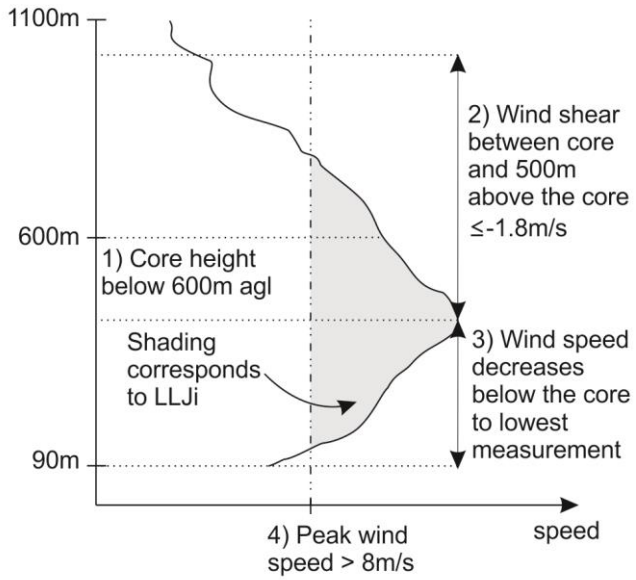

Figure 6-6: Cartoon summarising the LLJ detection scheme graphically. The y axis is height above ground level and the x axis is wind speed. The shading corresponds to the integral calculation done by the LLJi at this particular time step.

6.4.2. LLJs and cold pool outflows

On several mornings when LLJs are present at BBM, cold pool outflows also pass through the supersite. On these mornings, LLJ wind speed profiles are not always easily distinguishable from LLJ wind speed profiles on mornings without cold pools. To ensure that the analysis focuses initially on understanding LLJs rather than LLJ/cold pool combinations, mornings with cold pools ranked within the top 20 events of the month by *Allen et al.* [2013] are excluded from here onwards. This excludes 7/21 mornings (Table 6-2). The remaining 14 jets will be referred to as 'pure' LLJs. This approach also enables direct comparison with the Africa LAM, whose representation of cold pool outflows is poor [e.g. *Marsham et al.*, 2011], unsurprising for a model of 12km resolution and parameterised convection.

6.5. Africa LAM and ERAI simulations of the LLJ

6.5.1. Spatial position of the LLJ

Analysis of the Africa LAM 925hPa (roughly 400m) wind and specific humidity fields on the 14 'pure' LLJ mornings reveals that 6 LLJs are embedded in the dry ($q \approx 3g\ kg^{-1}$) northerly/northeasterly Harmattan flow and 5 LLJs are embedded in the relatively moist ($q \approx 9g\ kg^{-1}$) southerly/southwesterly monsoon flow (which is sometimes recirculated to arrive at BBM from another direction, e.g. WNW on 26 June). Jet directions are shown in Figure 6-7. On the remaining three mornings, the LLJ is simulated as part of an extensive westerly/northwesterly 'Atlantic inflow'. The LAM simulates the LLJs not as ribbons, but rather as sheets (≈100-500km wide). In some regions (e.g. between the Hoggar and the Atlas), the horizontal scale of the LLJs is probably set by the orography (flow channelling). The SHL also organises the flow (discussed later in Section 6.6.1) and the weak pressure gradient in its centre may act as a spatial boundary. Within each of the three types identified above there is variability with regards to the maximum LLJ wind speed (from 12-15 to 21-24ms^{-1}). The maximum LLJ wind speed is not necessarily found directly over BBM.

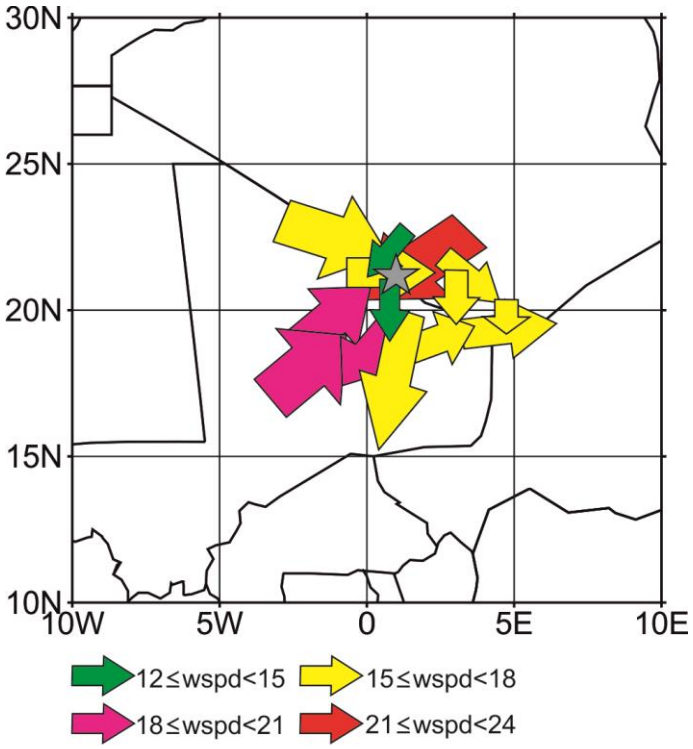

Figure 6-7: Spatial position of LLJs from the Africa LAM 0600 wind fields at 925hPa. Each arrow corresponds to a morning when a LLJ is detected at BBM (excluding those when cold pools were observed at BBM together with LLJs, see Section 6.4.2). For each of these mornings, the spatial position of the maximum wind speeds in the LLJ as simulated by the LAM is plotted. The arrow shows the direction of the LLJ, the colour the maximum wind speed and the width the span of the area of maximum wind speed. The location of BBM is shown as a star.

6.5.2. Comparison with observations at BBM

This section addresses key question 2: How well are LLJs at BBM represented by the Met Office Africa Limited Area Model and ERA-Interim reanalysis?

The lidar instrument makes it possible to compare LLJ wind observations at BBM with the Africa LAM simulations for the BBM gridbox. At 0600, simulated 925hPa wind direction on LLJ mornings is only greater than 22.5° out from observations on two occasions (not shown). On 28 June an observed south-westerly monsoon LLJ is simulated to arrive from the south. A more major simulation error occurs on 5 June,

when an observed south-westerly monsoon LLJ is simulated to reach BBM from the WNW.

The performance of the Africa LAM is significantly different depending on whether the LLJ is embedded in the monsoon or the Harmattan. The simulated 0600 composite wind speed profile for Harmattan LLJs at BBM shows excellent agreement to that measured by the lidar (Figure 6-8a). A clear LLJ is simulated by the LAM, with the core wind speed only fractionally too slow (12.9ms^{-1} compared to 13.1ms^{-1}). The core height is also accurately simulated. LAM wind speeds above 300m are between 0.5 and 2 ms^{-1} too fast but the surface wind speed is only underestimated by 0.8 ms^{-1}. This is in stark contrast to the ERAI reanalysis, which simulates the Harmattan LLJ structure very poorly, underestimating winds at all levels except the surface and 2km agl (Figure 6-8a). Maximum wind speeds are underestimated by 4ms^{-1}.

At 0900, approximately three hours after sunrise, wind speeds below 700m agl are simulated reasonably well by the LAM but wind speeds at the surface are underestimated by 1.8ms^{-1} (Figure 6-8b). Crucially for dust, surface wind speeds in the observed composite are above the BBM emission threshold, estimated at 8ms^{-1} [*Allen et al.*, 2013], but the simulated wind speeds are not. There is no 0900 timestep in ERAI reanalysis.

The LAM is less successful at simulating monsoon LLJs at BBM. At 0600, a weak LLJ structure is evident but wind speeds are underestimated at all heights below 2km agl by at least 1.5ms^{-1}, and underestimated by 8.5ms^{-1} in the jet core (Figure 6-8c). ERAI performs slightly better (jet core wind speeds underestimated by 6ms^{-1}) but the monsoon LLJ profile is still very poorly represented (Figure 6-8c). At 0900, wind speeds are simulated well by the LAM between 800m and 1400m agl but

underestimated elsewhere and by 6ms^{-1} at the surface (Figure 6-8d), again taking them below the local dust emission threshold. The underestimation of surface wind speeds by the LAM at 0900 in both Harmattan and monsoon LLJs suggests that the boundary layer processes responsible for momentum mix-down are not adequately represented. However, the Africa LAM simulates Harmattan LLJ profiles much better than monsoon LLJs, which suggests that the moist dynamics present a particular challenge for the model in the boundary layer. A detailed model-observation comparison is beyond the scope of this paper but will be addressed in future work.

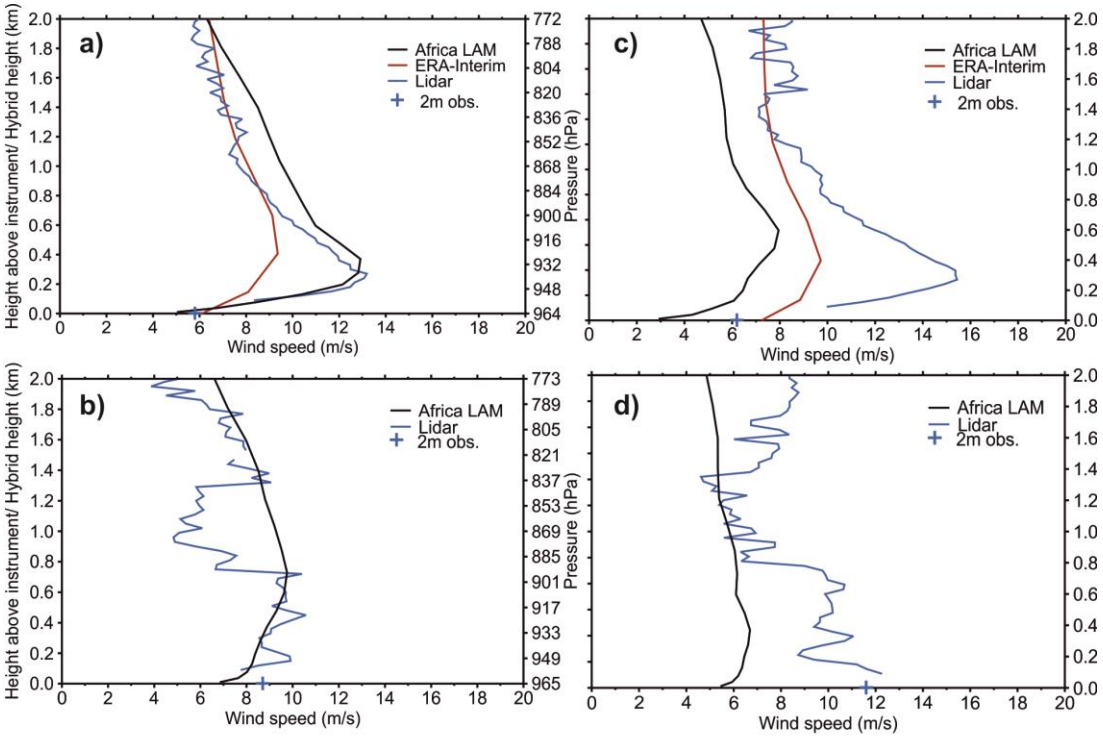

Figure 6-8: Composite wind speed-height profiles at BBM (ms^{-1}) for (left:) Harmattan LLJs, n=6 (right:) monsoon LLJs, n=5. Composites on top row are from 0600, composites on bottom row are from 0900. On each plot, the black curve represents the Africa LAM simulation (computed from the closest gridpoint to BBM) and the blue curve and cross the observations (lidar and 2m station measurements). At 0600 (panels a and c), ERAI reanalysis is plotted in red; there is no 0900 reanalysis. Lidar measurements are reported at height above instrument (=agl) and LAM at hybrid height. These are comparable since hybrid heights are sigma (i.e. terrain following) coordinates in the lower troposphere. ERAI is plotted on pressure levels. Mornings when both cold pools and LLJs were observed are not included (see Section 6.4.2).

6.6. Conditions for LLJ development

The following section addresses key question 3: Under what synoptic and local conditions is LLJ development favourable?

6.6.1. Synoptic-scale

An important control on the development of a LLJ is a sufficient background pressure gradient [*Stensrud*, 1996; *Rácz and Smith*, 1999]. This is not present every day over BBM. Unsurprisingly, on mornings when there is no LLJ at BBM, the 925hPa pressure gradient over BBM is weak compared to mornings when a LLJ is present (Figure 6-9). On LLJ mornings, the 925hPa pressure gradient ranged from 1.5gpm per degree latitude (12 June) to 6gpm per degree latitude (16 June, the strongest LLJ, Figure 6-5). (Pressure gradients were calculated in a rectangle centred on BBM from 18N to 24N, 0E to 2E.) The simulated pressure gradient over BBM is stronger during Harmattan LLJs than monsoon LLJs, resulting in stronger simulated 925hPa Harmattan winds over BBM (Figure 6-9e,f). It is likely however that the 925hPa monsoon winds over BBM (Figure 6-9f) are underestimated, given the comparison with observed LLJ profiles (section 6.5; Figure 6-8).

LLJ development over BBM is related to the position and strength of the Saharan Heat Low (SHL). On mornings when LLJs embedded in the monsoon flow are present over BBM, the SHL is centred just to the north-west of the supersite (Figure 6-9c). The SHL is well-defined even at 0600, with a strong colocation of the pressure minimum (<758gpm) and temperature maximum (>35°C). Winds are cyclonic around the SHL, resulting in south-westerlies at BBM and a strong (19ms^{-1}) easterly along the northern edge of the SHL where the pressure gradient is strongest (Figure 6-9c and f).

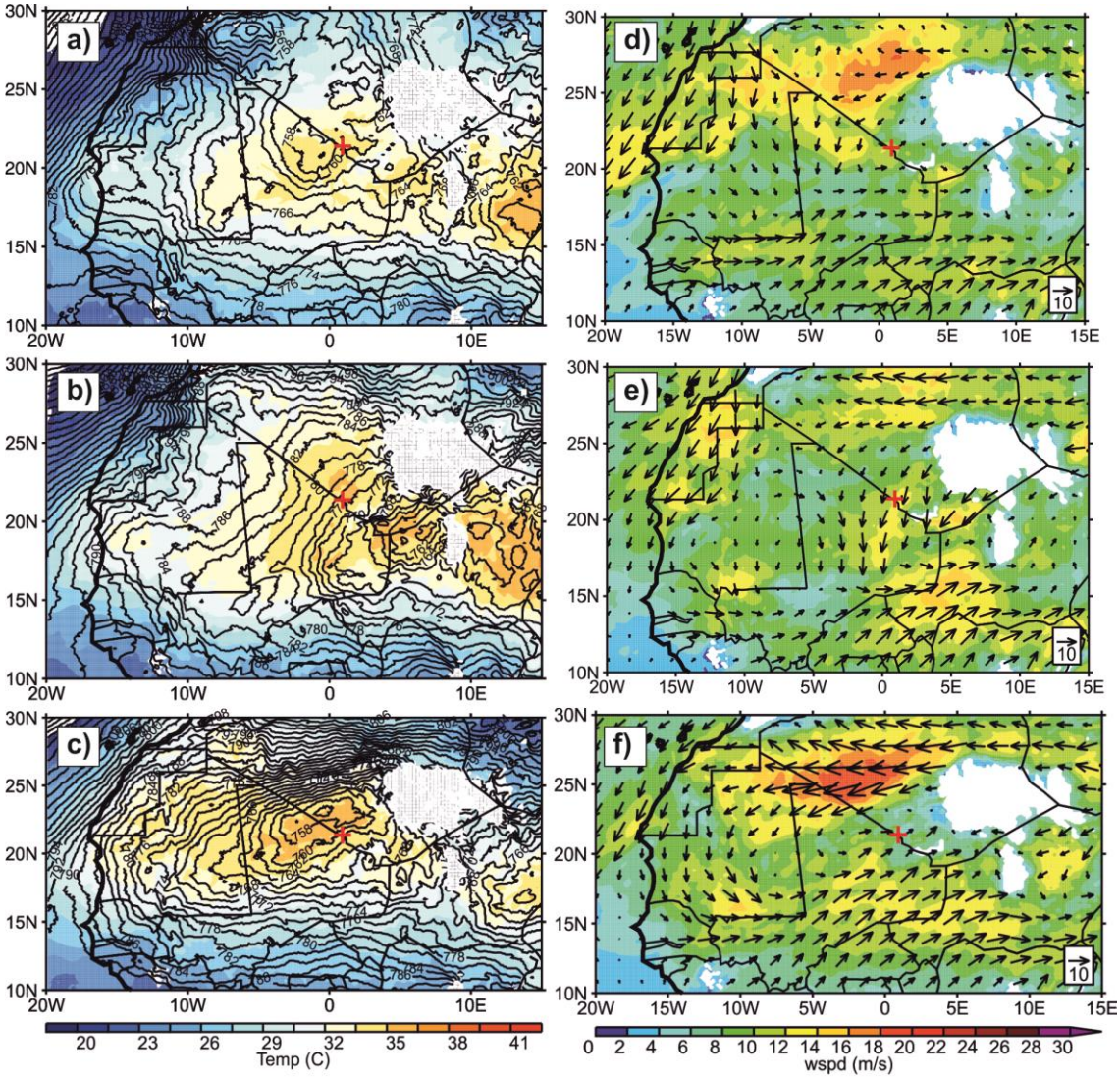

Figure 6-9: Left column: Africa LAM composites of 0600 geopotential height at 925hPa (gpm, lines) and 925hPa temperature (°C, colours). Right column: Africa LAM composites of 0600 wind at 925hPa (colours are wind speed in ms^{-1}). Top row: 'no LLJ' composites, n=5. Middle row: composites of LLJs forming part of the Harmattan flow; n=6. Bottom row: composites of LLJs forming part of the monsoon flow, n=5. Red cross marks location of BBM. White areas in right hand column indicate topography above 925hPa. Mornings when cold pools were observed are not included.

Marsham et al. [2013] identify three main synoptic-scale phases in June 2011 relevant to BBM: two periods when the centre of the SHL was close to BBM (prior to 8 June and from 13 June onwards) and a period when the centre was up to 10° further east (8-12 June). None of the monsoon LLJs at BBM occurs in the 8-12 June period, affirming

the importance of the SHL position for their formation. The SHL is centred just east of the Mali-Niger-Algeria triple point in the Harmattan LLJ composite (Figure 6-9b); with the SHL this far east, BBM is on the western edge of the cyclonic circulation and LLJs arrive at the supersite from the north-east.

6.6.2. Local-scale conditions for LLJ development

With a gradient wind in place, strong radiative cooling has been shown to be one effective way to promote LLJ development as it effectively decouples air aloft from the surface [*Blackadar,* 1957 and many studies since]. The cooling leads to a strong temperature inversion at the top of which the jet core is found [*Blackadar,* 1957]. Elements which could dampen the cooling include water vapour, cloud and dust (which absorb and re-emit infrared radiation).

In the night of 15-16 June (when the strongest LLJ is observed, highest LLJi and peak wind speed 23ms^{-1}, Table 6-2), favourable conditions for LLJ development are present. The 925hPa Africa LAM winds show a LLJ over BBM that is part of a wide (~300km) and strong (>20ms^{-1} at 0300 and 0600) north-easterly Harmattan flow originating west of the Hoggar Mountains (not shown). Although the SEVIRI cloud mask flags 65% of the nocturnal (1800-0600) timesteps as cloud, water vapour mixing ratio (WVMR) in the bottom 4000m agl remains uniformly low (~3.5g kg^{-1}) through the night and morning (Figure 6-10a). Nocturnal dust levels are below the IOP background nephelometer scattering value of 2x10^{-4}m^{-1} identified by *Allen et al.* [2013], and lidar backscatter is not greater than $10^{-5.5}$m^{-1}sr^{-1} in the bottom 3000m agl (not shown). As a result, a temperature inversion of 8°C develops by 0300 between the surface and 200m agl, and potential temperature (Θ) profiles show that this layer remains more stable than

the layer above until at least 0600 (Figure 6-10), allowing the winds at 200m to become decoupled from the surface.

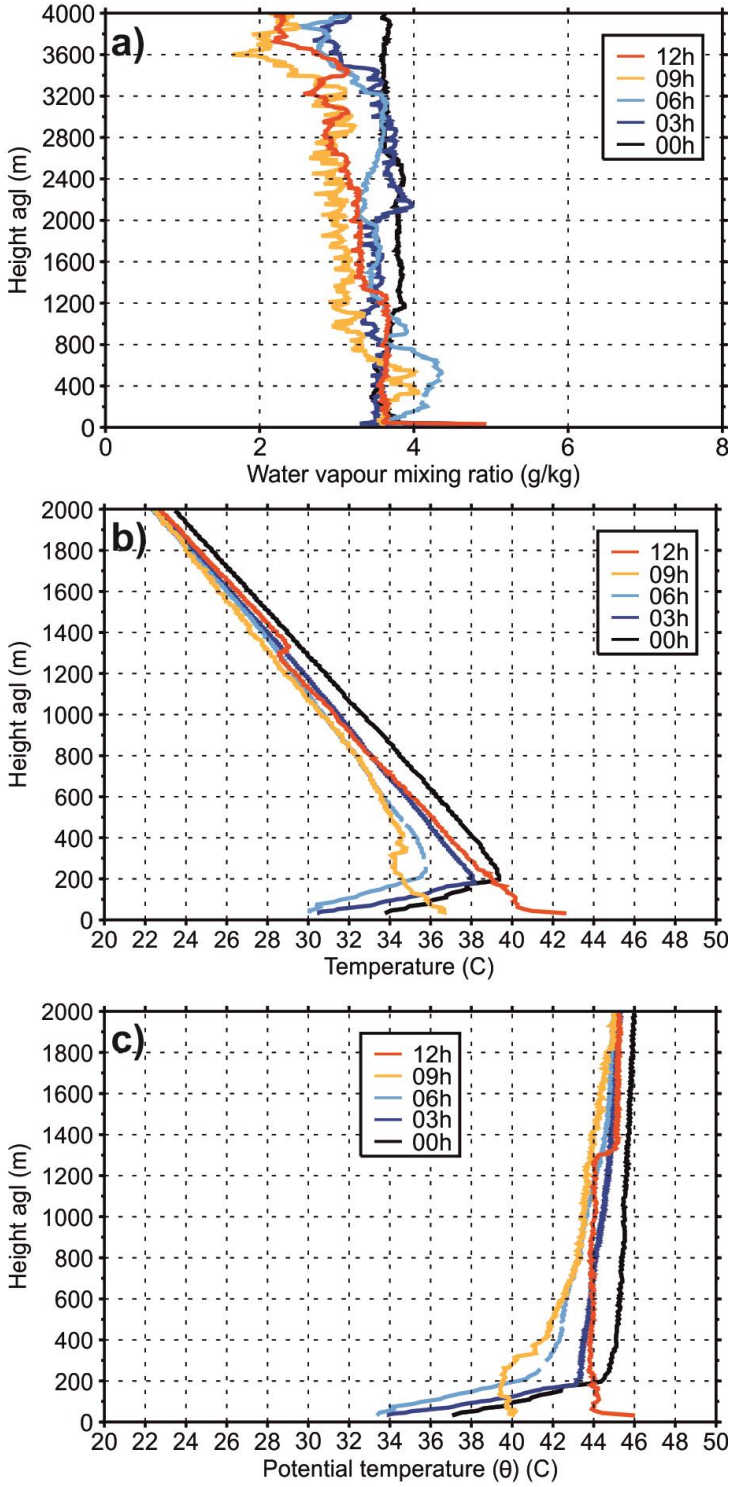

Figure 6-10: BBM radiosonde profiles for morning hours of 16 June 2011 (a:) Water vapour mixing ratio (g kg^{-1}) (b:) Temperature (°C) (c:) Potential temperature (°C). Note that the y axis of (a) extends higher than (b) and (c).

However, the same LLJ development conditions are not present for every LLJ. Indeed, during monsoon LLJs, the nocturnal surface temperature inversion at 0600 is weak, only 0.6°C/100m compared to 2.5°C/100m during Harmattan LLJs (Figure 6-11). The reduced low-level cooling during the development of the monsoon jets is likely due to longwave absorption by water vapour which, below 600m agl, is much higher (up to +4.5g kg^{-1}) during monsoon LLJs than Harmattan LLJs (Figure 6-12). (There is no cold pool signal since mornings with cold pools have been excluded, see Section 6.4.2.) The moist monsoon flow approaches overnight and is strongest at 0600 (Figure 6-12b), when boundary layer turbulence is minimal, as found by *Parker et al.* [2005]. The relationship between LLJ development and nocturnal dust and cloud cover was also examined but there was no statistically significant association (not shown).

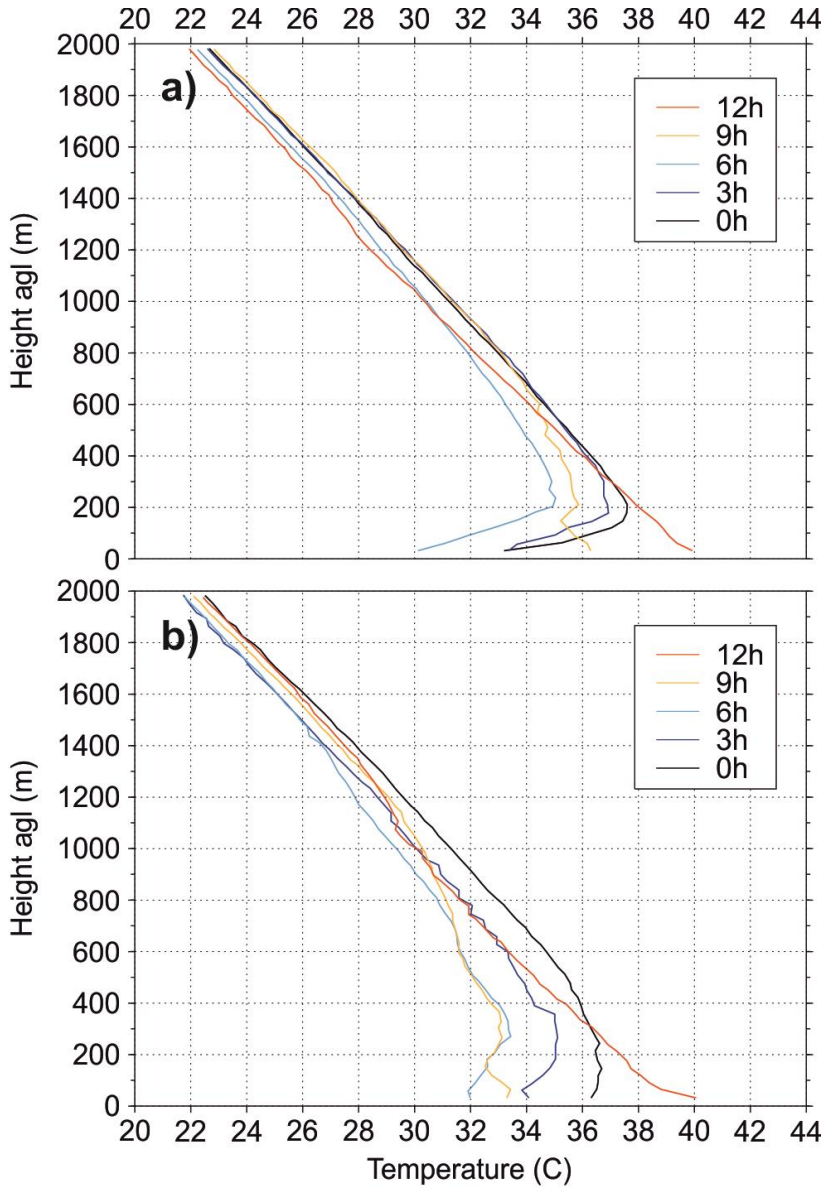

Figure 6-11: BBM composite radiosonde temperature profiles (°C) for mornings of June 2011 for (a:) LLJs embedded in the Harmattan flow (n=6) (b:) LLJs embedded in the monsoon flow (n=5). Mornings with cold pool outflows are excluded (see Section 6.4.2).

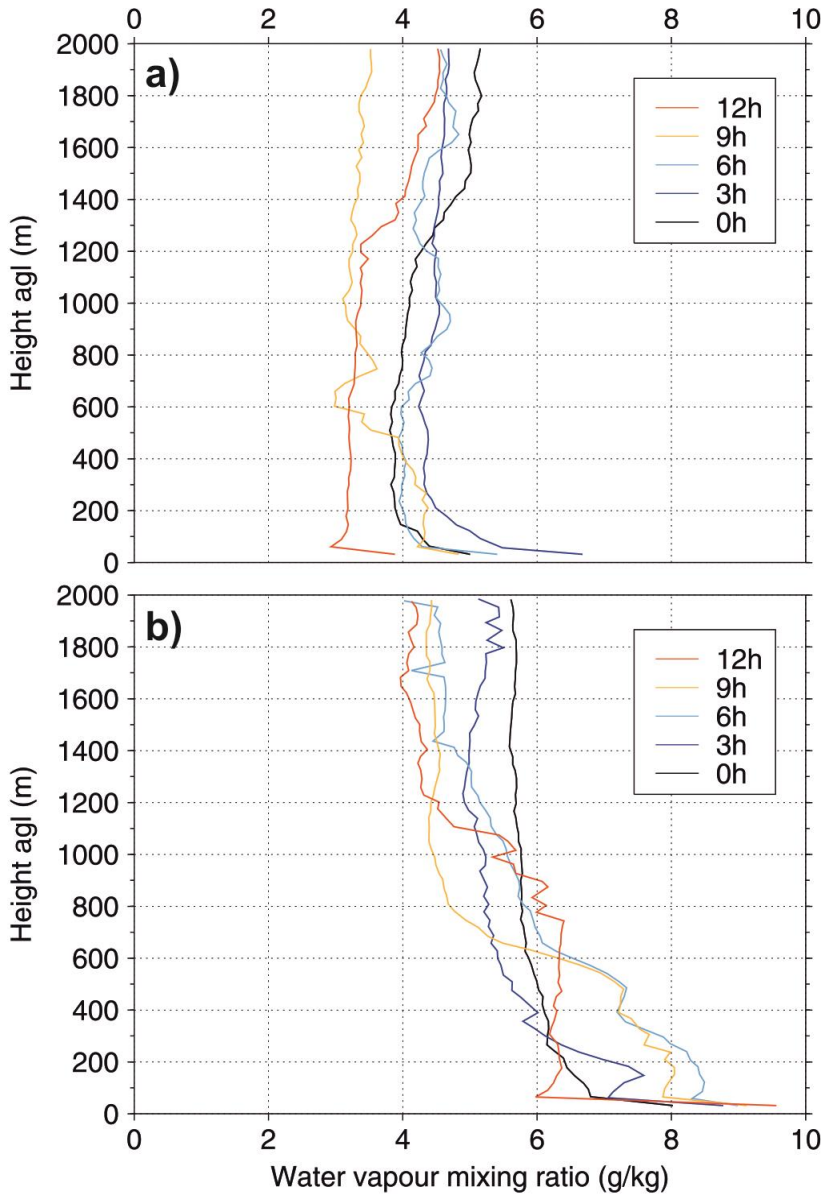

Figure 6-12: BBM composite radiosonde water vapour mixing ratio profiles (g kg^{-1}) for mornings of June 2011 for (a:) LLJs embedded in the Harmattan flow (n=6) (b:) LLJs embedded in the monsoon flow (n=5). Mornings with cold pool outflows are excluded (see Section 6.4.2).

6.7. Relationship between LLJs and dust emission

The following section addresses key question 4: What are the characteristics of LLJs associated with dust emission?

6.7.1. Characteristics of dust emitting LLJs

Dust emission does not occur on every morning that a LLJ is present. On most mornings when LLJs dominate the circulation (i.e. those not coincident with cold pools, Section 6.4.2), nephelometer scattering is below $2x10^{-4}m^{-1}$ (Table 6-4), considered a background level of dust at BBM in June 2011 [*Allen et al.*, 2013]. On only three of these 14 LLJ mornings is nephelometer scattering above $2x10^{-4}m^{-1}$ (16, 26 and 29 June, Table 6-4). These mornings are therefore candidates for LLJ-induced dust emission, as are 3 and 5 June, which are before the nephelometer was operational but when lidar backscatter peaked at $10^{-4.5}$ and 10^{-4} $m^{-1}sr^{-1}$ respectively, similar to the peaks on 16, 26 and 29 June (between $10^{-4.25}$ and 10^{-4} $m^{-1}sr^{-1}$, not shown). On 29 June, the LLJ appears to be associated with a monsoon surge, resulting in particularly intense and prolonged dust emission (Table 6-4; examined in detail in *Allen et al.* [2013]).

Table 6-4: Dust conditions for LLJs of June 2011 at BBM.†

Date	Morning dust conditions (peak nephelometer scattering, m^{-1} x10^4) [peak lidar backscatter, m^{-1} sr^{-1}]	Momentum mixed down (0500-0900)?	LLJi (m^2s^{-1})
	'Pure' LLJs (i.e. LLJs not coincident with cold pools in the morning)		
16	Considerable LLJ emission (4.5)	Y	94550
26	Strong LLJ emission (13)	Y	53580
29	Very strong LLJ emission (55)*	Y	44130
28	No emission (1.5)	N	29700
3	Considerable LLJ emission from 0800 [$10^{-4.75}$]; no data after 1000	Y^	24750
5	Strong LLJ emission [$10^{-4.25}$]	N/A Δ	23120
9	No LLJ emission (<1)	N	14350
14	No LLJ emission (<2)	N	10860
15	No LLJ emission (<2)	N§	7930
10	No LLJ emission (<1)	N§	7380
8	No LLJ emission (<1)	Y§	5060
20	No LLJ emission (<2)	N§	4650
12	No LLJ emission (<1)	N	3160
11	No LLJ emission (<1)	N§	1410
	LLJs coincident with cold pools in the mornings		
30	Thick dust (19) brought by cold pool until 0300; subsequently weak (2.5)	N¶	73480
21	Very thick dust brought by cold pool (27); no evidence of LLJ emission	NΔ	31240
25	Mix of thick cold pool dust (19) and considerable LLJ emission (6)	Y	24180
18	Mix of weak cold pool dust (3) and considerable LLJ emission (7)*	Y§	14710
13	Very thick dust (37) advected by cold pool from 0600; no evidence of LLJ emission*	NΔ	7010
23	Considerable (6) dust advected by cold pool between 0200-0300, weak (2.5) until 12h; no evidence of LLJ emission	N	6170
22	Very thick cold pool dust (22) between 0000-0300, thick (13) from 0300-0900, considerable (9) from 0900 with possible LLJ contribution	Y	3610

† Within each category ('pure' LLJ/LLJ and cold pool) dates are ordered according to LLJi (high to low). Nephelometer scattering used to describe dust conditions. Following *Allen et al.* [2013], nephelometer scattering ≤2x$10^{-4}$$m^{-1}$ is taken as background dust. Scattering ('s') then subdivided as follows: 'weak' (2<s≤4), 'considerable' (4<s≤10), thick/strong (10<s≤20), very thick/very strong (s>20). For periods prior to the activation of the nephelometer (i.e. before 6 June) lidar backscatter (in []) is given instead of nephelometer scattering, but these data may not be comparable due to attenuation of the signal in some cases. * denotes that further details of the event can be found in *Allen et al.* [2013]. Criterion used to represent momentum mix-down is a net positive change in momentum between 0500 and 0900 at 90m agl (lowest lidar measurement) AND 10m agl (from flux tower). ^ denotes where momentum measurements are not available and lidar wind speed is used as a proxy. § denotes where neither momentum nor lidar wind speed measurements are available and sodar wind speed is used as a proxy. ¶ denotes when momentum mix-down is detected between 0900 and 1200, Δ when momentum calculation is not possible during this time period due to missing observations (see Section 6.7.2.3).

Separately compositing LLJ wind profiles on dusty mornings (i.e. 3, 5, 16, 26, 29 June) and non-dusty mornings reveals that the LLJ is substantially stronger on dusty mornings than on non-dusty mornings (Figure 6-13). Indeed, at midnight on dusty mornings the LLJ is already stronger than the maximum strength the LLJ reaches on non-dusty mornings (11.5ms^{-1} at 03-04h). On dusty mornings, the LLJ reaches a maximum wind speed of 18.5ms^{-1} at 06-07h, roughly one hour after sunrise, and in the next hour decreases by less than 0.5ms^{-1}. It is not until 08-09h that the LLJ structure changes significantly: the core height rises to 500m agl and wind speeds reduce to 15.5ms^{-1}. Prior to 08-09h, the core height on dusty and non-dusty mornings is the same, 300m agl, but on dusty mornings the depth of wind speeds above 8ms^{-1} is twice as great, 90-1500m agl compared to 90-700m agl. This is reflected in the high LLJi values on dusty LLJ mornings (Table 6-4).

On dusty LLJ mornings, 10m wind speed begins to increase rapidly at 0700, and peaks at 15ms^{-1} at 0930, after which it declines. The wind speed curve from 0700-1300 resembles a Gaussian shape which matches closely with the lidar backscatter (Figure 6-14a). As the 10m wind speeds begin to increase, backscatter also increases through a deeper column of the atmosphere. When the wind speeds slacken, backscatter declines back to pre-sunrise values. The close correspondence between the wind speed and the backscatter is strong evidence for local dust emission, especially as winds are above the local emission threshold of 8ms^{-1} [*Allen et al.*, 2013] for six hours. On non-dusty LLJ mornings (Figure 6-14b), wind speeds from 0700-1300 follow a lower amplitude Gaussian pattern but never reach 8ms^{-1} and there is no evidence of corresponding dustiness in the lidar backscatter.

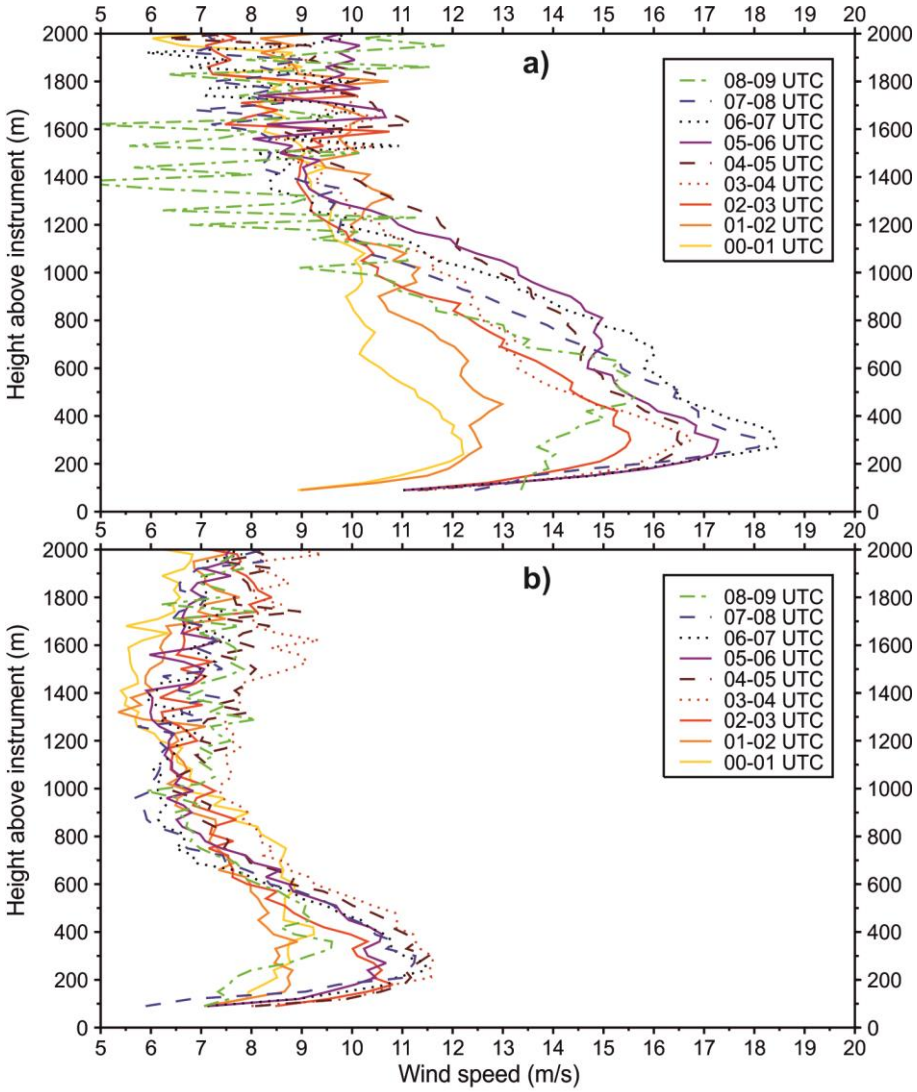

Figure 6-13: Lidar composite hourly-mean wind speed-height profiles (ms^{-1}, key in box) for a): LLJs that result in dust emission (n=5) b): LLJs that do not result in dust emission (n=9). Mornings when cold pools are coincident with LLJs are excluded.

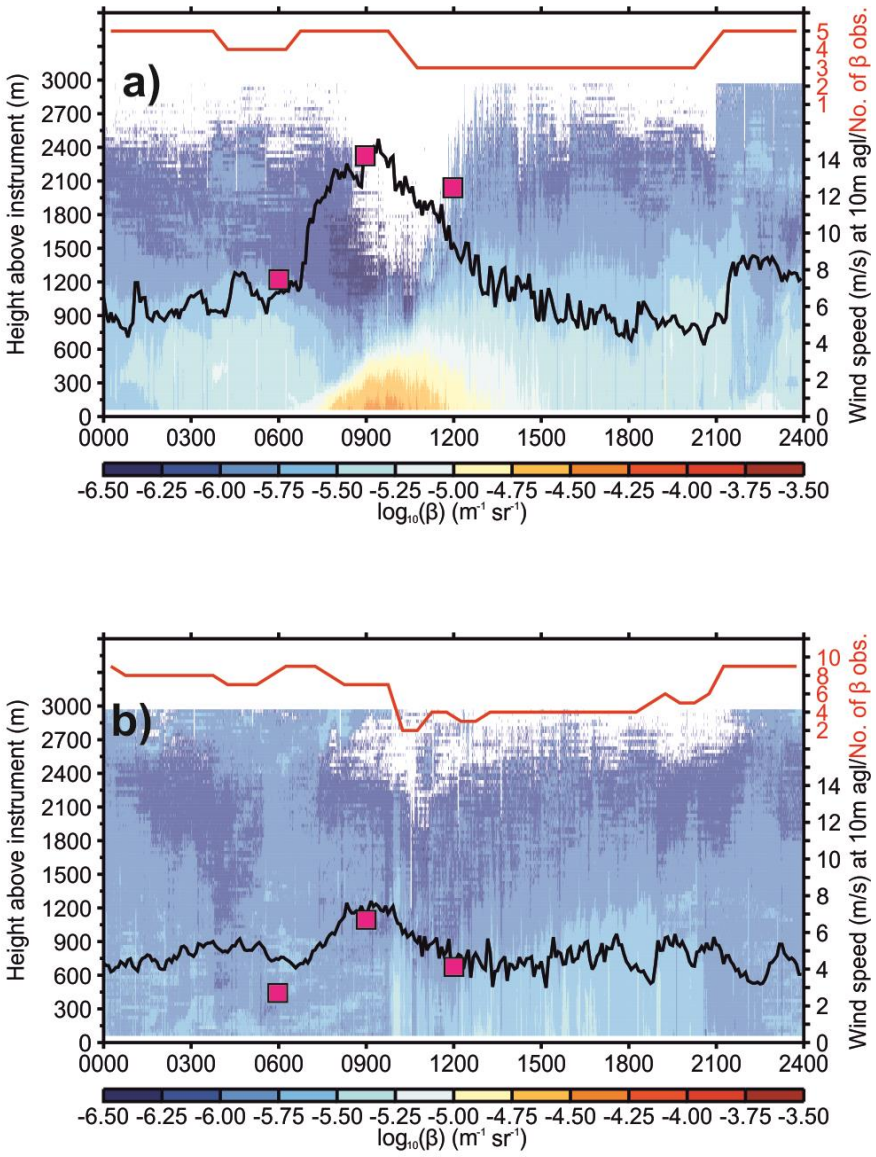

Figure 6-14: Lidar backscatter 'β' and 10m wind speed composites for (a) dusty LLJ days (n=5) and (b) non-dusty LLJ days (n=9). Mornings when LLJs were coincident with cold pools are excluded from the composites (Section 6.4.2). Colour contours show log_{10} lidar backscatter ($m^{-1}sr^{-1}$), resolved by height. Black curve shows 10 metre wind speed (5 min averages). Flux tower measurements are missing on some days; pink squares show composite wind speeds at 0600, 0900 and 1200 recalculated incorporating local synop station measurements. The red curve (red axis) shows the number of days available to make the backscatter composite at each 30 min interval. Note that the red axis is different in a) and b). Most missing backscatter is in the afternoon when the lidar was most prone to overheating.

The Gaussian patterns are not a product of the compositing process. On all LLJ mornings when flux tower data are available, a Gaussian pattern can be detected in the mid-late morning wind speed (not shown). When flux tower data are unavailable, local synop station winds are in broad agreement (Figure 6-14a, pink squares). Likewise, on all dust emitting LLJ mornings, lidar backscatter data when available follows a Gaussian shape, albeit with differing start times and durations (0700 to 0745 and 6h to 13.4h respectively). The composite can be interpreted with high confidence during the onset and peak of dust emission when backscatter data on all dust emitting LLJ mornings is available (Figure 6-14a, red line). Given the very clear differences between LLJs that lead to dust emission and those which do not (Figure 6-13 and Figure 6-14), it therefore appears that on non-dusty mornings, the LLJ is simply too weak to provide enough momentum to be mixed-down to the surface for emission. Additionally, on non-dusty mornings, the convective boundary layer (as identified by the depth of constant virtual potential temperature) is 100m shallower at 0900 than on dusty mornings (not shown), extending to only 100m agl. This suggests that turbulent mixing is also weaker on non-dusty mornings.

Three classes of wind profile have so far been identified at BBM: 'not LLJ', LLJ and now, 'dust emitting LLJ'. Objective criteria for distinguishing LLJ wind profiles from 'not LLJ' profiles were presented in Section 6.4. In order to distinguish dust emitting LLJs from non-emitting LLJs, two changes to the original LLJ detection scheme are introduced: i) wind speed below the core must not only decrease, but decrease with an average shear $\geq 0.6 ms^{-1}$ per 30m ii) the LLJ wind speed maximum must be $\geq 16 ms^{-1}$. These criteria are applied the 06-07h wind profiles (see Section 6.4). The below-core wind shear criterion appears to be of particular importance since it allows for the exclusion of 30 June, a morning when the LLJ is very strong (2nd highest LLJi and

peak wind speed of 17.2ms^{-1}) but does not lead to morning dust emission (Table 6-2). As before, the classification is tested with Discriminant Analysis, this time for three classes. The technique places 93% observations in the same class as identified *a priori*.

It is worth noting that application of the *Fiedler et al.* [2013] LLJ detection criteria to the BBM observations misses 3/5 LLJs that cause dust emission, primarily because the Fiedler et al (2013) above-core wind shear criterion is too strict for the observed profiles, which do not shear monotonically above the jet core but display 'reversal' periods. However, it is also important to be clear that the criteria presented above for distinguishing dust-emitting LLJs are based on only five cases. These were the only dust emitting LLJs in the IOP; nevertheless their infrequent occurrence means that the dust-emitting LLJ criteria might be better thought of as a summary of the commonalities between the five cases rather than a detection scheme.

6.7.2. Momentum mix-down

The following section addresses key question 5: Is dust emission consistent with the mix-down of momentum from the jet core?

Central to the theory of LLJ dust emission is that momentum is transferred towards the surface by turbulent mixing after sunrise [e.g. *Blackadar*, 1957; *Knippertz and Todd*, 2012]. This momentum is responsible for the high surface wind speeds at mid-morning which lead to dust emission. The general decline in 10-to-15m wind shear at BBM between 0630 and 1040 is consistent with momentum mix-down [*Marsham et al.*, 2013]. However, the BBM dataset also provides a rare opportunity to calculate momentum directly for the entire lower troposphere. Two case studies of dust emitting LLJs are presented next which clearly illustrate the operation of the momentum mix-down process.

6.7.2.1. 26 June 2011

26 June is chosen as a starting point because it has a strong LLJ (3rd strongest of June, Figure 6-5), strong dust emission and complete surface and boundary layer measurements. The 925hPa Africa LAM simulations (Figure 6-15) show that on this morning BBM is under the influence of aged monsoon air (specific humidity 8g kg^{-1}) which has been recirculated to arrive at the site from the north-west. The sodar measurements show the LLJ clearly, peaking at 0700 around 22 ms^{-1} at 300m agl with strong winds then encroaching towards the surface (Figure 6-16c). As expected, at the time of peak LLJ momentum (06-07h), 10m momentum is much lower, 238 kg ms^{-1} against 619 kg ms^{-1}. By 09-10h however, the time of maximum dust emission, 10m momentum has increased from 238 kg ms^{-1} to 437 kg ms^{-1}, the jet has shrunk in vertical extent and decayed from 619 kg ms^{-1} to just over 500 kg ms^{-1} (Figure 6-16d). 10m wind speeds reflect this increase and show a remarkably similar Gaussian structure to the nephelometer scattering and lidar backscatter (Figure 6-16, left).

Sunrise on 26 June 2011 is 0516 UTC. From 05 to 06h, 10m momentum increases by 20 kg ms^{-1} (not shown). From 06 to 07h, the first hour of surface temperature increase, momentum at the LLJ core, 300m, shows negligible change, whilst momentum below this height increases significantly, with a maximum increase of 150 kg ms^{-1} at 10m (Figure 6-17a). From 07 to 08h, the near surface is almost the only height gaining momentum, suggesting that the momentum from the LLJ has indeed been transported downwards. This is also exactly the period when backscatter begins to increase significantly (Figure 6-16).

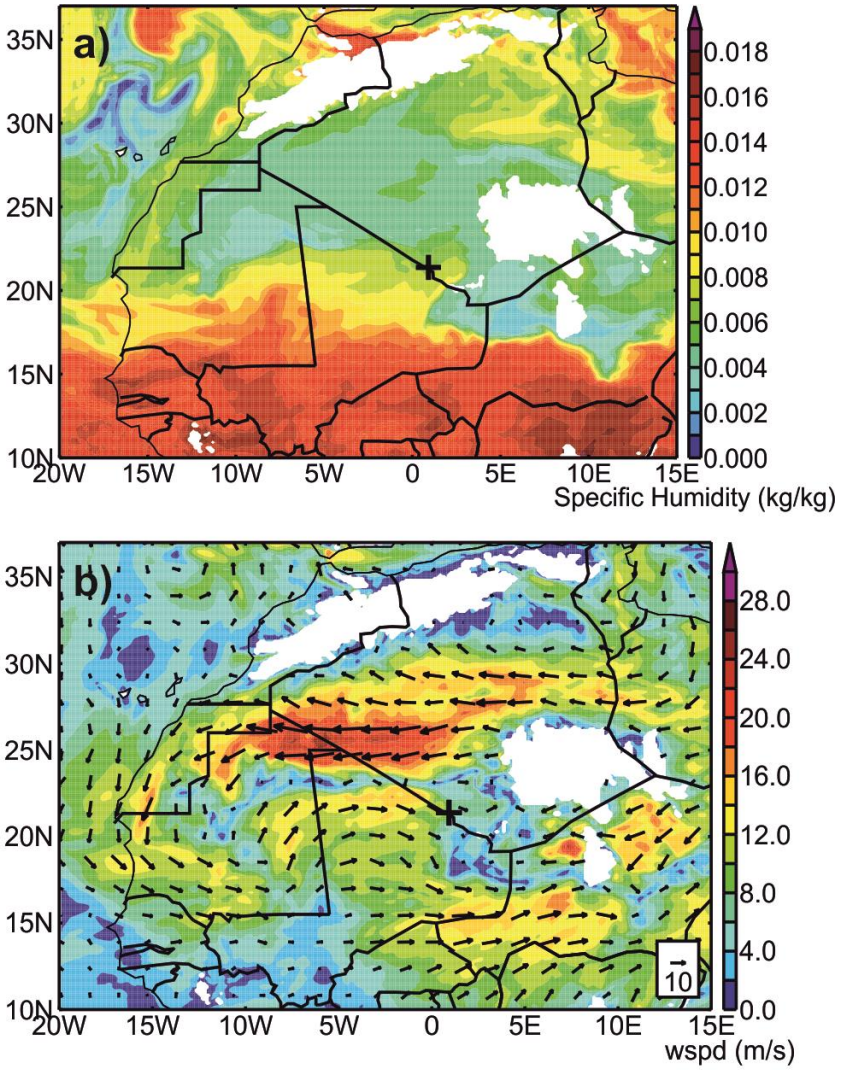

Figure 6-15: 26 June 2011 0600 UTC Africa LAM 925hPa (a:) specific humidity (kg kg^{-1}) (b:) wind speed (ms^{-1}) and vectors. Cross marks BBM location. White areas indicate topography above 925hPa.

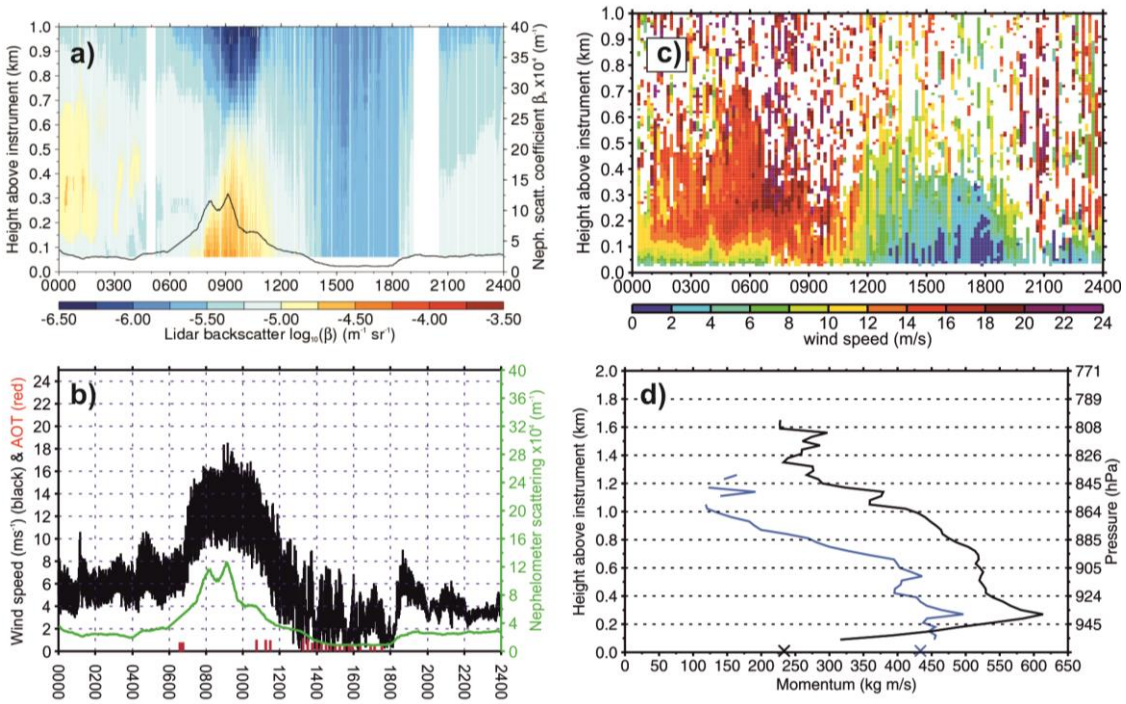

Figure 6-16: BBM, 26 June 2011. (a:) nephelometer scattering x10^4 (m^{-1}) and log_{10} lidar backscatter ($m^{-1}sr^{-1}$) time series. (b:) nephelometer scattering, 10m wind speed and AOT_{500} time series. (c:) sodar wind speed (ms^{-1}) time series. (d:) momentum profiles (kg ms^{-1}) for 06-07h (black) 09-10h (blue). 10m momentum is indicated with a cross. White areas in the sodar plot are missing data (dropout). Lidar backscatter data are missing from 0445-0515 and 1900-2030. In (b), periods without red bars do not indicate zero AOT but either (i) no AOT measurements taken (ii) AOT measurements removed as part of the AERONET level 1.5 cloud screening process.

6.7.2.2. 16 June 2011

The strongest LLJ by far at BBM is on 16 June (Figure 6-5). Its breakdown leads to considerable dust emission (Table 6-4). From 06 to 07h momentum at the jet core (~300m agl) shows negligible change; momentum in the layers below is decreasing and momentum in the layers above is mostly increasing (Figure 6-17b). From 07 to 08h there is a dramatic change. Momentum at 300m decreases by almost 240 kg ms^{-1} whilst momentum at 120m agl and below increases by over 80 kg ms^{-1}, again suggesting that the momentum is transferred towards the surface during this time interval, two hours after sunrise.

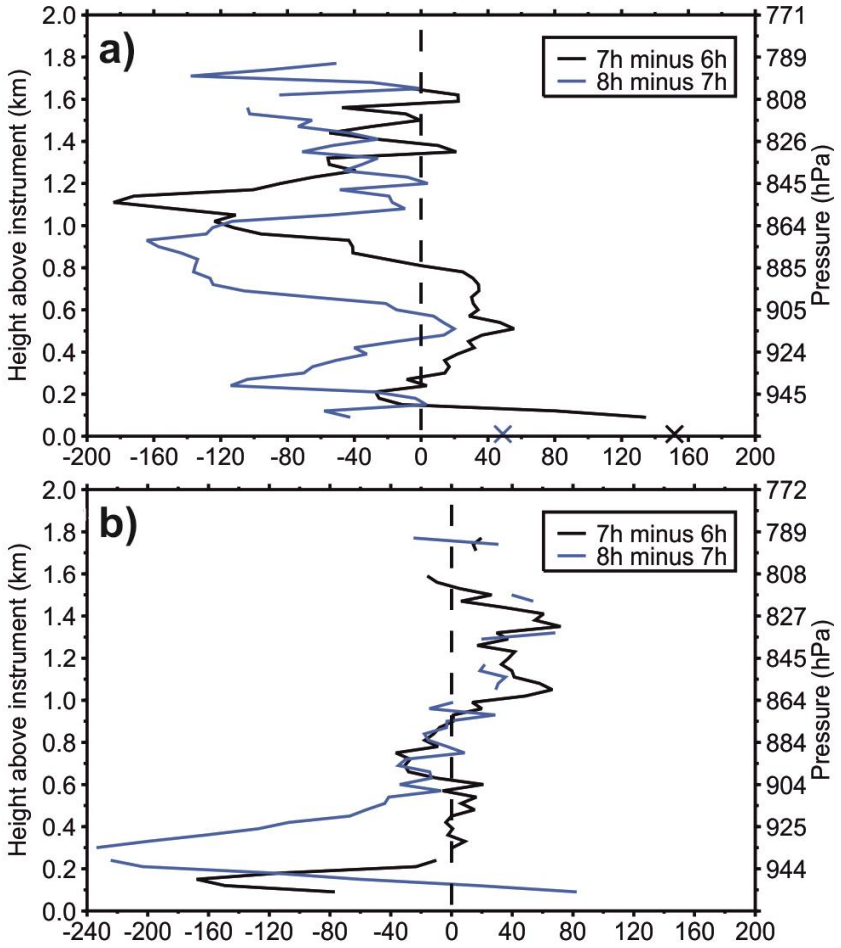

Figure 6-17: BBM momentum change profiles (kg ms^{-1} per hour) for a:) 26 June 2011 b:) 16 June 2011. Crosses marks 10m momentum change calculated from the flux tower (not available on 16 June).

6.7.2.3. Mix-down statistics

Momentum mix-down certainly appears to be the mechanism for dust emission from LLJs in the above cases. Of the five 'pure' LLJ mornings when LLJ-induced dust emission occurs, mix-down of momentum between 0500 and 0900 is observed on four (Table 6-4). On the remaining morning (5 June), momentum measurements (or a wind speed proxy) are not available. On the nine 'pure' LLJ mornings which do not lead to dust emission, momentum mix-down is not observed between 0500 and 0900 except on

8 June. The reason dust emission does not occur on the morning of 8 June (nephelometer scattering $<1x10^{4}m^{-1}$, Table 6-4) is likely because the LLJ is simply too weak to begin with (ranked 17th in LLJi, Figure 6-5).

On 17/21 LLJ mornings, momentum does not mix down between 0900 and 1200. Of the remaining four mornings, on one there are no data to make an assessment, on two mornings 90m momentum suggests mix-down but there are no 10m observations, and on only one LLJ morning (30 June) does momentum mix down between 0900 and 1200 (Table 6-4). The fact that in most cases momentum does not mix down between 0900 and 1200 is consistent with the decline of 10m winds after 0900 (e.g. Figures 14 and 16b). (Nine calculations of 0900-1200 momentum use sodar wind speed as a proxy due to missing lidar and/or radiosonde data.)

6.7.2.4. Dust from LLJs and cold pool outflows

This section considers LLJ cases which are coincident with cold pool outflows. It is clear that dust loadings are high on many of these mornings (Table 6-4). A perfect separation of dust produced by cold pools from dust associated with LLJs on these mornings is not possible. However, if nephelometer scattering and surface wind speed follow a coincident Gaussian pattern (as is the case on the 'pure LLJ' dust emission mornings) it is likely that LLJ breakdown is also contributing to the dust loadings. This is particularly clear on 18 June (examined in more detail in Section 7.2.2. of *Allen et al.* [2013]). Of the seven mornings when LLJs are coincident with cold pools, momentum mix-down between 0500 and 0900 occurs on 3 (including 18 June; Table 6-4). This suggests that on some occasions, morning LLJ breakdown continues in the presence of a cold pool, whilst on other occasions it does not.

Inspection of Table 6-2 and Table 6-4 identifies two 'anomalous' occasions when limited or no emission occurs, despite high LLJi and no strong cold pools in the late morning. These are examined next.

6.7.2.5. 30 June 2011

30 June is somewhat anomalous since it has the 2nd highest LLJi and yet backscatter and scattering are low in the mid-late morning ($2.5x10^{-4}m^{-1}$, Table 6-4). A comparison of momentum profiles with 26 June (which has a lower LLJi but higher emission) shows (i) the LLJ on 30 June decays between 05h and 07h whilst on 26 June it strengthens (ii) 10m momentum at 07h on 30 June is only 295 kg ms^{-1} compared to 385 kg ms^{-1} (Figure 6-18, left). As a result, 10m wind speed does not show the subsequent characteristic Gaussian LLJ curve and high peak (Figure 6-18, right) and therefore, although wind speeds are over the $8ms^{-1}$ threshold, there is little dust emission in the mid-late morning.

Between 0500 and 0900 on 30 June, momentum at 90m agl declines by 65 kg ms^{-1}. Momentum does not appear to mix down from the jet core before sunrise either: lidar profiles (available down to 90m agl) between 0100 and 0500 do not show wind speeds increasing below the jet core (not shown). The high scattering and backscatter prior to 0300 (Table 6-4) are very likely related to the very strong cold pool outflow which arrived at BBM at 2100 on 29 June (addressed in more detail in *Allen et al.*, [2013]). The outflow likely contributed to the high winds at 10m agl from 0000 to 0300 on 30 June. Thunderstorm outflows can display a LLJ wind profile behind the front [e.g. *Bowen*, 1996; *Darby et al.*, 2002], but the outflow is not the sole cause of the high wind speeds since a LLJ is also simulated by the Africa LAM in the early morning (not shown). (It is possible however that the model produces a LLJ instead of an outflow [*Heinold et al.*, 2013].)

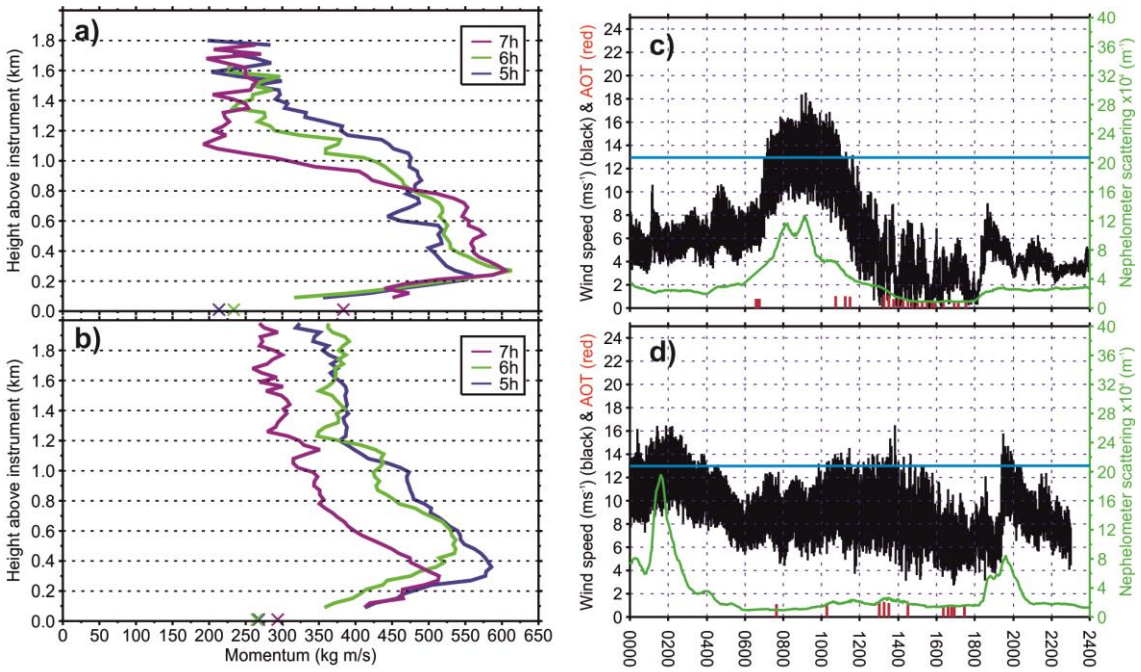

Figure 6-18. Left: BBM momentum profiles for (a:) 26 June 2011 (b:) 30 June. Crosses mark 10m flux tower calculations. Right (c:) 10m wind speed (ms^{-1}), nephelometer scattering $x10^4$ (m^{-1}) and AOT_{500} for 26 June (d:) for 30 June. Horizontal blue line marks 13 ms^{-1} wind speed for ease of comparison. In (c) and (d), periods without red bars do not indicate zero AOT but either (i) no AOT measurements taken (ii) AOT measurements removed as part of the AERONET level 1.5 cloud screening process.

The timing of LLJ development is important for dust emission. On 30 June, wind speeds between 90-600m agl begin to decline after 01-02h. On 16, 26 and 29 June, which are all dusty, this decline does not begin until five to six hours later (Figure 6-19). Furthermore, by 09-10h on 30 June, there are no levels between 90-600m with wind speeds >10ms^{-1}. After 0200, wind speeds at 10m agl also begin to decline (Figure 6-18d). Thus although the LLJ is very strong in the early morning, its decline in the hours prior to sunrise may explain why there is little if any dust emission in the mid-late morning. However, somewhat curiously, 30 June is also the only LLJ morning when momentum mixes down between 0900 and 1200. This may explain why the 10m wind speeds do not decrease after 0900, as on 26 June (Figure 6-18) and in the LLJ composite

(Figure 6-14). Inspection of the Africa LAM wind fields shows that BBM is on the very edge of a LLJ on the morning of 30 June (not shown): a small change in the orientation of the LLJ could result in a large increase or decrease in wind speeds over the site.

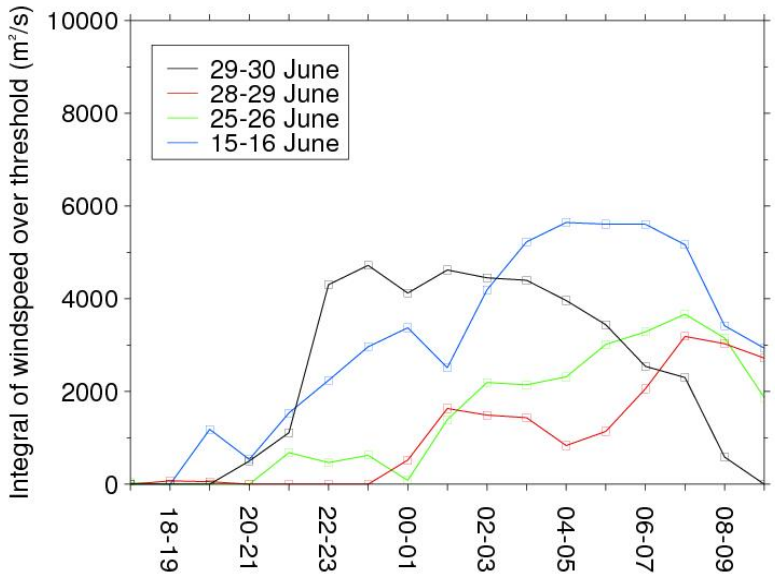

Figure 6-19: Timeseries of the integral of wind speed (m^2s^{-1}) over a threshold of $10ms^{-1}$ between 90m and 600m agl, for four selected night-morning transitions at BBM in June 2011. The x axis is time (UTC) in hourly intervals. Measurements are from the lidar.

It is strange that the nephelometer scattering between 0600 and 1800 on 30 June is so low (Figure 6-18d), often below the $2x10^{-4}$ m^{-1} threshold used for dust event detection, given that the wind speeds are generally above the local emission threshold (between 6 and 8 m s^{-1}, see *Allen et al.* [2013]). This may be because (i) the surface shear stress is not proportional to the 10m wind speed on this occasion (indeed, the shear velocity (gradient of the wind speed with height) changes much more rapidly from the jet core downward on 26 June than on 30 June (compare Figure 6-18 a and b); (ii) the nephelometer is not recording correctly; (iii) the wind speed emission threshold is inappropriate (although it seems to hold for other events and is similar to the threshold

reported by *Marsham et al.* [2013]); (iv) the wind speed threshold is appropriate but the erosivity has changed: on 29 June there was a monsoon surge whose moisture content may have strengthened the binding forces in the soil.

6.7.2.6. 28 June 2011

28 June is ranked 6th in the LLJi. As on 30 June, during the 0600-1200 period lidar backscatter and nephelometer scattering are very low ($10^{-5.5}$m^{-1}sr^{-1} and 1.5x10^{-4}m^{-1} respectively; Table 6-4). Flux tower wind speed is unavailable after 0700 but local observers reported 2m wind speeds to be unsurprisingly low: 6.2ms^{-1} at 0600 and 7.2ms^{-1} at 0900. Observations show that this is because momentum from the LLJ was simply not mixed down. Momentum at 90m (the lowest possible lidar observation) decreases by 95kg ms^{-1} between 0500 and 0900, and between 0600 and 0800 momentum is decreasing at almost every height below 2km (Figure 6-20).

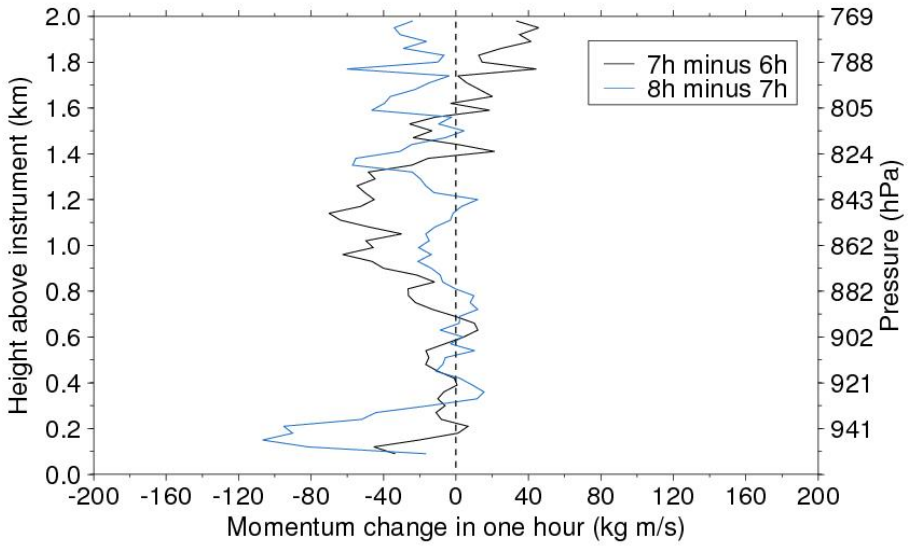

Figure 6-20: BBM 28 June 2011 momentum change profiles (kg ms^{-1} per hour). No flux tower data are available for 10m calculations.

6.8. Low level oscillations

The *Blackadar* [1957] theory of LLJ formation posits that the jet is initiated by an inertial oscillation as defined in Section 6.1. At BBM (21.38N) this would result in a ~32 hour oscillation period. If the decoupled period is assumed to be 10-12 hours, only a third of the inertial oscillation will be achieved at Saharan latitudes [*Knippertz and Todd*, 2012]. RCM experiments in the Bodélé show that this results in a highly super-geostrophic LLJ [*Todd et al.*, 2008].

Marsham et al. [2013, their figure 12a] show that the diurnal cycle in the June 2011 500m winds at BBM describes a clockwise rotation as expected. However, hodographs on individual days at BBM also display oscillations of much shorter period (as short as 5 or 6 hours, beginning at different times). For the nocturnal to late morning period (1800 to 1200), such oscillations occur on 59/292 (20%) possible occasions during the IOP (selected heights; see Table 6-5). They are almost all clockwise and are only present on certain days (Table 6-5). On most days their presence does not appear to be related to LLJ strength or lidar backscatter.

Table 6-5: Statistics showing the presence and nature of wind oscillations identified from daily hodographs from the IOP.†

Total occasions available for oscillations	292 (100%)
Total no. of observed oscillations	59 (20.2%)
Total no. of clockwise oscillations	53 (18.2%)
Of the 59 observed oscillations…	(100%)
No. of 'imperfect' oscillations	17 (28.8%)
No. of incomplete oscillations	16 (20.3%)
Favoured heights for oscillations	15m (18.6%) 10m (16.9%) 270m (11.9%)

Of the 43 completed oscillations…	(100%)
No. which lasted 5 hours	9 (20.9%)
No. which lasted 6 hours	7 (16.3%)
No. which lasted 7-9 hours	15 (34.9%)
No. which lasted 10 hours or more	12 (27.9%)
No. of days with oscillation(s) at any height (see caption for heights)	17/28

†Hodograph time period 1800 to 1200 chosen to include nocturnal LLJ growth, mix-down and surface wind speed maximum. Heights chosen for data availability reasons and to maximize observations near the jet core: 10m, 15m (measurements from the flux tower); 90m, 150m, 180m, 240m, 270m, 300m, 330m, 420m, 510m (measurements from the lidar). 'Occasion' defined as a given height on a given day where enough data are available to make an assessment. An 'imperfect' oscillation is one where not all the measurements fall on the circle.

There are two days however when these oscillations are particularly clear and do appear to have an association with the LLJ: 25 and 26 June. The oscillations can be seen in the jet core, 270 and 300m agl, from 0100 to 0800 (25 June) and from 0300 to 0800 (26 June, Figure 6-21). This timing is coincident with the growth-decay phase of the jet. There are no discernible oscillations below 270m agl except at 10m and 15m agl. At 10m and 15m agl, oscillations begin at 0600 (Figure 6-21), coincident with the start of the surface temperature increase (not shown). They last until 1200, spanning the period of the Gaussian-like increase and decrease in 10m winds caused by the occurrence then cessation of momentum mix-down (Figure 6-16b).

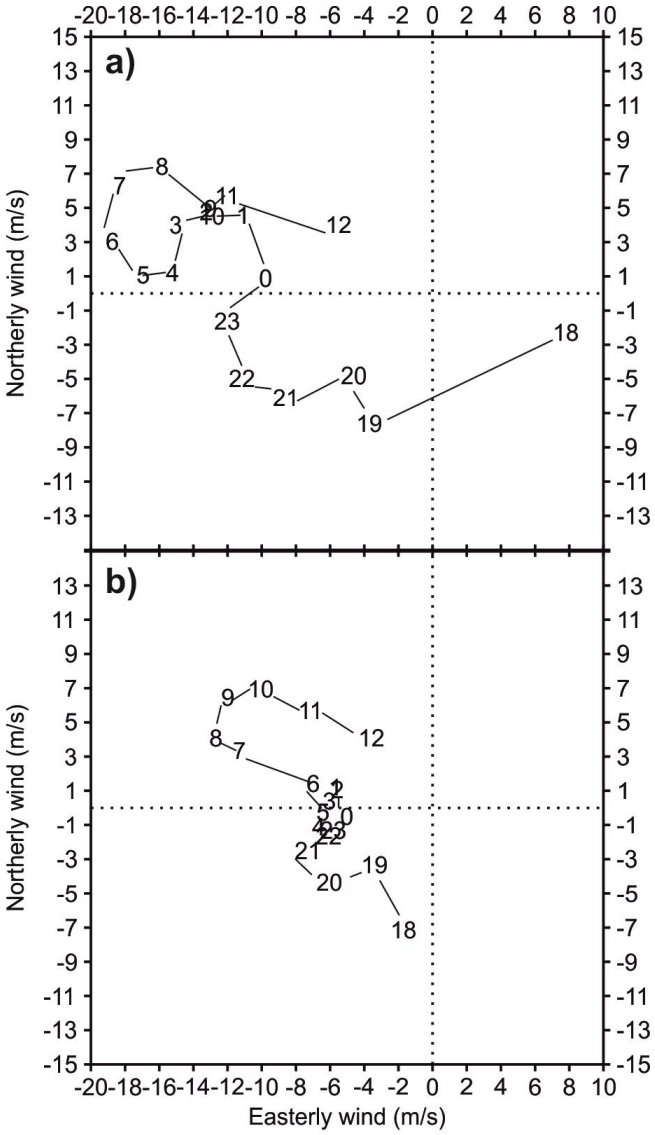

Figure 6-21. BBM hodographs from 1800 on 25 June 2011 to 1200 on 26 June. The figures shown on the hodograph represent the hour, starting from 1800 on 25 June 2011 ('18') and finishing at 1200 on 26 June ('12'). Broken lines are drawn at u=0 and v=0. (a:) 270m agl wind speed measurements from the lidar. (b:) 10m wind speed measurements from the flux tower. Both ms^{-1}.

6.9. Discussion and Conclusions

This paper presents observations of Saharan low level jets from the Fennec supersite at Bordj-Badji Mokhtar, Algeria, and addresses their correspondence with current theory on LLJ formation and relationship with dust emission. Five key questions were posed in

the introduction: (i) What are the observed characteristics of the LLJ in the central Sahara at BBM in summer? (ii) How well are LLJs at BBM represented by the Africa LAM and ERAI? (iii) Under what synoptic and local conditions is LLJ development favourable? (iv) What are the characteristics of LLJs associated with dust emission? (v) Is dust emission consistent with the mix-down of momentum from the jet core? These will now be addressed in turn.

The LLJ is clearly evident in the June 2011 mean diurnal wind cycle (Figure 6-1), as also shown by *Marsham et al.* [2013], but it is only present on 21/28 of these mornings. Its core is at 300m agl (approximately 935hPa). Peak composite wind speeds in the core are 13.5ms^{-1} (12ms^{-1} in the all-June composite) and occur between 0400 and 0500. There is significant variability in 10m wind speeds and wind speeds within the jet core during the month (Figure 6-2 and Figure 6-3). Composite temperatures (2m height, Figure 6-3) begin to increase half an hour after sunrise (0513h on 15 June), and the decay of the jet begins between 0500 and 0600. 10m wind speeds lag behind those in the jet core; peak 10m wind speed, 7.5ms^{-1} (7ms^{-1} in the all-June composite), occurs between 0900 and 1000, five hours after the LLJ peak (Table 6-1, Table 6-3). This is similar to the lag in the Bodélé Depression: a near-surface wind speed peak at around 0900 was observed during BoDEx, four hours after surface temperatures began to increase [*Washington et al.*, 2006a]. In south-west Niger the mix-down of the LLJ was found to be slower: *Parker et al.* [2005] report observed surface winds not peaking until 1100. At Fennec supersite 2, at Zouerate in Mauritania, LLJ mix-down is slower still: the Atlantic Inflow allows the LLJ to persist until 0900-1200, with a prolonged but moderate peak in surface winds over the course of the afternoon [*Todd et al.*, 2013].

LLJ detection at BBM is based on three criteria: (i) wind speed maximum (below 600m agl) >8ms^{-1} (ii) wind shear between the LLJ core and 500m above the core ≤ -1.8 ms^{-1} (iii) wind speed under the core decreases all the way to the lowest lidar measurement (90m agl). Of the 28 mornings when lidar data were available, LLJs were detected on 21.

A low level jet index (LLJi) was developed to compare the strength of the LLJs at BBM during the IOP. It is defined as the summation of wind speed exceeding a threshold in the LLJ core over the nocturnal-early morning period (Equation 1). The LLJi time series shows that there is significant variability in LLJ strength over the course of the month (Figure 6-5). Additionally the LLJi shows that the strongest winds were produced by a relatively small number of events: 85% of the total LLJi is contained in 10/21 LLJs. The LLJi is based on high quality, high resolution data from a prime location for dust emission. However, the data were obtained over one summer month and the definitions used do depend on the conditions present during the limited period of observations.

The Africa LAM (key question 2) simulates Harmattan LLJ profiles accurately at BBM during the IOP, particularly at 0600 (Figure 6-8). Winds in the core of monsoon LLJs however are underestimated by 8.5ms^{-1}. Surface wind speeds during the breakdown period of both monsoon and Harmattan LLJs are underestimated by up to 6ms^{-1}. Critically, these underestimations result in surface wind speeds below the local threshold for dust emission. Further work will examine the causes and implications of these underestimates; it may be that the moist dynamics of monsoon LLJs present a particular challenge for the model in the boundary layer.

ERAI representation of monsoon jets at BBM is better than the LAM. However, it is still poor (core wind speeds underestimated by 6ms^{-1} at 0600, Figure 6-8). ERAI

representation of Harmattan jets at BBM is also poor (core wind speeds underestimated by 4ms^{-1} at 0600). These findings demonstrate that ERAI does indeed underestimate LLJ strength in the morning, as suggested by *Fiedler et al.* [2013]. There is little LLJ structure in the 0600 ERAI wind profiles compared to the lidar observations during the IOP at BBM. This is also the case for monsoon LLJs simulated by the LAM. Application of reanalysis-based LLJ detection criteria to observations is inappropriate at BBM. Caution should be exercised when using ERAI as a surrogate for observations of LLJs elsewhere in the central Sahara, and likewise the LAM for monsoon LLJs. However, the LAM simulates Harmattan LLJs very accurately. *Ashpole and Washington* [2013] point to the Harmattan LLJ being the dominant LLJ wind direction in the central Sahara for dust emission. Since this form of the LLJ is more important than the monsoon jet as a whole across the central Sahara in the summer, there is a clear case for favouring the LAM dataset.

LLJ development at BBM (key question 3) is favourable under conditions of a strong synoptic-scale pressure gradient. When this is not present, when the heat low is weak in the BBM region, there is little or no LLJ formation (Figure 6-9a,b). Under conditions of a strong synoptic-scale pressure gradient, LLJs at BBM during the IOP can be split into two main types, those embedded in the moist monsoon flow (5 LLJs) and those embedded in the dry Harmattan flow (6 LLJs; mornings when cold pools were observed coincident with LLJs are excluded in both cases). There is a clear association between the SHL position and the classification of the LLJ. When the SHL is east of BBM, the cyclonic circulation promotes north-easterly LLJs over BBM (Figure 6-9c,d). When the SHL is to the north-west of BBM, the cyclonic circulation promotes south-westerly LLJs over BBM (Figure 6-9e,f). This highlights the importance of correct model simulation of the position and strength of the SHL. South-westerly LLJs accelerating

towards the SHL have been shown to be an important feature of the diurnal monsoon circulation [*Parker et al.*, 2005]; the monsoon flow intensifies overnight as boundary layer turbulence dies down.

The local conditions for LLJ development are appreciably different depending on whether the LLJ is embedded in the Harmattan or the monsoon flow. Harmattan LLJs are associated with stronger surface temperature inversions than monsoon LLJs: on average 2.5°C/100m at 0600 compared with 0.6°C/100m (Figure 6-11). The strongest LLJ, which is embedded in the Harmattan, has a surface temperature inversion of 2.2°C/100m (Figure 6-10b). This highly stably-stratified nocturnal boundary layer will promote the decoupling of the winds in the LLJ core from the surface. However, many strong LLJs, particularly those embedded in the monsoon, have much weaker surface temperature inversions (Figure 6-11). Unlike for the LLJs in Mali documented by *Bain et al.* [2010], stronger temperature inversions did not necessarily result in stronger jets. *Kutsher et al.* [2012] document LLJs in the Negev Desert which do not depend on strong surface temperature inversions to form, since the LLJs can be advected as part of the sea breeze circulation. The West African Monsoon could to some extent also be thought of as 'advecting' the monsoon LLJs to BBM.

Harmattan and monsoon LLJs develop with considerably different lower-tropospheric moisture conditions (Figure 6-12). The reduced near-surface cooling during the nights and early mornings of monsoon LLJs is most likely because the monsoon LLJs bring relatively high levels of water vapour with them below ~600m agl (Figure 6-12b). There is no evidence of turbulent mixing below the LLJ core in the BBM nocturnal potential temperature profiles: *Kutsher et al.* [2012] found such a mechanism and showed that it could counterbalance nocturnal radiative cooling.

Only particularly strong and deep LLJs lead to dust emission (Figure 6-13; key question 4). Dust emitting LLJs at BBM all have core wind speeds ≥16ms^{-1} and below core wind shear ≥0.6ms^{-1} per 30m. At midnight on dusty mornings the LLJ is already stronger than the maximum strength the LLJ reaches on non-dusty mornings (thus there is a ~6 h predictive capability for dust emitting LLJs). The depth of wind speeds above 8ms^{-1} is also twice as great, 90-1500m agl compared to 90-700m agl. Therefore there is a much greater 'source' of momentum. A deeper convective boundary layer promotes momentum mix-down to the surface (a larger number of turbulent eddies penetrate to jet core height), where post-sunrise wind speeds display a Gaussian increase and decay, closely matched by the lidar backscatter from 0700 to 1300 (Figure 6-14a). During this period 10m wind speeds are above the local dust emission threshold of 8ms^{-1} [*Allen et al.*, 2013].

Higher LLJ wind speeds on dusty mornings have also been found by other studies. In their sub-domain including BBM, *Fiedler et al.* [2013] find that the median LLJ core wind speed for dust emitting LLJs is 7ms^{-1} faster than that for all LLJ periods (16ms^{-1} compared to 9ms^{-1}). During BoDEx, LLJ core wind speeds on dusty mornings were, depending on the hour, up to 10ms^{-1} faster than on non-dusty mornings [*Washington et al.*, 2006a].

Unlike most previous studies where wind speed is used as a proxy for momentum, the simultaneous availability of radiosondes, lidar and flux tower instrumentation has allowed momentum profiles to be calculated explicitly for the IOP (key question 5). These show that, on all occasions when LLJ-induced dust emission occurs, momentum does indeed mix down from the LLJ core to the surface between 0500 and 0900, after the onset of surface heating (Table 6-4). The use of momentum change profiles makes it

particularly easy to see the transfer of momentum between one hour and the next at a selection of levels through the atmosphere. Good examples of this occur in the 0700-0800 time interval: on 26 June (Figure 6-17a) the near surface is almost the only height gaining momentum coincident with a significant increase in backscatter; on 16 June momentum at 300m decreases by almost 240 kg ms^{-1} whilst momentum at 120m agl and below increases by over 80 kg ms^{-1} (Figure 6-17b).

Momentum is not always mixed down. On the nine 'pure' LLJ mornings which do not lead to dust emission, momentum mix-down between 0500 and 0900 is not observed except on 8 June. On this morning the weakness of the LLJ (Figure 6-5) probably explains why no dust emission occurs. On 17/21 LLJ mornings, momentum does not mix down between 0900 and 1200. This is consistent with the general decrease in surface wind speeds after 0900 on LLJ mornings (Figures 14, 16b and 18c). Without momentum being mixed to the surface, the surface wind speeds decline. This suggests that the period of 0600-1200 chosen by *Marsham et al.* [2013] to span momentum mix-down is too generous for most cases at BBM (this timing may be different elsewhere), although, given uncertainties due to missing data, there are between 1-4 cases when LLJ momentum does mix down from 0900-1200. This compares with 8-9 cases when momentum mixes down from 0500-0900 (Table 6-4).

Some cold pool outflows (e.g. 13 and 21 June) appear to disrupt the mix-down process: momentum does not mix down between 0500 and 0900 on either of these mornings (Table 6-4). Using regional model LM-MUSCAT, *Heinold et al.* [2008] also found that thermal stratification suppresses turbulent mix-down of momentum in the Sahara, although this stratification was specifically due to the presence of dust, which is not always the cause of the stratification at BBM. During three mornings when LLJs were

coincident with cold pool outflows (e.g. 18 June, Table 6-4), momentum does mix down between 0500 and 0900, however. On these mornings it is plausible that the LLJ also contributes to the dust loadings, especially if a Gaussian pattern in the surface wind speeds can be identified. Following the results of 4km-resolution explicit convection simulations over the West African domain, *Heinold et al.* [2013] suggest that aged cold pools that glide above a stable nocturnal boundary layer can trigger LLJ formation. This mechanism is not the main trigger for LLJ formation during the IOP (the LLJs observed at BBM are simulated by the 12km resolution Africa LAM, which parameterises convection and has very poor representation of cold pools (see also *Marsham et al.* [2011]). However, the coincidence of LLJ and cold pool outflow is reasonably frequent: of the 21 mornings when LLJs were detected, cold pools occurred on 7. This is similar to the results of *Heinold et al.* [2013], who found that for 23% dust emissions in the model domain both LLJs and cold pools were detected together.

LLJs are common features in desert regions, where they can be an important mechanism for dust emission. The Bodélé LLJ in Chad has been well documented [e.g. *Washington et al.*, 2006a], but the remoteness and difficulty of working in the summertime central Sahara has meant that until the Fennec project, direct observations of these features here has been very limited. This paper has presented the first detailed analysis of central Saharan LLJs from ground-based observations and demonstrated their strong association with the heat low. Whilst LLJs occur on most mornings, their presence cannot be taken as a guarantee of dust emission, even over a highly erodible surface: only the strongest LLJs lead to momentum mix-down and emission. The study is limited to one location and one summer however; further Fennec work will expand the analysis beyond BBM and out to other years.

6.10. Acknowledgements

Fennec was funded by a NERC consortium grant (NE/G017166/1). The authors thank Chidong Zhang and two anonymous reviewers for their comments which improved the manuscript. The authors also wish to thank the following individuals and institutions. For establishing and instrumenting the supersite: B Abderrahmane, M Bart, BJ Brooks, C Cavazos-Guerra, F Davies, S Engelstaedter, L Garcia-Carreras, M Gascoyne, M Hobby, A Lima, M Limam, JH Marsham, V Martins, JB McQuaid, A O'Leary, B Ouchene, A Ouladichir, DJ Parker, A Saci, M Salah-Ferroudj, D Sidali, MC Todd, the AERONET PHOTONS team, ONM Algérie, the University of Leeds and the University of Sussex. For providing the SEVIRI imagery at http://www.fennec.imperial.ac.uk: H Brindley and J Banks. For the Africa-LAM dataset: UK Met Office. For the ERAI dataset: European Centre for Medium-Range Weather Forecasts. For helpful suggestions and discussion: I Ashpole, S Engelstaedter and JH Marsham. We also thank FGAM (Facility for Ground-based Atmospheric Measurement), UK Met Office and NCAS (National Centre for Atmospheric Science) for the use of the sodar, lidar and radiosonde units. Datasets are available through the British Atmospheric Data Centre.

6.11. References

Allen, C. J. T., R. Washington, and S. Engelstaedter (2013), Dust emission and transport mechanisms in the central Sahara: Fennec ground-based observations from Bordj Badji Mokhtar, June 2011, *Journal of Geophysical Research: Atmospheres*, *118*, 6212–6232, doi: 10.1002/jgrd.50534.

Andreas, E., K. Claffy, and A. Makshtas (2000), Low-Level Atmospheric Jets And Inversions Over The Western Weddell Sea, *Boundary-Layer Meteorology*, *97*(3), 459-486, doi: 10.1023/a:1002793831076.

Ansmann, A., M. Tesche, P. Knippertz, E. Bierwirth, D. Althausen, D. Müller, and O. Schulz (2009), Vertical profiling of convective dust plumes in southern Morocco during SAMUM, *Tellus B*, *61*(1), 340-353, doi: 10.1111/j.1600-0889.2008.00384.x.

Ashpole, I., and R. Washington (2012), An automated dust detection using SEVIRI: A multiyear climatology of summertime dustiness in the central and western Sahara, *J. Geophys. Res.*, *117*(D8), D08202, doi: 10.1029/2011jd016845.

Ashpole, I., and R. Washington (2013), A new high-resolution central and western Saharan summertime dust source map from automated satellite dust plume tracking, *Journal of Geophysical Research D: Atmospheres*, *118*(13), 6981-6995, doi: 10.1002/jgrd.50554.

Bain, C. L., D. J. Parker, C. M. Taylor, L. Kergoat, and F. Guichard (2010), Observations of the Nocturnal Boundary Layer Associated with the West African Monsoon, *Monthly Weather Review*, *138*(8), 3142-3156, doi: 10.1175/2010mwr3287.1.

Banta, R. M., R. K. Newsom, J. K. Lundquist, Y. L. Pichugina, R. L. Coulter, and L. Mahrt (2002), Nocturnal Low-Level Jet Characteristics Over Kansas During Cases-99, *Boundary-Layer Meteorology*, *105*(2), 221-252, doi: 10.1023/a:1019992330866.

Basu, S., J. F. Vinuesa, and A. Swift (2008), Dynamic LES modeling of a diurnal cycle, *Journal of Applied Meteorology and Climatology*, *47*(4), 1156-1174, doi: 10.1175/2007JAMC1677.1.

Bechtold, P., M. Köhler, T. Jung, F. Doblas-Reyes, M. Leutbecher, M. J. Rodwell, F. Vitart, and G. Balsamo (2008), Advances in simulating atmospheric variability with the ECMWF model: From synoptic to decadal time-scales, *Quarterly Journal of the Royal Meteorological Society*, *134*(634), 1337-1351, doi: 10.1002/qj.289.

Blackadar, A. K. (1957), Boundary layer wind maxima and their significance for the growth of nocturnal inversion, *Bull. Am. Meteorol. Soc*, *38*(5), 283-290.

Bou Karam, D., C. Flamant, P. Tulet, J.-P. Chaboureau, A. Dabas, and M. C. Todd (2009), Estimate of Sahelian dust emissions in the intertropical discontinuity region of the West African Monsoon, *Journal of Geophysical Research-Atmospheres*, *114*, doi: 10.1029/2008jd011444.

Bou Karam, D., C. Flamant, P. Knippertz, O. Reitebuch, J. Pelon, M. Chong, and A. Dabas (2008), Dust emissions over the Sahel associated with the West African monsoon intertropical discontinuity region: A representative case-study, *Quarterly Journal of the Royal Meteorological Society*, *134*(632), 621-634, doi: 10.1002/qj.244.

Bowen, B. M. (1996), Example of reduced turbulence during thunderstorm outflow, *Journal of Applied Meteorology*, *35*(6), 1028-1032, doi: 10.1175/1520-0450(1996)035<1028:EORTDT>2.0.CO;2.

Brown, A. R., R. J. Beare, J. M. Edwards, A. P. Lock, S. J. Keogh, S. F. Milton, and D. N. Walters (2008), Upgrades to the Boundary-Layer Scheme in the Met Office Numerical Weather Prediction Model, *Boundary-Layer Meteorology*, *128*(1), 117-132, doi: 10.1007/s10546-008-9275-0.

Browning, K., and R. Wexler (1968), The determination of kinematic properties of a wind field using Doppler radar, *J. Appl. Meteorol.*, *7*, 105-113, doi: 10.1175/1520-0450(1968)007<0105:TDOKPO>2.0.CO;2.

Cuesta, J., C. Lavaysse, C. Flamant, M. Mimouni, and P. Knippertz (2010), Northward bursts of the West African monsoon leading to rainfall over the Hoggar Massif, Algeria, *Quarterly Journal of the Royal Meteorological Society*, *136*, 174-189, doi: 10.1002/qj.439.

Cuesta, J., D. Edouart, M. Mimouni, P. H. Flamant, C. Loth, F. Gibert, F. Marnas, A. Bouklila, M. Kharef, B. Ouchene, M. Kadi, and C. Flamant (2008), Multiplatform observations of the seasonal evolution of the Saharan atmospheric boundary layer in Tamanrasset, Algeria, in the framework of the African Monsoon Multidisciplinary Analysis field campaign conducted in 2006, *Journal of Geophysical Research-Atmospheres*, *113*, doi: 10.1029/2007jd009417.

Darby, L. S., R. M. Banta, W. A. Brewer, W. D. Neff, R. D. Marchbanks, B. J. McCarty, C. J. Senff, A. B. White, W. M. Angevine, and E. J. Williams (2002), Vertical variations in O3 concentrations before and after a gust front passage, *Journal of Geophysical Research: Atmospheres*, *107*(D13), ACH 9-1-ACH 9-11, doi: 10.1029/2001jd000996.

de Longueville, F., P. Ozer, S. Doumbia, and S. Henry (2012), Desert dust impacts on human health: an alarming worldwide reality and a need for studies in West Africa, *International Journal of Biometeorology*, 1-19, doi: 10.1007/s00484-012-0541-y.

Dee, D. P., S. M. Uppala, A. J. Simmons, P. Berrisford, P. Poli, S. Kobayashi, U. Andrae, M. A. Balmaseda, G. Balsamo, P. Bauer, P. Bechtold, A. C. M. Beljaars, L. van de Berg, J. Bidlot, N. Bormann, C. Delsol, R. Dragani, M. Fuentes, A. J. Geer, L. Haimberger, S. B. Healy, H. Hersbach, E. V. Hólm, L. Isaksen, P. Kållberg, M. Köhler, M. Matricardi, A. P. McNally, B. M. Monge-Sanz, J. J. Morcrette, B. K. Park, C. Peubey, P. de Rosnay, C. Tavolato, J. N. Thépaut, and F. Vitart (2011), The ERA-Interim reanalysis: configuration and performance of the data assimilation system, *Quarterly Journal of the Royal Meteorological Society*, *137*(656), 553-597, doi: 10.1002/qj.828.

Diab, R. D., R. A. Preston-Whyte, and R. Washington (1991), Distribution of rainfall by synoptic type over natal, South Africa, *International Journal of Climatology*, *11*(8), 877-888, doi: 10.1002/joc.3370110806.

Dukić, V., M. Hayden, A. A. Forgor, T. Hopson, P. Akweongo, A. Hodgson, A. Monaghan, C. Wiedinmyer, T. Yoksas, M. C. Thomson, S. Trzaska, and R. Pandya (2012), The Role of Weather in Meningitis Outbreaks in Navrongo, Ghana: A Generalized Additive Modeling Approach, *Journal of Agricultural, Biological, and Environmental Statistics*, *17*(3), 442-460, doi: 10.1007/s13253-012-0095-9.

Emmel, C., P. Knippertz, and O. Schulz (2010), Climatology of convective density currents in the southern foothills of the Atlas Mountains, *J. Geophys. Res.*, *115*(D11), D11115, doi: 10.1029/2009jd012863.

Engelstaedter, S., I. Tegen, and R. Washington (2006), North African dust emissions and transport, *Earth-Science Reviews*, *79*(1–2), 73-100, doi: 10.1016/j.earscirev.2006.06.004.

Evan, A. T., G. R. Foltz, D. Zhang, and D. J. Vimont (2011), Influence of African dust on ocean-atmosphere variability in the tropical Atlantic, *Nature Geoscience*, *4*(11), 762-765, doi: 10.1038/ngeo1276.

Fernald, F. (1984), Analysis of atmospheric lidar observations: some comments, *Applied Optics*, *23*(5), 652-653, doi: 10.1364/AO.23.000652.

Fernald, F., B. Herman, and J. Reagan (1972), Determination of aerosol height distributions by Lidar, *J. Appl. Meteorol.*, *11*, 482-489, doi: 10.1175/1520-0450(1972)011<0482:DOAHDB>2.0.CO;2.

Fiedler, S., K. Schepanski, B. Heinold, P. Knippertz, and I. Tegen (2013), Climatology of Nocturnal Low-Level Jets over North Africa and Implications for Modeling Mineral Dust Emission, *Journal of Geophysical Research: Atmospheres*, *118*, 6100–6121, doi: 10.1002/jgrd.50394.

García, O. E., J. P. Díaz, F. J. Expósito, A. M. Díaz, O. Dubovik, Y. Derimian, P. Dubuisson, and J. C. Roger (2012), Shortwave radiative forcing and efficiency of key aerosol types using AERONET data, *Atmospheric Chemistry and Physics*, *12*(11), 5129-5145, doi: 10.5194/acp-12-5129-2012.

Garrity, C. M., R. S. Cerveny, and E. A. Wentz (2010), Vertical moisture profile characteristics of severe surface drought and surface wetness in the western United States: 1973–2002, *International Journal of Climatology*, *30*(6), 894-900, doi: 10.1002/joc.1944.

Haywood, J. M., R. P. Allan, I. Culverwell, T. Slingo, S. Milton, J. Edwards, and N. Clerbaux (2005), Can desert dust explain the outgoing longwave radiation anomaly over the Sahara during July 2003?, *J. Geophys. Res.*, *110*(D5), D05105, doi: 10.1029/2004jd005232.

Heinold, B., I. Tegen, K. Schepanski, and O. Hellmuth (2008), Dust radiative feedback on Saharan boundary layer dynamics and dust mobilization, *Geophysical Research Letters*, *35*(20), L20817, doi: 10.1029/2008gl035319.

Heinold, B., P. Knippertz, J. H. Marsham, S. Fiedler, N. S. Dixon, K. Schepanski, B. Laurent, and I. Tegen (2013), The role of deep convection and nocturnal low-level jets for dust emission in summertime West Africa: Estimates from convection-permitting simulations, *Journal of Geophysical Research: Atmospheres*, *118*, 4385–4400, doi: 10.1002/jgrd.50402.

Hobby, M., M. Gascoyne, J. H. Marsham, M. Bart, C. J. T. Allen, S. Engelstaedter, D. M. Fadel, A. Gandega, R. Lane, J. B. McQuaid, B. Ouchene, A. Ouladichir, D. J. Parker, P. Rosenberg, M. S. Ferroudj, A. Saci, F. Seddik, M. Todd, D. Walker, and R. Washington (2013), The Fennec Automatic Weather Station (AWS) Network: Monitoring the Saharan Climate System, *Journal of Atmospheric and Oceanic Technology*, *30*(4), 709-724, doi: 10.1175/jtech-d-12-00037.1.

Holben, B. N., T. F. Eck, I. Slutsker, D. Tanré, J. P. Buis, A. Setzer, E. Vermote, J. A. Reagan, Y. J. Kaufman, T. Nakajima, F. Lavenu, I. Jankowiak, and A. Smirnov (1998), AERONET - A federated instrument network and data archive for aerosol characterization, *Remote Sensing of Environment*, *66*(1), 1-16, doi: 10.1016/s0034-4257(98)00031-5.

Kallistratova, M. A., and R. D. Kouznetsov (2012), Low-Level Jets in the Moscow Region in Summer and Winter Observed with a Sodar Network, *Boundary-Layer Meteorology*, *143*(1), 159-175, doi: 10.1007/s10546-011-9639-8.

Klett, J. D. (1981), Stable analytical inversion solution for processing lidar returns, *Applied Optics*, *20*(2), 211-220, doi: 10.1364/AO.20.000211.

Knippertz, P. (2008), Dust emissions in the West African heat trough the role of the diurnal cycle and of extratropical disturbances, *Meteorologische Zeitschrift*, *17*(5), 553-563, doi: 10.1127/0941-2948/2008/0315.

Knippertz, P., and M. C. Todd (2012), Mineral dust aerosols over the Sahara: Meteorological controls on emission and transport and implications for modeling, *Reviews of Geophysics*, *50*(1), doi: 10.1029/2011RG000362.

Kutsher, J., N. Haikin, A. Sharon, and E. Heifetz (2012), On the Formation of an Elevated Nocturnal Inversion Layer in the Presence of a Low-Level Jet: A Case Study, *Boundary-Layer Meteorology*, 1-9, doi: 10.1007/s10546-012-9720-y.

Lensky, I. M., and D. Rosenfeld (2008), Clouds-Aerosols-Precipitation Satellite Analysis Tool (CAPSAT), *Atmos. Chem. Phys.*, *8*(22), 6739-6753, doi: 10.5194/acp-8-6739-2008.

Lock, A. P. (2001), The Numerical Representation of Entrainment in Parameterizations of Boundary Layer Turbulent Mixing, *Monthly Weather Review*, *129*(5), 1148-1163, doi: 10.1175/1520-0493(2001)129<1148:tnroei>2.0.co;2.

Lock, A. P., A. R. Brown, M. R. Bush, G. M. Martin, and R. N. B. Smith (2000), A New Boundary Layer Mixing Scheme. Part I: Scheme Description and Single-Column Model Tests, *Monthly Weather Review*, *128*(9), 3187-3199, doi: 10.1175/1520-0493(2000)128<3187:anblms>2.0.co;2.

Lothon, M., F. Saïd, F. Lohou, and B. Campistron (2008), Observation of the Diurnal Cycle in the Low Troposphere of West Africa, *Monthly Weather Review*, *136*(9), 3477-3500, doi: 10.1175/2008mwr2427.1.

Madougou, S., F. Saïd, B. Campistron, M. Lothon, and C. Kebe (2012), Results of UHF radar observation of the nocturnal low-level jet for wind energy applications, *Acta Geophys.*, *60*(5), 1413-1453, doi: 10.2478/s11600-012-0062-4.

Mahowald, N., S. Kloster, S. Engelstaedter, J. K. Moore, S. Mukhopadhyay, J. R. McConnell, S. Albani, S. C. Doney, A. Bhattacharya, M. A. J. Curran, M. G. Flanner, F. M. Hoffman, D. M. Lawrence, K. Lindsay, P. A. Mayewski, J. Neff, D. Rothenberg, E. Thomas, P. E. Thornton, and C. S. Zender (2010), Observed 20th century desert dust variability: impact on climate and biogeochemistry, *Atmos. Chem. Phys. Discuss.*, *10*(5), 12585-12628, doi: 10.5194/acpd-10-12585-2010.

Marsham, J. H., D. J. Parker, C. M. Grams, C. M. Taylor, and J. M. Haywood (2008), Uplift of Saharan dust south of the intertropical discontinuity, *J. Geophys. Res.*, *113*(D21), D21102, doi: 10.1029/2008jd009844.

Marsham, J. H., P. Knippertz, N. S. Dixon, D. J. Parker, and G. M. S. Lister (2011), The importance of the representation of deep convection for modeled dust-generating winds over West Africa during summer, *Geophys. Res. Lett.*, *38*(16), L16803, doi: 10.1029/2011gl048368.

Marsham, J. H., M. Hobby, C. J. T. Allen, J. R. Banks, M. Bart, B. J. Brooks, C. Cavazos-Guerra, S. Engelstaedter, M. Gascoyne, A. R. Lima, J. V. Martins, J. B. McQuaid, A. O'Leary, B. Ouchene, A. Ouladichir, D. J. Parker, A. Saci, M. Salah-Ferroudj, M. C. Todd, and R. Washington (2013), Meteorology and dust in the central Sahara: Observations from Fennec supersite-1 during the June 2011 Intensive Observation Period, *Journal of Geophysical Research: Atmospheres*, *118*, 4069–4089, doi: 10.1002/jgrd.50211.

Michailidou, C., P. Maheras, A. Arseni-Papadimititriou, F. Kolyva-Machera, and C. Anagnostopoulou (2009), A study of weather types at Athens and Thessaloniki and their relationship to circulation types for the cold-wet period, part II: discriminant analysis, *Theoretical and Applied Climatology*, *97*(1-2), 179-194, doi: 10.1007/s00704-008-0058-9.

Newsom R. K., Berg L. K., Shaw W. J. and Fischer M. L. (2015), Turbine-scale wind field measurements using dual-Doppler lidar, Wind Energ., 18, 219–235, doi: 10.1002/we.1691.

Nunalee, C. G., and S. Basu (2013), Mesoscale modeling of coastal low-level jets: implications for offshore wind resource estimation, *Wind Energy*, *17*, 1199-1216, doi: 10.1002/we.1628.

Parker, D. J., R. R. Burton, A. Diongue-Niang, R. J. Ellis, M. Felton, C. M. Taylor, C. D. Thorncroft, P. Bessemoulin, and A. M. Tompkins (2005), The diurnal cycle of the West African monsoon circulation, *Quarterly Journal of the Royal Meteorological Society*, *131*(611), 2839-2860, doi: 10.1256/qj.04.52.

Pearson, G., F. Davies, and C. Collier (2009), An analysis of the performance of the UFAM pulsed Doppler lidar for observing the boundary layer, *Journal of Atmospheric and Oceanic Technology*, *26*(2), 240-250, doi: 10.1175/2008JTECHA1128.1.

Rácz, Z., and R. K. Smith (1999), The dynamics of heat flows, *Quarterly Journal of the Royal Meteorological Society*, *125*(553), 225-252, doi: 10.1002/qj.49712555313.

Sandu, I., A. Beljaars, P. Bechtold, T. Mauritsen, and G. Balsamo (2013), Why is it so difficult to represent stably stratified conditions in numerical weather prediction (NWP) models?, *Journal of Advances in Modeling Earth Systems*, *5*(2), 117-133, doi: 10.1002/jame.20013.

Schepanski, K., I. Tegen, M. C. Todd, B. Heinold, G. Bönisch, B. Laurent, and A. Macke (2009), Meteorological processes forcing Saharan dust emission inferred from MSG-SEVIRI observations of subdaily dust source activation and numerical models, *J. Geophys. Res.*, *114*(D10), D10201, doi: 10.1029/2008jd010325.

Shapiro, A., and E. Fedorovich (2010), Analytical description of a nocturnal low-level jet, *Quarterly Journal of the Royal Meteorological Society*, *136*(650), 1255-1262, doi: 10.1002/qj.628.

Smith, R. N. B. (1990), A scheme for predicting layer clouds and their water content in a general circulation model, *Quarterly Journal of the Royal Meteorological Society*, *116*(492), 435-460, doi: 10.1002/qj.49711649210.

Solmon, F., N. Elguindi, and M. Mallet (2012), Radiative and climatic effects of dust over West Africa, as simulated by a regional climate model, *Climate Research*, *52*(1), 97-113, doi: 10.3354/cr01039.

Stanelle, T., B. Vogel, H. Vogel, D. Bäumer, and C. Kottmeier (2010), Feedback between dust particles and atmospheric processes over West Africa during dust episodes in March 2006 and June 2007, *Atmos. Chem. Phys.*, *10*(22), 10771-10788, doi: 10.5194/acp-10-10771-2010.

Stensrud, D. J. (1996), Importance of low-level jets to climate: A review, *Journal of Climate*, *9*(8), 1698-1711, doi: 10.1175/1520-0442(1996)009<1698:IOLLJT>2.0.CO;2.

Todd, M. C., R. Washington, S. Raghavan, G. Lizcano, and P. Knippertz (2008), Regional model simulations of the Bodélé low-level jet of Northern Chad during the Bodélé dust experiment (BoDEx 2005), *Journal of Climate*, *21*(5), 995-1012, doi: 10.1175/2007JCLI1766.1.

Todd, M. C., C. J. T. Allen, M. Bart, M. Bechir, J. Bentefouet, B. J. Brooks, C. Cavazos-Guerra, T. Clovis, S. Deyane, M. Dieh, S. Engelstaedter, C. Flamant, L. Garcia-Carreras, A. Gandega, M. Gascoyne, M. Hobby, C. Kocha, C. Lavaysse, J. H. Marsham, J. V. Martins, J.

B. McQuaid, J. B. Ngamini, D. J. Parker, T. Podvin, A. Rocha-Lima, S. Traore, Y. Wang, and R. Washington (2013), Meteorological and dust aerosol conditions over the Western Saharan region observed at Fennec supersite-2 during the Intensive Observation Period in June 2011, *Journal of Geophysical Research: Atmospheres*, *118*, 8426–8447, doi: 10.1002/jgrd.50470.

Tompkins, A. M., C. Cardinali, J. J. Morcrette, and M. Rodwell (2005), Influence of aerosol climatology on forecasts of the African Easterly Jet, *Geophys. Res. Lett.*, *32*(10), L10801, doi: 10.1029/2004gl022189.

van de Wiel, B. J. H., A. F. Moene, G. J. Steeneveld, P. Baas, F. C. Bosveld, and A. A. M. Holtslag (2010), A conceptual view on inertial oscillations and nocturnal low-level jets, *Journal of the Atmospheric Sciences*, *67*(8), 2679-2689, doi: 10.1175/2010JAS3289.1.

Walters, D. N., M. J. Best, A. C. Bushell, D. Copsey, J. M. Edwards, P. D. Falloon, C. M. Harris, A. P. Lock, J. C. Manners, C. J. Morcrette, M. J. Roberts, R. A. Stratton, S. Webster, J. M. Wilkinson, M. R. Willett, I. A. Boutle, P. D. Earnshaw, P. G. Hill, C. MacLachlan, G. M. Martin, W. Moufouma-Okia, M. D. Palmer, J. C. Petch, G. G. Rooney, A. A. Scaife, and K. D. Williams (2011), The Met Office Unified Model Global Atmosphere 3.0/3.1 and JULES Global Land 3.0/3.1 configurations, *Geosci. Model Dev.*, *4*(4), 919-941, doi: 10.5194/gmd-4-919-2011.

Washington, R., and M. C. Todd (2005), Atmospheric controls on mineral dust emission from the Bodélé Depression, Chad: The role of the low level jet, *Geophys. Res. Lett.*, *32*(17), L17701, doi: 10.1029/2005gl023597.

Washington, R., M. C. Todd, S. Engelstaedter, S. Mbainayel, and F. Mitchell (2006a), Dust and the low-level circulation over the Bodélé Depression, Chad: Observations from BoDEx 2005, *J. Geophys. Res.*, *111*(D3), D03201, doi: 10.1029/2005jd006502.

Washington, R., M. C. Todd, G. Lizcano, I. Tegen, C. Flamant, I. Koren, P. Ginoux, S. Engelstaedter, C. S. Bristow, C. S. Zender, A. S. Goudie, A. Warren, and J. M. Prospero (2006b), Links between topography, wind, deflation, lakes and dust: The case of the Bodélé Depression, Chad, *Geophys. Res. Lett.*, *33*(9), L09401, doi: 10.1029/2006gl025827.

Washington, R., C. Flamant, D. J. Parker, J. H. Marsham, J. B. McQuaid, H. Brindley, M. C. Todd, E. Highwood, C. Ryder, J. P. Chaboureau, C. Kocha, M. Bechir, and A. Saci (2012), Fennec - The Saharan Climate System, *CLIVAR Exchanges*, *17*(3), 31-33.

7. Dust detection from ground-based observations in the summer global dust maximum: results from Fennec 2011 and 2012 and implications for modelling and field observations

Christopher J. T. Allen, R. Washington and A. Saci

Published in Journal of Geophysical Research Atmospheres 4 February 2015[15]

doi: 10.1002/2014JD022655

Abstract

In boreal summer, the central Sahara is the dustiest place on Earth. Fennec supersite 1 is located within the dust maximum. With two field seasons completed, June 2011 (IOP1) and June 2012 (IOP2), we now have an initial measure of their representativeness. Although the number of dust event hours in IOP2 is up to 169 h (60%) more than in IOP1, the relative importance of the different dust mechanisms is the same. In both years, emission by cold pool outflows from deep convection causes most dust, followed by dust advection, monsoon surges, low level jet emission and lastly dry convective plumes. Given the dominance of cold pools, it is very important that they be incorporated in dust modelling efforts over the region. Because cold pools frequently occur at night and are associated with cloud cover, instruments that can monitor in these conditions are particularly valuable in this region. Sun photometer aerosol optical depth retrievals for example are only available for 23% (41%) of the time cold pool emission occurs at the supersite in IOP1 (IOP2). Deployment of instrumentation in remote regions being difficult and expensive, choosing the optimal instrument payload pays

[15] Note that following Minor Corrections required by the DPhil examiners (requested after this chapter was published) the content of this chapter is not identical to the published version.

dividends. With this motivation, we evaluate the different dust detection instrumentation deployed at the supersite and develop an approach which can identify and characterise individual dust emission mechanisms with a high degree of success purely from routine meteorological observations and remote sensing. This identification is however much more challenging in the case of dust advection.

7.1. Introduction

It is well-established that North Africa is the dustiest place in the world [e.g. *Prospero et al.*, 2002; *Washington et al.*, 2003; *Ginoux et al.*, 2012], but it is only recently that the central Sahara, the prime boreal summer dust source [*Ashpole and Washington*, 2012], has been subject to a comprehensive campaign of instrumentation: Fennec [*Washington et al.*, 2012]. As part of Fennec, eight automatic weather stations were deployed in the central Sahara [*Hobby et al.*, 2013] and two supersites were established, in Bordj-Badji Mokhtar, Algeria [*Marsham et al.*, 2013] and Zouerat, Mauritania [*Todd et al.*, 2013]. Observations from these supersites have provided new insights into Saharan dust, including among others the links between dust, cloud and the surface energy balance [*Marsham et al.*, 2013]; the relative importance of dust production mechanisms [*Allen et al.*, 2013; *Marsham et al.*, 2013]; the operation of the low level jet dust emission mechanism [*Allen and Washington*, 2014] and the role of the Atlantic Inflow on the diurnal cycle of the boundary layer [*Todd et al.*, 2013].

Considerable progress on African meteorology and climatology have been derived from short-term, intensive campaigns with the African Monsoon Multidisciplinary Analysis (AMMA) [*Redelsperger et al.*, 2006] and Fennec [*Washington et al.*, 2012] serving as prime examples for the west and north African region respectively. The extreme remoteness of major source regions of mineral aerosols in the central Sahara has led to

short-term campaigns in order to make costs and logistics manageable. As a result, the benchmark statistics relating to the meteorology of dust producing mechanisms emerging from field experiments such as BoDEx and Fennec, against which model development is posed, are derived from sub-seasonal campaigns typically in just one calendar year. In the case of Fennec, *Allen et al.* [2013] have shown that cold pool outflows, which constitute considerable challenges for numerical simulation, account for 45% of total emissions in the central Sahara. What is not clear is whether June 2011, the period from which this statistic was derived, can be regarded as representative of the mean summer conditions in the Sahara. There is growing evidence based on remote sensing [e.g. *Ashpole and Washington*, 2013b; *Awad and Mashat*, 2014; *Ridley et al.*, 2014] and observations distant from dust source regions [e.g. *Prospero and Lamb*, 2003; *Engelstaedter et al.*, 2006; *Mona et al.*, 2006] that Saharan dust output displays considerable interannual variability.

This variability in dust output has been linked to variability in assorted North African atmospheric phenomena. African Easterly Waves for example, which show significant interannual variability [*Thorncroft and Hodges*, 2001], can promote cold pool emission and also transport dust aloft towards the Atlantic [*Jones et al.*, 2003; *Knippertz and Todd*, 2010; *Zuluaga et al.*, 2012]. Interannual variability in the West African Monsoon [reviewed by *Rodríguez-Fonseca et al.*, 2011] is also linked to variability in dust emission: *Ashpole and Washington* [2013b] find that the dustiest summers are associated with a ≈ 3 ms^{-1} positive south-westerly anomaly in 925hPa wind speed that extends from northern Mali into central Algeria. A strong moist monsoon inflow can lead to dust emission as an intrusive surge or by promoting cold pool activity [*Bou Karam et al.*, 2008; *Marsham et al.*, 2008; *Allen et al.*, 2013; *Marsham et al.*, 2013];

strong low level jets (LLJs) are also frequently embedded in the moist monsoon inflow [*Parker et al.*, 2005; *Allen and Washington*, 2014].

Fennec was fortunate to be funded for an unplanned, albeit scaled-down second season in the Sahara in 2012. As a result of this opportunity, the aims of this paper are (a) ontological: a comparison of June 2011 and June 2012 in order to establish the degree of similarity of dust generating mechanisms operating in the remote Sahara and thereby to provide some constraint on interannual variability and (b) methodological: an analysis of the extent to which limited instrumentation can reproduce diagnostics of dust mechanisms compared with more comprehensive instrument deployment. The value in the latter lies in knowing the optimal level of instrumentation given the expense of importing, transporting and deploying instrumentation to remote regions - impediments that have long acted as a brake on knowledge of the meteorology of key dust producing regions.

Section 7.2 describes the datasets and field instrumentation employed; Section 7.3 describes the dust detection methodology for June 2012; this is then validated in Section 7.4. Sections 7.5-7.8 compare the characteristics of the dust events of June 2011 and June 2012 and Section 7.9 assesses the instrumentation. A discussion and conclusions are presented in Section 7.10.

7.2. Datasets and instrumentation

This paper focuses on Fennec supersite 1, the most comprehensively instrumented Fennec ground station, located at the existing synoptic station of Bordj-Badji Mokhtar (BBM) in south-west Algeria (21.38N, 0.92E; altitude 420m asl; WMO ID: 60686). BBM is located very close to the centre of the boreal summer global climatological dust maximum [e.g. *Ashpole and Washington*, 2012] and is proximate to several frequently

active dust sources [*Ashpole and Washington*, 2013a] making it an ideal location to study dust emission processes. Figure 7-1 shows the location of BBM in North Africa.

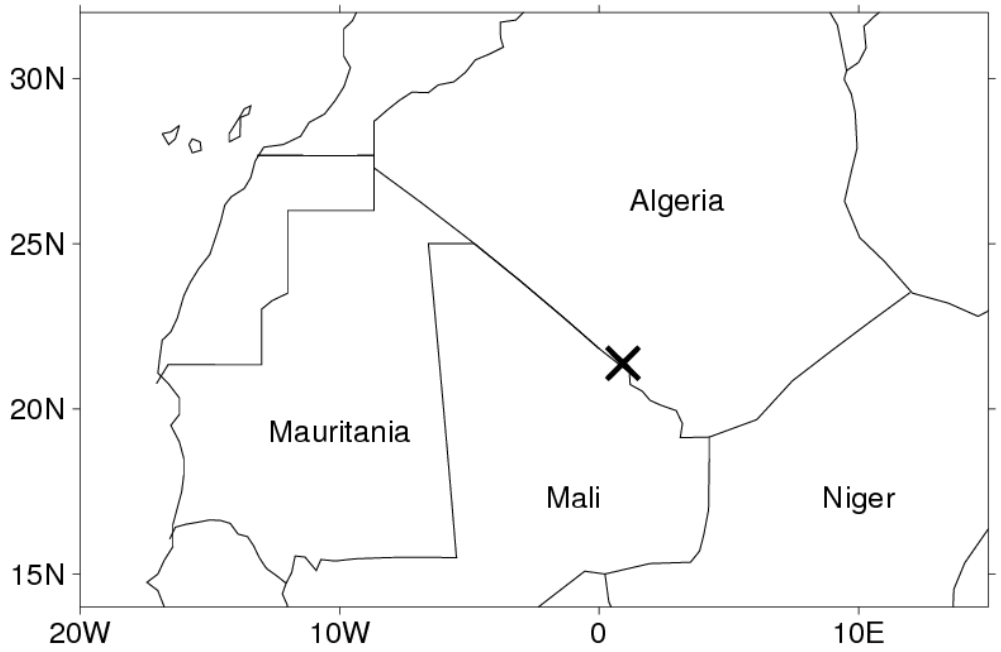

Figure 7-1: The location of Fennec supersite 1: Bordj Badji Mokhtar, Algeria (marked with a cross).

Fennec instrumentation has been deployed at BBM since June 2011 as part of the Fennec extended observation period (EOP), with additional instruments being available during the June 2011 intensive observation period (IOP) and, to a much lesser extent, the June 2012 IOP. The instruments, their accuracy and deployment lengths are described in Table 7-1. False colour imagery with 15 minute temporal resolution from the Spinning Enhanced Visible & Infrared Imager (SEVIRI) on board the Meteosat Second Generation satellite at 0N, 0E [*Lensky and Rosenfeld*, 2008] is used to identify the presence of cloud and to help classify dust events. A detailed evaluation of the SEVIRI dust detection algorithm is provided by *Brindley et al.* [2012]. A SEVIRI cloud mask product (available from the EUMETSAT data archive

(archive.eumetsat.int/umarf/)) is employed to detect cloud over BBM. In addition, we use an objective dust presence dataset, the SEVIRI Dust Flag (SDF) [*Ashpole and Washington*, 2012] with 15 minute, 0.03° resolution to help detect dust over BBM. SDF is a threshold-based automated dust detection scheme that is based on the widely-used but qualitative thermal infrared SEVIRI Dust Scheme [*Lensky and Rosenfeld*, 2008]. A major advantage of SDF compared with other satellite dust detection datasets is its 24-hour temporal coverage.

Table 7-1: Instruments available in June 2011 and June 2012†

Instrument	Accuracy	June 2011	June 2012	Notes
'Flux tower' (10m and 15m agl sonic anemometers)	0.1ms^{-1} (wind speed)	6th-30th	1st-30th	
'Flux tower' (2m agl sensors)	2% (RH), 0.3°C (T), 0.5hPa (P)	6th-30th	1st-30th	
Cimel sun photometer (formed part of the AERONET project [*Holben et al.*, 1998]). Level 1.5 data (cloud-screened) is used as it is common to 2011 and 2012.	0.01 (440nm AOD)	4th-30th	1st-30th	Measurements not continuous – data gaps discussed in Section 7.9.1
Vaisala RS92 GPS radiosondes (launched at up to 3-hourly intervals)	0.2ms^{-1} (wind speed)	8th-30th	2nd-25th	Not launched at 0600 on all of these mornings
HALO Photonics Streamline 1.55µm Doppler lidar (measurements taken every 30m from 90m agl to 9990m agl)	0.1ms^{-1} (wind speed)	3rd-30th	N/A	Wind speed and direction derived using a modified velocity-azimuth display algorithm [*Browning and Wexler*, 1968; *Banta et al.*, 2002].
Inverse nephelometer (2m agl, 670nm)	10^{-7}m^{-1} (scattering)	5th-30th	N/A	
Scintec MFAS phased array sodar	0.3 ms^{-1} (wind speed)	2nd-30th	N/A	

† RH=relative humidity, T=temperature, P=pressure, agl=above ground level. Accuracy is reported for the variables used in this paper. Filters from the vacuum pump aerosol sampler are still being analysed and the data are not used in this paper. An automatic weather station was available in June 2012, with instruments as per the flux tower (described by *Hobby et al.* [2013]). It was not used in this analysis. Further details of the instrumentation at BBM can be found in *Marsham et al.* [2013].

For both years, conditions (cloud and dust) reported by the weather observers at BBM are used, as well as local synop station measurements of meteorological variables when Fennec measurements are unavailable. Observers reported conditions on 101 synoptic hours in June 2011 and 92 in June 2012. They did not report conditions at night. The Africa Limited Area Model (LAM), a configuration of the Met Office Unified Model [*Walters et al.*, 2011] is used in Section 7.8 to ascertain the orientation of four LLJs in June 2012 for which no radiosondes are available. The four LLJ orientations are the same in the ERA-Interim reanalysis product. A detailed description of the Africa LAM is given in *Allen and Washington* [2014] and of ERA-Interim in *Dee et al.* [2011].

7.3. Dust detection methodology for June 2012

During the June 2011 IOP (IOP1), the instrumental set-up at BBM was conducive to identifying and characterising dust events and the meteorological mechanisms responsible for them (method and results documented in *Allen et al.* [2013]). For the June 2012 IOP (IOP2), the more limited instrumentation available makes this more difficult. In particular, the loss of the nephelometer and the lidar makes it impossible to simply apply the dust mechanism identification approach of *Allen et al.* [2013] to IOP2. We therefore use a data-denial approach on the IOP1 dataset (i.e. we only use instruments also available in IOP2) to develop identification criteria which can be applied to IOP2. This approach is taken since the classification of IOP1 dust events based on IOP2 instrumentation is verifiable given the spectrum of available instrumentation in IOP1. The criteria are designed to be objective wherever possible. We present the data-denial identification criteria in this section and present a quantitative measure of their skill in Section 7.4.

7.3.1. Detection of dust presence

For IOP2, the only dataset that can be used to infer dust presence during the day and the night is SDF. A limitation of SDF is that it is relatively poor at flagging dust when the overall loading is low (AOD< ~1) [*Ashpole and Washington*, 2012]. As a result, we combine local observers' observations of the dust conditions with SDF to develop a set of 'SDF and observers rules' to determine dust presence. These are summarised in Table 7-2. The SDF and observers rules are applied to aid dust mechanism identification as explained in the following subsections.

Table 7-2: SDF and observers rules

SDF and observers dust conditions†	Ruling
SDF=1 and dust visually observed	Dust
SDF=1 and observations clear	Dust
SDF=0 and dust visually observed	Dust
SDF=0 and observations clear	No dust
SDF=1 and no observations made	Dust
SDF=0 and no observations made	Dust if meteorological criteria satisfied (Section 7.3)

†SDF is a binary measure, 1=dust flagged, 0=dust not flagged. Conditions are as reported by the local weather observers.

7.3.2. Low level jet dust emission detection

Low level jets (LLJs) form primarily at night when winds above the nocturnal temperature inversion become decoupled from surface friction [*Blackadar*, 1957]. Turbulent mixing increases after sunrise and the momentum from the LLJ can be mixed down to the surface [e.g. *Lothon et al.*, 2008; *Allen and Washington*, 2014], leading to dust emission [*Washington et al.*, 2006; *Todd et al.*, 2008; *Marsham et al.*, 2013; *Allen and Washington*, 2014]. Low level jet (LLJ) dust emission detection is a two stage

process. First, a LLJ has to be detected above the surface. Second, momentum mix-down from the LLJ must result in high surface wind speeds and dust emission.

The LLJ detection scheme developed by *Allen and Washington* [2014] is used to identify LLJs. The scheme searches the 0600 wind profiles for wind speed maxima below 600m above ground level (agl). (This upper limit avoids detecting elevated wind maxima which are not LLJs, these have been found at BBM [*Allen and Washington*, 2014] and in northern Algeria [*Cowie et al.*, 2014]). The maxima are classified as LLJs if (i) they are > 8 ms^{-1} (ii) the wind shear between the wind maximum (the LLJ 'core') and 500m above the core is ≤ -1.8 ms^{-1} (iii) the wind speed under the core decreases downwards to the lowest measurement. *Allen and Washington* [2014] apply these criteria to lidar wind profiles, but since the lidar is unavailable for IOP2 we use radiosonde wind profiles. Using radiosonde rather than lidar measurements to detect LLJs during IOP1 results in correct LLJ classification on all but three out of the 22 occasions when radiosondes were launched at 0600 in IOP1. Two of these are when LLJs and cold pools occurred simultaneously, when one might expect wind profiles to be changing rapidly.

Allen and Washington [2014] show that the presence of a LLJ is not a guarantee of dust emission, since momentum does not always mix down to the surface. Indeed, in dusty regions it is possible that daytime turbulent mixing in the boundary layer actually decreases, because the dust reduces the sunlight reaching the surface [*R L Miller et al.*, 2004; *Pérez et al.*, 2006]. A detected LLJ is considered to lead to dust emission if (i) the 10m wind speed is above an emission threshold (Section 7.4) (ii) the pattern of 10m wind speed increase and decrease is approximately Gaussian (as found by *Allen and Washington* [2014]) (iii) the wind speed increase does not begin before sunrise (iv) the

SDF and observers rules are passed (Table 7-2). On mornings when no 0600 radiosonde wind profile measurements are available (8 mornings in IOP1 and 8 mornings in IOP2), the detection rests on fulfilling these four criteria alone.

7.3.3. Cold pool outflow emission detection

Cold pool outflows form when downdrafts from deep convection spread away from the parent storm as a density current [e.g. *S D Miller et al.*, 2008; *Roberts and Knippertz*, 2014]. At the leading edge of the outflow, where turbulence is high, substantial 'walls' of dust can be raised [*Flamant et al.*, 2007; *Knippertz et al.*, 2007; *S D Miller et al.*, 2008; *Williams et al.*, 2009; *Emmel et al.*, 2010; *Solomos et al.*, 2012; *Allen et al.*, 2013; *Marsham et al.*, 2013]. Inspection of 10m wind speed during the cold pool emission events of IOP1 (as identified by *Allen et al.* [2013]) shows that every cold pool emission event begins with a jump in wind speed of at least $3ms^{-1}$ in 15 min. We therefore use a jump in wind speed of at least $3ms^{-1}$ in 15 min as a first condition. The second condition is that wind speed must be above an emission threshold, since by definition this is a search for dust emitting cold pools (see also Section 7.4). One characteristic of cold pools is that as they pass over a point, they frequently cause a measureable change in temperature, water vapour mixing ratio (WVMR) and/or pressure [e.g. *S D Miller et al.*, 2008; *Emmel et al.*, 2010; *Marsham et al.*, 2013]. This is often but not always the case for cold pool outflows observed at BBM. During the day, continuous temperature fluctuations are recorded which have a magnitude similar to that associated with the passing of moderate or weak cold pools (≈±1°C/15 min), so it is difficult to determine when these changes are actually due to cold pools. Furthermore, during IOP1 surface temperature, humidity and pressure measurements are missing for a total of 245, 245 and 147 hours respectively after the instruments were activated. As a result of all these factors, we do not use temperature, pressure or moisture changes as a criterion for cold

pool emission detection, although if these are present, they help confirm the detection. We do however use the SEVIRI false colour dust detection imagery to check whether identification as a cold pool is appropriate, once the wind speed filters have been passed. Dust from large cold pools is often clearly visible in SEVIRI, and the presence of deep convection is a strong clue for potential cold pool activity [e.g. *Solomos et al.*, 2012; *Allen et al.*, 2013; *Marsham et al.*, 2013; *Roberts and Knippertz*, 2014].

In brief, the criteria for cold pool emission are (i) event starts with a jump in wind speed of at least $3ms^{-1}$ in 15 min (ii) wind speeds remain above an emission threshold (iii) SDF and observers rules are passed (Table 7-2) (iv) convective cloud is present over BBM in SEVIRI false colour imagery, or the dust can be back-tracked to deep convection. There is some risk that a single event may be artificially split into two or more separate events, this is discussed in Section 7.6. However, it will not change the calculations of their total duration or total dustiness during the IOPs.

7.3.4. Dry convective plume emission

Dust can also be raised by dry convection, either in non-rotating plumes (diameter ~100m) [*Ansmann et al.*, 2009] or rotating vortices known as dust devils (diameter ~7m) [*Balme and Greeley*, 2006]. Dusty dry convective events are relatively short-lived, on the order of a few minutes for dust devils and an hour or so for dry convective plumes [*Ansmann et al.*, 2009]. Light winds ($<7ms^{-1}$) are required to allow dry convective plumes and dust devils to develop [*Oke et al.*, 2007]. Dry convective plumes are usually associated with a pressure drop at the surface, known as a 'pressure well' [*Balme and Greeley*, 2006; *Lorenz*, 2012]. In a thermodynamical model for dust devils, *Renno et al.* [1998] show that the net work done by a dust devil is proportional to the surface

pressure drop, and that the wind speed around a dust devil solely depends on this value, making the pressure well a particularly important variable to consider.

The criteria for dry convective plume emission detection are (i) event starts with a jump in wind speed of at least $3ms^{-1}$ in 15 min and a pressure decrease (pressure 'well') of at least 0.7hPa in 15 min (ii) wind speeds prior to the pressure well must be less than $7ms^{-1}$ (following *Oke et al.* [2007] and *Ansmann et al.* [2009]) (iii) wind speeds following the wind speed jump remain above the emission threshold (Section 7.4), but for no longer than two hours (iv) the event must occur in the afternoon (i.e. after midday but before sunset). The final criterion is to help distinguish dry convective plumes from the convective mixing which can bring down momentum from LLJs, typically in the morning. Dry convection thus plays a role in two dust emission processes here but the above criteria focus on the short-lived convective plumes and dust devils caused by afternoon gustiness, having already identified periods of LLJ emission in Section 7.3.2. (Dry convection is implicitly included in the LLJ breakdown identification.)

Since dry convective plumes are short-lived, they are not required to pass the SDF and observers rules (observers report at most every three hours and it is unlikely that dust from dry convective plumes would be visible from a geostationary satellite due to limitations on the spatial resolution of imagery). Dust devils are not explicitly distinguished from dry convective plumes in this analysis; they are smaller and shorter-lived and difficult to detect with only one mast. Missing pressure measurements make it probable that some events are missed. It is likely that the contribution of dry convective plumes and dust devils is underestimated in both IOPs.

7.3.5. Dust advection

Without the lidar or nephelometer, detection of advected dust at BBM is difficult. Two classes of advected dust are distinguished: 'advection: unknown cause' and 'probably cold pool' advection. For the former, the following criteria are adopted: (i) SDF or visually observed dust present, but not identified so far as an emission mechanism (ii) wind speed below an emission threshold. For the latter, (i) the event begins with a fluctuation in pressure of at least 0.7hPa in 15 mins and/or an increase in water vapour mixing ratio (WVMR) of 1g kg^{-1} in 5 mins (ii) wind speed is below an emission threshold (iii) event passes SDF and observers rules (Table 7-2). In both 'advection: unknown cause' and 'probably cold pool' advection, once an event passes the criteria it continues to be classed as advection until dust is no longer identified by SDF or the observers, as long as wind speed is below the emission threshold. The 'advection: unknown cause' category could contain dust from many origins, including aged cold pools with no pressure or WVMR signatures, or advection related to larger scale processes such as Saharan cyclones or African Easterly Waves.

7.3.6. Monsoon surges

Monsoon surges are large scale incursions of the summer moist monsoon inflow into the central Sahara [e.g. *Couvreux et al.*, 2010]. They can raise dust directly by acting as density currents or indirectly by promoting deep convection and cold pool outflows [e.g. *Bou Karam et al.*, 2008; *Marsham et al.*, 2008]. In this paper, the term 'monsoon surge' will only be applied to surge events that produce dust. *Allen et al.* [2013] did not explicitly identify any monsoon surges during IOP1. They are not always distinguishable from LLJs and cold pool outflows as they can share similar characteristics [*Bou Karam et al.*, 2008; *Marsham et al.*, 2008; *Flamant et al.*, 2009; *Marsham et al.*, 2013]. During IOP2 however, classification of monsoon surges was

easier. On three occasions, SEVIRI imagery showed very wide (500-1000km) dust fronts approaching BBM during the late night/early morning from the south or south east; WVMR rose from background values of < 4g kg^{-1} to up to 14g kg^{-1} (at a rate of up to 7g kg^{-1} h^{-1}); peak wind speeds in the boundary layer were over 13ms^{-1} but did not have LLJ profiles (Section 7.3.2); 10m wind speeds began to increase before sunrise and persisted above 6ms^{-1} for up to 15 hours.

Figure 7-2 summarises the data-denial dust detection methodology.

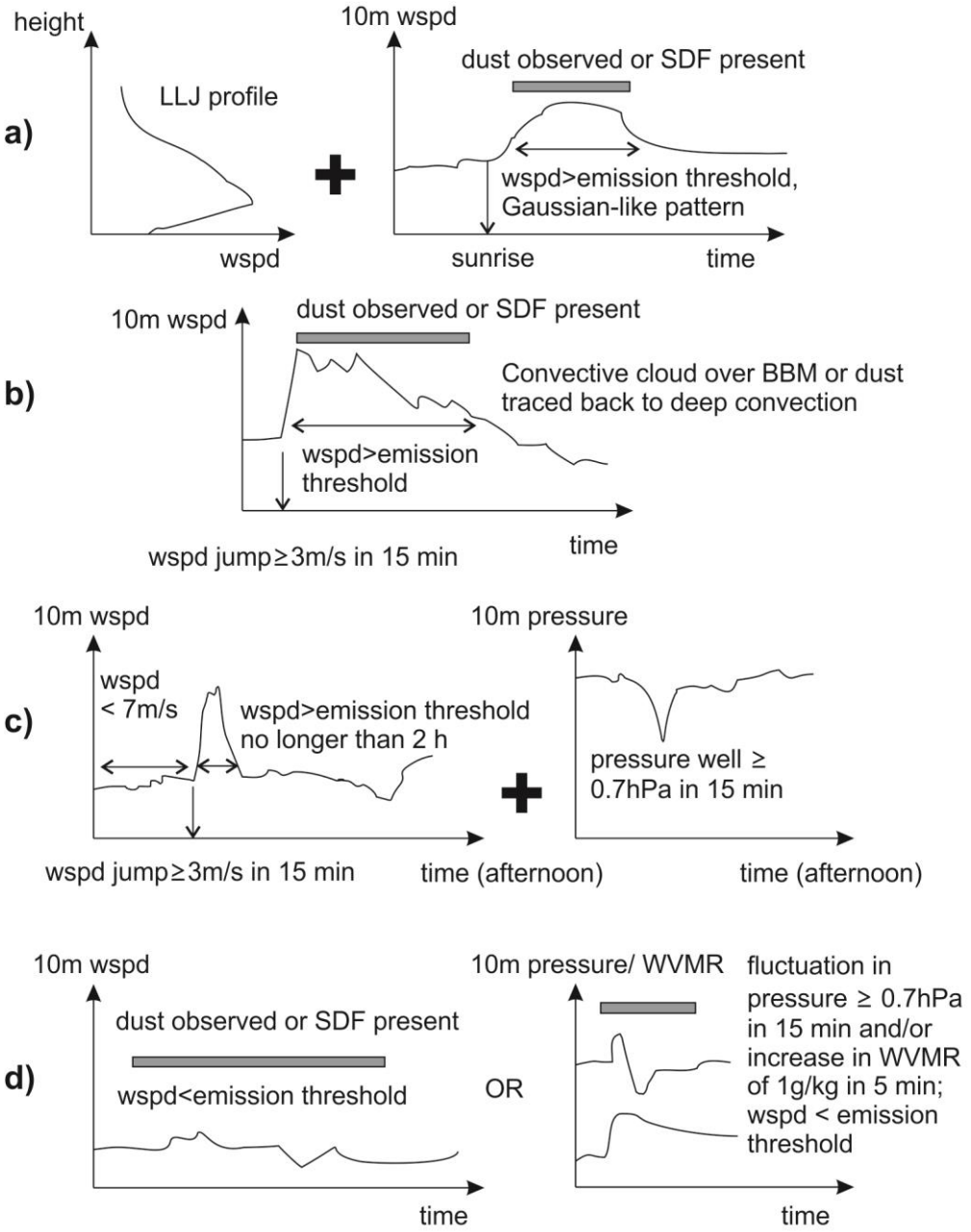

Figure 7-2: Cartoon summarising data denial dust detection methodology. (a) LLJ emission, (b) cold pool emission, (c) dry convective plume emission, (d) dust advection: 'unknown cause' (left) and 'probably cold pool' (right). 'wspd' = wind speed. For details see Section 7.3.

7.4. Validation of data-denial dust detection methodology

The data-denial dust detection methodology described in Section 7.3 is validated by comparing it with a refined version of the *Allen et al.* [2013] dust detection results. The

refinement is to allow classification of separate advection and emission periods within individual dust events, rather than classing each event once based on whether it is mostly advecting or emitting dust. This refinement is introduced because some cold pool outflows can contain both periods of dust emission (e.g. at the leading edge) and advection (e.g. behind it) [*S D Miller et al.*, 2008; *Emmel et al.*, 2010]. The same emission threshold (6 ms^{-1}) is used for both years.

The *Allen et al.* [2013] approach used nephelometer scattering as a sampling base and also made heavy use of the height-resolved lidar backscatter profiles to characterise dust events. Both instruments were unavailable during IOP2 and therefore also to the data denial approach. The nephelometer was unavailable before 2020 h on 5 June 2011 and missed two dust emission-inducing LLJs on the mornings of 3 and 5 June (described in *Allen and Washington* [2014]); these LLJs are included in the validation.

Validation of the data denial identification method (Section 7.3) can result in four outcomes. (i) True positive (data denial method identifies the same dust mechanism as actually observed). (ii) False positive (data denial identifies a dust mechanism when no dust mechanism is observed). (iii) False negative (a 'miss': data denial fails to identify the correct dust mechanism, or does not identify one at all). (iv) True negative (data denial correctly identifies that no dust mechanism is occurring). The bias ratio can also be used to provide a basic evaluation of the data denial method for each dust mechanism; it is defined as total forecast event hours ÷ total observed event hours [*Wilks*, 2006]. Values <1 are underpredictions and values >1 are overpredictions.

The data denial method is very successful in detecting cold pool emission, LLJ emission and dry convective plumes. For these the true positive rate is around 0.9, the false positive rate is below 0.015 and the bias ratio is close to 1 for each event class (red

symbols, Figure 7-3). With no nephelometer or lidar, detection of local emission using the data denial approach is unsurprisingly more successful than detection of advected dust (Figure 7-3, compare orange symbols with red symbols). Without using SDF or local observers as part of the criteria, the true positive rate for advected dust is very low, below 0.1, and the bias ratio is very poor, 0.15 (orange star, Figure 7-3). Including SDF or observers' observations results in a marked improvement in the true positive rate, from below 0.1 to 0.3 (orange crosses, Figure 7-3), and including both improves it significantly further (orange circle, Figure 7-3). However, the true positive rate is still only 0.47: a large proportion of the advected dust observed during IOP1 is missed. The false positive rate is low however, only 0.02. We apply the data denial dust advection detection to IOP2, but highlight that confidence is appreciably lower than for local dust emission detection.

For all dust mechanisms, the false positive rate is very low (Figure 7-3). This is probably because BBM is within a dust source area itself, a palaeolake [*Ashpole and Washington*, 2013a] therefore emission is not supply-limited (the palaeolake surface is readily erodible). Hence if an emission mechanism is operating, dust uplift will occur. There is little difference in the success of the dust detection methodology between day and night because the only data source used that is not available at night is the local observers (the sun photometer is not used for dust detection).

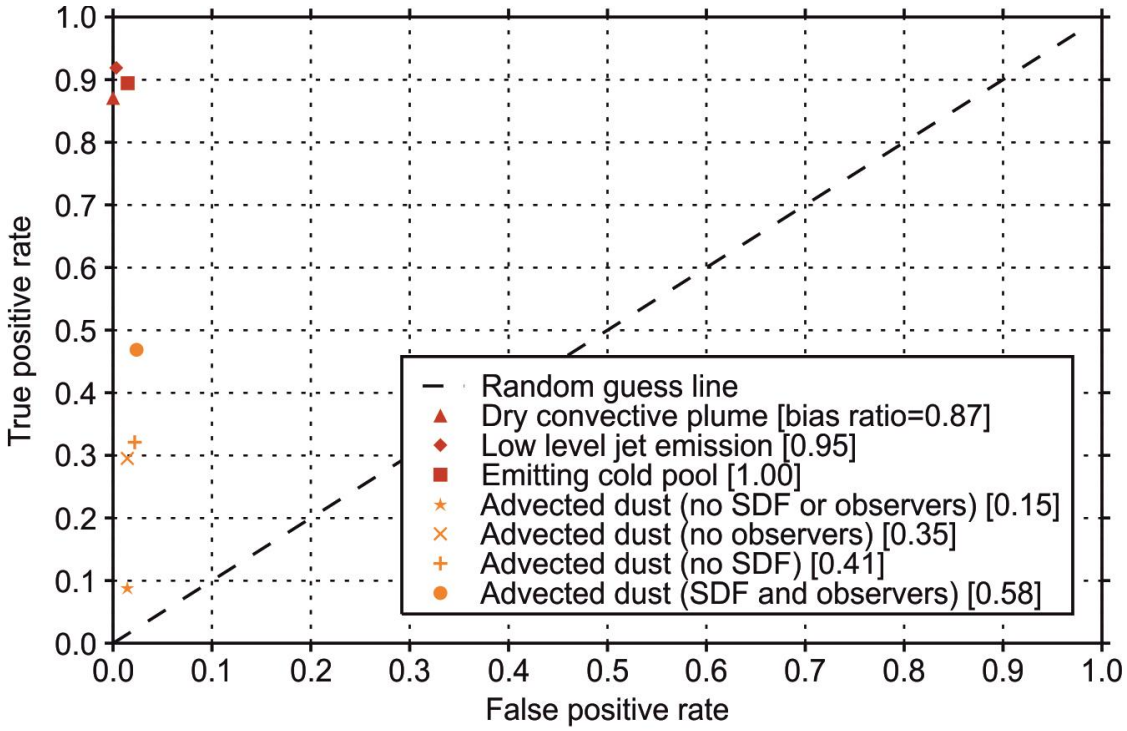

Figure 7-3: Receiver Operating Characteristic (ROC) diagram showing ability of dust mechanism identification criteria developed using data denial approach (Section 7.3) to detect observed dust mechanisms during IOP1. The true positive rate (left axis) is the number of true positives divided by the number of observed positives. The false positive rate (bottom axis) is the number of false positives divided by the number of observed negatives. A symbol in the top left would indicate a perfect prediction. A random guess would result in a point on the diagonal line. The dust mechanisms are each assigned symbols as shown in the key, with slightly altered identification criteria noted by ( ). The values in [ ] represent the bias ratio, defined as the total forecast event hours ÷ total observed event hours. Values <1 are underpredictions and values >1 are overpredictions. (Emitted cold pools are slightly overpredicted, the bias ratio is rounded to 2 d.p.)

We do not validate the monsoon surge data-denial detection since *Allen et al.* [2013] did not explicitly identify any monsoon surges during IOP1. They did however recognise that there were two occasions when event attribution is particularly difficult and monsoon surges may have been detected as a LLJ and advected dust in a cold pool (see also Section 7.3.6). In the remainder of the paper we class these two events in IOP1 as monsoon surges. In the supporting information (chapter appendix) we show that the

relative importance of the dust mechanisms is only altered subtly if they are classed otherwise.

7.5. Time partitioning of dust mechanisms

One area of research which has been called for in recent years is a quantitative assessment of the relative importance of dust production mechanisms in the Sahara [e.g. *Bou Karam et al.*, 2008; *Marsham et al.*, 2008]. Progress has been made on this front with modelling [e.g. *Marsham et al.*, 2011; *Heinold et al.*, 2013], reanalysis [e.g. *Fiedler et al.*, 2013], and also from observations during IOP1 [*Allen et al.*, 2013; *Marsham et al.*, 2013]. As with many remote field campaigns however, the IOP1 observations are from just one calendar year. The fortune to be granted a second field season means that a valuable first assessment can be made of the representativeness of the dust mechanisms observed in this all-important region. The dust detection methodology described and validated in the sections above makes this possible.

Three different estimations have been given for the IOP2 dust production hours (Figure 7-4). The time resolution is 15 min (the maximum resolution of SDF). The blue box ('lower limit') gives the value based on dust mechanism identification following the methodology outlined in Section 7.3. The open circle ('estimate') does the same but allows the occasional periods where dust could plausibly be produced by two different mechanisms to be counted twice. This allows for incorporation of classification uncertainty. It leads to no change to the dust production hours in the case of advected dust, and only small or moderate changes in the other cases (Figure 7-4). The third approach (red diamond, 'bias ratio correction') divides the 'lower limit' values in Figure 7-4 by the appropriate bias ratio (see Section 7.4 and Figure 7-3). This provides a basic correction for the number of hours that are missed by the dust detection techniques. A

bias ratio correction is not applied to monsoon surges since there is uncertainty in their detection in IOP1 (Section 7.4 and chapter appendix). As expected from the low true positive rate of dust advection detection (Figure 7-3, orange circle), the bias ratio correction leads to a large increase in the duration of dust advection for IOP2, from 128 h to 218 h (Figure 7-4). For the other dust mechanisms, the bias ratio correction results in very small changes (no more than 3 h, Figure 7-4), as expected from their high true positive rates (Figure 7-3, red symbols). Regardless of the estimation method chosen for the duration of the dust events during IOP2, the ranking remains identical.

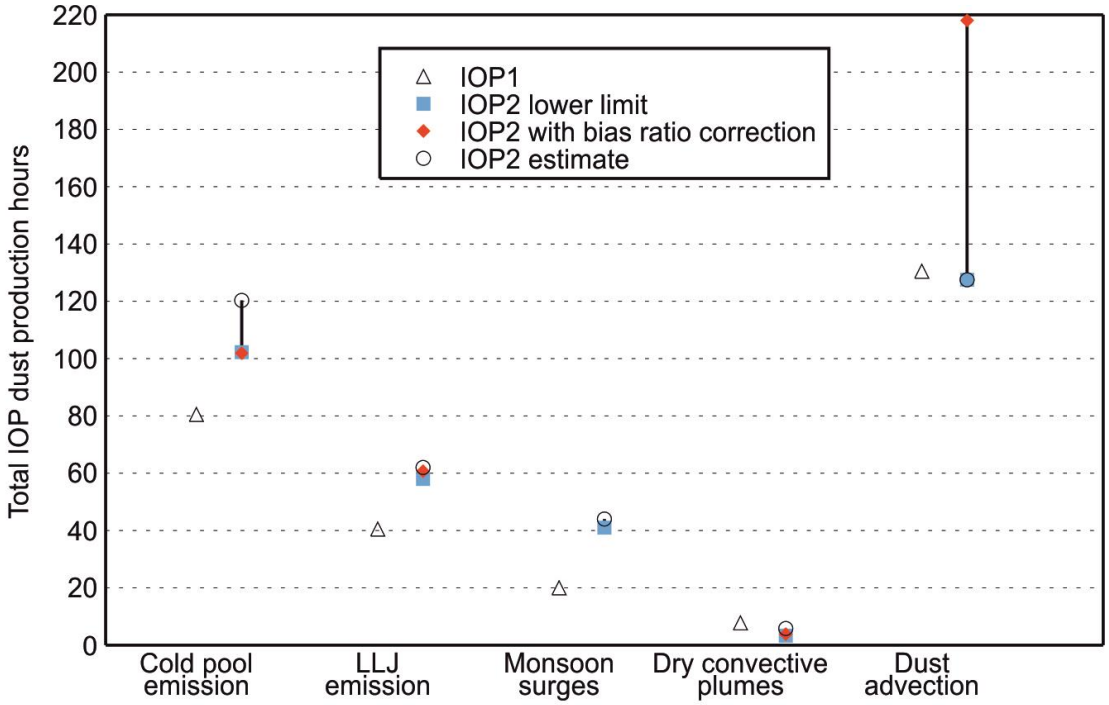

Figure 7-4: Partitioning of dust mechanisms by duration for IOP1 (June 2011) and IOP2 (June 2012). The bottom axis is the dust production mechanism and the left axis is the total duration of time that a dust production mechanism is in operation. Different symbols for IOP2 represent different calculations of dust production hours. See Section 7.5 for full details. IOP1 durations are from *Allen et al.* [2013] but expanded back from the evening of 5 June 2011 (when the nephelometer was activated) to the morning of 3 June 2011 (when the lidar was activated). This allows the inclusion of dust emission from LLJs identified on 3 and 5 June 2011 (see *Allen and Washington* [2014]). The values expressed as percentages can be found in Table 7-3.

In terms of the total amount of time a given dust mechanism is operating, the relative importance of the dust mechanisms during IOP2 is very similar to IOP1 and the ranking is identical (Figure 7-4, Table 7-3). During both Junes, dust advection occurs for more time than any other mechanism (131h in IOP1, ≥128h in IOP2), followed by cold pool emission (81h in IOP1, ≥102h in IOP2) then LLJ emission (41h in IOP1, ≥58h in IOP2), monsoon surges (20h in IOP1, ≥41h in IOP2) and finally dry convective plumes (8h in IOP1, ≥3h in IOP2). The times as percentages of the IOP totals can also be found in Table 7-3.

Table 7-3: Comparison of IOP1 and IOP2 dust production hours†

	IOP1 hours	IOP2 hours	Percentage of IOP1 hours	Percentage of IOP2 hours	Percentage change in hours (IOP2-IOP1)
Dust advection	131	128-218	19%	18-30%	-2 to +66%
Cold pool emission	81	102-120	12%	14-17%	+26 to +48%
LLJ emission	41	58-62	6%	8-9%	+41 to +51%
Monsoon surges	20	41-44	3%	6%	+105 to +120%
Dry convective plumes	8	3-6	1%	0.4-0.8%	-25 to -63%
Total dust production	281	332-450	42%	46-63%	+18 to +60%

† IOP hours are taken from Figure 7-4 and are rounded to the nearest whole number; the rows are in descending order (i.e. ranked). 'Total dust production' hours are the sum of the five rows above. The total number of hours used for percentage calculations in columns 4 and 5 is 28*24 in IOP1 (no dust classification was made prior to the lidar activation on 3 June, Table 7-1) and 30*24 in IOP2. The IOP1 percentage hours are slightly different from *Allen et al.* [2013] because (i) here we incorporate monsoon surges (ii) the emission/advection classification is refined (Section 7.4) (iii) *Allen et al.* [2013] defined the start of the IOP as 5 June, when the nephelometer was activated.

During IOP2, cold pool emission, LLJ emission and monsoon surges occurred for a longer time than during IOP1 (Figure 7-4). The difference is an increase of up to 39 h (48%) for cold pool emission, up to 21 h (51%) for LLJ emission and up to 24 h (120%) for monsoon surges (Table 7-3). During IOP2, dry convective plumes occurred for a shorter time than during IOP1. The difference is a decrease of up to 5 h (63%) (Table 7-3). Without bias ratio correction, dust advection during IOP2 occurred for a shorter time than during IOP1. The difference is a decrease of 3 h (2%) (Table 7-3). With bias ratio correction however, the amount of time dust advection occurred is much greater during IOP2 then IOP1, an increase of 87 h (66%). Overall, there were up to 169 (60%) more dust production hours in IOP2 than IOP1 (Table 7-3).

7.6. Duration of individual dust events

The *total* duration of time that dust mechanisms occupy (Section 7.5) is only one way to compare their characteristics. The number and duration of individual dust events is also informative given that the residence time of dust in the atmosphere is important to interactions with radiation and cloud, for example. For this purpose, cold pools cannot be split between emitting cold pools and 'probably cold pool' advection (Section 7.3.5): whilst some cold pools purely emit or advect dust, in others there may be periods where dust emission is occurring (e.g. at the leading edge) and periods in the same outflow when wind speeds are below the emission threshold [*S D Miller et al.*, 2008; *Emmel et al.*, 2010].

In IOP2, there were more events in each class than in IOP1 (Figure 7-5, top line). There is no statistically significant difference between IOP1 and IOP2 in the proportion of events in each class however (2 sample χ^2 test, 90% confidence level). Apart from monsoon surges, the duration of individual events in IOP2 was shorter. Indeed, the

median duration in IOP2 was always shorter than the lower quartile in IOP1 (Figure 7-5). In both June months, the longest event was a cold pool outflow: 23 h in IOP1 and 19 h in IOP2 (Figure 7-5). In IOP2, monsoon surges are the category with the second-longest events (lasting from 12.25 to 16 h) but the duration of monsoon surges in IOP1 is more varied (from 5 to 15 h). The maximum duration of LLJ emission events is very similar in both Junes (13 h in IOP1 and 12.75 h in IOP2) but there is more difference in the median durations (6.25 h in IOP1 and 4.25 h in IOP2). Dry convective plumes are, by nature and design (Section 7.3.4), the shortest-lived events (maximum durations 2 h in IOP1 and 1.5 h in IOP2).

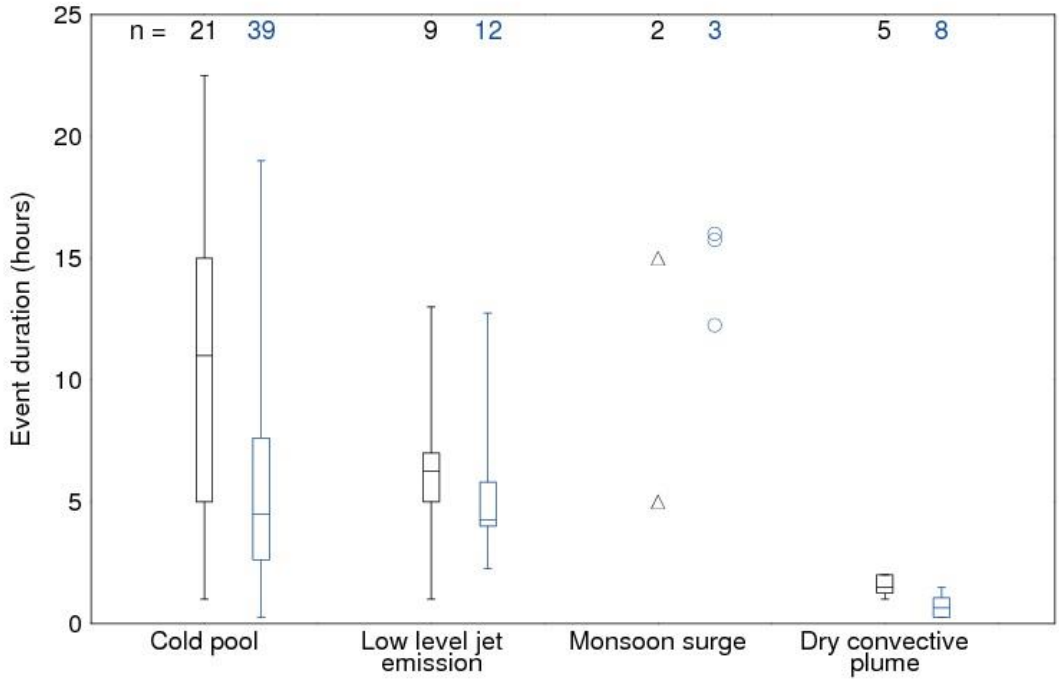

Figure 7-5: Boxplots comparing duration characteristics of individual dust events for IOP1 (black) and IOP2 (blue).The whiskers span the maximum range. Since there were only two and three monsoon surges in IOP1 and IOP2 respectively, boxplots for monsoon surges are not drawn but the duration of each of these events is noted with symbols as per Figure 4. The number of events in each class is shown at the top of the plot. The 'estimate' approach is used for classification (Section 7.5, open circles and triangles in Figure 7-4). (The bias ratio correction approach cannot be used since it does not provide any information about individual events.) The 'cold pool' class includes emitted and advected cold pool dust, see Section 7.6.

The most significant difference between the two Junes is the cold pool category. In IOP1, there are 21 cold pools with a median duration of 11 h; in IOP2 there are 39 cold pools with a median duration of 4.5 h. It is possible that some of this difference relates to the difficulty of detecting advected dust without the lidar or nephelometer (Figure 7-3). As stated above, an individual cold pool can have periods of active dust emission and periods when dust is only advected. If only some of these advection periods are not detected in IOP2, then one cold pool event may be artificially split into two or more shorter events. Indeed, in IOP1, 5 haboobs that contain a mixture of advected and emitted dust are artificially split into 10 separate events by the data-denial identification criteria.

7.7. Intensity of dust events

So far, the comparisons have only provided information on the duration of dust events, either as totals (Section 7.5) or as individual events (Section 7.6). The dustiness, or intensity, of the events is another important measure, as it is an important control on interactions with radiation [e.g. *Redmond et al.*, 2010; *Gu et al.*, 2012]. Unfortunately, there was no lidar or nephelometer available in IOP2, which is a major drawback for understanding the intensity of the dust events in June 2012. However, the sun photometer was operational during both Junes (albeit only during daytime), providing measurements of AOD.

The intensity of LLJ emission events was similar in both IOPs, with the dustiest LLJ emission event of IOP1 (IOP2) having an AOD of 2.4 (2.6) and the least dusty having an AOD of 0.7 (0.5) (Figure 7-6). The AODs are skewed towards the lower range of the spectrum in both cases. The intensity of cold pool emission events is harder to compare, since for 15 (22) events in IOP1 (IOP2) sun photometer AODs are not measured, and

only 2 cold pool emission events have measurements in IOP1. However, the dustiest available cold pool emission event of IOP1 is much more intense than the dustiest available cold pool emission event of IOP2 (AOD 2.8 against 1.3, Figure 7-6). Although a considerable number of AOD measurements of dust advection events are unavailable, enough measurements exist for a rough comparison. The distribution of dust advection AODs is fairly even in both IOPs, but in IOP1 the AODs are offset towards higher values (IOP1 range 0.7-3.3, IOP2 range 0.2-1.7; Figure 7-6). The small number of monsoon surges makes comparison difficult, but the monsoon surges in IOP1 were less dusty than the one available monsoon surge in IOP2 (AODs 1.1 and 2.4 in IOP1 against 2.7 in IOP2; Figure 7-6). From the measurements available, dry convective plumes appear to be more intense in IOP1 (AOD ~1.2) than IOP2 (~0.4), although 6 dry convective plumes in IOP2 do not have AOD measurements. Wind speeds during dry convective plumes were always stronger in IOP1 (not shown).

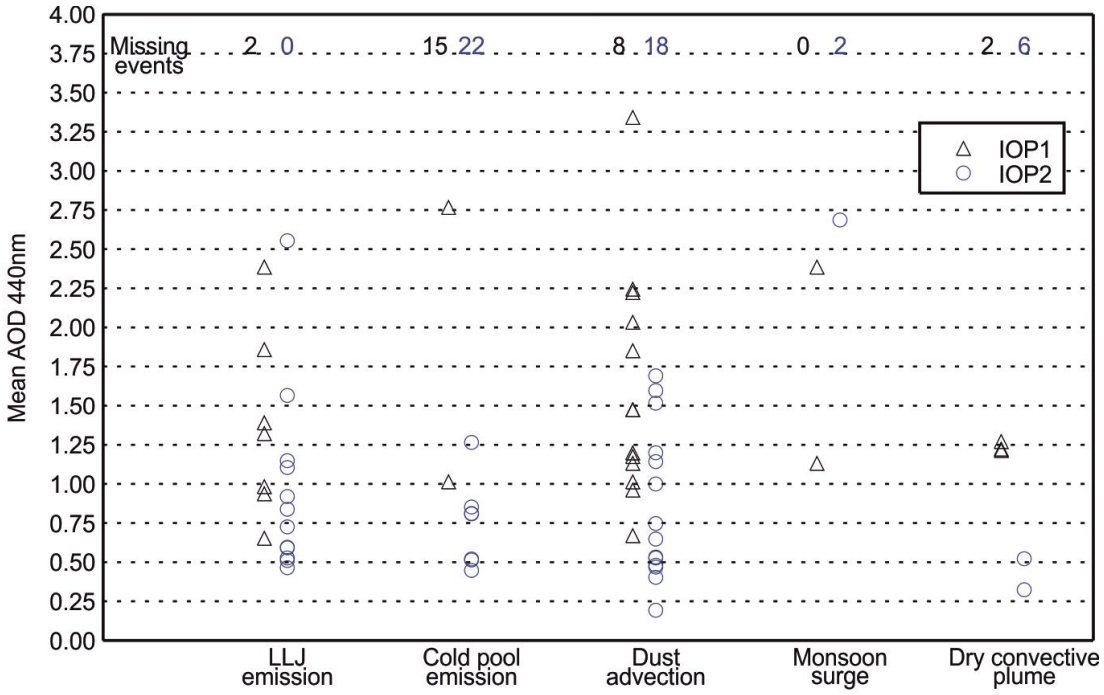

Figure 7-6: Comparison of AODs for individual dust events in IOP1 (black) and IOP2 (blue). Each symbol represents the mean AOD of a dust event as measured by the sun photometer. The events are split by category (bottom axis). The 'estimate' approach is used for category classification (Section 7.5, open circles and triangles as in Figure 7-4). The number of missing events in each category is noted at the top of the chart (discussed in detail in Section 7.9.1.1). An event is considered missing if it does not have any AOD measurements (if there is only one, this is considered to be the 'mean').

Sun photometer AODs cannot be used to calculate total dust loadings over the course of the month since they are unavailable under cloud or at night (see Section 7.9.1.1 for a detailed assessment of this drawback). Nephelometer scattering is used for this purpose in *Allen et al.* [2013], but the nephelometer is unavailable in IOP2. However, the time that dust events last is known for both IOPs, at 15 min resolution (Section 7.5). For IOP1, ratios can be defined between the total time of each event class and the total nephelometer scattering of that class (the 'scattering ratio'). By multiplying the total time of each event class by its scattering ratio, the total nephelometer scattering of each event class in IOP2 can be estimated to first order (the 'predicted scattering'). Clearly,

the predicted scattering is an approximation that assumes that the relationship between event duration and dustiness holds between the two June months, and apart from LLJs there is some evidence from the AODs that daytime dustiness is different between the two Junes (Figure 7-6). However, in the absence of instrumentation that can measure dust continuously in IOP2, it allows a rough comparison of dustiness to be made between the two field seasons.

Predicted scattering in IOP2 is higher than scattering in IOP1 for cold pool emission (an increase of between 1.02 and 1.9 m^{-1}), LLJ emission (an increase of between 0.32 and 0.39 m^{-1}) and monsoon surges (an increase of between 1.06 and 1.21 m^{-1}) (Figure 7-7). It is marginally lower in IOP2 for dry convective plumes. For dust advection, it is marginally lower in IOP2 unless a bias ratio correction is applied (Section 7.4) which results in an increase in IOP2 of 2.25 m^{-1} (Figure 7-7). Overall, Figure 7-7 suggests that IOP2 is dustier than IOP1. The total difference between predicted scattering in IOP2 and scattering in IOP1 is up to 9.08 m^{-1} which is an increase of up to 63% from IOP1 to IOP2. As mentioned, predicted scattering is a fairly rudimentary metric, but such an increase in dustiness compares well with the number of times dust is detected by SDF over BBM, which increases by 67% from IOP1 to IOP2. In both years, the ranking of the dust events by scattering is the same, with cold pool emission being the most important and dry convective plumes being the least important (Figure 7-7).

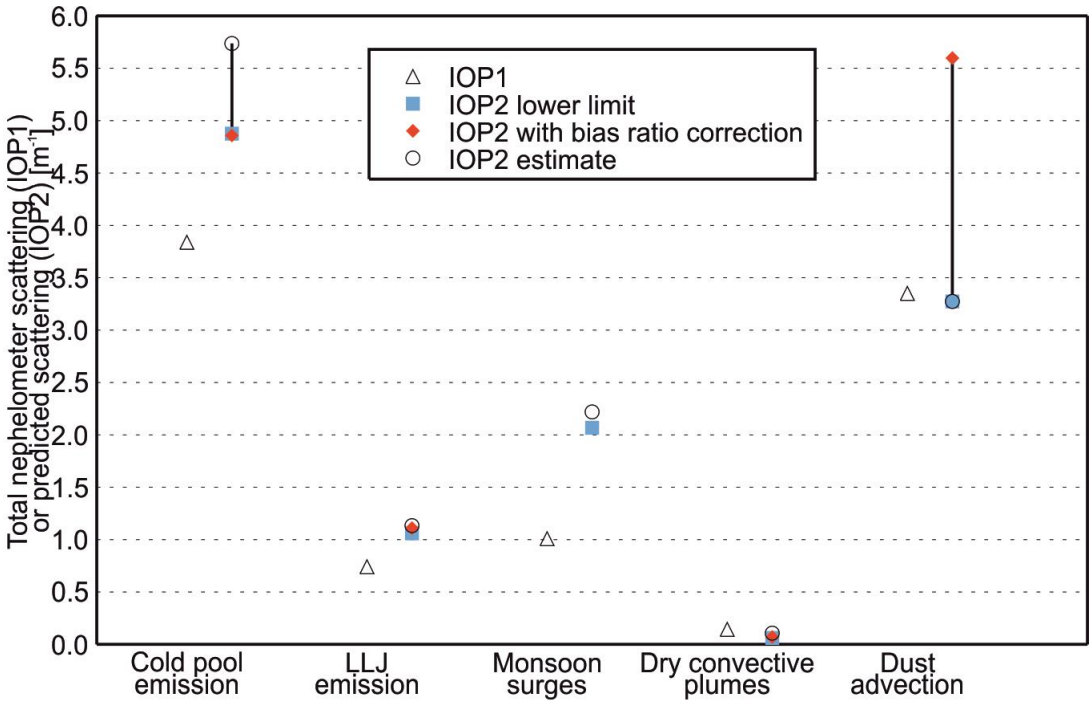

Figure 7-7: Partitioning of dust events by dustiness for IOP1 and IOP2. The bottom axis is the event class and the left axis is the total nephelometer scattering (for IOP1) or the total predicted scattering (for IOP2). See Section 7.7 for how the predicted scattering is calculated. For IOP2, different symbols indicate the different methods used to estimate the dust production hours (see Section 7.5). In IOP1 the nephelometer was not activated until the evening of 5 June so predicted scattering is used for events before nephelometer activation.

7.8. Comparison of low level jets

Of all the different dust event types, LLJs are the one which allows the most faithful comparison between IOP1 and IOP2. This is because (i) the detection method in IOP2 is very accurate (Figure 7-3), (ii) AODs are available for most LLJ events (Figure 7-6), (iii) radiosondes are launched at 0600 on 22 mornings during IOP2 and are timed well with respect to LLJ detection. As mentioned above, the number and duration of LLJ emission events is similar (Figure 7-5) and the dust emission is of a similar intensity (Figure 7-6). Note that not all LLJs necessarily lead to dust emission (Section 7.3.2; see also *Allen*

and Washington [2014]). In this section we compare all LLJs, not just those which led to dust emission.

The number of LLJs that are detected by the *Allen and Washington* [2014] scheme (Section 7.3.2) is 21 in IOP1 and 13 in IOP2 (Table 7-4**)**. In IOP2, an additional 5 LLJs were inferred from surface wind speeds (Section 7.3.2). In IOP1 (IOP2) There were 2 (3) mornings when wind profiles were not measured so it is possible there could have been non-dust emitting LLJs on these occasions (Table 7-4). Thus 21-23 LLJs were detected in IOP1 and 18-21 in IOP2.

Table 7-4: Comparison of LLJ characteristics between IOP1 and IOP2

Comparison	IOP1	IOP2
No. of LLJs	21 + up to 2 more (missing lidar and radiosondes)	13 + 5 inferred from surface winds + up to 3 more (missing radiosondes)
Mean wind speed max. below 600m agl at 0600 when LLJs are detected	13 ms^{-1}	14 ms^{-1}
Mean LLJ core height (0600)	270m agl	370m agl
No. of LLJs embedded in the northeasterly Harmattan flow §	6	5Δ
No. of LLJs embedded in the moist monsoon inflow §	5	8Δ
No. of LLJs that lead to dust emission	5 'pure' † + 4 with some cold pool overlap	7 'pure' † + 5 with some cold pool overlap

§ Excludes mornings when LLJs overlap with cold pools
Δ Two of these assessments are made using the Africa LAM since radiosondes were not launched
† 'Pure' LLJ emission is dust emission caused by a LLJ only (i.e. no dust contribution from other dust mechanisms).

The mean LLJ core wind speed in both Junes was very similar, 13 ms^{-1} and 14 ms^{-1} in IOP1 and IOP2 respectively. The mean core height was different however, 270m and 370m agl respectively (Table 7-4). Unlike in IOP1, more LLJs were embedded in the moist monsoon inflow than in the dry northeasterly Harmattan in IOP2, but this difference is not very large (Table 7-4). In IOP1 (IOP2), 9 (12) LLJs led to dust emission, with 4 (5) overlapping with cold pool outflows.

In IOP1, LLJ orientation can be split into a roughly northerly component and a south-westerly component (Figure 7-8). In IOP2, the orientations are more varied, with 3 from the ESE, a direction no LLJs were oriented in IOP1. There are also none from the south-west. However, this may be because no sondes were launched after 25 June, and the moist monsoon inflow has more influence on the Sahara in late June and early July [*Sultan and Janicot*, 2003]. A detailed examination of the LLJ in June 2012 is beyond the scope of this study.

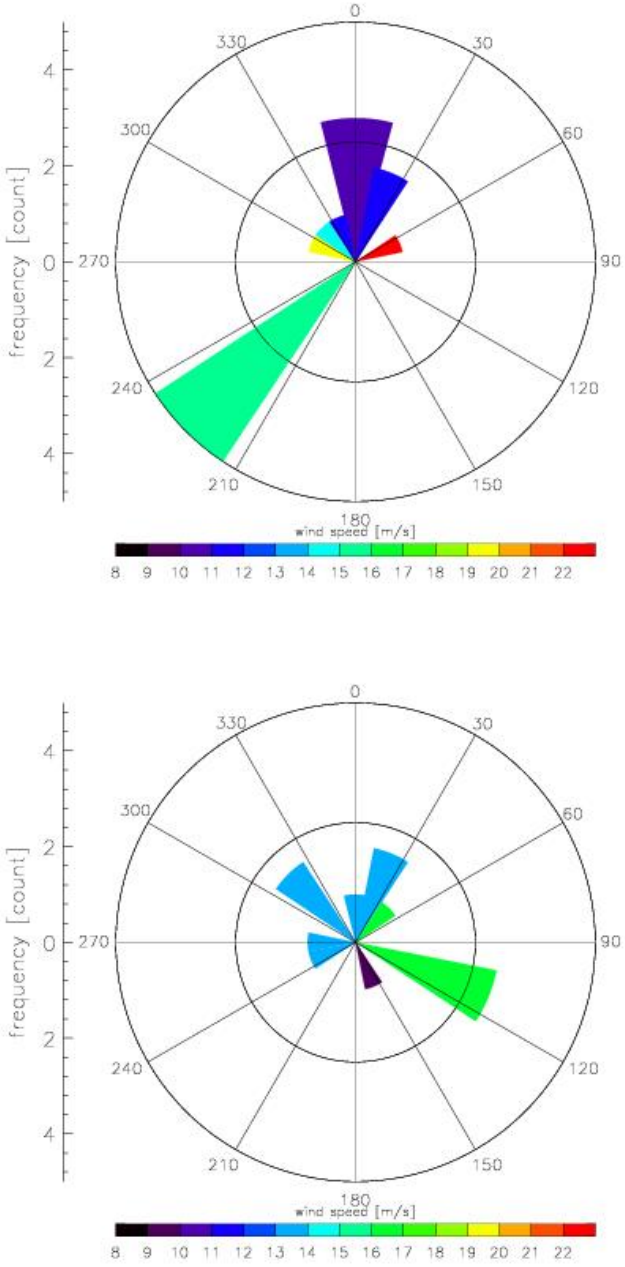

Figure 7-8: Wind roses for LLJs in IOP1 (above) and IOP2 (below), at 0600. Wind speeds and directions are taken at the mean LLJ core height (270m agl for IOP1 and 370m agl for IOP2). The segment direction denotes where the wind is blowing from (e.g. 0° = northerly). Mornings when cold pool outflows were concurrent with LLJs are excluded.

7.9. Optimal instrumentation for dust detection from fieldwork

Since dust sources, particularly in the central Sahara, are frequently remote and difficult to access [*Washington et al.*, 2003; *Ginoux et al.*, 2012; *Ashpole and Washington*, 2013a], optimal instruments for field campaigns are those which provide high quality information about dust conditions whilst themselves being as small, light and affordable as possible. It was shown in Section 7.4 that even without ground instruments which detect dust, field observations can be used together with remote sensing to identify and characterise individual dust *emission* mechanisms with a high degree of success (Figure 7-3). For this purpose, the most important measurements come from the anemometer (near-surface wind speeds for all dust event types), the pressure and humidity sensors (for dry convection and cold pool detection), the radiosondes (for LLJ detection) and SEVIRI (useful for most event types but particularly cold pool identification). Admittedly radiosondes are not particularly practical for remote campaigns because of the need to transport heavy gas canisters; alternatives include sodar (although dropout was a problem in Fennec) or lidar (addressed in more detail below).

The two major setbacks of not using dedicated dust instrumentation are (i) it is difficult to detect dust *advection* (although SDF and observers' reports improve capacity to do this, Figure 7-3); (ii) such approaches provide only limited quantitative information on the intensity (dustiness) of dust events. The question then arises, which dust instrument is optimal, given the constraints of remote fieldwork? Below we evaluate the ground-based dust detection instrumentation used at BBM in Fennec.

7.9.1. Measurement availability

The nephelometer provided continuous measurements at 4 s resolution (averaged to 1 min) during IOP1, with only two gaps (for 9 h on 15 June and 8 h on 23 June). The lidar

took measurements at 1.4 s (averaged to 10 s) but there were several data gaps due to overheating. These data gaps totalled approximately 128 h during IOP1 (18% total IOP duration). Lidar backscatter measurements were also attenuated for a total of approximately 26 h (4% total IOP duration) during the thickest dust events, the attenuation starting from heights ranging from 200m to 600m agl. The availability of sun photometer measurements is addressed below.

7.9.1.1. Availability of sun photometer measurements

A serious limitation of the sun photometer at BBM during the IOPs is that measurements are unavailable for a large number of events (Figure 7-6, top line). The photometer cannot take measurements at night, and cloud-contaminated AOD measurements must be removed. Since a significant proportion, if not the majority of dust emission in the region occurs at night or is associated with cloud [*Marsham et al.*, 2011; *Allen et al.*, 2013; *Ashpole and Washington*, 2013b; *Heinold et al.*, 2013; *Marsham et al.*, 2013]. AOD measurements are therefore not representative of the overall or average atmospheric dust loading. This is addressed further in the discussion.

LLJ emission is the only category where sun photometer AOD measurements are available in both IOPs for >50% of the total time dust is produced by this mechanism (hereafter the 'event time') (Figure 7-9). This is unsurprising as LLJ emission usually occurs in the morning in the southern Sahara [*Washington et al.*, 2006; *Schepanski et al.*, 2009; *Fiedler et al.*, 2013; *Allen and Washington*, 2014], when the sun photometer can take measurements. LLJs were only associated with a total of 7 hours of cloud cover over BBM in IOP1, and 0 hours in IOP2 (Figure 7-9).

By contrast, in both IOPs, emitting cold pools had sun photometer AODs available for <50% event time (just 23% in IOP1 and 41% in IOP2; Figure 7-9). The main reason for

this was the large number of hours emitting cold pools occurred at night (53 hours in IOP1 and 55 hours in IOP2; Figure 7-9). The secondary reason was cloud cover (7 hours in IOP1 and 20 hours in IOP2). Monsoon surges, dry convective plumes and advected dust had sun photometer AODs available for >50% event time in IOP1 and <50% event time in IOP2 (Figure 7-9). Apart from LLJ dust emission, cloud cover was a bigger problem in IOP2 than in IOP1. This is consistent with the moist monsoon inflow being stronger and penetrating further north in 2012 than in 2011 [*Cornforth*, 2013].

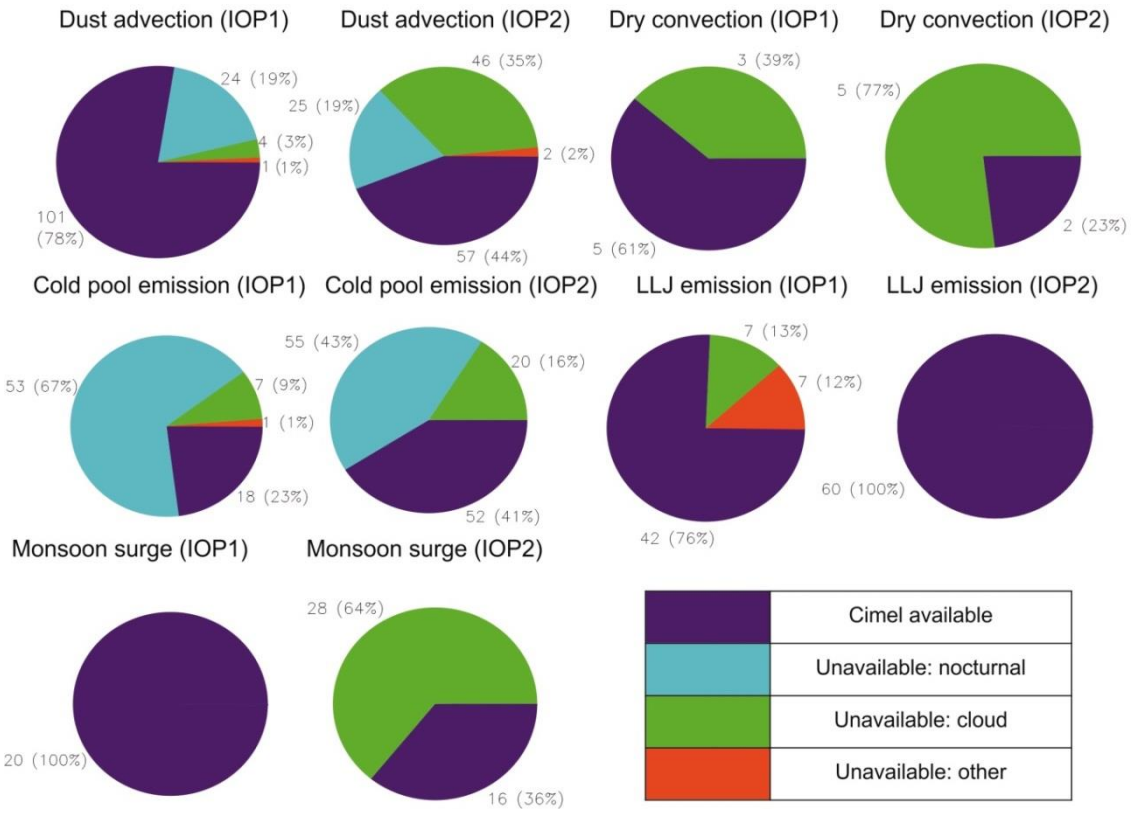

Figure 7-9: Availability of sun photometer AODs by dust event type (labelled). The numbers are the total hours sun photometer AOD measurements are available or unavailable (see colour key) for a given dust event type. The percentages are the percentage of the total duration of a given dust event type when sun photometer AOD measurements are available or unavailable. The 'estimate' approach is used for category classification (Section 7.5, open circles and triangles in Figure 7-4). Cloud was detected using the SEVIRI cloud mask product which has 15 min resolution (Section 7.2). 'Unavailable: other' means that sun photometer AODs should have been available but were not, because of calibration error, mechanical problems or possibly user interference.

7.9.1.2. Other instrument properties

As a result of its relatively small size and low weight, operation at high temperatures and measurement availability at night and under cloud, the nephelometer stands out as the optimal instrument from the ones compared here for dust fieldwork in remote desert locations, especially those where cloud cover is frequent, such as BBM in summer (Table 7-5). The lidar has the added advantage of providing height-resolved dust measurements and wind profiles; however this is offset by its large size and weight, the necessity for air conditioning on very hot days and the fact that in the dustiest conditions, attenuation reduces the data quality (Table 7-5). The sun photometer does not suffer from the latter two problems but it is severely limited in regions where dust production occurs at night or under cloud (Section 7.9.1.1; Table 7-5).

Table 7-5: Summary of relative merits of dust detection instruments during IOP1

Instrument	Works at night?	Can be used with cloud?	Does not need air conditioning?	Not attenuated by thick dust?	Provides height resolved measurements?	Approx packing volume	Approx packing mass
Nephelometer	✔	✔	✔	✔		0.08 m^3	20 kg
Lidar	✔	✔			✔	1.5 m^3	100 kg
Sun photometer			✔	✔		0.47 + 0.37 m^3 §	70 + 26 kg §

§ In the case of the sun photometer, the second value given for the volume and mass is for the satellite transmission equipment, which is optional.

There is a strong correlation between the sun photometer AOD and the nephelometer scattering (Spearman Rank (r_s) 0.86, n=634, Figure 7-10). This is perhaps surprising given that air is drawn into the nephelometer chamber at 2m agl whilst the AOD is a total-column measurement. However, the correlation is much weaker in dustier

conditions. For example, if only the points with AOD≥0.5 are correlated, r_s is reduced to 0.70. If only the points with nephelometer scattering ≥$2x10^{-4}m^{-1}$ (the dust event threshold in *Allen et al.* [2013]) are correlated, r_s is only 0.43. Therefore both instruments agree well when there is low dust, but when there is high dust at the surface (i.e. high nephelometer scattering), the AOD is not always proportionately high (Figure 7-10).

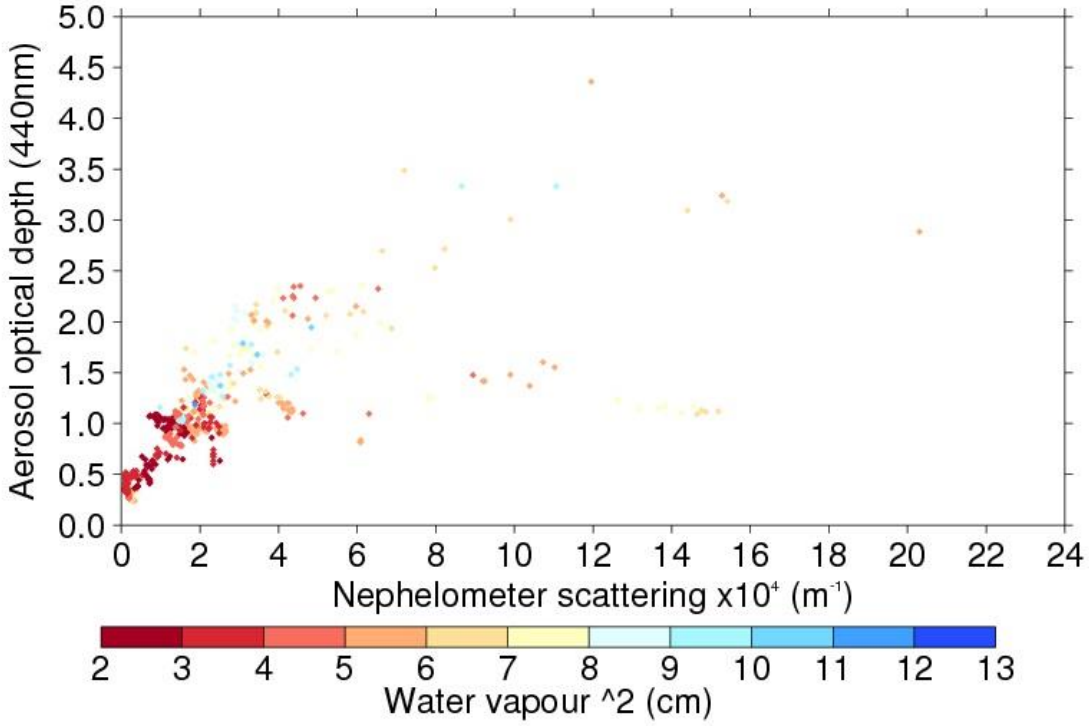

Figure 7-10: Scatter plot of nephelometer scattering against sun photometer aerosol optical depth, for June 2011. Since AOD measurements were less regular than nephelometer measurements, each point represents an AOD measurement and the corresponding (in time) nephelometer scattering. n=634. The colours show the square of the column water vapour for each point (derived from the sun photometer measurements by AERONET). The column water is squared to highlight differences in moisture.

At low nephelometer scattering, column water values are particularly low (Figure 7-10), supporting the findings of *Marsham et al.* [2013] that the driest period of IOP1 was the

least dusty. The dustiest points are not associated with the highest column water, but Figure 7-10 covers less than half of the IOP since nocturnal and cloudy periods cannot be included (Section 7.9.1.1), and it is these periods when cold pool outflows (associated with high moisture levels) are frequent.

7.10. Discussion and conclusions

The Fennec field campaign of 2011 was the first to instrument the remote central Sahara [*Washington et al.*, 2012]. However, with only one season of measurements, it is not possible to say whether the dust events of June 2011 were the exception or the rule. The opportunity to undertake a second field season (albeit scaled-down) has helped address this question.

At BBM, the total amount of time occupied by dust events was greater in IOP2 than IOP1 for cold pool emission, LLJ induced emission and monsoon surges (Figure 7-4). The difference was an increase of up to 39 h (48%), 21 h (51%) and 24 h (120%) respectively (Table 7-3). The 2012 West African Monsoon was more active than the 2011 monsoon (averaged normalized April-October rainfall departure for 20 Sahelian stations [*Boyd et al.*, 2013]); this would likely enhance cold pool and monsoon surge activity. Indeed, *Ashpole and Washington* [2013b] show that interannual variability of summer dust occurrence in the central Sahara is to a large extent controlled by the moist monsoon inflow, with greater monsoon activity associated with higher dust presence. *Cornforth* [2013] shows that the inter-tropical discontinuity (averaged between 10°W and 10°E) was over 1° north of its climatological position in late June 2012, bringing deep moist convection closer to BBM.

The total time occupied by dry convective plumes was 5 h (63%) less in IOP2 than IOP1. In IOP2, uncertainty in dust advection detection results in a difference that is

either a small decrease (3 h, 2%) or substantial increase (87 h, 66%) (Figure 7-4, Table 7-3). Overall, the number of dust event hours in IOP2 was 51-169 h (18-60%) more than in IOP1. In both Junes, dust advection occupied the longest amount of time (IOP1 19%, IOP2 ≥18%), followed by cold pool emission (IOP1 12%, IOP2 ≥14%), LLJ emission (6%, ≥8%), monsoon surges (3%, ≥6%) then dry convective plumes (1%, ≥0.4%) (Table 7-3), i.e. the ranking of the mechanisms by time is the same in both IOPs. The importance of dust advection is in agreement with the climatological study of *Cowie et al.* [2014], who use a longer record of observers' observations across the Sahara and show that advected dust occurs more frequently than locally emitted dust at BBM.

In IOP2, with the exception of monsoon surges, dust events were more frequent and shorter-lasting than in IOP1 (Figure 7-5). Between the two Junes however there was no statistically significant difference in the proportion of events of each mechanism type. Using a rudimentary method to predict nephelometer scattering for IOP2, this season is found to be dustier overall than IOP1 (up to 63% dustier), and dustier specifically in the case of cold pool emission, LLJ emission and monsoon surges (Figure 7-7). Due to predicted scattering assuming the preservation of relationships between event duration and nephelometer scattering from IOP1 into IOP2, this result should be treated carefully, but it does compare well with the number of times dust is detected by SDF over BBM, which increases by 67% from IOP1 to IOP2.

In both IOPs, the ranking of the events by scattering is the same: cold pool emission produces the most scattering, followed by dust advection, monsoon surges, LLJ emission then dry convective plumes (Figure 7-7). In essence, the results presented here show that whilst June 2012 was a dustier season than June 2011, the same dust

mechanisms dominated in both years. In other words, the BBM observations show a large interannual variability in dust output from the central Sahara, but little variability in the relative contribution of the dust producing mechanisms. There is thus even more incentive than before to focus research, model development and observational networks on the key mechanisms. The relatively small contribution of dust emission from LLJs is intriguing, especially as LLJs are thought to be fairly commonplace across the Sahara [*Schepanski et al.*, 2009; *Fiedler et al.*, 2013]. Using an atmospheric general circulation model which incorporated the radiative effects of mineral dust, *R L Miller et al.* [2004] and *Pérez et al.* [2006] found that, by reducing incoming solar radiation, the dust led to a reduction in boundary layer turbulent mixing and a reduction in downward transport of momentum to the surface. BBM is close to the global dust maximum in summer [e.g. *Ashpole and Washington*, 2012], so it is possible that these high dust levels result in less momentum mix-down and resultant dust emission from LLJs than might be expected given their frequent occurrence.

The findings reported here confirm the primacy of cold pools for dust emission in the central Sahara, as found by other observational [*Allen et al.*, 2013; *Marsham et al.*, 2013] and model [*Marsham et al.*, 2011; *Heinold et al.*, 2013] studies. This is problematic for current numerical modelling, as configurations without explicit convection struggle to generate cold pool outflows [*Reinfried et al.*, 2009; *Marsham et al.*, 2011; *Cavazos-Guerra and Todd*, 2012; *Solomos et al.*, 2012]. As well as the implications for dust emission, missing cold pools contribute significantly to a warm and dry model bias in the region [*Garcia-Carreras et al.*, 2013].

Since cold pools frequently occur at night, round the clock dust monitoring is particularly valuable in the summertime central Sahara. Instruments such as lidars and

nephelometers are therefore particularly useful, as is 24-hour satellite dust retrieval such as SDF [*Ashpole and Washington*, 2012]. It also invites consideration of more novel instrumentation, such as the lunar photometer [e.g. *Barreto et al.*, 2013]. Whilst the sun photometer provides excellent quantitative information on dust conditions and dust properties, it is handicapped in the central Sahara where the prime dust emission mechanism occurs frequently at night or under cloud, when sun photometer retrievals are not possible. Indeed, sun photometer AODs are only available for 23% (41%) of the time cold pool emission occurs at BBM in IOP1 (IOP2) (Figure 7-9). They provide much more information about LLJ emission - sun photometer AODs available for 76% (100%) time LLJ emission occurs in IOP1 (IOP2) – but LLJs are a less significant dust mechanism at BBM (Figure 7-4 and Figure 7-7). The missing periods of sun photometer data correspond to 43% of the attributed scattering in IOP1 and 57-58% of the predicted scattering in IOP2. The percentage calculation assumes that daytime and cloud-free dust events are as intense as night-time and cloud-covered dust events, which may not be true (and is not possible to check for IOP2), but the key message is that roughly half of the dust in the field seasons is missed by the sun photometer.

Sun photometer measurements are frequently used to evaluate (or tune) dust loading in numerical models [e.g. *Huneeus et al.*, 2011; *Pérez et al.*, 2011; *Haustein et al.*, 2012; *Tegen et al.*, 2013] and satellite retrieval [e.g. *Kahn et al.*, 2009; *Klüser and Schepanski*, 2009; *Carrer et al.*, 2010; *Amiridis et al.*, 2013]. However, doing this for the summertime central Sahara this will likely underestimate the actual dust burden as so few cold pool outflows can be captured by the photometer. This is supported by the work of *Kocha et al.* [2013], who show that AOD simulations by the AROME model in the Adrar region of the Sahara (containing BBM) when only simulated under clear-sky conditions, result in a mean reduction of simulated AOD of 0.2 through the diurnal

cycle, compared to continuous simulations. *Kocha et al.* [2013] found that AODs over the Adrar region peaked at 2200 h, consistent with the dominance of cold pool outflows found in this investigation and in the studies mentioned above.

During daylight hours, the AOD of cold pool emission, dust advection and dry convective plumes is higher in IOP1 than IOP2 (Figure 7-6). IOP-mean sun photometer AOD decreases from 0.98 in IOP1 to 0.73 in IOP2. This belies the increase in dustiness found by SDF and predicted scattering. The sun photometer is unavailable for 107 h when dust events are occurring in IOP1 and 181 h when dust events are occurring in IOP2. In percentage terms it is unavailable for 37% time dust events are occurring in IOP1 and 49% time dust events are occurring in IOP2. In IOP2 it is unavailable for most of the time that dust advection, dry convection, cold pool emission and monsoon surges are occurring (Figure 7-9). Therefore there is good reason to be suspicious of the apparent decrease in dustiness suggested by the monthly-mean AODs. We therefore advocate strongly against uncritical use of monthly-mean AODs in dust studies of this region, or regions dominated by cold pool dust production.

When using sun photometer measurements to evaluate models or satellite retrievals, at the least the model or satellite values should only be averaged for the daylight period, as done by *Tegen et al.* [2013]. The sun photometer of course provides useful information on column aerosol properties (which do not have a simple relationship with the surface) and authors are generally aware of its limitations; we feel however that it is important to present a quantification of the information that may be lost as we have done in Figure 7-9. Using the sun photometer alone would certainly give the wrong conclusions about which dust mechanisms are most important in this region of the Sahara.

At other times of year and in other regions of the North Africa, the balance of importance between the different dust mechanisms is shifted. For example, it is clear that in the Bodélé Depression the semi-permanent LLJ is the main mechanism for dust emission year round and particularly in winter [*Washington and Todd*, 2005; *Washington et al.*, 2006; *Fiedler et al.*, 2013]. ECMWF ERA-40 reanalysis shows that northeasterly Harmattan LLJs are also common (~50% nights) in winter across a wide band (roughly 10-20°N) of North Africa [*Schepanski et al.*, 2009], with BBM on the northern edge of this zone. In summer, reanalysis and SYNOP observations show that LLJs are particularly frequent over Western Sahara and northern Mauritania, the Sahel and southern Sahara and also central and western Algeria [*Schepanski et al.*, 2009; *Fiedler et al.*, 2013; *Cowie et al.*, 2014].

Current understanding suggests that cold pools likewise occur over a wide domain in North Africa. They have been shown to be of particular importance in the southern foothills of the Atlas Mountains, especially from April to September [*Emmel et al.*, 2010]; in the Sahel and particularly the western Sahel in summer [*Williams*, 2008; *Cowie et al.*, 2014]; in central Mali and eastern Mauritania [*Heinold et al.*, 2013] and even more widely across western Africa in late summer [*Marsham et al.*, 2011], where the authors argue they may be responsible for around half the dust uplift. Cold pools are thus certainly not a phenomenon restricted to BBM and its environs, although the evidence suggests that they are most frequent in the summer months, as would be expected with the northernmost penetration of the moist West African Monsoon and the associated deep convection.

In both IOPs, dry convective plumes/dust devils are found to be the least important mechanism for dust production (present ≤1% time, Table 7-3). Because there was only

one mast at BBM, it is highly likely that many dust devils or dry convective plumes passed close to the site but were not recorded by the pressure sensor or anemometers. Thus their importance at BBM is almost certainly underestimated. However, given the predominance of larger scale dust mechanisms at BBM it is hard to imagine that close to 35% of the dust at could be due to dry convective plumes/dust devils, which is the global estimate calculated by *Koch and Renno* [2005]. Note however that the definition of dry convective plumes only extends to dust raised by afternoon gustiness (Section 7.3.4): dry convection is additionally responsible for mixing LLJ momentum down to the surface and this is implicitly included in the LLJ partitioning category.

This paper has shown that even without ground instruments which detect dust, field observations can be used together with remote sensing to identify and characterise individual dust emission mechanisms with a high degree of success (Figure 7-2, Figure 7-3; Sections 7.3 and 7.4). Given the expense of importing and deploying instrumentation to remote regions, the potential for inferring dust mechanisms from standard meteorological equipment and widely-available satellite products is valuable. Unfortunately, such approaches suffer from two major drawbacks: they give limited quantitative information about the actual intensity (dustiness) of the dust events and are poor at detecting dust which is being advected rather than locally emitted (Figure 7-3), which is a significant hurdle since dust advection occurs for more time than any single other mechanism in IOP1 or IOP2. We note however the value of SDF and the observations made by the local observers, without which the detection of advected dust would be significantly more difficult (Figure 7-3). With some exceptions [e.g. *Cowie et al.*, 2013; *Cowie et al.*, 2014], observers' reports are no longer regularly used in dust research in the region, despite being a valuable resource.

Nonetheless, deploying a dedicated dust detection instrument alongside regular field equipment is preferable. Given the need for an instrument that is operational continuously, and the incentive to keep payloads light and manageable on remote field campaigns, the nephelometer comes out as the best overall performer of the dust detection instruments deployed at BBM (Table 7-5).

Most conventional field campaigns in north Africa have involved large deployment of instrumentation and needed significant human and financial resources, for example AMMA [*Redelsperger et al.*, 2006], the Saharan Mineral Dust Experiment (SAMUM) [*Ansmann et al.*, 2011] and Fennec [*Washington et al.*, 2012]. This makes organizing and delivering such programmes very taxing. It appears however that with the choice of the right instrumentation, a more limited payload can also deliver very comprehensive results. The Bodélé Dust Experiment [*Washington et al.*, 2006] is a case in point. In the case of the central Sahara, a nephelometer and automatic weather station combination would go a long way towards identifying and quantifying dust events. Of course the instrumentation that is deployed needs to be able to answer the questions that are posed. But the great advantage of inexpensive and lightweight deployments is that they can be replicated in many places, and for a long duration of time. Such approaches should be given serious consideration when planning future field research in remote regions.

7.11. Acknowledgements

Fennec was funded by a NERC consortium grant (NE/G017166/1). The authors wish to thank the following individuals and institutions. For comments which improved the manuscript: Zhanqing Li, Ron Miller and two anonymous reviewers. For establishing and instrumenting the supersite: B Abderrahmane, M Bart, BJ Brooks, C Cavazos-Guerra, F Davies, S Engelstaedter, L Garcia-Carreras, M Gascoyne, M Hobby, A Lima, M Limam, JH Marsham, V Martins, JB McQuaid, A O'Leary, B Ouchene, A Ouladichir, DJ Parker, M Salah-Ferroudj, D Sidali, MC Todd, the AERONET PHOTONS team, ONM Algérie, the University of Leeds and the University of Sussex. For providing the SEVIRI imagery at http://www.fennec.imperial.ac.uk: H Brindley and J Banks. For the Africa-LAM dataset: UK Met Office. For the SDF dataset: I Ashpole. CA is also particularly grateful to I Ashpole for helpful discussion of all stages of the manuscript. We also thank FGAM (Facility for Ground-based Atmospheric Measurement), UK Met Office and NCAS (National Centre for Atmospheric Science) for the use of the sodar, lidar and radiosonde units. Datasets are available through the British Atmospheric Data Centre or upon request from the authors.

7.12. Chapter appendix: Relative importance of dust mechanisms with and without monsoon surges in IOP1

In IOP1, there is uncertainty with regard to the classification of two events as monsoon surges (as presented in the body of the paper) or as a LLJ and advected dust in a cold pool (see Sections 7.3.6 and 7.4). In this appendix we show that the relative importance of the dust mechanisms only changes subtly if these two events are re-classed as a LLJ and advected dust in a cold pool. By design, monsoon surges now contribute 0 hours to the IOP1 total, LLJ emission increases by 15 hours and dust advection increases by 5 hours (compare the filled and open triangles in Figure S1 below). Reclassifying monsoon surges in IOP1 in this way does not change the ranking of the top three mechanisms in terms of total dust production hours: they remain dust advection, cold pool emission and LLJ emission. The only change to the IOP1 ranking is that dry convective plumes and monsoon surges swap fourth and last place (Figure S1). Regardless of the classification in IOP1, the comparison with IOP2 stays the same (Figure S1). Cold pool emission, LLJ emission and monsoon surges occur for a longer period of time in IOP2 than IOP1. Dry convective plumes occur for a longer period of time in IOP1 than IOP2. Finally, as before, the comparison for dust advection depends on whether a bias ratio correction is used in IOP2 (discussed in Section 7.5).

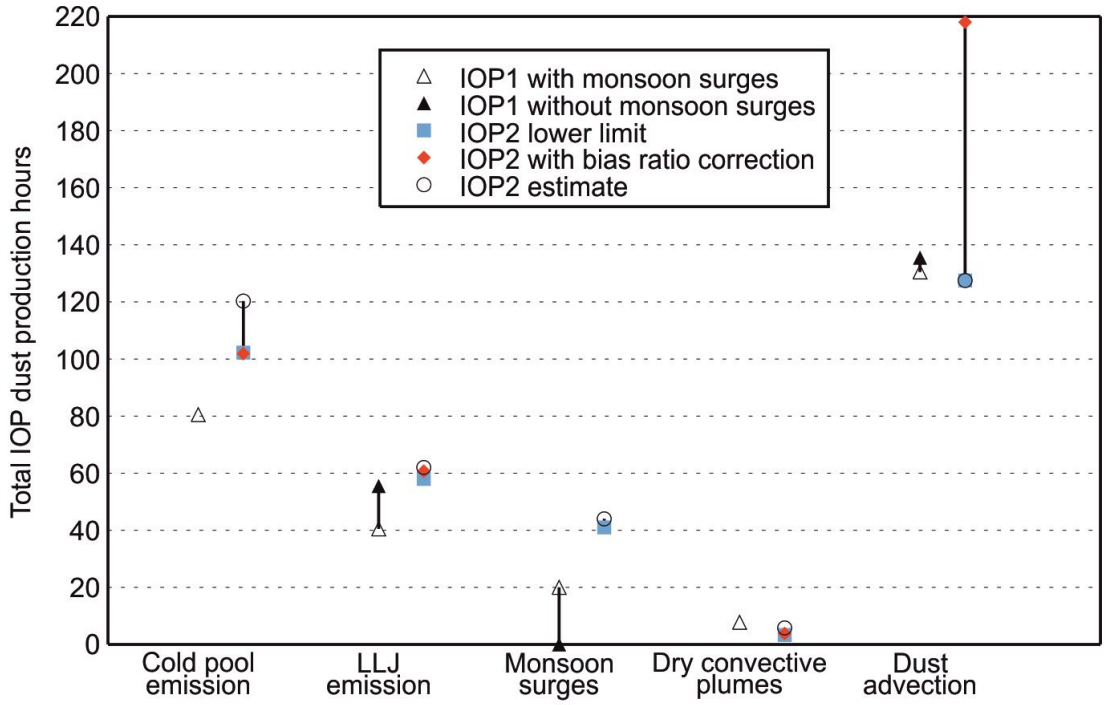

Figure S1. As Figure 7-4 but including classification in IOP1 both with and without monsoon surges.

7.13. References

Allen, C. J. T., and R. Washington (2014), The low-level jet dust emission mechanism in the central Sahara: Observations from Bordj-Badji Mokhtar during the June 2011 Fennec Intensive Observation Period, *Journal of Geophysical Research: Atmospheres*, doi: 10.1002/2013jd020594.

Allen, C. J. T., R. Washington, and S. Engelstaedter (2013), Dust emission and transport mechanisms in the central Sahara: Fennec ground-based observations from Bordj Badji Mokhtar, June 2011, *Journal of Geophysical Research: Atmospheres*, *118*, 6212–6232, doi: 10.1002/jgrd.50534.

Amiridis, V., U. Wandinger, E. Marinou, E. Giannakaki, A. Tsekeri, S. Basart, S. Kazadzis, A. Gkikas, M. Taylor, J. Baldasano, and A. Ansmann (2013), Optimizing CALIPSO Saharan dust retrievals, *Atmos. Chem. Phys.*, *13*(23), 12089-12106, doi: 10.5194/acp-13-12089-2013.

Ansmann, A., M. Tesche, P. Knippertz, E. Bierwirth, D. Althausen, D. Müller, and O. Schulz (2009), Vertical profiling of convective dust plumes in southern Morocco during SAMUM, *Tellus B*, *61*(1), 340-353, doi: 10.1111/j.1600-0889.2008.00384.x.

Ansmann, A., A. Petzold, K. Kandler, I. N. A. Tegen, M. Wendisch, D. Müller, B. Weinzierl, T. Müller, and J. Heintzenberg (2011), Saharan Mineral Dust Experiments SAMUM–1 and SAMUM–2: what have we learned?, *Tellus B*, *63*(4), 403-429, doi: 10.1111/j.1600-0889.2011.00555.x.

Ashpole, I., and R. Washington (2012), An automated dust detection using SEVIRI: A multiyear climatology of summertime dustiness in the central and western Sahara, *J. Geophys. Res.*, *117*(D8), D08202, doi: 10.1029/2011jd016845.

Ashpole, I., and R. Washington (2013a), A new high-resolution central and western Saharan summertime dust source map from automated satellite dust plume tracking, *Journal of Geophysical Research D: Atmospheres*, *118*(13), 6981-6995, doi: 10.1002/jgrd.50554.

Ashpole, I., and R. Washington (2013b), Intraseasonal variability and atmospheric controls on daily dust occurrence frequency over the central and western Sahara during the boreal summer, *Journal of Geophysical Research: Atmospheres*, *118*(23), 2013JD020267, doi: 10.1002/2013jd020267.

Awad, A. M., and A.-W. S. Mashat (2014), Synoptic features associated with dust transition processes from North Africa to Asia, *Arab J Geosci*, *7*(6), 2451-2467, doi: 10.1007/s12517-013-0923-4.

Balme, M., and R. Greeley (2006), Dust devils on Earth and Mars, *Reviews of Geophysics*, *44*(3), doi: 10.1029/2005RG000188.

Banta, R. M., R. K. Newsom, J. K. Lundquist, Y. L. Pichugina, R. L. Coulter, and L. Mahrt (2002), Nocturnal Low-Level Jet Characteristics Over Kansas During Cases-99, *Boundary-Layer Meteorology*, *105*(2), 221-252, doi: 10.1023/a:1019992330866.

Barreto, A., E. Cuevas, B. Damiri, C. Guirado, T. Berkoff, A. J. Berjón, Y. Hernández, F. Almansa, and M. Gil (2013), A new method for nocturnal aerosol measurements with a lunar photometer prototype, *Atmos. Meas. Tech.*, *6*(3), 585-598, doi: 10.5194/amt-6-585-2013.

Blackadar, A. K. (1957), Boundary layer wind maxima and their significance for the growth of nocturnal inversion, *Bull. Am. Meteorol. Soc*, *38*(5), 283-290.

Bou Karam, D., C. Flamant, P. Knippertz, O. Reitebuch, J. Pelon, M. Chong, and A. Dabas (2008), Dust emissions over the Sahel associated with the West African monsoon intertropical discontinuity region: A representative case-study, *Quarterly Journal of the Royal Meteorological Society*, *134*(632), 621-634, doi: 10.1002/qj.244.

Boyd, E., R. J. Cornforth, P. J. Lamb, A. Tarhule, M. I. Lele, and A. Brouder (2013), Building resilience to face recurring environmental crisis in African Sahel, *Nature Clim. Change*, *3*(7), 631-637, doi: 10.1038/nclimate1856.

Brindley, H., P. Knippertz, C. Ryder, and I. Ashpole (2012), A critical evaluation of the ability of the Spinning Enhanced Visible and Infrared Imager (SEVIRI) thermal infrared red-green-blue rendering to identify dust events: Theoretical analysis, *Journal of Geophysical Research D: Atmospheres*, *117*(7), doi: 10.1029/2011JD017326.

Browning, K., and R. Wexler (1968), The determination of kinematic properties of a wind field using Doppler radar, *J. Appl. Meteorol.*, *7*, 105-113, doi: 10.1175/1520-0450(1968)007<0105:TDOKPO>2.0.CO;2.

Carrer, D., J.-L. Roujean, O. Hautecoeur, and T. Elias (2010), Daily estimates of aerosol optical thickness over land surface based on a directional and temporal analysis of SEVIRI MSG visible observations, *Journal of Geophysical Research: Atmospheres*, *115*(D10), D10208, doi: 10.1029/2009jd012272.

Cavazos-Guerra, C., and M. C. Todd (2012), Model Simulations of Complex Dust Emissions over the Sahara during the West African Monsoon Onset, *Advances in Meteorology*, *2012*, 17, doi: 10.1155/2012/351731.

Cornforth, R. J. (2013), West African Monsoon 2012, *Weather*, *68*(10), 256-263, doi: 10.1002/wea.2161.

Couvreux, F., F. Guichard, O. Bock, B. Campistron, J. P. Lafore, and J. L. Redelsperger (2010), Synoptic variability of the monsoon flux over West Africa prior to the onset, *Quarterly Journal of the Royal Meteorological Society*, *136*(S1), 159-173, doi: 10.1002/qj.473.

Cowie, S. M., P. Knippertz, and J. H. Marsham (2013), Are vegetation-related roughness changes the cause of the recent decrease in dust emission from the Sahel?, *Geophysical Research Letters*, *40*(9), 1868-1872, doi: 10.1002/grl.50273.

Cowie, S. M., P. Knippertz, and J. H. Marsham (2014), A climatology of dust emission events from northern Africa using long-term surface observations, *Atmos. Chem. Phys.*, *14*(16), 8579-8597, doi: 10.5194/acp-14-8579-2014.

Dee, D. P., S. M. Uppala, A. J. Simmons, P. Berrisford, P. Poli, S. Kobayashi, U. Andrae, M. A. Balmaseda, G. Balsamo, P. Bauer, P. Bechtold, A. C. M. Beljaars, L. van de Berg, J. Bidlot, N. Bormann, C. Delsol, R. Dragani, M. Fuentes, A. J. Geer, L. Haimberger, S. B. Healy, H. Hersbach, E. V. Hólm, L. Isaksen, P. Kållberg, M. Köhler, M. Matricardi, A. P. McNally, B. M. Monge-Sanz, J. J. Morcrette, B. K. Park, C. Peubey, P. de Rosnay, C. Tavolato, J. N. Thépaut, and F. Vitart (2011), The ERA-Interim reanalysis: configuration and performance of the data assimilation system, *Quarterly Journal of the Royal Meteorological Society*, *137*(656), 553-597, doi: 10.1002/qj.828.

Emmel, C., P. Knippertz, and O. Schulz (2010), Climatology of convective density currents in the southern foothills of the Atlas Mountains, *J. Geophys. Res.*, *115*(D11), D11115, doi: 10.1029/2009jd012863.

Engelstaedter, S., I. Tegen, and R. Washington (2006), North African dust emissions and transport, *Earth-Science Reviews*, *79*(1–2), 73-100, doi: 10.1016/j.earscirev.2006.06.004.

Fiedler, S., K. Schepanski, B. Heinold, P. Knippertz, and I. Tegen (2013), Climatology of Nocturnal Low-Level Jets over North Africa and Implications for Modeling Mineral Dust Emission, *Journal of Geophysical Research: Atmospheres*, *118*, 6100–6121, doi: 10.1002/jgrd.50394.

Flamant, C., P. Knippertz, D. J. Parker, J. P. Chaboureau, C. Lavaysse, A. Agusti-Panareda, and L. Kergoat (2009), The impact of a mesoscale convective system cold pool on the northward propagation of the intertropical discontinuity over West Africa, *Quarterly Journal of the Royal Meteorological Society*, *135*(638), 139-159, doi: 10.1002/qj.357.

Flamant, C., J. P. Chaboureau, D. J. Parker, C. M. Taylor, J. P. Cammas, O. Bock, F. Timouk, and J. Pelon (2007), Airborne observations of the impact of a convective system on the planetary boundary layer thermodynamics and aerosol distribution in the inter-tropical discontinuity region of the West African Monsoon, *Quarterly Journal of the Royal Meteorological Society*, *133*(626), 1175-1189, doi: 10.1002/qj.97.

Garcia-Carreras, L., J. H. Marsham, D. J. Parker, C. L. Bain, S. Milton, A. Saci, M. Salah-Ferroudj, B. Ouchene, and R. Washington (2013), The impact of convective cold pool outflows on model biases in the Sahara, *Geophysical Research Letters*, *40*(8), 1647-1652, doi: 10.1002/grl.50239.

Ginoux, P., J. M. Prospero, T. E. Gill, N. C. Hsu, and M. Zhao (2012), Global-scale attribution of anthropogenic and natural dust sources and their emission rates based on MODIS Deep Blue aerosol products, *Reviews of Geophysics*, *50*(3), doi: 10.1029/2012RG000388.

Gu, Y., K. N. Liou, J. H. Jiang, H. Su, and X. Liu (2012), Dust aerosol impact on North Africa climate: a GCM investigation of aerosol-cloud-radiation interactions using A-Train satellite data, *Atmos. Chem. Phys.*, *12*(4), 1667-1679, doi: 10.5194/acp-12-1667-2012.

Haustein, K., C. Pérez, J. M. Baldasano, O. Jorba, S. Basart, R. L. Miller, Z. Janjic, T. Black, S. Nickovic, M. C. Todd, R. Washington, D. Müller, M. Tesche, B. Weinzierl, M. Esselborn, and A. Schladitz (2012), Atmospheric dust modeling from meso to global scales with the online NMMB/BSC-Dust model – Part 2: Experimental campaigns in Northern Africa, *Atmos. Chem. Phys.*, *12*(6), 2933-2958, doi: 10.5194/acp-12-2933-2012.

Heinold, B., P. Knippertz, J. H. Marsham, S. Fiedler, N. S. Dixon, K. Schepanski, B. Laurent, and I. Tegen (2013), The role of deep convection and nocturnal low-level jets for dust emission in summertime West Africa: Estimates from convection-permitting simulations, *Journal of Geophysical Research: Atmospheres*, *118*, 4385–4400, doi: 10.1002/jgrd.50402.

Hobby, M., M. Gascoyne, J. H. Marsham, M. Bart, C. J. T. Allen, S. Engelstaedter, D. M. Fadel, A. Gandega, R. Lane, J. B. McQuaid, B. Ouchene, A. Ouladichir, D. J. Parker, P. Rosenberg, M. S. Ferroudj, A. Saci, F. Seddik, M. Todd, D. Walker, and R. Washington (2013), The Fennec Automatic Weather Station (AWS) Network: Monitoring the Saharan Climate System, *Journal of Atmospheric and Oceanic Technology*, *30*(4), 709-724, doi: 10.1175/jtech-d-12-00037.1.

Holben, B. N., T. F. Eck, I. Slutsker, D. Tanré, J. P. Buis, A. Setzer, E. Vermote, J. A. Reagan, Y. J. Kaufman, T. Nakajima, F. Lavenu, I. Jankowiak, and A. Smirnov (1998), AERONET - A federated instrument network and data archive for aerosol characterization, *Remote Sensing of Environment*, *66*(1), 1-16, doi: 10.1016/s0034-4257(98)00031-5.

Huneeus, N., M. Schulz, Y. Balkanski, J. Griesfeller, J. Prospero, S. Kinne, S. Bauer, O. Boucher, M. Chin, F. Dentener, T. Diehl, R. Easter, D. Fillmore, S. Ghan, P. Ginoux, A. Grini, L. Horowitz, D. Koch, M. C. Krol, W. Landing, X. Liu, N. Mahowald, R. Miller, J. J. Morcrette, G. Myhre, J. Penner, J. Perlwitz, P. Stier, T. Takemura, and C. S. Zender (2011), Global dust model intercomparison in AeroCom phase I, *Atmos. Chem. Phys.*, *11*(15), 7781-7816, doi: 10.5194/acp-11-7781-2011.

Jones, C., N. Mahowald, and C. Luo (2003), The Role of Easterly Waves on African Desert Dust Transport, *Journal of Climate*, *16*(22), 3617-3628, doi: 10.1175/1520-0442(2003)016<3617:troewo>2.0.co;2.

Kahn, R., A. Petzold, M. Wendisch, E. Bierwirth, T. Dinter, M. Esselborn, M. Fiebig, B. Heese, P. Knippertz, D. MÜLler, A. Schladitz, and W. Von Hoyningen-Huene (2009), Desert dust aerosol air mass mapping in the western Sahara, using particle properties derived from space-based multi-angle imaging, *Tellus B*, *61*(1), 239-251, doi: 10.1111/j.1600-0889.2008.00398.x.

Klüser, L., and K. Schepanski (2009), Remote sensing of mineral dust over land with MSG infrared channels: A new Bitemporal Mineral Dust Index, *Remote Sensing of Environment*, *113*(9), 1853-1867, doi: 10.1016/j.rse.2009.04.012.

Knippertz, P., and M. C. Todd (2010), The central west Saharan dust hot spot and its relation to African easterly waves and extratropical disturbances, *J. Geophys. Res.*, *115*(D12), D12117, doi: 10.1029/2009jd012819.

Knippertz, P., C. Deutscher, K. Kandler, T. Müller, O. Schulz, and L. Schütz (2007), Dust mobilization due to density currents in the Atlas region: Observations from the Saharan Mineral Dust Experiment 2006 field campaign, *J. Geophys. Res.*, *112*(D21), D21109, doi: 10.1029/2007jd008774.

Koch, J., and N. O. Renno (2005), The role of convective plumes and vortices on the global aerosol budget, *Geophys. Res. Lett.*, *32*(18), L18806, doi: 10.1029/2005gl023420.

Kocha, C., P. Tulet, J. P. Lafore, and C. Flamant (2013), The importance of the diurnal cycle of Aerosol Optical Depth in West Africa, *Geophysical Research Letters*, *40*(4), 785-790, doi: 10.1002/grl.50143.

Lensky, I. M., and D. Rosenfeld (2008), Clouds-Aerosols-Precipitation Satellite Analysis Tool (CAPSAT), *Atmos. Chem. Phys.*, *8*(22), 6739-6753, doi: 10.5194/acp-8-6739-2008.

Lorenz, R. D. (2012), Observing desert dust devils with a pressure logger, *Geosci. Instrum. Method. Data Syst.*, *1*(2), 209-220, doi: 10.5194/gi-1-209-2012.

Lothon, M., F. Saïd, F. Lohou, and B. Campistron (2008), Observation of the Diurnal Cycle in the Low Troposphere of West Africa, *Monthly Weather Review*, *136*(9), 3477-3500, doi: 10.1175/2008mwr2427.1.

Marsham, J. H., D. J. Parker, C. M. Grams, C. M. Taylor, and J. M. Haywood (2008), Uplift of Saharan dust south of the intertropical discontinuity, *J. Geophys. Res.*, *113*(D21), D21102, doi: 10.1029/2008jd009844.

Marsham, J. H., P. Knippertz, N. S. Dixon, D. J. Parker, and G. M. S. Lister (2011), The importance of the representation of deep convection for modeled dust-generating winds over West Africa during summer, *Geophys. Res. Lett.*, *38*(16), L16803, doi: 10.1029/2011gl048368.

Marsham, J. H., M. Hobby, C. J. T. Allen, J. R. Banks, M. Bart, B. J. Brooks, C. Cavazos-Guerra, S. Engelstaedter, M. Gascoyne, A. R. Lima, J. V. Martins, J. B. McQuaid, A. O'Leary, B. Ouchene, A. Ouladichir, D. J. Parker, A. Saci, M. Salah-Ferroudj, M. C. Todd, and R. Washington (2013), Meteorology and dust in the central Sahara: Observations from Fennec supersite-1 during the June 2011 Intensive Observation Period, *Journal of Geophysical Research: Atmospheres*, *118*, 4069–4089, doi: 10.1002/jgrd.50211.

Miller, R. L., J. Perlwitz, and I. Tegen (2004), Feedback upon dust emission by dust radiative forcing through the planetary boundary layer, *Journal of Geophysical Research: Atmospheres*, *109*(D24), D24209, doi: 10.1029/2004jd004912.

Miller, S. D., A. P. Kuciauskas, M. Liu, Q. Ji, J. S. Reid, D. W. Breed, A. L. Walker, and A. A. Mandoos (2008), Haboob dust storms of the southern Arabian Peninsula, *Journal of Geophysical Research D: Atmospheres*, *113*(1), doi: 10.1029/2007JD008550.

Mona, L., A. Amodeo, M. Pandolfi, and G. Pappalardo (2006), Saharan dust intrusions in the Mediterranean area: Three years of Raman lidar measurements, *Journal of Geophysical Research: Atmospheres*, *111*(D16), D16203, doi: 10.1029/2005jd006569.

Oke, A. M. C., N. J. Tapper, and D. Dunkerley (2007), Willy-willies in the Australian landscape: The role of key meteorological variables and surface conditions in defining frequency and spatial characteristics, *Journal of Arid Environments*, *71*(2), 201-215, doi: 10.1016/j.jaridenv.2007.03.008.

Parker, D. J., R. R. Burton, A. Diongue-Niang, R. J. Ellis, M. Felton, C. M. Taylor, C. D. Thorncroft, P. Bessemoulin, and A. M. Tompkins (2005), The diurnal cycle of the West African monsoon circulation, *Quarterly Journal of the Royal Meteorological Society*, *131*(611), 2839-2860, doi: 10.1256/qj.04.52.

Pérez, C., S. Nickovic, G. Pejanovic, J. M. Baldasano, and E. Özsoy (2006), Interactive dust-radiation modeling: A step to improve weather forecasts, *Journal of Geophysical Research: Atmospheres*, *111*(D16), D16206, doi: 10.1029/2005jd006717.

Pérez, C., K. Haustein, Z. Janjic, O. Jorba, N. Huneeus, J. M. Baldasano, T. Black, S. Basart, S. Nickovic, R. L. Miller, J. P. Perlwitz, M. Schulz, and M. Thomson (2011), Atmospheric dust modeling from meso to global scales with the online NMMB/BSC-Dust model – Part 1: Model description, annual simulations and evaluation, *Atmos. Chem. Phys.*, *11*(24), 13001-13027, doi: 10.5194/acp-11-13001-2011.

Prospero, J. M., and P. J. Lamb (2003), African Droughts and Dust Transport to the Caribbean: Climate Change Implications, *Science*, *302*(5647), 1024-1027, doi: 10.1126/science.1089915.

Prospero, J. M., P. Ginoux, O. Torres, S. E. Nicholson, and T. E. Gill (2002), Environmental characterization of global sources of atmospheric soil dust identified with the NIMBUS 7 Total Ozone Mapping Spectrometer (TOMS) absorbing aerosol product, *Rev. Geophys.*, *40*(1), 1002, doi: 10.1029/2000rg000095.

Redelsperger, J.-L., C. D. Thorncroft, A. Diedhiou, T. Lebel, D. J. Parker, and J. Polcher (2006), African Monsoon Multidisciplinary Analysis: An International Research Project and Field Campaign, *Bulletin of the American Meteorological Society*, *87*(12), 1739-1746, doi: 10.1175/bams-87-12-1739.

Redmond, H. E., K. D. Dial, and J. E. Thompson (2010), Light scattering and absorption by wind blown dust: Theory, measurement, and recent data, *Aeolian Research*, *2*(1), 5-26, doi: 10.1016/j.aeolia.2009.09.002.

Reinfried, F., I. Tegen, B. Heinold, O. Hellmuth, K. Schepanski, U. Cubasch, H. Huebener, and P. Knippertz (2009), Simulations of convectively-driven density currents in the Atlas region using a regional model: Impacts on dust emission and sensitivity to horizontal resolution and convection schemes, *Journal of Geophysical Research: Atmospheres*, *114*(D8), D08127, doi: 10.1029/2008jd010844.

Renno, N. O., M. L. Burkett, and M. P. Larkin (1998), A Simple Thermodynamical Theory for Dust Devils, *Journal of the Atmospheric Sciences*, *55*(21), 3244-3252, doi: 10.1175/1520-0469(1998)055<3244:asttfd>2.0.co;2.

Ridley, D. A., C. L. Heald, and J. M. Prospero (2014), What controls the recent changes in African mineral dust aerosol across the Atlantic?, *Atmos. Chem. Phys.*, *14*(11), 5735-5747, doi: 10.5194/acp-14-5735-2014.

Roberts, A. J., and P. Knippertz (2014), The formation of a large summertime Saharan dust plume: Convective and synoptic-scale analysis, *Journal of Geophysical Research: Atmospheres*, *119*(4), 1766-1785, doi: 10.1002/2013jd020667.

Rodríguez-Fonseca, B., S. Janicot, E. Mohino, T. Losada, J. Bader, C. Caminade, F. Chauvin, B. Fontaine, J. García-Serrano, S. Gervois, M. Joly, I. Polo, P. Ruti, P. Roucou, and A. Voldoire (2011), Interannual and decadal SST-forced responses of the West African monsoon, *Atmospheric Science Letters*, *12*(1), 67-74, doi: 10.1002/asl.308.

Schepanski, K., I. Tegen, M. C. Todd, B. Heinold, G. Bönisch, B. Laurent, and A. Macke (2009), Meteorological processes forcing Saharan dust emission inferred from MSG-SEVIRI observations of subdaily dust source activation and numerical models, *J. Geophys. Res.*, *114*(D10), D10201, doi: 10.1029/2008jd010325.

Solomos, S., G. Kallos, E. Mavromatidis, and J. Kushta (2012), Density currents as a desert dust mobilization mechanism, *Atmospheric Chemistry and Physics*, *12*(22), 11199-11211, doi: 10.5194/acp-12-11199-2012.

Sultan, B., and S. Janicot (2003), The West African monsoon dynamics. Part II: The "preonset" and "onset" of the summer monsoon, *Journal of Climate*, *16*(21), 3407-3427, doi: 10.1175/1520-0442(2003)016<3407:TWAMDP>2.0.CO;2.

Tegen, I., K. Schepanski, and B. Heinold (2013), Comparing two years of Saharan dust source activation obtained by regional modelling and satellite observations, *Atmos. Chem. Phys.*, *13*(5), 2381-2390, doi: 10.5194/acp-13-2381-2013.

Thorncroft, C., and K. Hodges (2001), African Easterly Wave Variability and Its Relationship to Atlantic Tropical Cyclone Activity, *Journal of Climate*, *14*(6), 1166-1179, doi: 10.1175/1520-0442(2001)014<1166:aewvai>2.0.co;2.

Todd, M. C., R. Washington, S. Raghavan, G. Lizcano, and P. Knippertz (2008), Regional model simulations of the Bodélé low-level jet of Northern Chad during the Bodélé dust experiment (BoDEx 2005), *Journal of Climate*, *21*(5), 995-1012, doi: 10.1175/2007JCLI1766.1.

Todd, M. C., C. J. T. Allen, M. Bart, M. Bechir, J. Bentefouet, B. J. Brooks, C. Cavazos-Guerra, T. Clovis, S. Deyane, M. Dieh, S. Engelstaedter, C. Flamant, L. Garcia-Carreras, A. Gandega, M. Gascoyne, M. Hobby, C. Kocha, C. Lavaysse, J. H. Marsham, J. V. Martins, J. B. McQuaid, J. B. Ngamini, D. J. Parker, T. Podvin, A. Rocha-Lima, S. Traore, Y. Wang, and R. Washington (2013), Meteorological and dust aerosol conditions over the Western Saharan region observed at Fennec supersite-2 during the Intensive Observation Period in June 2011, *Journal of Geophysical Research: Atmospheres*, *118*, 8426–8447, doi: 10.1002/jgrd.50470.

Walters, D. N., M. J. Best, A. C. Bushell, D. Copsey, J. M. Edwards, P. D. Falloon, C. M. Harris, A. P. Lock, J. C. Manners, C. J. Morcrette, M. J. Roberts, R. A. Stratton, S. Webster, J. M. Wilkinson, M. R. Willett, I. A. Boutle, P. D. Earnshaw, P. G. Hill, C. MacLachlan, G. M. Martin, W. Moufouma-Okia, M. D. Palmer, J. C. Petch, G. G. Rooney, A. A. Scaife, and K. D. Williams (2011), The Met Office Unified Model Global Atmosphere 3.0/3.1 and JULES Global Land 3.0/3.1 configurations, *Geosci. Model Dev.*, *4*(4), 919-941, doi: 10.5194/gmd-4-919-2011.

Washington, R., and M. C. Todd (2005), Atmospheric controls on mineral dust emission from the Bodélé Depression, Chad: The role of the low level jet, *Geophys. Res. Lett.*, *32*(17), L17701, doi: 10.1029/2005gl023597.

Washington, R., M. C. Todd, N. J. Middleton, and A. S. Goudie (2003), Dust-Storm Source Areas Determined by the Total Ozone Monitoring Spectrometer and Surface Observations, *Annals of the Association of American Geographers*, *93*(2), 297-313, doi: 10.1111/1467-8306.9302003.

Washington, R., M. C. Todd, S. Engelstaedter, S. Mbainayel, and F. Mitchell (2006), Dust and the low-level circulation over the Bodélé Depression, Chad: Observations from BoDEx 2005, *J. Geophys. Res.*, *111*(D3), D03201, doi: 10.1029/2005jd006502.

Washington, R., C. Flamant, D. J. Parker, J. H. Marsham, J. B. McQuaid, H. Brindley, M. C. Todd, E. Highwood, C. Ryder, J. P. Chaboureau, C. Kocha, M. Bechir, and A. Saci (2012), Fennec - The Saharan Climate System, *CLIVAR Exchanges*, *17*(3), 31-33.

Wilks, D. S. (2006), *Statistical Methods in the Atmospheric Sciences*, 627 pp., Academic Press, London.

Williams, E. (2008), Comment on "Atmospheric controls on the annual cycle of North African dust" by S. Engelstaedter and R. Washington, *J. Geophys. Res.*, *113*(D23), D23109, doi: 10.1029/2008jd009930.

8. Dust mechanisms across the central-western Sahara in June 2011: observations and modelling

Christopher J. T. Allen and Richard Washington

Submitted for publication in Aeolian Research

Abstract

The central Sahara is the dustiest region in the world in summer. Until recently, ground observations were only available at its fringes. The Fennec Project has documented dust emission and transport processes in detail from observations in the central-western Sahara (CWS) at Bordj-Badji Mokhtar, Algeria, and Zouerat, Mauritania. However, these are only two points. The Fennec automatic weather station network provides the first ever opportunity to expand this analysis across the remote CWS. Using a combination of new automatic weather station observations, numerical modelling and satellite retrieval, summertime atmospheric dust production mechanisms across the remote CWS are identified. In June 2011, low-level jets (LLJs) and cold pool outflows are the most frequently detected mechanisms. LLJs are associated with Atlantic ventilation to the north-west of the CWS and the large scale north-easterly Harmattan flow in the northern CWS. Cold pools are most prevalent in the south-east CWS. Although LLJs generally occur more frequently than cold pools, only 12-36% of those detected are strong enough to lead to dust emission. Cold pools are less frequently identified than LLJs at most CWS stations, but frequency of cold pool occurrence is not the best way to quantify their importance for dust emission either, because cold pools are both longer lasting and more 'efficient' (more dust per hour of occurrence) dust producers than LLJs. The Met Office Global (GLOBAL) and Africa Limited Area

(ALAM) models underpredict the occurrence of surface wind speeds > 6 m s^{-1}, and thus will strongly underestimate dust emission. The models do not simulate surface wind speeds more successfully at stations where cold pools are less frequent. On roughly 40% mornings, surface wind speeds simulated by ALAM at 0900 (the usual time of LLJ breakdown) do not show an increase as observed. This suggests that ALAM struggles to mix momentum down to the surface on these occasions. GLOBAL model output is not available at 0900: therefore it is not known how well or poorly the model simulates changes in surface winds caused by LLJ breakdown. Archiving model data at 0900 is very important for understanding Saharan atmospheric dynamics and dust emission. Improvements in model-driven dust emission in the CWS seem likely to stem from improved temporal resolution of model output, increased horizontal resolution to the point where convection is explicitly resolved, and/or inclusion of subgrid-scale wind variability.

8.1. Introduction

The central Sahara is widely recognised to be the planet's dustiest region in boreal summer [*Prospero et al.*, 2002; *Washington et al.*, 2003; *Engelstaedter et al.*, 2006]. However, because of its extreme remoteness and hostile climate, observations of the region have until recently been limited to its fringes. As the importance of dust in the climate system is being increasingly recognised [e.g. *Jickells et al.*, 2005; *Shao et al.*, 2011], addressing this observation gap has become an increasing priority. In 2011, the Fennec Project [*Washington et al.*, 2012] embarked on a comprehensive and ambitious ground-based and airborne survey of the climate of the central-western Sahara (CWS). Eight automatic weather stations (AWS) were deployed across the region from western Mauritania to central Algeria [*Hobby et al.*, 2013]. Two supersites with a comprehensive suite of meteorological instrumentation were established at Zouerat,

Mauritania [*Todd et al.*, 2013] and Bordj Badji Mokhtar (BBM), Algeria [*Marsham et al.*, 2013]. Radiosondes were launched from the supersites and additionally from the Algerian stations of Tindouf, In Salah and Tamanrasset. Finally, a total of 48 research flights were flown by the UK BAe-146 Large Atmospheric Research Aircraft and the French Falcon 20 across the northern and western parts of the CWS [*Ryder et al.*, 2015]. Figure 8-1 shows the extent of the field observations.

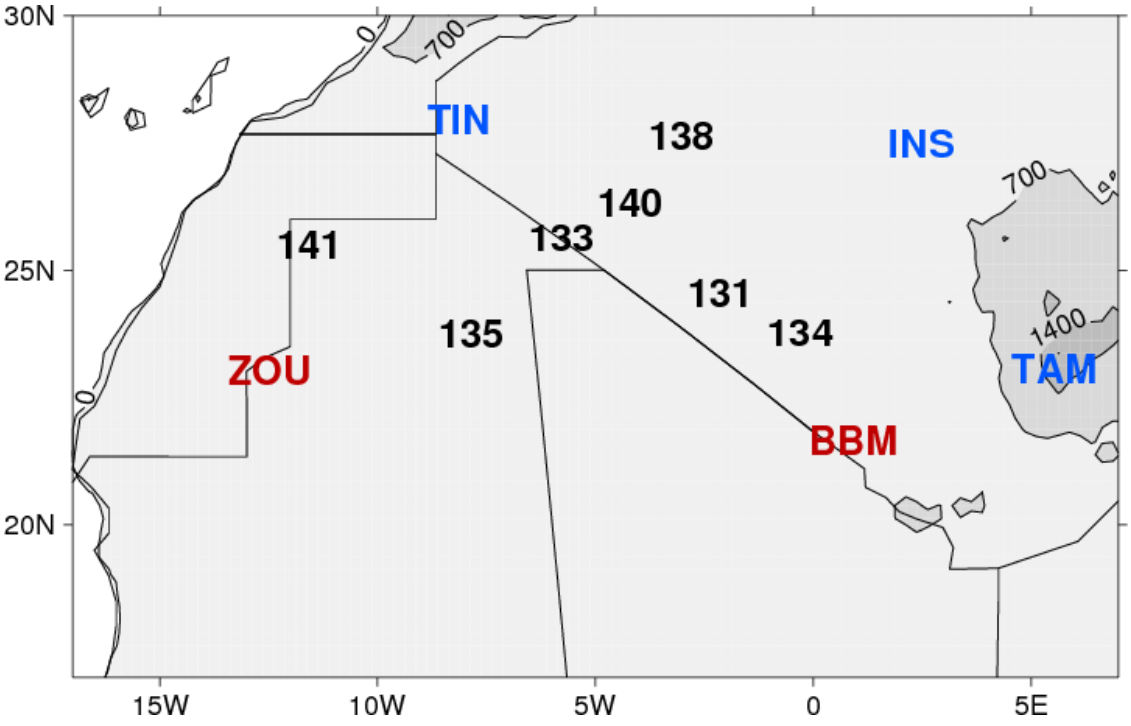

Figure 8-1: Map of CWS showing location of Fennec AWSs (black), supersites (red) and radiosonde stations (blue). Note that radiosondes were also launched from ZOU and BBM. ZOU=Zouerat, BBM=Bordj Badji Mokhtar, TIN=Tindouf, INS=In Salah, TAM=Tamanrasset. Greyscale background is elevation (700m contour step).

Detailed research into dust conditions from Fennec ground-based observations has so far focused on the supersites of Zouerat (22.75°N, 12.48°W; elevation 343 m; WMO ID 61404) and BBM (21.38N, 0.92E; elevation 420m; WMO ID 60686). These studies [*Allen et al.*, 2013; *Garcia-Carreras et al.*, 2013; *Marsham et al.*, 2013; *Todd et al.*, 2013; *Allen and Washington*, 2014; *Allen et al.*, 2015] have explored the atmospheric

dynamics and the mechanisms of dust emission and transport, as well as assessing the fidelity of models to reproduce these features. The Fennec AWS and radiosonde network provides an unparalleled opportunity to extend this work across the wider CWS. This is important in order to establish if and how the key dust processes vary across the domain and as a corollary, whether the supersites are representative of the rest of the CWS. From a modelling perspective, BBM, which is near the heart of the dust maximum [*Ashpole and Washington*, 2012], presents a particular challenge since the dominant dust mechanisms are cold pool outflows [*Garcia-Carreras et al.*, 2013; *Marsham et al.*, 2013; *Allen et al.*, 2015], which are very poorly simulated by models without explicit convection [e.g. *Reinfried et al.*, 2009; *Marsham et al.*, 2011; *Solomos et al.*, 2012].

Until now, our understanding of the dust mechanisms operating in the CWS has necessarily been dependent on satellite retrieval, modelling, and the few geographically-limited observations at synoptic meteorological stations that are available. The aims of this paper are therefore to develop a methodology that can identify the key dust processes across the CWS using the AWS measurements, then to use these results to establish how the dust processes vary geographically, and finally to assess the fidelity of the models in capturing the observed surface winds. Section 8.2 describes the instrumentation and datasets employed. The dust mechanisms and the methodology used to detect them are described in Section 8.3. Section 8.4 discusses the spatial variability of the dust mechanisms across the CWS. The surface winds and the fidelity of two Met Office models in capturing them are addressed in Section 8.5. A discussion is presented in Section 8.6 followed by conclusions in Section 8.7.

8.2. Instrumentation and datasets

8.2.1. Ground-based

This paper makes use of the ground-based observations at the Fennec supersites of BBM and Zouerat, the Fennec remote AWS network and Fennec radiosonde launches in the CWS. Their locations are shown in Figure 8-1. The study time period is the June 2011 Intensive Observation Period (IOP1). The instrumentation at BBM and Zouerat is described in detail by *Marsham et al.* [2013] and *Todd et al.* [2013] respectively and more briefly below and in Table 8-1. During IOP1, the instruments at BBM included a 15-metre mast with sonic anemometers at 10 m and 15 m (the 'flux tower'); pressure, temperature and humidity sensors; a Scintec MFAS phased array sodar; a Halo Photonics Streamline 1.55 μm Doppler lidar; an inverse nephelometer (670nm, fixed at 2 m height); a Cimel Sun Photometer and Vaisala RS92 GPS radiosondes launched up to every 3 hours. The instruments at Zouerat during IOP1 included an identical flux tower, pressure, temperature and humidity sensors; a Cimel Sun Photometer; pilot balloons (launched twice daily); a Scintec MFAS phased array sodar and Vaisala RS92 GPS radiosondes launched up to every 3 hours. Instrument accuracy and data availability is given in Table 8-1.

Table 8-1: Details of instruments deployed at BBM and Zouerat §

Instrument	Accuracy	Availability (BBM)‡	Availability (Zouerat)‡
'Flux tower' (10m and 15m agl sonic anemometers)	0.1ms^{-1} (wind speed)	6th-30th	1st-30th†
'Flux tower' (2m agl sensors)	2% (RH), 0.3°C (T), 0.5hPa (P)	6th-30th	1st-30th†
Cimel sun photometer (formed part of the AERONET project [*Holben et al.*, 1998]).	0.01 (440nm AOD)	4th-30th	1st-30th
Vaisala RS92 GPS radiosondes (launched at up to 3-hourly intervals)	0.2ms^{-1} (wind speed)	8th-30th	1st-30th
HALO Photonics Streamline 1.55µm Doppler lidar	0.1ms^{-1} (wind speed), ≤0.9° (wind direction)	3rd-30th	Not deployed
Inverse nephelometer (2m agl, 670nm)	10^{-7}m^{-1} (scattering)	5th-30th	Not deployed
Scintec MFAS phased array sodar	0.3 ms^{-1} (wind speed)	2nd-30th	1st-30th
Pilot balloons (twice daily)	Variable (user-dependent)	Not deployed	11-30th

§For full details see *Marsham et al.* [2013] and *Todd et al.* [2013]. RH=relative humidity, T=temperature, P=pressure, AOD=aerosol optical depth.
‡June 2011
†Substantial data loss after 20 June

During IOP1, Vaisala RS92 GPS radiosondes were not only launched at the supersites but also at Tindouf, In Salah and Tamanrasset in Algeria (Figure 8-1). At Tindouf, the radiosonde measurements were recorded at a coarser vertical resolution – only at 'mandatory' and 'significant' levels[16]. As a result, at Tindouf there were only up to 8 (and usually fewer) data points recorded in the bottom ~2km of the troposphere. These measurements are not comprehensive enough to unambiguously detect or characterise LLJs, so the Tindouf radiosondes were not used in this study. Future campaigns that

[16] The 'mandatory' levels are the surface, 1000, 925, 850, 700, 500, 400, 300, 250, 200, 150, 100, 70, 50, and 10 hPa, and the 'significant' levels are those at which abrupt changes in temperature and/or dewpoint temperature occur (to ensure that linear interpolation yields values of temperature which do not differ from the observed value by 1°C below 300 hPa and 2°C after that).

seek to understand Saharan boundary layer phenomena should ensure that radiosonde measurements (winds in particular) are archived at an appropriate vertical resolution.

The AWS instrumentation is described in full in *Hobby et al.* [2013] and more briefly below and in Table 8-2. The AWSs measured 2 m wind speed and direction, temperature, humidity, pressure, upwelling and downwelling radiation, ground heat flux, and ground temperature. The data were recorded at 3 min 20 s resolution, which is three times as frequent as the World Meteorological Organisation standard for winds and gusts. With the exception of AWS 141, both cup and sonic anemometers were available to measure wind speeds. Inspection of the wind speed time series (not shown) shows that the sonic anemometers tend to 'saturate' at wind speeds greater than ~9 m s^{-1} when stronger winds are recorded by the cup anemometers. The cause of this underestimation of high wind speeds by the sonic anemometers is still under investigation. Cup anemometer measurements are therefore used wherever possible and when the sonic anemometers are used this is clearly stated. After deployment in the remote desert (Figure 8-1), a very difficult task successfully completed by partners at the Mauritanian and Algerian Meteorological Services, the AWSs were completely unmanned.

Table 8-2: Details of AWS instruments §

Instrument	Accuracy	Height agl
Sonic anemometer (2D wind speed and direction)	0.3 m s^{-1}‡ 3°	2m
Cup anemometer	0.5 m s^{-1}	2m
Vane anemometer	3°	2m
Temperature sensor	0.2°C	2m
Humidity sensor	2%	2m
Pressure sensor	0.5hPa	1m

§Only instruments used in this study are listed. Full details are in *Hobby et al.* [2013].
‡There were problems with the sonic anemometer at high wind speeds (see Section 8.2.1)

At four AWSs, battery voltage began to decrease rapidly soon after deployment in June 2011, ultimately leading to station failure within a few days (Table 8-3). It is thought that the cause of this failure was a rapid decrease in solar cell efficiency at unexpectedly high solar cell temperature (102.5°C) [*Hobby et al.*, 2013]. Unfortunately, due to the great difficulty of travelling and working in the remote central Sahara in summer, the problem could not be addressed until after the IOP.

Table 8-3: AWS data availability in June 2011 §

Station number	Data availability
131	1-8 June
133	1-5 June
134	1-30 June
135	2-3 June
138	1-30 June
140	1-4 June
141	2-30 June‡

§ The locations of the stations can be found in Figure 8-1
‡ AWS 141 did not have a cup anemometer

8.2.2. Satellite

False-colour satellite imagery from the Spinning Enhanced Visible & Infrared Imager (SEVIRI) is used to help identify dust events across the CWS. The algorithm, developed by *Lensky and Rosenfeld* [2008], assigns colours to features as follows: deep cumulonimbus, dark red; thick water clouds, gold; clouds with small particles, green; thin cirrus, black; desert dust, pink; surface quartz sand, light blue/grey. SEVIRI is on board the Meteosat Second Generation satellite at 0N, 0E which gives the imager an excellent view of the CWS. It has a temporal resolution of 15 min. SEVIRI imagery is regularly used in studies of Saharan dust [e.g. *Schepanski et al.*, 2007; *Cuesta et al.*, 2009; *Bou Karam et al.*, 2014; *Roberts and Knippertz*, 2014]. Its main limitation is that

the algorithm struggles to detect dust when column water vapour is relatively high (>20-25 mm), or a temperature inversion is present [*Brindley et al.*, 2012].

In addition to the SEVIRI false colour imagery, we make use of an automated objective dataset of dust presence, the SEVIRI dust flag (SDF), developed by *Ashpole and Washington* [2012]. SDF exploits the brightness temperature signal of dust across three channels to flag pixels as either dusty or not dusty. The advantages of SDF are that it is objective, it has 24 h coverage and shares the high (15 min) temporal resolution of the SEVIRI imagery. However, SDF is relatively poor at detecting dust when the loading is low (aerosol optical depths less than ~1) [*Ashpole and Washington*, 2012].

8.2.3. Numerical model

One of the objectives of the Fennec Project is to evaluate and develop Met Office numerical weather prediction tools over the Sahara. Here we use and compare two configurations of the Met Office Unified Model, described by *Walters et al.* [2011]: the Global Model (GLOBAL) and the Africa Limited Area Model (ALAM). GLOBAL covers the entire global atmosphere with a horizontal resolution is 25km. The time-step is 10 min. There are 70 levels in the vertical. The lowest level is at 10m; levels are terrain following in the lower troposphere. GLOBAL assimilates data globally using Hybrid Incremental 4D-Var. Forecast run times are at 00z, 06z, 12z and 18z. For June 2011, GLOBAL data from intermediate forecast steps are not yet available and we use the six-hourly archived output data.

ALAM covers the African continent, the southern Mediterranean and the Arabian Peninsula (Figure 8-2) at a higher horizontal resolution of 12km. The time step is 4 min. The vertical resolution is identical to GLOBAL. The parameterization of vertical mixing within the boundary layer is not identical but it is designed to be as similar as possible:

both ALAM and GLOBAL are part of the Met Office Unified Model system. (By keeping model physics similar across resolutions, the Met Office seeks to achieve 'seamless' prediction across spatial and temporal scales.) ALAM receives its boundary conditions from GLOBAL, applied in a ten-point rim around the edge of the ALAM domain. ALAM is only initialised from GLOBAL when it is first started, and thereafter runs an independent data assimilation cycle from within the domain. Sea surface temperatures are held constant during runs. There were two forecast runs per day (at 06z and 18z), but only data from the 18z initialisation are available. Experience during the Fennec flight campaign [*Ryder et al.*, 2015] showed that there was little sensitivity to the initialisation time. For any given day, the ALAM output data used is three-hourly from initialisation at 18z. ALAM has been shown to simulate LLJs in the northerly/north-easterly Harmattan flow very well at BBM compared to lidar wind profiles [*Allen and Washington*, 2014] and also very well across the wider CWS compared to aircraft measurements [*Ryder et al.*, 2015].

Figure 8-2: The domain of the Met Office Africa Limited Area Model (ALAM).

In Section 8.4.1 we use ERA-Interim reanalysis (ERAI) from the European Centre for Medium-Range Weather Forecasts to provide an independent view of the large scale West African circulation during June 2011. ERAI has 6-hourly resolution of model output, horizontal resolution of 0.75° (roughly 83 km in the central Sahara), and 60 levels in the vertical, which are terrain following in the lower troposphere [*Dee et al.*, 2011].

8.3. Dust mechanisms and their detection across the AWS network

There are several different wind mechanisms in the CWS that have the capability to uplift dust. Here we describe them and the methodology employed for their identification over the AWSs. Since there were no dedicated dust instruments or observers at the AWSs (except at station 141, which had a dust sampler [*Todd et al.*, 2013]), we do not attempt to calculate the dust burden associated with the dust mechanisms, but are able to present dust mechanism frequency counts across all stations. The limitations of this approach are assessed in the Discussion (Section 8.6).

8.3.1. Low level jets

In the summertime, the Saharan Heat Low (SHL) is located over the CWS [e.g. *Lavaysse et al.*, 2009], with the inter-tropical discontinuity (ITD) separating the dry north-easterly Harmattan winds from the moist south-westerly monsoon flow. The large-scale pressure gradient into the SHL is a synoptic-scale control on dust emission [*Knippertz and Todd*, 2012]. Low-level jets (LLJs) forming on both sides of the ITD can lead to dust emission when momentum is mixed down to the surface [*Schepanski et al.*, 2009; *Fiedler et al.*, 2013; *Heinold et al.*, 2013; *Allen and Washington*, 2014], although trajectory analysis of the dust emanating from individual sources suggests that it is only in the CWS north of the ITD that LLJs are the dominant process [*Ashpole and*

Washington, 2013b]. This is broadly in agreement with the findings of *Fiedler et al.* [2013] who show, using ERAI, that from June to August LLJs contribute more substantially to dust emission north of 20°N. The Fennec observations at the western CWS station of Zouerat show that LLJs occur on most mornings of June 2011, but that they do not lead to substantial dust emission because the Atlantic Inflow impedes the mix-down of momentum to the surface [*Todd et al.*, 2013].

When height-resolved wind observations are available (e.g. radiosondes, lidar), LLJs can be identified from their wind profiles. For example, *Allen and Washington* [2014] developed a set of objective criteria for detecting LLJs from 0600 wind profiles at BBM during IOP1. They chose 0600 because it is a time when vertical wind shear is still clearly present in the LLJ profile, the LLJ is close to breakdown (and therefore relates closely to potential dust emission), and it is an hour commonly used for radio-soundings and model output. The criteria consist of four tests which must be met: (i) jet core (i.e. wind speed maximum) below 600 m agl (ii) wind shear between the core and 500 m above the core $\leq$-1.8 m s^{-1} (iii) wind speed decreases from below the core to the surface (or lowest measurement) (iv) core wind speed > 8 m s^{-1}. There are no universally accepted LLJ detection criteria [*Kallistratova and Kouznetsov*, 2012; *Nunalee and Basu*, 2013] but *Allen and Washington* [2014] is an appropriate choice here because it is optimised for the central Sahara in June. An alternative choice would be the criteria of *Fiedler et al.* [2013] but these were shown to miss 3/5 LLJs which led to dust emission over BBM [*Allen and Washington*, 2014].

Unfortunately, there are no wind profile observations over the AWSs. If they are good enough, it is possible to use model-simulated wind profiles as a substitute. To assess whether this is appropriate, we present a brief evaluation of modelled LLJs compared to

Fennec radiosonde launches at BBM, Tamanrasset, In Salah and Zouerat (hereafter, the 'radiosonde stations').

8.3.1.1 Met Office model LLJ detection

Observed LLJs are identified by applying the *Allen and Washington* [2014] LLJ detection criteria to all the available 0600 radio-soundings at the radiosonde stations in June 2011. LLJs were observed on 34 out of 47 (i.e. 72%) possible occasions when 0600 observations were available at the radiosonde stations. The detection criteria are also applied to GLOBAL and ALAM at the same locations on the same mornings. Interestingly, GLOBAL simulates LLJ core wind speeds within 2 m s^{-1} of the observed core wind speeds more frequently than ALAM (45% occasions against 35% occasions). GLOBAL also simulates LLJ core wind speed absolute errors > 5 m s^{-1} compared with observed core wind speeds less frequently than ALAM (16% occasions against 29% occasions). For example, at In Salah on 22 June, a LLJ is detected in the radiosounding, GLOBAL and ALAM, but ALAM overestimates the strength of the jet core by 5.1 m s^{-1} (Figure 8-3). It appears that the higher horizontal resolution of ALAM does not necessarily result in improvements in LLJ characteristics. *Schepanski et al.* [2014] also find that model representation of a LLJ in the Sahel is generally insensitive to changes in model horizontal resolution (4km, 12km or 36km). Both GLOBAL and ALAM have the same vertical resolution and a similar boundary layer scheme so it is possible that the more accurate LLJ profile simulations by GLOBAL at the radiosonde stations are due to information from beyond the limited area model domain not available to ALAM (see also Section 8.2.3). The prime large-scale control on the formation of LLJs is the pressure gradient. The domain of ALAM ends at 20°W (see Figure 8-2), which does not include the Azores High. ALAM is only initialised from GLOBAL when it is first

started and is one-way nested, so it may be missing interactions between the Azores High and the Saharan pressure gradient. However, for the purpose of solely detecting the presence of LLJs, which is the main objective here, GLOBAL and ALAM do similarly well. The bias ratio (number of yes (i.e. LLJ) simulations ÷ number of yes observations [*Wilks*, 2006]) is 0.84 for GLOBAL and 0.85 for ALAM. Thus both GLOBAL and ALAM underforecast the occurrence of LLJs, but not substantially. As a result, GLOBAL and ALAM are judged to be appropriate for detecting LLJs over the AWSs in the absence of wind profile observations.

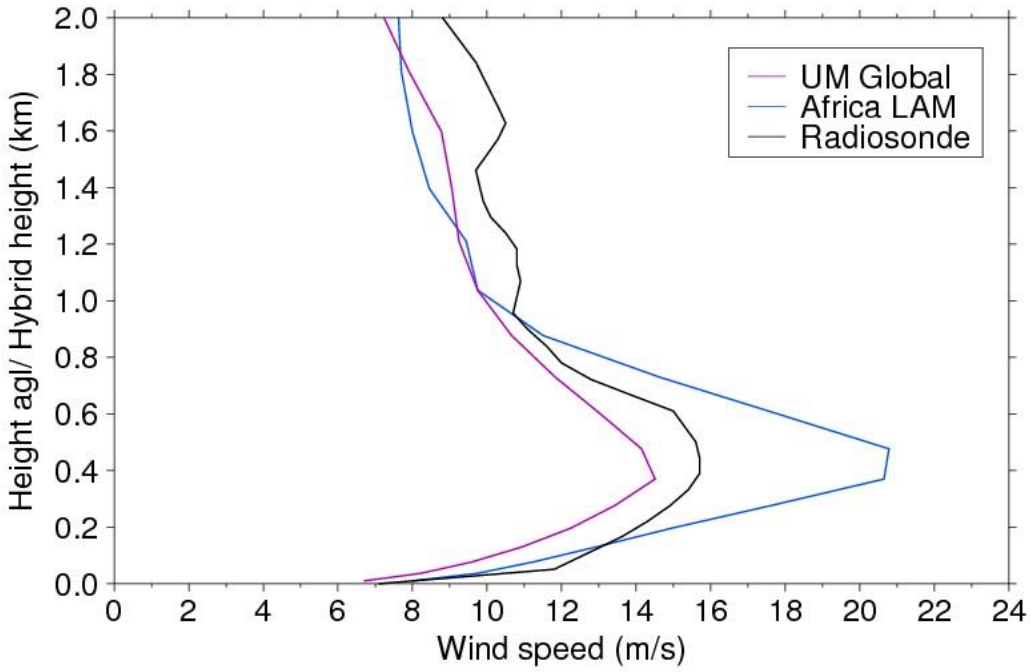

Figure 8-3: Observed (radiosonde) and simulated (GLOBAL and ALAM) wind speed profiles at In Salah at 0600 on 22 June 2011. Height agl and hybrid height are comparable since hybrid heights are sigma coordinates (i.e. terrain following) in the lower troposphere.

8.3.1.2 LLJ detection methodology over the AWSs

The full LLJ detection methodology for the AWSs is as follows. Mornings when either the ALAM or GLOBAL detect LLJs over the AWSs are noted (following the criteria described in Section 8.3.1 above). The SEVIRI imagery is checked for evidence of LLJs (fast developing streams of pink dust[17]; see also *Ashpole and Washington* [2013b]). The AWS surface wind speed observations are inspected for periods when momentum from a LLJ is likely mixing down to the surface (Gaussian-like increase in surface wind speed after sunrise, see also *Allen and Washington* [2014] and *R L Miller et al.* [2004]). Note that momentum does not always mix down to the surface - particularly if the LLJ is weak [*Allen and Washington*, 2014] or if surface heating is significantly reduced by elevated dust [*R L Miller et al.*, 2004; *Pérez et al.*, 2006] - and AWS observations are not available on every day so AWS observations are not themselves sufficient to detect LLJs.

The lower estimate of LLJ frequency at an AWS is the lower of the ALAM/GLOBAL detections plus any events when the AWS observations and/or SEVIRI suggest that a LLJ is present but not simulated. The upper estimate of LLJ frequency is the higher of the ALAM/GLOBAL detections plus any events when the AWS observations and/or SEVIRI suggest that a LLJ is present but not simulated. The LLJ detection methodology is summarized in Figure 8-4. Note that this approach only attempts to detect the presence of LLJs; it does not explicitly identify those which are responsible for dust emission. This is not possible because dust detection instrumentation is not available at the AWSs. Model surface (i.e. 10m) wind speeds are not used as part of the LLJ

[17] These LLJ dust streams can be distinguished from cold pool outflow dust in SEVIRI because (i) their first appearance is usually under clear skies (not an outward propagation from deep convection as for cold pools), (ii) they do not lead to arcus clouds at their leading edge, as do some cold pools (iii) cold pool fronts are prependicular to the direction of propagation whilst LLJ dust streams are elongated parallel to the direction of propagation.

detection methodology because these will be compared against the observations in later sections.

Three examples of the LLJ detection process are presented next, illustrating LLJ detection from SEVIRI, LLJ detection from surface wind speed observations and LLJ detection from model wind profiles.

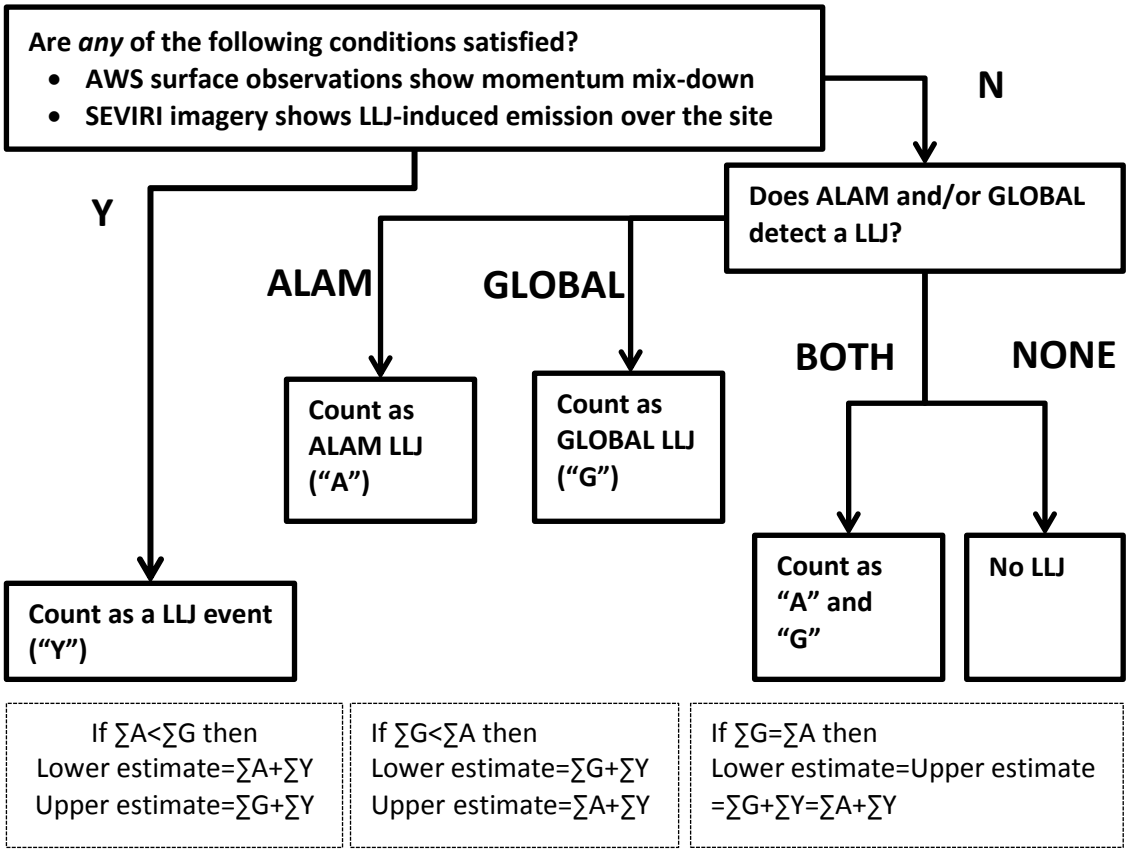

Figure 8-4: LLJ detection methodology over the AWSs (see Section 8.3.1 for detailed description).

On the late morning of 29 June 2011 SEVIRI clearly shows a streak of dust emanating south-westward from AWS 135, a tell-tale indication of LLJ-induced dust emission (Figure 8-5a). The event is therefore counted as a "Y" (Figure 8-4). There are no AWS 135 surface wind speed observations available on 29 June, although they would not be

necessary to confirm the detection in any case because the evidence from SEVIRI is strong enough alone (Figure 8-4). On the morning of 3 June 2011 AWS 134 records a Gaussian-like increase in surface wind speed, increasing from 5 m s^{-1} at 0600 to 12 m s^{-1} at 0900 then decaying back to 5 m s^{-1} by 1200 (Figure 8-5b). Such a pattern is indicative of momentum mix-down and so the event is classed as a "Y" (Figure 8-4). On this occasion SEVIRI does not show any evidence of a LLJ, but this may be because a temperature inversion is present, there are high levels of moisture in the atmosphere or the amount of dust raised is small and difficult to detect. On 10 June 2011 there is no evidence from SEVIRI or from surface wind speeds at AWS 138 that a LLJ is present (Figure 8-5c). However, both ALAM and GLOBAL simulate LLJs at 0600 (Figure 8-5d) so the event is counted as an "A" and "G" LLJ (Figure 8-4).

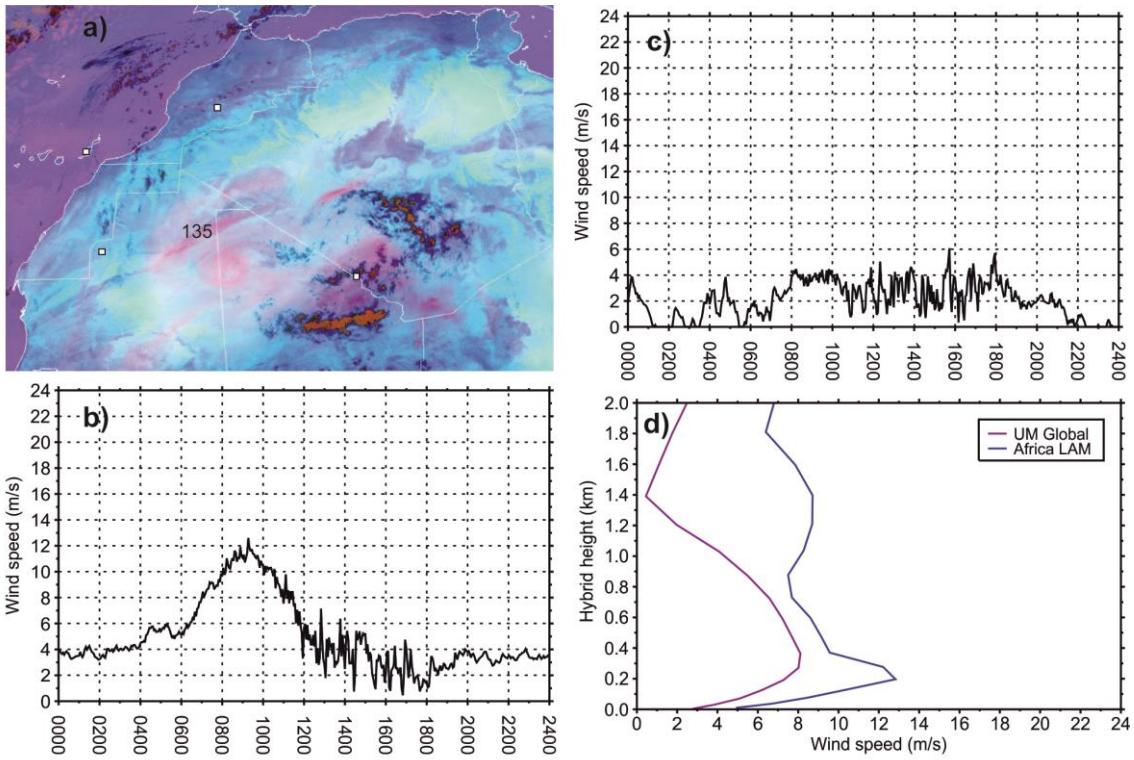

Figure 8-5. (a) SEVIRI false colour imagery showing LLJ-induced dust emission (elongated pink stripe from NE to SW) over AWS 135 (labelled) at 1115 on 29 June 2011. The white squares are other Fennec sites, clockwise from top: Ouarzazate, BBM, Zouerat, Fuerteventura. (b) 2m wind speed timeseries at AWS 134 on 3 June 2011. (c) 2m wind speed timeseries at AWS 138 on 10 June 2011. (d) GLOBAL and ALAM wind profiles above AWS 138 at 0600 on 10 June 2011.

8.3.2. Cold pool outflows

In the Sahara south of ~23°N[18] and in the Sahel, cold pool outflows are a dominant mechanism of dust emission and transport in summer [*Marsham et al.*, 2011; *Allen et al.*, 2013; *Heinold et al.*, 2013; *Marsham et al.*, 2013; *Allen et al.*, 2015]. Cold pools form when evaporating precipitation in the mid-levels (800-500hPa) cools the surrounding air and leads to strong downdrafts (the downdrafts can be further promoted by the drag imparted on the air by falling precipitation). These downdrafts spread away from the parent storm as a density current, raising dust at the leading edge and mostly transporting it in the tail [e.g. *Knippertz et al.*, 2007; *S D Miller et al.*, 2008]. At BBM in June 2011, 72% of the dust was caused by cold pools: 45% in local emission and 27% in long-range transport [*Allen et al.*, 2013]. Because cold pools are strongly tied to convective processes, they are typically missed or poorly represented in models where the convection is parameterized [e.g. *Reinfried et al.*, 2009; *Marsham et al.*, 2011; *Solomos et al.*, 2012]. However, when models can be run with explicit convection, cold pools are shown to account for roughly half the dust emission in the Saharan region [*Marsham et al.*, 2011; *Heinold et al.*, 2013]. During their period of simulation with the Met Office Unified Model at 4km resolution (26 July to 2 September 2006), *Heinold et al.* [2013] found that cold pool dust emission was concentrated in the CWS region, extending from eastern Mauritania to western Algeria roughly between 16 and 22°N. Cold pools are also observed in the southern foothills of the Atlas Mountains, predominantly from April to September [*Emmel et al.*, 2010].

A combination of AWS measurements and SEVIRI imagery are used to detect cold pools. Since cold pool outflows originate from deep convection, they frequently cause

[18] For reference, BBM is at 21.4°N

increases in moisture as they pass over a site [e.g. *Emmel et al.*, 2010; *Marsham et al.*, 2013]. *Allen et al.* [2015] use an increase in water vapour mixing ratio (WVMR) of $\geq$1 g kg^{-1} in 5 min as part of their cold pool detection methodology at BBM. The AWSs record measurements every 3 min 20 s, so here we use a criterion of WVMR increase of $\geq$1 g kg^{-1} in 6 min 40 s (400 s). When this condition is satisfied, a 'definite' cold pool is recorded, unless there is evidence that the moisture has been brought in by a monsoon surge (Section 8.3.3).

Cold pools may also cause sudden changes in temperature (increase or decrease), pressure (increase or increase followed by decrease), wind speed (increase) and wind direction as they pass a site [e.g. *Knippertz et al.*, 2007; *S D Miller et al.*, 2008; *Allen et al.*, 2013]. Where such fluctuations are present but the WVMR criterion is not met, these events are designated as 'possible' cold pools. At AWS 141 (Figure 8-1), it is likely that moisture is also transported to the station by the Atlantic Inflow [*Grams et al.*, 2010; *Todd et al.*, 2013]. The Atlantic Inflow shares many of the characteristics of a density current [*Grams et al.*, 2010], therefore the AWS measurements are not used to detect cold pools at AWS 141. We do not attempt to distinguish between cold pools that are advecting dust and those which are locally emitting dust because (i) we do not know the local dust emission thresholds at the AWSs (ii) there are many days with missing AWS measurements (Section 8.2.1).

Separately, SEVIRI imagery is used to identify cold pool outflows crossing the AWSs. Cold pools are frequently visible on SEVIRI images as bright pink or dark pink/blue fronts propagating from deep convective systems, [e.g. *Ashpole and Washington,* 2013b; *Bou Karam et al.*, 2014; *Roberts and Knippertz,* 2014]. When there is no doubt from the imagery that a cold pool outflow has crossed an AWS this is recorded as a 'definite'

cold pool; where the signal is weak or deep convection is directly over the site this is designated a ‘possible’ cold pool.

The cold pool detections from the AWS measurements and SEVIRI are brought together to generate a lower and upper estimate of cold pool frequency over each AWS as follows. The lower estimate is the sum of all ‘definite’ events (not counting an event twice if it is detected in both AWS measurements and SEVIRI). The upper estimate is the lower estimate plus the count of any remaining ‘possible’ events (not counting an event twice if it is detected in both AWS measurements and SEVIRI). If an event is designated ‘definite’ by AWS (SEVIRI) but ‘possible’ by SEVIRI (AWS) then it is counted as a ‘definite’ cold pool. By combining the AWS observations and SEVIRI imagery we aim to overcome some of the deficiencies of each (e.g. missing data in the AWSs, limitations of SEVIRI to detect dust under high column water). A flowchart illustrating the cold pool detection process is in Figure 8-6.

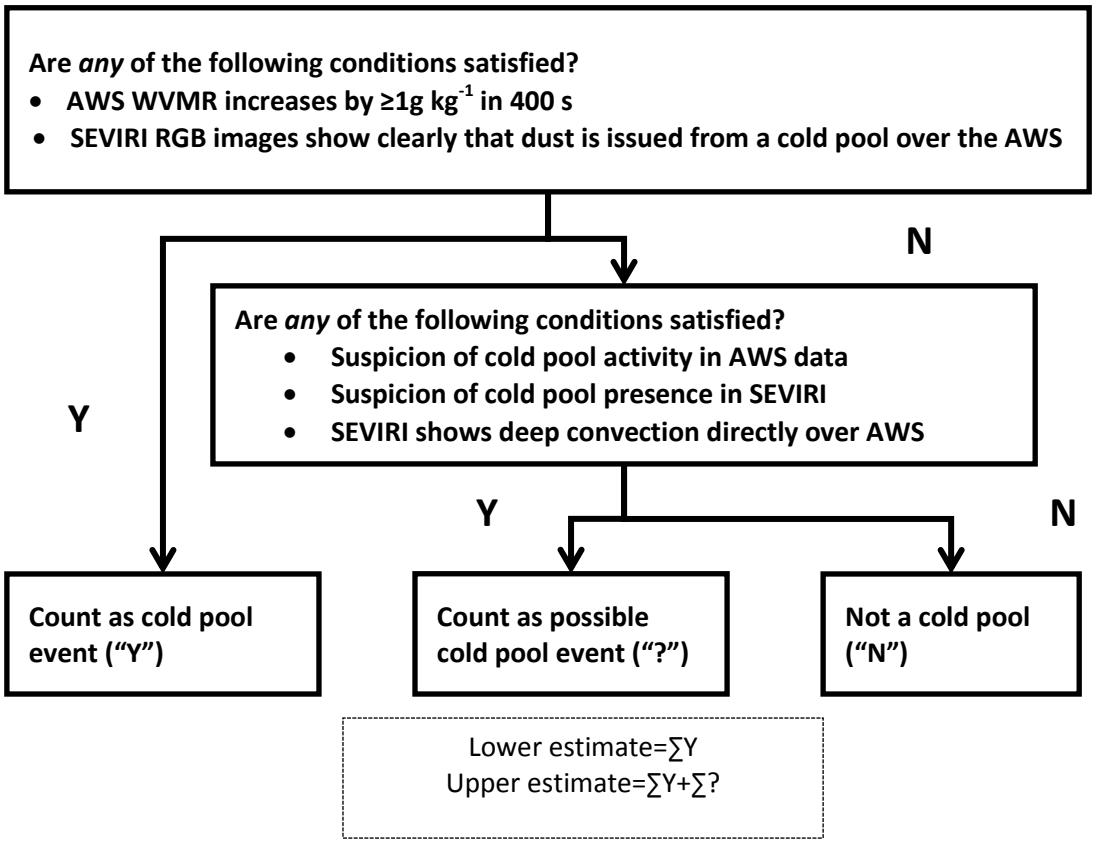

Figure 8-6: Cold pool detection methodology over the AWSs (see Section 8.3.2 for detailed description).

8.3.2.1 Case studies of cold pool outflow detection

Two case studies of the cold pool outflow detection procedure are presented here: first exemplifying a 'definite' detection and second exemplifying a 'possible detection'. At 0008 h on 21 June 2011, AWS 138 recorded a jump in WVMR of 2 g kg^{-1} in 400 s (Figure 8-7a). SEVIRI clearly showed a cold pool outflow about 600 km wide reaching the station at midnight from an expanse of deep convection which had formed over the Atlas Mountains the previous evening (Figure 8-7b). The deep convection is bright red and the leading edge of the cold pool (further south) extends roughly WSW-ENE (crossing AWS 138) and can be identified by a sharp change in the colours from light

blue/purple to light pink. Thus the event was designated a ‘definite’ cold pool (Figure 8-6). Further evidence for the passing of the cold pool front included an increase in wind speeds of 8 m s^{-1} in the same period as the WVMR increase (Figure 8-7a).

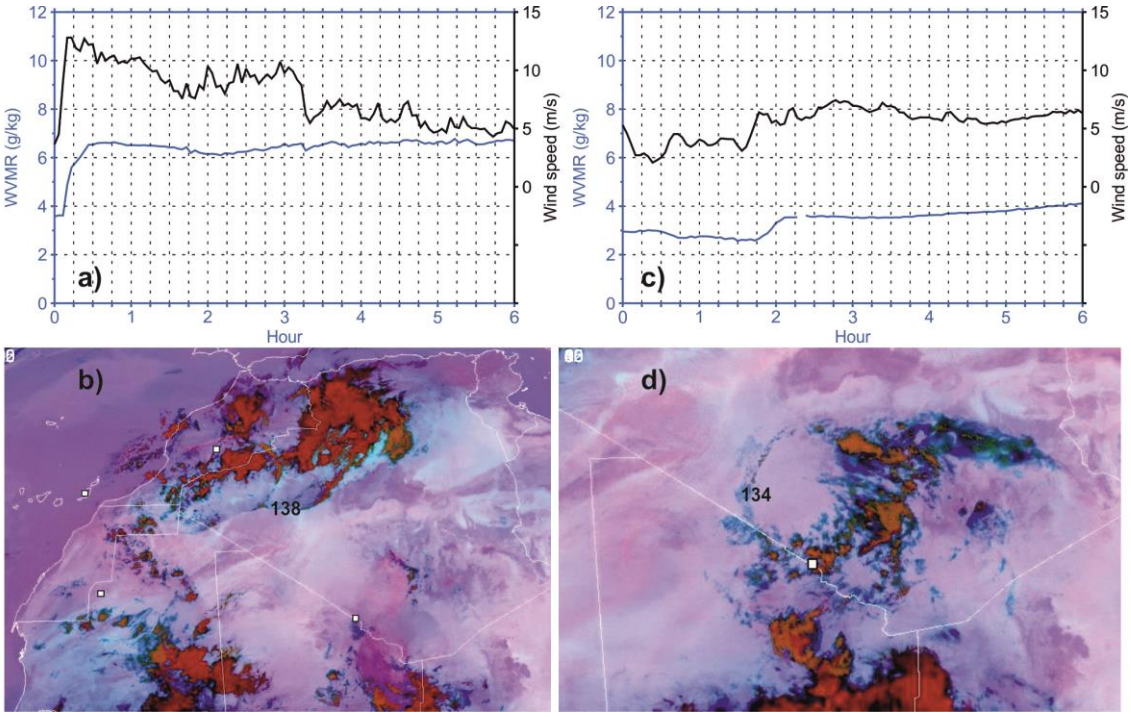

Figure 8-7. (a) WVMR (blue) and 2m wind speed (black) timeseries at AWS 138 for the early morning of 21 June 2011. Note that the scale of the wind speed axis has been chosen to avoid overlap with WVMR for clarity. (b) SEVIRI false colour imagery at midnight on 21 June 2011. AWS 138 labelled. White squares are as Figure 8-5a. (c) As (a) but for AWS 134 on 29 June 2011. (d) SEVIRI false colour imagery at 0200 on 29 June 2011. AWS 134 labelled. White square is location of BBM.

At 0145 on 29 June 2011, AWS 134 recorded an increase in WVMR of 1 g kg^{-1} in 15 min (Figure 8-7c). This is not enough to satisfy the cold pool detection criteria (Figure 8-6), but immediately preceded by a 3 m s^{-1} increase in wind speed (Figure 8-7c) it suggests that one may be passing the station. Additionally, SEVIRI shows that the station is under a band of arcus-like clouds (Figure 8-7d), which may form at the leading edge of cold pool outflows [*Knippertz et al.*, 2007; *Allen et al.*, 2013]. To the

east of AWS 134 there is a cluster of mesoscale convective systems (Figure 8-7d) which developed over the previous 36 hours. There is no 'pink dust' visibly emanating from the mesoscale convective systems but this is likely because the air has a high water vapour content, making dust detection difficult for the algorithm [*Brindley et al.*, 2012]. These observations are sufficient to designate the event a 'possible' cold pool (Figure 8-6).

If a cold pool and a LLJ are detected simultaneously, both are recorded. This is not thought to be a deficiency of the detection methodology. For example, in explicit convection (4km resolution) simulations using the Met Office Unified Model in late summer over the north-west African domain, *Heinold et al.* [2013] found that 23% dust emission occurred when both cold pools and LLJs were detected together. This was seen to happen 7 times at BBM during June 2011 [*Allen and Washington*, 2014]. Cold pools and LLJs were detected simultaneously 11 times across the seven AWSs in the same period.

8.3.3. Monsoon surges

At a larger scale than cold pool outflows, monsoon surges also raise dust in the CWS in summer [*Flamant et al.*, 2007; *Bou Karam et al.*, 2008; *Marsham et al.*, 2013; *Allen et al.*, 2015]. The moist southerly monsoon flow can act as an intrusive density current, emitting dust at its leading edge, and also promotes cold pool activity by bringing moisture into the CWS [*Bou Karam et al.*, 2008]. Using an objective satellite dust detection method, *Ashpole and Washington* [2013a] show that climatologically, summer monsoon surges into the SHL region are associated with particularly high dust detection frequency.

Monsoon surges are identified at an AWS when (i) observed WVMR (or modelled WVMR if observations are unavailable) $\geq$12 g kg^{-1} (following *Flamant et al.* [2007]) and (ii) the ITD is at or north of the AWS. The ITD is defined as the zero-wind interface between the southerly/south-westerly monsoon and the northerly/north-easterly Harmattan at 925hPa, as used in *Flamant et al.* [2007] and *Couvreux et al.* [2010]. This can only be diagnosed from the models. If both models show that the ITD is at or north of the AWS then it is counted as a definite monsoon surge; if only one model shows this then it is counted as a possible monsoon surge. If detection of a monsoon surge is coincident with detection of a cold pool or LLJ then the monsoon surge detection takes precedence. This is because monsoon surges share many characteristics of cold pools and LLJs [*Bou Karam et al.*, 2008; *Marsham et al.*, 2008; *Flamant et al.*, 2009; *Marsham et al.*, 2013], but neither cold pools nor LLJs should cause spatially extensive northward deformations of the ITD like monsoon surges.

8.3.4. Dry convective plumes and dust devils

At the smallest spatial and temporal scale, dry convection can raise dust directly in non-rotating updrafts (dry convective plumes) or rotating vortices (dust devils). The former may have a lifetime of a few hours and diameter ~100m [e.g. *Ansmann et al.*, 2009], the latter a few minutes and diameter ~7m [e.g. *Balme and Greeley*, 2006]. *Renno et al.* [1998] show that the net work performed by a dust devil solely depends on the surface pressure drop, sometimes known as the pressure well. Light winds (<7 m s^{-1}) are required for dry convective plumes or dust devils to develop [*Oke et al.*, 2007], although wind speeds within them easily exceed this. The contribution of dust devils and dry convective plumes to the global dust budget has been estimated at 35% by *Koch and Renno* [2005] but at only 3.4% by *Jemmett-Smith et al.* [2015], the latter in much closer agreement to the <2% contribution estimated at BBM in June 2011 [*Allen et al.*, 2013].

As with momentum mix-down from LLJs, it is possible that under very dusty conditions, such as the CWS in summer, dust emission by dry convection is impeded [*R L Miller et al.*, 2004; *Pérez et al.*, 2006].

We use the criteria of *Allen et al.* [2015] to detect dry convective plumes/dust devils (the two are difficult to separate with the available measurements). The criteria are (i) event starts with a jump in wind speed of at least $3ms^{-1}$ in 15 min and a pressure well of at least 0.7hPa in 15 min (ii) wind speeds prior to the pressure well must be less than $7ms^{-1}$ (iii) wind speeds following the wind speed jump remain above 6 m s^{-1} but for no longer than two hours (iv) the event must occur in the afternoon (i.e. after midday but before sunset) to separate it from LLJ break-down. Since AWS measurements are missing on a large number of days (Table 8-3), the number of dry convective plumes detected will almost certainly be an underestimate.

It is important to recognise that dry convection occurs throughout daylight hours in the Sahara, as heating of the ground surface generates turbulent eddies which can have a range of scales up to the boundary layer height. It is these turbulent eddies that result in momentum mix-down from LLJs. In this paper however, the term 'dry convective plume' is restricted to afternoon gustiness which raises dust in discrete updrafts. The role of dry convection - which includes momentum mix-down from aloft – is therefore broader than what here are described as 'dry convective plumes'.

8.3.5. Other dust events

There are other processes which may lead to dust emission and transport over the CWS, although this is often via embedded smaller-scale dust mechanisms. African Easterly Waves (AEWs) have been shown to be associated with dust entrainment into the atmosphere [e.g. *Jones et al.*, 2003], but their role is probably an indirect rather than

direct one. *Knippertz and Todd* [2010] demonstrate that AEWs promote dust emission (i) by bringing low-level moisture northward into the CWS, mobilizing dust at the monsoon leading edge and promoting cold pool outflows (ii) by increasing the surface pressure gradient and promoting LLJs in the northeasterly flow. Dust emission in North Africa also has associations with stationary depressions and mobile cyclones, although these are more important in spring than summer [e.g. *Bou Karam et al.*, 2010; *Schepanski and Knippertz*, 2011; *Fiedler et al.*, 2014]. Whilst there is some evidence that suggests that these synoptic-scale features can raise dust directly [*Bou Karam et al.*, 2009; *Fiedler et al.*, 2014], frequently the dust emission is likely caused by smaller-scale embedded mechanisms such as LLJs or cold pool outflows [*Knippertz and Fink,* 2006; *Fiedler et al.*, 2014]. As a result, we do not explicitly search for AEW- or depression-related dust mechanisms.

However, to increase confidence that no important dust-producing mechanisms have been missed, we perform a check using SDF (which has not been employed in the methodology so far). The SDF timeseries are examined over each AWS. If there are any periods with SDF present for 30 min (i.e. two time steps) or longer that do not correspond with one of the dust mechanisms identified so far (i.e. LLJ, cold pool, monsoon surge, dry convective plume), then the event is classified as 'other dust'. (The SDF timeseries over each AWS is generated using a 0.1x0.1 degree box centred over the station; if dust is flagged at any pixel in this box then SDF is considered present for that time step.)

Over the duration of the whole IOP at all AWSs, there are only two 'other dust' events, lasting a total of 3 h. We are therefore confident that no important dust mechanisms have been missed.

8.3.6. Detection comparison with Fennec supersites

The Fennec supersites of BBM and Zouerat benefited from much more comprehensive instrumentation that the AWSs (compare Table 8-1 and Table 8-2). This instrumentation made detailed documentation of dust and atmospheric conditions at the supersites possible. Therefore, as a further check of the fidelity of the dust detection methodology over the AWSs presented above (the 'AWS methodology'), we apply it to the Fennec supersites of BBM and Zouerat for IOP1 and compare the results with those from detailed studies of the supersites presented in *Allen et al.* [2015] and *Todd et al.* [2013]. Using the sonde data presented in *Todd et al.* [2013], 24 LLJs at Zouerat can be identified; the AWS methodology applied to Zouerat identifies 21-23 (upper and lower estimate, see Figure 8-4). *Allen et al.* [2015] identify 21 LLJs at BBM; the AWS methodology applied to BBM identifies 21-24. The AWS methodology for LLJ detection therefore does well overall. Since it slightly underpredicts at one supersite and slightly overpredicts at another there is merit in calculating the lower and upper estimates (Figure 8-4).

Todd et al. [2013] identify 4 cold pools at Zouerat in IOP1; the AWS methodology applied to Zouerat identifies 6-7 (upper and lower estimate, see Figure 8-6). *Allen et al.* [2015] identify 21 cold pools at BBM in IOP1; the AWS methodology applied to BBM identifies 23-29. The main reason for these higher values is that when deep convection develops over BBM this is always counted as a 'possible' cold pool (Figure 8-6), when a cold pool does not always materialise. This is less of a problem at the remote AWSs which are further from the sources of moisture south of the ITD. However, since there is also a small cold pool overestimation at Zouerat, we have more confidence in the 'lower estimate' cold pool calculation than the 'upper estimate' cold pool calculation.

No monsoon surges are detected over Zouerat during IOP1 by *Todd et al.* [2013]; neither are any detected by the AWS methodology. Two monsoon surges are detected over BBM by *Allen et al.* [2015] and by the AWS methodology, both towards the end of the month as expected. The monsoon surge detection is therefore considered appropriate. Finally, the dry convective plume methodology is exactly the same here as in *Allen et al.* [2015], where it is shown to perform very well when compared with measurements including the lidar and nephelometer.

8.4. Variability in dust mechanisms across the CWS

With a satisfactory methodology developed for detecting the different dust mechanisms at the AWSs during IOP1 (Section 8.3), it is now possible to examine how they vary across the region. The incidence of the different dust mechanisms across the CWS is summarised in Table 8-4. LLJs are more frequent than any other mechanism at all stations except BBM, where they are joint first with cold pools. (Note again that the detection methodology for LLJs is only able to detect jet presence, not whether the LLJ results in dust emission, Section 8.3.1.) Cold pools are the second most frequent dust mechanism at all stations except BBM, where they are joint first with LLJs. Monsoon surges are not detected except at BBM where only two are detected, which is not surprising because (i) BBM is the southernmost station (ii) monsoon surges are expected to be more common in July than June, after full summer monsoon onset. Dry convective plumes are only detected at AWS 138 (2) and BBM (5). If there were fewer missing observations at the AWSs (Table 8-3) it is almost certain that this number would be higher, although it is worth pointing out that AWS 138 has complete measurements and still only records two dry convective plumes in 30 days. The station with the largest dust mechanism count is unambiguously BBM (49), in good agreement with its proximity to the global summertime dust maximum as identified by SDF

[*Ashpole and Washington*, 2012]. It is harder to identify which station has the lowest dust mechanism count because of the uncertainty ranges, but it is probably AWS 135 or AWS 133 (Table 8-4), both in north-eastern Mauritania.

Table 8-4: Incidence of dust mechanisms at stations across the CWS during June 2011 §

	Zouerat	141	135	133	140	138	131	134	BBM
LLJ	24	25-29	11-18	14-19	15-22	21-22	19-27	24-26	21
Cold pool	4	5-8	9-16	7-12	7-14	7-12	8-10	9-11	21
Monsoon surge	0	0	0	0	0	0	0	0	2
Dry convective plume	0	0	0	0	0	2	0	0	5
Total	28	30-37	20-34	21-31	22-36	28-34	27-37	33-37	49

§ Stations are listed left to right from west to east. Statistics for Zouerat and BBM are taken from *Todd et al.* [2013] and *Allen et al.* [2015] respectively. Confidence is slightly lower at AWS 141 than the other stations because only a sonic and no cup anemometer is available (see Section 8.2.1).

There is an interesting spatial pattern to the frequency of LLJs and cold pool outflows, the principal dust mechanisms in the CWS (Figure 8-8). At stations to the north-west and north-east of the CWS, LLJs are clearly more frequent than cold pools, with little uncertainty in their detection. *Fiedler et al.* [2013] identify the north-west CWS as a LLJ hot spot in ERAI in summer due to Atlantic ventilation; this likely explains the high incidence of LLJs at Zouerat and AWS 141 (Figure 8-8). *Fiedler et al.* [2013] do not identify central-western Algeria as a LLJ hot spot, although using ERA-40 *Schepanski et al.* [2009] show that LLJs occur here frequently in summer, in agreement with the high incidence of LLJs at AWSs 138, 131 and 134 (Figure 8-8). These LLJs are likely embedded in the dry north-easterly Harmattan flow. To the centre of the CWS (AWSs 135, 133 and 140), there is more uncertainty in detection of LLJs and cold pools, and more overlap between LLJ and cold pool frequency (Figure 8-8). BBM is somewhat exceptional in that it has an equal and high number of cold pools and LLJs. It

has the highest number of cold pools, which is unsurprising given its location in the south of the CWS. These findings agree well with the SDF satellite analysis of *Ashpole and Washington* [2013b], who find that dust events in the southern CWS are frequently (often >60% time) associated with deep convection, with no dominant dust transport direction, pointing to cold pools as the dominant dust mechanism here. Also consistent with the results presented here, *Ashpole and Washington* [2013b] point to the dominance of LLJ dust emission in the north-east CWS, as the dust events there have a dominant south-westward trajectory, consistent with the Harmattan wind. Interestingly however, the frequency of cold pools does not follow a simple decreasing pattern northwards; there are still an appreciable number (up to 14) registered at the two northernmost AWSs, 140 and 138 (Figure 8-8).

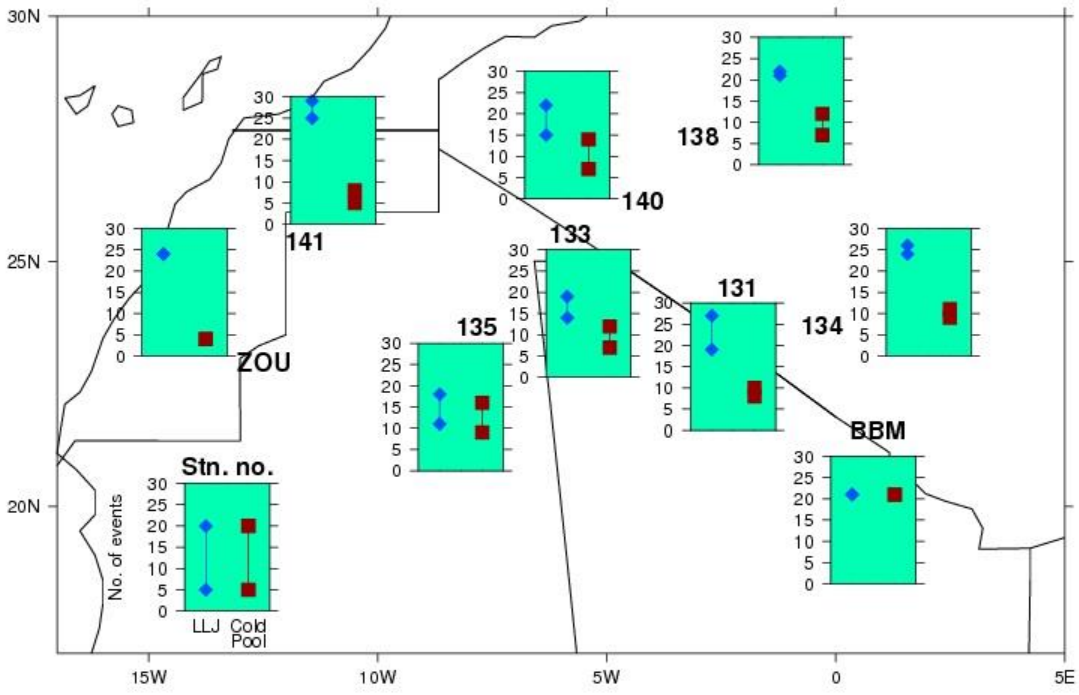

Figure 8-8: Incidence of LLJs and cold pools in June 2011 (charts) at the Fennec supersites and remote AWSs (located on map). A key is presented in the bottom left. The location of each station is at the centre of each label. ZOU=Zouerat, BBM=Bordj Badji Mokhtar. Upper and lower estimates for the AWSs are calculated as described in Section 8.3. Counts for Zouerat and BBM are taken from *Todd et al.* [2013] and *Allen et al.* [2015] respectively.

8.4.1. Regional-scale controls on dust mechanism variability across the CWS

Model composites of 925hPa temperature and geopotential height for June 2011 show the SHL (as identified by the temperature maximum and geopotential height minimum) centred near BBM (Figure 8-9, left). Both ALAM and ERAI (which was not used in the dust mechanism identification methodology and is presented to provide an independent view) show a similar large-scale circulation structure, although the values of the temperature maximum and geopotential height minimum are different (33.5°C in ALAM and 35°C in ERAI, 764 gpm in ALAM and 752 gpm in ERAI). North and east of the SHL, the pressure gradient is very steep in both models (Figure 8-9, left). In conjunction with the temperature gradient, this sets up a clear easterly and north-easterly flow between the Hoggar and Atlas mountain ranges, which reaches the easternmost AWSs (Figure 8-9, right). The high number of LLJs detected at AWSs 131, 134, 138 and 140 (Figure 8-8) is thus a consequence of their location in the large scale mean Harmattan flow into the SHL. These strong winds, time-averaged in Figure 8-9, are a regular feature, occurring in ALAM on at least 24 mornings in June 2011 in the topographic gap between the Hoggar and the Atlas Mountains (Figure 8-10).

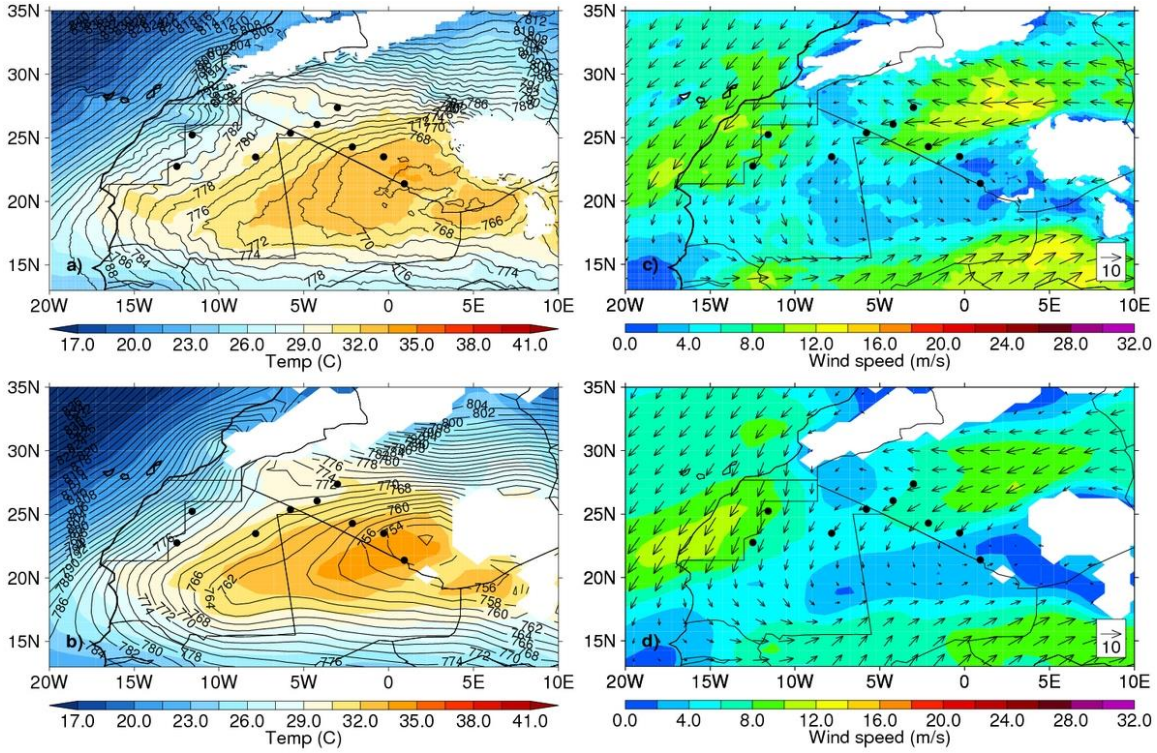

Figure 8-9: Composite maps of June 2011 925hPa temperature and geopotential height (left) and 925hPa winds (right). Upper panels are from 0600 ALAM simulations and lower panels are from 0600 ERAI simulations. The boxed arrow in the bottom right of panels (c) and (d) represents a 10 m s^{-1} wind vector. The black circles are the locations of the Fennec supersites and AWSs (see Figure 8-8 for labels). Topography above the 925hPa level is shown in white.

The second region where the pressure gradient is particularly strong is along the coast (Figure 8-9, left). The strong winds ventilate the western edge of the SHL (Figure 8-9), and likely result in the high number of LLJ detections at Zouerat and AWS 141, where they are particularly common (Figure 8-8 and Figure 8-10).

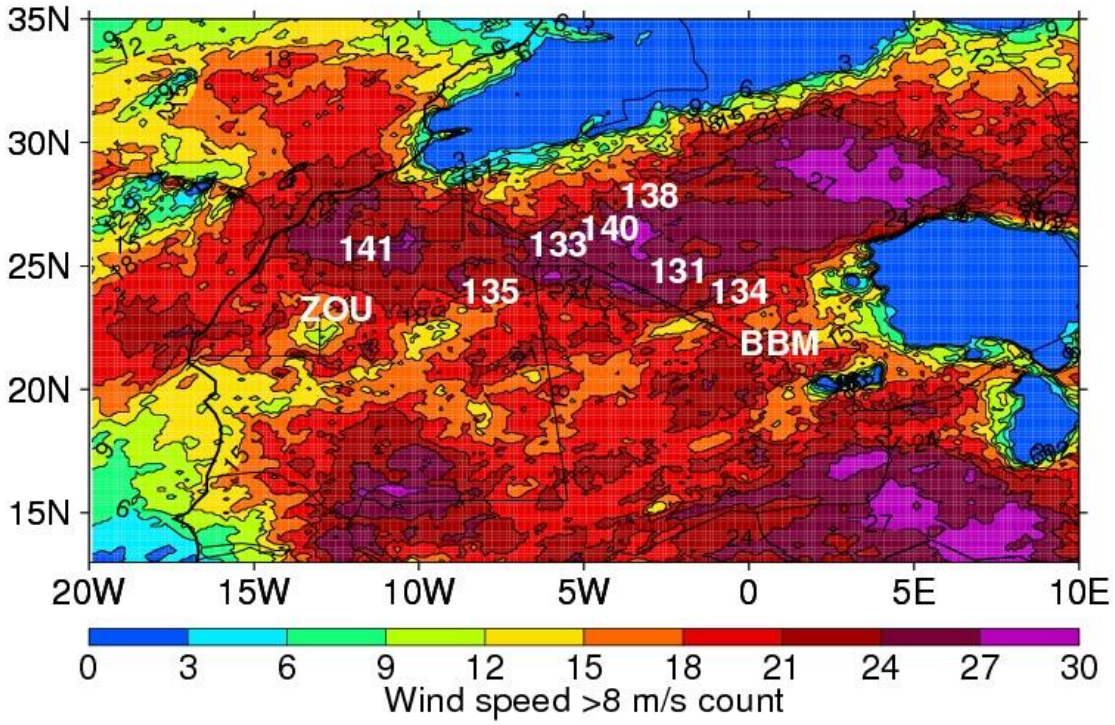

Figure 8-10: Contour map showing number of times ALAM 925hPa wind speed exceeds 8 m s^{-1}, summed for every morning (i.e. every 0600 timestep) of June 2011. E.g. if wind speeds at a gridbox exceed 8m/s on every morning the value will be 30. Stations are labelled in white.

Neither ALAM, nor ERAI nor GLOBAL have high enough spatial resolution to simulate cold pools. Their distribution across the CWS (Figure 8-8) is in part due to the proximity of the south-easternmost stations to the moisture brought to the southern reaches of the Sahara by the south-westerly monsoon winds (Figure 8-9, right). Backtracking the cold pools to their point of origin (not shown) using SEVIRI imagery shows that 41% of cold pools detected at the AWSs originate from northern Mali or southern Algeria, roughly corresponding to the 'Mali-Algeria border' and 'Mali-Algeria-Niger triple point' dust hotspots identified by *Ashpole and Washington* [2013a]. However, the two northernmost AWSs, 138 and 140, also have a relatively high frequency of cold pool occurrence (Figure 8-8). SEVIRI imagery shows that of the cold

pools detected at stations 138 and 140, 58% and 36% respectively originate over the Atlas, particularly from Morocco or north-east Algeria. Some of these Atlas cold pools travel even further south: at the remaining AWSs (141, 135, 133, 131 and 134) 18-25% detected cold pools arrive from the Atlas region, in the most extreme case having travelled roughly 1500 km. Comprehensive studies of cold pool activity in the Sahara should therefore not just focus on the southern (summer monsoon-influenced) reaches of the desert.

8.5. Surface wind speeds across the CWS

The wind measurements that the AWSs recorded are a valuable tool for understanding dust emission and for model evaluation. Since the lowest model wind speeds are at 10 m height in ALAM and GLOBAL, for comparison it is necessary to scale the AWS 2 m wind speeds to 10 m. This is done using the commonly-used wind profile power law relationship

$$wspd_{pred} = wspd_{obs} * (Z_{pred}/Z_{obs})^{\alpha} \qquad [1]$$

where Z_{pred} is the height at which the wind speed is being predicted (i.e. 10 m), Z_{obs} is the height at which the wind speed is known (i.e. 2 m), $wspd_{pred}$ is the wind speed at Z_{pred}, $wspd_{obs}$ is the wind speed that is observed and α is an exponent set to 1/7.

To test the suitability of the wind profile power law, 2 m AWS wind measurements at BBM in June 2012 (there was no AWS at BBM in June 2011) are used to predict the 10 m wind speed. These predictions can be verified because the flux tower 10 m wind measurements are also available in June 2012. For this purpose the flux tower measurements are averaged to the same time resolution as the AWS cup anemometer (200 s). Both qualitatively and quantitatively there is good agreement between the predicted and observed 10 m wind speeds (Figure 8-11), with the Spearman Rank

correlation coefficient at 0.81 (n=10792). Errors between 0600 and 1800 are <0.5 m s^{-1} (within the uncertainty of the cup anemometer, Table 8-2) and do not exceed ~1 m s^{-1} at other times.

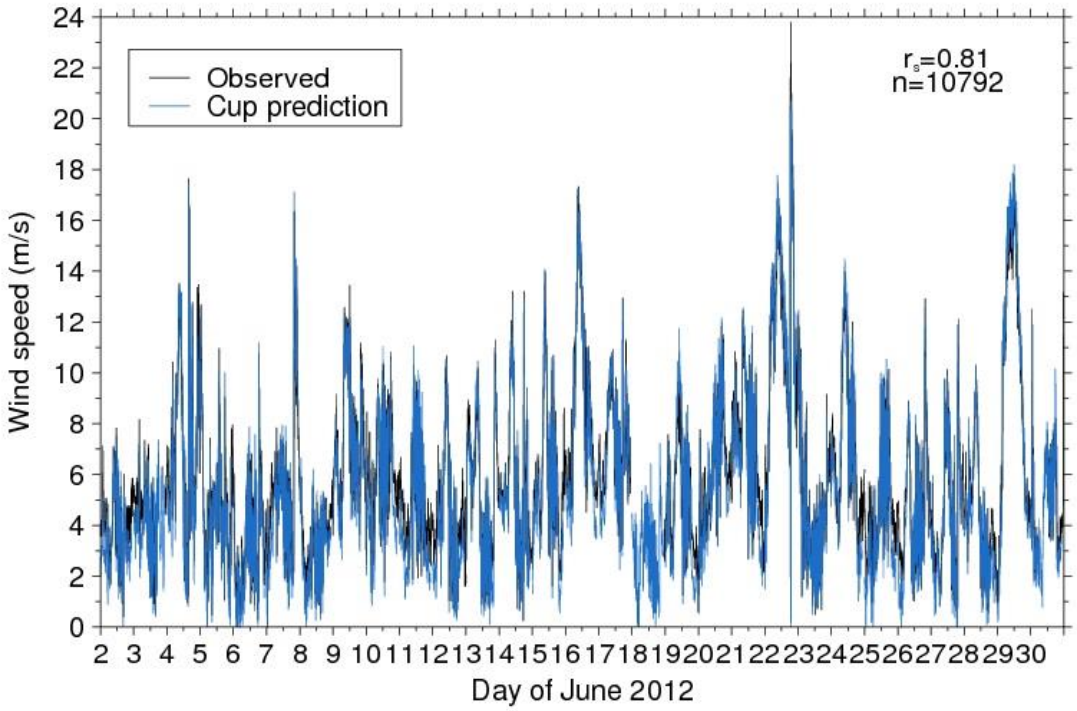

Figure 8-11: Time series of observed 10 m wind speeds at BBM in June 2012 (black) and predicted 10 m wind speeds obtained using the wind profile power law (Equation 1) applied to the AWS cup anemometer measurements at 2 m (blue). In the top right are shown the Spearman Rank correlation coefficient (r_s) between the two curves and the number of observations used (n). AWS data is not available on 1 June 2012 at BBM.

8.5.1. Observed surface wind speed variability

Surface (i.e. 10 m) wind speeds at most AWSs and at BBM have a roughly unimodal and positively-skewed distribution (Figure 8-12). At three AWSs (131, 133, 134) the modal wind speed is 2-3 m s^{-1}. At BBM the modal wind speed is 4-5 m s^{-1} and at AWS 138 it is 6-7 m s^{-1}. AWS 140 has an apparently bimodal wind speed distribution, with a peak at 2-3 m s^{-1} and a smaller peak at 8-9 m s^{-1}, this second peak perhaps due to the

location of AWS 140 at a point where strong 925hPa winds are frequent (Figure 8-10), increasing the likelihood of momentum mix-down. However, AWS 140 only has 4 days of measurements during the IOP (Table 8-3), so confidence in its wind measurements is reduced. All stations have a long tail extending out to at least 15-16 m s^{-1} and in most cases further, up to 19-20 m s^{-1} (Figure 8-12). This long tail is particularly important for dust emission, since dust emission is a threshold process more closely proportional to the cube of wind speed than wind speed alone [e.g. *Bagnold*, 1941; *Gillette*, 1974; *Darmenova et al.*, 2009]; this relationship is also seen to be the case at BBM [*Allen et al.*, 2013, their Table 3].

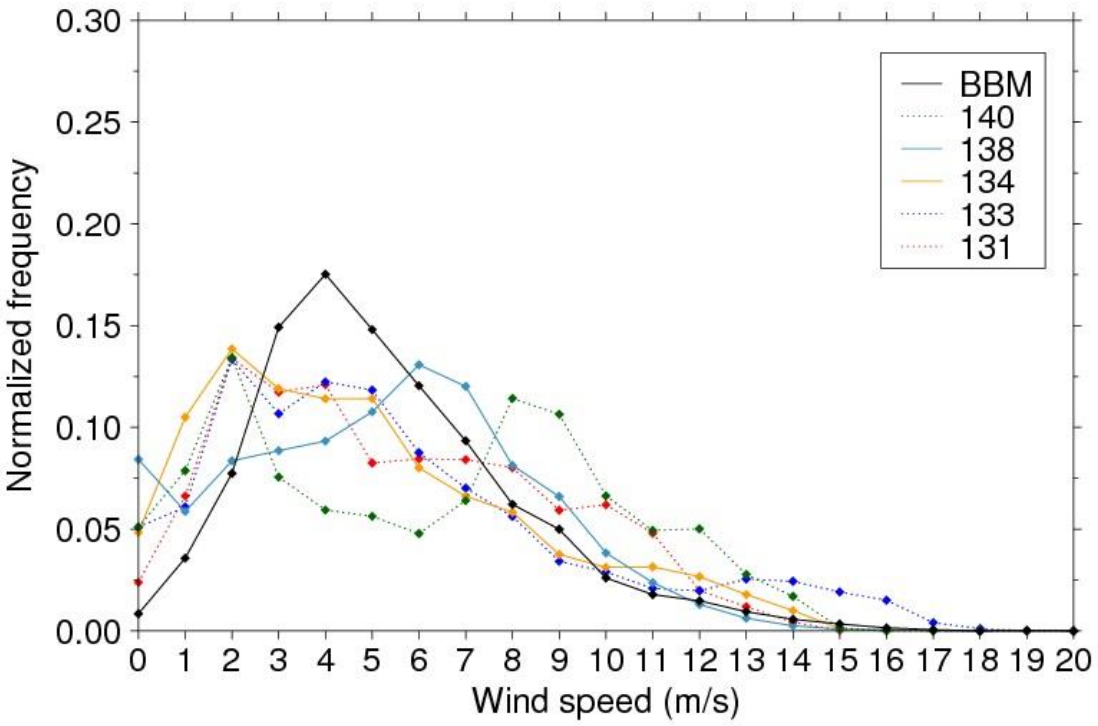

Figure 8-12. Histogram showing normalized frequency of wind speed at 10 m height at BBM and AWSs where there are at least four days of measurements (Table 8-3). AWSs which have complete measurements for June 2011 are shown in solid lines; AWSs which do not are shown in dotted lines. BBM has measurements for most of June 2011 (Table 8-1). AWS 141 is not included because it does not have a cup anemometer (see Section 8.2.1). Bins are constructed so that the corresponding wind speed on the x-axis refers to the lower bound (e.g. the first diamonds are for the 0-1 m s^{-1} bin).

Focusing on the stations which have complete or near-complete observations (i.e. those plotted in solid lines on Figure 8-12) it is not immediately clear why the wind speeds are distributed differently. AWSs 134 and 138 record a similar number of cold pools and LLJs (Figure 8-8), but quite different modal surface wind speeds (2-3 m s^{-1} and 6-7 m s^{-1}, Figure 8-12). The explanation may be the position of AWS 138, which is the northernmost station and, in ALAM at least, lies in a region where strong 925hPa winds are more common than at AWS 134 (Figure 8-10). If LLJs tend to be stronger over AWS 138 than AWS 134, then a larger proportion of them is likely lead to momentum mix-down to the surface and higher surface wind speeds. The modal surface wind speed at BBM (4-5 m s^{-1}) is between the modal wind speeds of AWSs 134 and 138 (Figure 8-12), possibly reflecting that, whilst strong 925hPa wind speeds are less common at BBM than at AWS 138 (Figure 8-10), BBM receives more cold pools than AWS 134 (Figure 8-8). There is no obvious relationship between the length or 'fatness' of the surface wind speed tail and the number of cold pools and the number of LLJs.

8.5.2. Modelled surface wind speed variability

If numerical models are used to model dust emission or to drive off-line dust emission schemes, the surface wind speeds must be simulated as accurately as possible. Here we compare the surface wind speed distributions of the three stations with complete or near-complete observations (BBM, AWSs 134 and 138) with ALAM and GLOBAL. Model and observed surface wind speeds are at 10 m height (see Section 8.5). Note that the model surface wind speeds were not used as part of the dust mechanism detection methodology (Section 8.3) because this would likely underestimate the occurrence of momentum mix-down (as indeed shown to be the case below). AWSs 134 and 138 are LLJ-dominated whilst BBM records an equal number of cold pools and LLJs (Figure 8-8). At all three stations, the models significantly overpredict surface wind speeds

between roughly 1 and 6 m s^{-1} (Figure 8-13). GLOBAL shows the most extreme overpredictions of low wind speeds at all stations, and in particular at BBM. This suggests that either the lower spatial resolution or lower time resolution of GLOBAL model output compared to ALAM reduces its accuracy (both have the same vertical resolution and a similar boundary layer scheme). This will be discussed further below. Both models (with two odd exceptions in GLOBAL at AWS 134) underpredict surface wind speeds greater than 6 m s^{-1} (Figure 8-13). Their lack of a 'long tail' is a serious problem for dust emission since the threshold wind speed for emission across different parts of the Sahara is at least 6 m s^{-1}, and frequently twice as high [*Helgren and Prospero*, 1987; *Chomette et al.*, 1999; *Todd et al.*, 2007; *Allen et al.*, 2013; *Marsham et al.*, 2013]. Moreover, as mentioned above, dust emission is proportional to the cube of the wind speed. At BBM, the underprediction of the high surface wind speeds is at least in part because the models do not generate cold pools, which are particularly frequent here. Since LLJs themselves are generally well simulated (Section 8.3.1), the underprediction of the surface winds speeds by ALAM at the LLJ-dominated AWSs 134 and 138 is likely caused by difficulties simulating the transport of the momentum towards the surface, and hence the model boundary layer dynamics. It is not known whether GLOBAL suffers from similar difficulties because the data is only archived at 6 h resolution. This is a serious limitation because it misses the peak momentum mix-down time at 0900 (discussed further below).

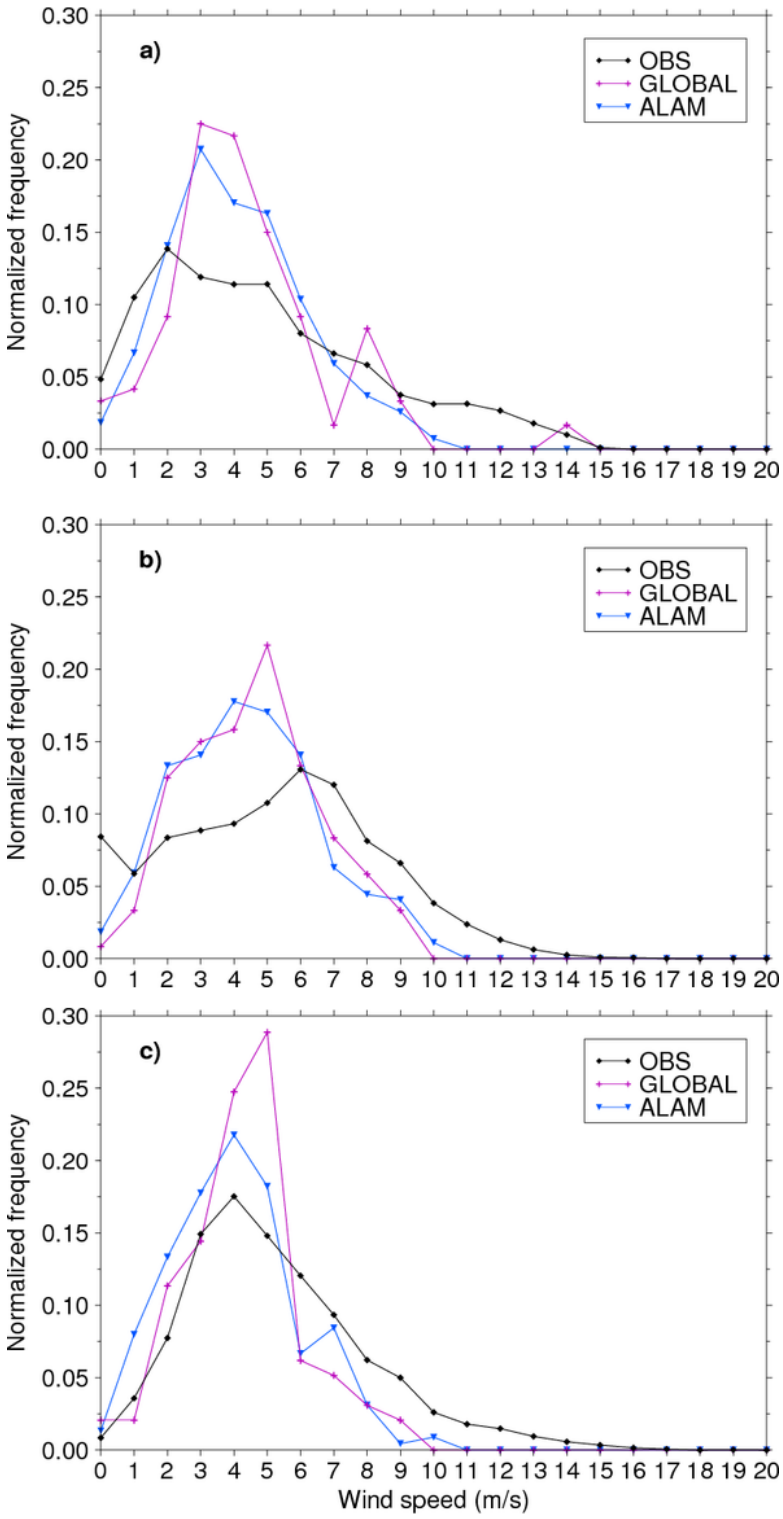

Figure 8-13: Histograms showing normalized frequency of 10 m wind speed for June 2011 in the observations (OBS, black), ALAM (blue) and GLOBAL (purple). Each panel shows a different location: (a) AWS 134, (b) AWS 138, (c) BBM. Bins are constructed so that the corresponding wind speed on the x-axis refers to the lower bound (e.g. the first symbols are for the 0-1 m s^{-1} bin).

Across all the stations (Figure 8-8), there are 77 occasions in June 2011 when station wind speed observations suggest that LLJ momentum is mixing down (see also Section 8.3.10; sonic anemometer measurements have to be used for AWS 141). On 48 (i.e. 62%) of these occasions, ALAM simulates a similarly timed Gaussian-like (or at least triangular) increase and decrease in surface wind speeds after sunrise, suggesting that it has 'captured' something of the momentum mix-down in these cases. However, there is still a significant minority (38%) of cases when ALAM does not capture momentum mix-down. Examples of 'successful' and 'unsuccessful' ALAM momentum mix-down are shown in Figure 8-14a and b respectively. At AWS 131 on 4 June 2011 ALAM simulates a LLJ and also manages to capture the observed increase and decrease in wind speeds at the surface between 0600 and 1200, even simulating the magnitude of the peak very close to observations (Figure 8-14a). However, at AWS 134 on 17 June 2011, despite simulating a LLJ ALAM fails to capture the momentum mix down which peaks at 0900 in the observations (Figure 8-14b).

The peak 0600 ALAM wind speed below 600 m agl (see Section 8.3.1) averaged on days when ALAM 'captures' momentum mix-down is 14.6 m s^{-1}. On days when ALAM surface winds do not capture momentum mix-down it is 11.6 m s^{-1} (not shown). This suggests that if ALAM doesn't simulate a 'strong enough' jet, momentum will not mix down to the surface in the model. Indeed, on 14 of the 77 occasions (i.e. 18%) when station wind speed observations suggest that LLJ momentum is mixing down, ALAM does not simulate a LLJ profile at all. However, the strength or presence of a LLJ in the model is not alone sufficient to explain why model momentum does not always mix down: there are 10 mornings when surface observations suggest momentum mix-down, ALAM simulates a strong (core wind speed $\geq$14 m s^{-1}) LLJ but does not capture momentum mix-down at the surface (e.g. Figure 8-14b). Therefore it is likely that the

model boundary layer is not transporting momentum from the LLJ core downwards as it should in these cases. A detailed assessment of the causes for this is beyond the scope of this paper.

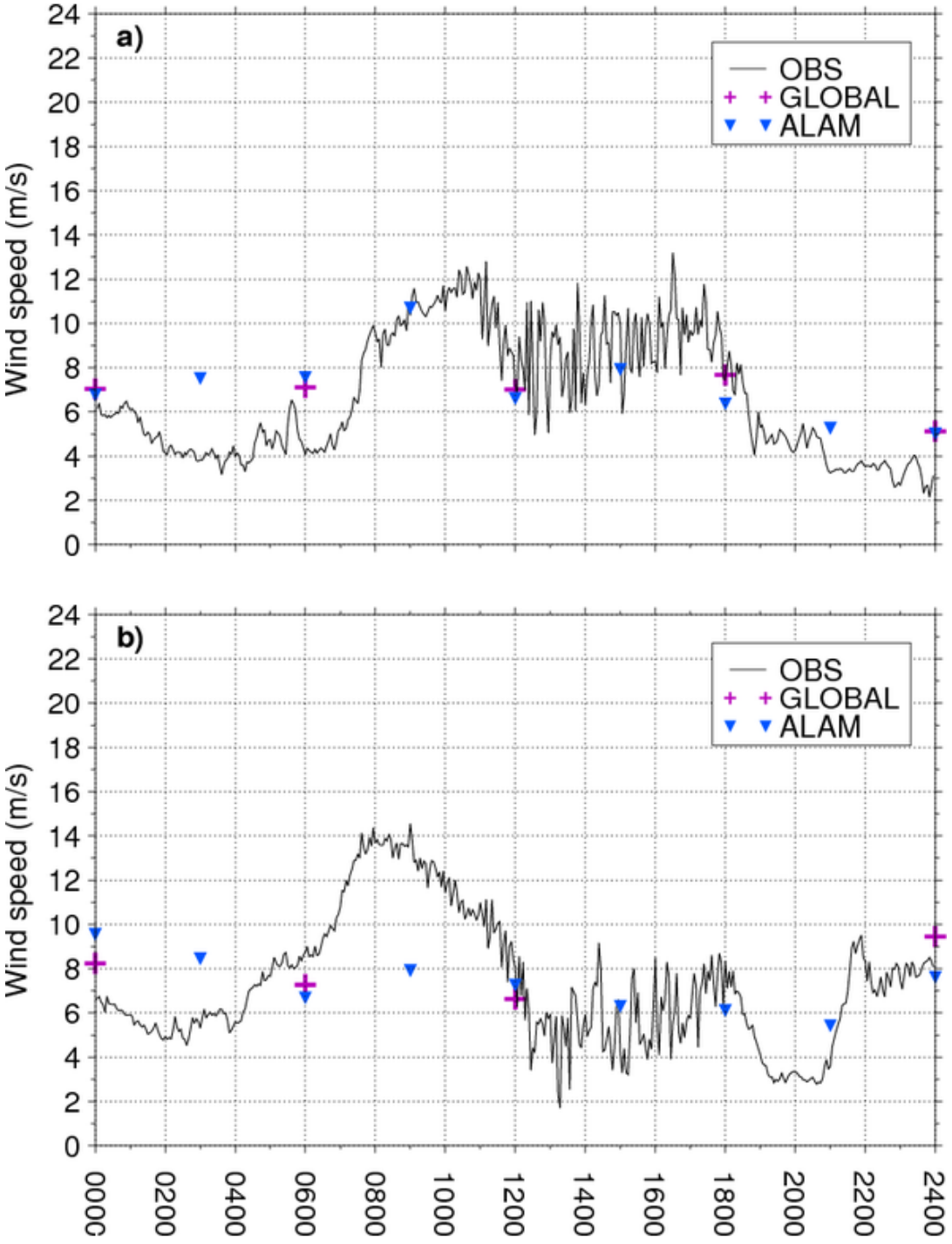

Figure 8-14: Timeseries of observed and modelled 10 m wind speed at (a) AWS 131 on 4 June 2011 (b) AWS 134 on 17 June 2011.

Of the 77 occasions when station surface wind speed observations suggest that LLJ momentum is mixing down, GLOBAL only 'captures' this pattern in surface wind speeds 16 times (21%) – doing much worse than ALAM, which has a success rate of 62% (see above). Both models have the same vertical resolution and a similar boundary layer scheme, so this is unlikely to be the cause of the difference. It is possible that the problem lies in the reduced spatial resolution of GLOBAL, but this did not appear to impact its simulation of LLJs themselves (Section 8.3.1). What is certain is that having output data only every six hours (as in GLOBAL here) is a severe limitation. Of the 77 occasions when station surface wind speed observations suggest that LLJ momentum is mixing down, on 46 (60%) the peak surface wind speeds occur within an hour of 0900, and are therefore not recorded by GLOBAL (e.g. Figure 8-14). It is therefore crucial that studies that use models to calculate dust emission in the Sahara archive data at least every three hours, and in particular in the mid-morning. This has also been highlighted by *Fiedler et al.* [2013].

8.6. Discussion

8.6.1. Importance of different dust mechanisms across the CWS

This study has used new Fennec ground observations to identify the main dust producing mechanisms in the remote CWS in June 2011 and documented their variability across the region (Table 8-4, Figure 8-8). The two most frequently occurring mechanisms are cold pool outflows and LLJs. Dry convective plumes/dust devils and monsoon surges are mostly negligible in these measurements (Table 8-4). In the case of dry convective plumes/dust devils, their calculated frequency is almost certainly an underestimate. This is because, unlike the detection of other mechanisms which also employs satellite and model data, the detection of dry convective plumes/dust devils is

based entirely on the meteorological measurements available which have many gaps (Table 8-3). However, where data is complete or near-complete (e.g. AWS 138 or BBM) the number is still small (Table 8-4). Of course, many could pass near the sensors but not close enough to be detected, which is another source of underestimation, and a more general problem for detection of small-scale dust mechanisms. However, it seems unlikely that the error is such that it could come close to make dry convective plumes/dust devils responsible for 35% of dust emission, the global estimate calculated by *Koch and Renno* [2005]. Indeed, *Jemmett-Smith et al.* [2015] estimate that the global contribution of dry convective plumes and dust devils is just 3.4%, much closer to the <2% estimate at BBM found by *Allen et al.* [2013]. The discrepancy between the estimates of *Jemmett-Smith et al.* [2015] and *Koch and Renno* [2005] results from a 2.5 times smaller dust source area available in *Jemmett-Smith et al.* [2015] (the study uses the source map of *Ginoux et al.* [2001]) and 2.5 times fewer hours of dry convective plume/dust devil activity in *Jemmett-Smith et al.* [2015], which the authors suggest is because of strong winds over intense dust sources suppressing dry convective plume/dust devil formation. Note however that the definition of dry convective plumes here only extends to dust raised by afternoon gustiness (Section 8.3.4): dry convection is additionally responsible for mixing LLJ momentum down to the surface and this is implicitly included in the LLJ partitioning category.

In the case of monsoon surges, the low number detected (Table 8-4) is not so surprising given that the southerly monsoon flow reaches further north in July than June, in agreement with the fact that the two monsoon surges that were detected were at the southernmost station, BBM, and in the last five days of June. With regard to other 'candidate' dust mechanisms such as AEWs, depressions and cyclones, we suggest that these may be acting mostly indirectly to produce dust via embedded cold pool outflows

or LLJs, as has been seen in satellite and reanalysis data [e.g. *Knippertz and Todd*, 2010]: the detection criteria appear not to have missed any major dust producing mechanisms (Section 8.3.5).

Given the data availability, it was only possible to provide counts of the incidence of dust mechanisms, not event durations or measures of dustiness. The contributions of the dust mechanisms in these terms warrants some consideration, since it is dust concentration and residence time in the atmosphere that is important for radiative forcing and possible feedbacks on the meteorology [e.g. *R L Miller et al.*, 2004; *Ryder et al.*, 2013]. The LLJ criteria record LLJs themselves rather than dust emission caused by LLJs (Section 8.3.1). When SEVIRI suggests that a dust-producing LLJ is present then this is recorded as a LLJ (Figure 8-4), but this only happens 15 times and LLJs are detected up to 208 times across the CWS (Table 8-4). By contrast, of the up-to 108 times cold pools are detected (Table 8-4), on 78 (i.e. 72%) occasions associated cold pool dust is also visible in SEVIRI. This is not to say that LLJs only lead to dust emission on 15 occasions across the CWS: SEVIRI has well-known difficulties detecting dust in the morning when temperature inversions are present or under moist conditions [*Brindley et al.*, 2012]. Indeed at BBM in June 2011 two of the strongest dust-emitting LLJs did not have a signal in SEVIRI [*Allen et al.*, 2013]. However, what is clear is that not all LLJs lead to dust emission. At BBM in June 2011, 21 LLJs were detected but only five (i.e. 24%) resulted in dust emission [*Allen and Washington*, 2014].

To address this further, we consider the observed characteristics of the dust emitting LLJs at BBM. These can be well constrained since in IOP1 BBM had high resolution wind profile and dust measurements from a lidar, high resolution dust measurements from a nephelometer and high resolution surface wind speed measurements from the

flux tower. The observed characteristics of the dust emitting LLJs were found to be core wind speeds ≥16 m s^{-1}, below-core wind shear ≥0.6 m s^{-1}/30m, and wind shear between the core and 500 m above the core ≤-1.8 m s^{-1} [*Allen and Washington*, 2014]. *Fiedler et al.* [2013], who use ERAI and an offline dust emission model over North Africa, find that the median LLJ wind speed during dust emission ranges from 14-16 m s^{-1}, in good agreement with the 16 m s^{-1} threshold found at BBM. In ALAM, 69 of the 194 LLJs detected over the CWS stations in June 2011 (i.e. 36%) share the BBM observed 'dust emitting jet' characteristics. In GLOBAL however, only 15 of the 123 LLJs detected (i.e. 12%) are 'dust emitting'. Whilst ALAM has excellent representation of northerly/north-easterly Harmattan LLJs at BBM [*Allen and Washington*, 2014], GLOBAL simulates the wind speeds at the radiosonde stations closer to the observations (Section 8.3.1). It is therefore not clear which is likely to be more accurate across the remote CWS. But what is clear is that the LLJ contribution to dust emission is much less than their frequency (Figure 8-8) might suggest, as dust emission caused by LLJs likely occurs on only a minority (12-36%) of cases.

In terms of their duration, at BBM in both June 2011 and June 2012 individual cold pool outflow events tended to last longer than individual LLJ-induced emission events [*Allen et al.*, 2015]. In June 2011, the authors found the median duration of cold pools to be 11 h and of LLJ-induced emission 6.25 h. If these differences are preserved across the CWS then cold pools are likely to be larger contributors to dust burden than their frequency (Figure 8-8) might suggest. Exceptions would be if the cold pools are travelling long distances to the stations (as is the case for a non-negligible minority of events across the CWS, Section 8.4.1), since it is likely that their dust load is reduced by gravitational settling, particularly if emission is no longer taking place.

An idea of the 'efficiency' of different dust mechanisms is given in Figure 11 of *Allen et al.* [2013]. The authors partition dust mechanisms at BBM by the percentage time they occupy, and also the percentage nephelometer scattering (i.e. dustiness) they cause. Although cold pool emission only occurs for 17% of the IOP, it is responsible for 45% nephelometer scattering. Cold pool advection occurs for 18% of the IOP, but is responsible for a disproportionately large amount of nephelometer scattering, 27%. By contrast, LLJ-induced emission occurs for 12% of the IOP, but only results in 14% of nephelometer scattering. These relationships suggest that cold pools are more 'efficient' at producing dust than LLJ-induced emission, yet again raising their importance for dust production beyond what might be expected from their frequency of occurrence.

To summarise, the frequency of cold pools and LLJs (Figure 8-8) does not by itself tell us about the importance of the mechanisms for dust. Since the majority of LLJs do not result in dust emission and if they do it (i) lasts for less time on average than cold pools and (ii) raises dust less efficiently, their frequency of occurrence exaggerates their importance. Conversely, given that the average duration of cold pools is longer than LLJ-induced emission, and that they are more efficient at producing dust, their frequency of occurrence understates their importance. BBM provides a case in point: although the number of LLJs and cold pools is the same in June 2011 (Table 8-4), it is well established that cold pools are responsible for far more dust at the site [*Allen et al.*, 2013; *Marsham et al.*, 2013]. At all the other stations, LLJs are more frequent than cold pools (Figure 8-8). If these values are adjusted according to the reasoning above so that LLJs are ascribed less importance for dust and cold pools more, then their contribution becomes more similar, and indeed this is what is found by *Heinold et al.* [2013], who used convection-permitting simulations of the Met Office Unified Model over summertime West Africa and found that 40% of dust emission was from LLJs and 40%

from cold pools. Unfortunately there were no dust-measuring instruments at the AWSs so a more detailed quantitative comparison cannot be made.

8.6.2. Model simulation of surface wind speeds across the CWS

The importance of correctly simulating 10m wind speeds for dust emission was convincingly demonstrated by *Laurent et al.* [2008]. The authors calculated dust production in the Bodélé Depression, the world's largest single dust source [*Washington et al.*, 2003], using an explicit mineral dust emission scheme driven with two different soil databases and four different 10m wind databases (from mesoscale numerical models). *Laurent et al.* [2008] found that the major uncertainty in dust emission was due to the 10m wind, with the difference between the four wind databases resulting in more than an order of magnitude difference in dust emission. Such divergences can arise because dust emission is a function of the third power of wind speed, meaning that small underestimations of wind speed result in large underestimations of dust emission.

At AWSs 134 and 138 (which have complete wind data for June 2011, Table 8-3) and at BBM (which has near-complete wind data, Table 8-1), the frequency of 10 m wind speeds greater than about 6 m s^{-1} is almost always underestimated in both ALAM and GLOBAL (Figure 8-13). With an isolated exception in GLOBAL at AWS 134, 10m wind speeds greater than 11 m s^{-1} are completely missed (Figure 8-13). Both models lack the 'long tail' in wind speeds that is observed and instead overpredict wind speeds below 6 m s^{-1}. Since dust emission thresholds across the Sahara are at least 6 m s^{-1}, and frequently twice as high [*Helgren and Prospero*, 1987; *Chomette et al.*, 1999; *Todd et al.*, 2007; *Allen et al.*, 2013; *Marsham et al.*, 2013], wind speeds from these models cannot be expected to lead to realistic dust emission, at least at these three stations.

Given the cubic dependence of dust emission on wind speed, the models' lack of a long tail will result in significant underestimates of dust emission.

Despite the increase in horizontal resolution available to ALAM compared to GLOBAL (12km compared to 25km), 10 m wind speeds are not simulated noticeably more accurately (except for a reduced overprediction of wind speeds less than 6 m s^{-1} (Figure 8-13), which is of little consequence for dust emission). Both models have the same vertical resolution and a similar boundary layer scheme. However, the higher time resolution of ALAM model output (3-hourly compared to 6-hourly for GLOBAL) is an advantage when it comes to simulating surface wind speeds related to LLJs. On 60% occasions when station surface wind speed observations suggest that LLJ momentum is mixing down, the peak surface wind speeds occur within an hour of 0900. With GLOBAL wind speeds only available at 0000, 0600, 1200 and 1800, these peak surface wind speeds are missed. Thus even though GLOBAL simulates the 0600 LLJ wind profiles more accurately than ALAM at the radiosonde stations (possibly suggesting that information from beyond the limited area model domain is important for LLJ simulation, Section 8.3.1), this advantage is lost because only 6-hourly data is available. The importance of high temporal resolution of model output for LLJ-induced emission has also been highlighted by *Fiedler et al.* [2013], who use ERAI.

Numerical models which do not simulate convection explicitly (horizontal resolution coarser than roughly 7km) have poor or no representation of cold pools [*Reinfried et al.*, 2009; *Marsham et al.*, 2011; *Solomos et al.*, 2012]. The observed 'long tail' of high winds at BBM, which is dominated by cold pools, is underpredicted by GLOBAL and ALAM (Figure 8-13c). The long tail of high winds at AWSs 134 and 138, which are dominated by LLJs, is also underpredicted by GLOBAL and ALAM (Figure 8-13a,b).

Since ALAM and GLOBAL simulate LLJs reasonably well, it is likely that the underprediction of high wind speeds at the surface at these two stations results from (i) output not being archived at 0900 (GLOBAL) (ii) difficulty mixing momentum from the LLJs downwards (ALAM, unknown for GLOBAL). The latter problem has also been documented over the Sahara in the regional model COSMO-MUSCAT [*Heinold et al.*, 2011].

Improvements in dust emission in both global and regional models can be made by including subgrid-scale surface wind variability [*Lunt and Valdes,*2002; *Cakmur et al.*, 2004; *R L Miller et al.*, 2006; *Marcella and Eltahir*, 2010]. At each gridbox, a probability distribution of wind speed is constructed and emission depends on the fraction of the wind speed distribution above the emission threshold, rather than depending on the explicitly resolved wind speed [*Cakmur et al.*, 2004]. The authors show that, due to subgrid wind variability, the mean wind speed (as calculated from the probability distribution) is always higher than the explicitly resolved wind speed. Including subgrid variability results in a significant improvement of the simulated aerosol optical thicknesses compared to the Total Ozone Mapping Spectrometer satellite retrieval: over the Sahara in June, the underestimation of aerosol optical thickness was reduced from 0.55 to 0.1 [*Cakmur et al.*, 2004].

Cakmur et al. [2004] and *R L Miller et al.* [2006] consider three different velocity scales for subgrid variability: mechanical mixing in the boundary layer due to surface drag, gust fronts created by moist downdraughts (i.e. cold pool outflows) and dry convective thermals. All three are present in the Sahara in summer. Including such subgrid-scale wind variability would be likely to improve the ALAM and GLOBAL wind speed distributions, and any dust schemes driven by them. Interestingly, *Cakmur et al.* [2004]

find that the contribution of dry convective thermals to the subgrid wind variability is the most important for improving dust loadings. Fennec ground-based observations suggest that dry convective plumes are only responsible for a small fraction of dust (<2% at BBM [*Allen et al.*, 2013]). They are infrequent in observations across the CWS (Table 8-4). However, their definition is strict here and only refers to dust-raising afternoon gustiness caused by thermals. More broadly speaking, dry convection plays a dual role in that it is also an important driver of momentum mix-down from LLJs [e.g. *Blackadar*, 1957] which can then result in dust emission [e.g. *Washington et al.*, 2006; *Knippertz*, 2008; *Schepanski et al.*, 2009; *Allen and Washington*, 2014]. This role of dry convection is not included in the 'dry convective plume' category (see Section 8.3.4) but implicitly in detection of LLJ mixdown. Since models do not always capture momentum mix-down (e.g. Figure 8-14), including subgrid-scale wind variability from dry convection may improve the surface wind speeds in regions where LLJs occur.

8.7. Conclusion

Fennec ground-based observations have been used in conjunction with model and satellite data to document the wind mechanisms across the CWS which have the capability to lead to dust emission ('dust mechanisms'). By far the most frequent mechanisms are cold pool outflows and LLJs (Table 8-4). LLJs are most frequent in the north-west and north-east CWS (Figure 8-8), where they are associated with ventilation of the SHL from the Atlantic in the north-west and the Harmattan flow into the SHL in the north-east (Figure 8-9). In the central CWS LLJs are still more frequent than cold pools but their detection uncertainty is larger (Figure 8-8). Dust mechanisms occur more frequently at BBM than any other station, in agreement with its position near the boreal summer global dust maximum [*Ashpole and Washington*, 2012]. BBM is somewhat unusual in recording a very high frequency of cold pools (Figure 8-8). However, cold

pools are recorded at every station. Northern Mali and southern Algeria are the most frequent source regions of cold pools reaching the Fennec stations, although a noteworthy minority originate over the Atlas, particularly from Morocco or north-east Algeria, in some cases travelling over 1000km into the desert interior.

The frequency of the dust mechanisms is not directly proportional to their contribution to the Saharan dust burden. Although LLJs themselves are very frequent, only an estimated 12-36% of those detected will be strong enough to lead to dust emission. The capability of LLJs to lead to dust emission is weakened by the Atlantic Inflow at Zouerat [*Todd et al.*, 2013] and presumably this will also be the case at AWS 141, which shares the same climatological setting. At BBM, dust emission by LLJs has been found to be less efficient than cold pool dust emission [*Allen et al.*, 2013], and LLJ dust emission typically lasts for a shorter time period [*Allen et al.*, 2015]. If these characteristics are common to the rest of the CWS then the importance of LLJs to the dust burden is exaggerated by their frequency and the importance of cold pools is understated.

Wind speeds over 6 m s^{-1} at the AWSs and at BBM are significantly underpredicted. Since wind speed thresholds for dust emission are at least 6 m s^{-1} across the Sahara and dust emission is proportional to the cube of wind speed, these model underpredictions will result in large underestimations of dust emission. At stations where LLJs occur, high temporal resolution of model output is vital for capturing momentum mix-down, which takes place within an hour of 0900 on 60% occasions, and thus cannot be captured by models with archived output only every six hours. The improved horizontal resolution of ALAM compared to GLOBAL (12km and 25km respectively) does not appear to improve simulation of LLJs or surface wind speeds. Improvements in model-

driven dust emission in the CWS therefore seem likely to stem from improved temporal resolution of model output, increased horizontal resolution to the point where convection is explicitly resolved and/or inclusion of subgrid-scale wind variability.

8.8. Acknowledgements

Fennec was funded by a NERC consortium grant (NE/G017166/1). The authors wish to thank the following individuals and institutions. For building the bespoke AWS and supersite instrumentation: M Hobby, M Gascoyne, University of Leeds. For establishing and operating the supersites and/or deploying the AWSs: B Abderrahmane, M Bart, M Bechir, BJ Brooks, C Cavazos-Guerra, F Davies, S Engelstaedter, DM Fadel, A Gandega, L Garcia-Carreras, M Gascoyne, M Hobby, A Lima, M Limam, JH Marsham, V Martins, JB McQuaid, A O'Leary, B Ouchene, A Ouladichir, DJ Parker, A Saci, M Salah-Ferroudj, F Seddik, D Sidali, M Sidi, MC Todd, S Traore, the AERONET PHOTONS team, ONM Algérie, ONM Mauritanie, ASECNA, the University of Leeds, the University of Oxford and the University of Sussex. For providing the SEVIRI imagery at http://www.fennec.imperial.ac.uk: H Brindley and J Banks. For the ALAM and GLOBAL model datasets: UK Met Office. For the SDF dataset: I Ashpole. We also thank FGAM (Facility for Ground-based Atmospheric Measurement), UK Met Office and NCAS (National Centre for Atmospheric Science) for the use of the sodar, lidar and radiosonde units. Datasets are available upon request from the authors.

8.9. References

Allen, C. J. T., and R. Washington (2014), The low-level jet dust emission mechanism in the central Sahara: Observations from Bordj-Badji Mokhtar during the June 2011 Fennec Intensive Observation Period, *Journal of Geophysical Research: Atmospheres*, doi: 10.1002/2013jd020594.

Allen, C. J. T., R. Washington, and S. Engelstaedter (2013), Dust emission and transport mechanisms in the central Sahara: Fennec ground-based observations from Bordj Badji Mokhtar, June 2011, *Journal of Geophysical Research: Atmospheres*, *118*, 6212–6232, doi: 10.1002/jgrd.50534.

Allen, C. J. T., R. Washington, and A. Saci (2015), Dust detection from ground-based observations in the summer global dust maximum: Results from Fennec 2011 and 2012 and implications for modeling and field observations, *Journal of Geophysical Research: Atmospheres*, *120*(3), 897-916, doi: 10.1002/2014jd022655.

Ansmann, A., M. Tesche, P. Knippertz, E. Bierwirth, D. Althausen, D. Müller, and O. Schulz (2009), Vertical profiling of convective dust plumes in southern Morocco during SAMUM, *Tellus B*, *61*(1), 340-353, doi: 10.1111/j.1600-0889.2008.00384.x.

Ashpole, I., and R. Washington (2012), An automated dust detection using SEVIRI: A multiyear climatology of summertime dustiness in the central and western Sahara, *J. Geophys. Res.*, *117*(D8), D08202, doi: 10.1029/2011jd016845.

Ashpole, I., and R. Washington (2013a), Intraseasonal variability and atmospheric controls on daily dust occurrence frequency over the central and western Sahara during the boreal summer, *Journal of Geophysical Research: Atmospheres*, *118*(23), 2013JD020267, doi: 10.1002/2013jd020267.

Ashpole, I., and R. Washington (2013b), A new high-resolution central and western Saharan summertime dust source map from automated satellite dust plume tracking, *Journal of Geophysical Research D: Atmospheres*, *118*(13), 6981-6995, doi: 10.1002/jgrd.50554.

Bagnold, R. A. (1941), *The Physics of Blown Sand and Desert Dunes*, Methuen, London.

Balme, M., and R. Greeley (2006), Dust devils on Earth and Mars, *Reviews of Geophysics*, *44*(3), doi: 10.1029/2005RG000188.

Blackadar, A. K. (1957), Boundary layer wind maxima and their significance for the growth of nocturnal inversion, *Bull. Am. Meteorol. Soc*, *38*(5), 283-290.

Bou Karam, D., C. Flamant, J. Cuesta, J. Pelon, and E. Williams (2010), Dust emission and transport associated with a Saharan depression: February 2007 case, *Journal of Geophysical Research-Atmospheres*, *115*, doi: 10.1029/2009jd012390.

Bou Karam, D., C. Flamant, P. Tulet, M. C. Todd, J. Pelon, and E. Williams (2009), Dry cyclogenesis and dust mobilization in the intertropical discontinuity of the West African Monsoon: A case study, *Journal of Geophysical Research-Atmospheres*, *114*, doi: 10.1029/2008jd010952.

Bou Karam, D., C. Flamant, P. Knippertz, O. Reitebuch, J. Pelon, M. Chong, and A. Dabas (2008), Dust emissions over the Sahel associated with the West African monsoon intertropical discontinuity region: A representative case-study, *Quarterly Journal of the Royal Meteorological Society*, *134*(632), 621-634, doi: 10.1002/qj.244.

Bou Karam, D., E. Williams, M. Janiga, C. Flamant, M. McGraw-Herdeg, J. Cuesta, A. Auby, and C. Thorncroft (2014), Synoptic-scale dust emissions over the Sahara Desert initiated by a moist convective cold pool in early August 2006, *Quarterly Journal of the Royal Meteorological Society*, *140*(685), 2591-2607, doi: 10.1002/qj.2326.

Brindley, H., P. Knippertz, C. Ryder, and I. Ashpole (2012), A critical evaluation of the ability of the Spinning Enhanced Visible and Infrared Imager (SEVIRI) thermal infrared red-green-blue rendering to identify dust events: Theoretical analysis, *Journal of Geophysical Research D: Atmospheres*, *117*(7), doi: 10.1029/2011JD017326.

Cakmur, R. V., R. L. Miller, and O. Torres (2004), Incorporating the effect of small-scale circulations upon dust emission in an atmospheric general circulation model, *Journal of Geophysical Research: Atmospheres*, *109*(D7), D07201, doi: 10.1029/2003jd004067.

Chomette, O., M. Legrand, and B. Marticorena (1999), Determination of the wind speed threshold for the emission of desert dust using satellite remote sensing in the thermal infrared, *Journal of Geophysical Research-Atmospheres*, *104*(D24), 31207-31215, doi: 10.1029/1999jd900756.

Couvreux, F., F. Guichard, O. Bock, B. Campistron, J. P. Lafore, and J. L. Redelsperger (2010), Synoptic variability of the monsoon flux over West Africa prior to the onset, *Quarterly Journal of the Royal Meteorological Society*, *136*(S1), 159-173, doi: 10.1002/qj.473.

Cuesta, J., J. H. Marsham, D. J. Parker, and C. Flamant (2009), Dynamical mechanisms controlling the vertical redistribution of dust and the thermodynamic structure of the West Saharan atmospheric boundary layer during summer, *Atmospheric Science Letters*, *10*(1), 34-42, doi: 10.1002/asl.207.

Darmenova, K., I. N. Sokolik, Y. Shao, B. Marticorena, and G. Bergametti (2009), Development of a physically based dust emission module within the Weather Research and Forecasting (WRF) model: Assessment of dust emission parameterizations and input parameters for source regions in Central and East Asia, *Journal of Geophysical Research: Atmospheres*, *114*(D14), n/a-n/a, doi: 10.1029/2008jd011236.

Dee, D. P., S. M. Uppala, A. J. Simmons, P. Berrisford, P. Poli, S. Kobayashi, U. Andrae, M. A. Balmaseda, G. Balsamo, P. Bauer, P. Bechtold, A. C. M. Beljaars, L. van de Berg, J. Bidlot, N. Bormann, C. Delsol, R. Dragani, M. Fuentes, A. J. Geer, L. Haimberger, S. B. Healy, H. Hersbach, E. V. Hólm, L. Isaksen, P. Kållberg, M. Köhler, M. Matricardi, A. P. McNally, B. M. Monge-Sanz, J. J. Morcrette, B. K. Park, C. Peubey, P. de Rosnay, C. Tavolato, J. N. Thépaut, and F. Vitart (2011), The ERA-Interim reanalysis: configuration and performance of the data assimilation system, *Quarterly Journal of the Royal Meteorological Society*, *137*(656), 553-597, doi: 10.1002/qj.828.

Emmel, C., P. Knippertz, and O. Schulz (2010), Climatology of convective density currents in the southern foothills of the Atlas Mountains, *J. Geophys. Res.*, *115*(D11), D11115, doi: 10.1029/2009jd012863.

Engelstaedter, S., I. Tegen, and R. Washington (2006), North African dust emissions and transport, *Earth-Science Reviews*, *79*(1–2), 73-100, doi: 10.1016/j.earscirev.2006.06.004.

Fiedler, S., K. Schepanski, B. Heinold, P. Knippertz, and I. Tegen (2013), Climatology of Nocturnal Low-Level Jets over North Africa and Implications for Modeling Mineral Dust Emission, *Journal of Geophysical Research: Atmospheres*, *118*, 6100–6121, doi: 10.1002/jgrd.50394.

Fiedler, S., K. Schepanski, P. Knippertz, B. Heinold, and I. Tegen (2014), How important are atmospheric depressions and mobile cyclones for emitting mineral dust aerosol in North Africa?, *Atmos. Chem. Phys.*, *14*(17), 8983-9000, doi: 10.5194/acp-14-8983-2014.

Flamant, C., P. Knippertz, D. J. Parker, J. P. Chaboureau, C. Lavaysse, A. Agusti-Panareda, and L. Kergoat (2009), The impact of a mesoscale convective system cold pool on the northward propagation of the intertropical discontinuity over West Africa, *Quarterly Journal of the Royal Meteorological Society*, *135*(638), 139-159, doi: 10.1002/qj.357.

Flamant, C., J. P. Chaboureau, D. J. Parker, C. M. Taylor, J. P. Cammas, O. Bock, F. Timouk, and J. Pelon (2007), Airborne observations of the impact of a convective system on the planetary boundary layer thermodynamics and aerosol distribution in the inter-tropical discontinuity region of the West African Monsoon, *Quarterly Journal of the Royal Meteorological Society*, *133*(626), 1175-1189, doi: 10.1002/qj.97.

Garcia-Carreras, L., J. H. Marsham, D. J. Parker, C. L. Bain, S. Milton, A. Saci, M. Salah-Ferroudj, B. Ouchene, and R. Washington (2013), The impact of convective cold pool outflows on model biases in the Sahara, *Geophysical Research Letters*, *40*(8), 1647-1652, doi: 10.1002/grl.50239.

Gillette, D. A. (1974), On the production of soil wind erosion aerosols having the potential for long-range transport, *J. Rech. Atmos.*, *8*, 735-744.

Ginoux, P., M. Chin, I. Tegen, J. M. Prospero, B. Holben, O. Dubovik, and S.-J. Lin (2001), Sources and distributions of dust aerosols simulated with the GOCART model, *Journal of Geophysical Research: Atmospheres*, *106*(D17), 20255-20273, doi: 10.1029/2000jd000053.

Grams, C. M., S. C. Jones, J. H. Marsham, D. J. Parker, J. M. Haywood, and V. Heuveline (2010), The Atlantic inflow to the Saharan heat low: observations and modelling, *Quarterly Journal of the Royal Meteorological Society*, *136*(S1), 125-140, doi: 10.1002/qj.429.

Heinold, B., I. Tegen, S. Bauer, and M. Wendisch (2011), Regional modelling of Saharan dust and biomass-burning smoke Part 2: Direct radiative forcing and atmospheric dynamic response, *63*(4).

Heinold, B., P. Knippertz, J. H. Marsham, S. Fiedler, N. S. Dixon, K. Schepanski, B. Laurent, and I. Tegen (2013), The role of deep convection and nocturnal low-level jets for dust emission in summertime West Africa: Estimates from convection-permitting simulations, *Journal of Geophysical Research: Atmospheres*, *118*, 4385–4400, doi: 10.1002/jgrd.50402.

Helgren, D. M., and J. M. Prospero (1987), Wind Velocities Associated with Dust Deflation Events in the Western Sahara, *Journal of Climate and Applied Meteorology*, *26*(9), 1147-1151, doi: 10.1175/1520-0450(1987)026<1147:wvawdd>2.0.co;2.

Hobby, M., M. Gascoyne, J. H. Marsham, M. Bart, C. J. T. Allen, S. Engelstaedter, D. M. Fadel, A. Gandega, R. Lane, J. B. McQuaid, B. Ouchene, A. Ouladichir, D. J. Parker, P. Rosenberg, M. S. Ferroudj, A. Saci, F. Seddik, M. Todd, D. Walker, and R. Washington (2013), The Fennec Automatic Weather Station (AWS) Network: Monitoring the Saharan Climate System, *Journal of Atmospheric and Oceanic Technology*, *30*(4), 709-724, doi: 10.1175/jtech-d-12-00037.1.

Holben, B. N., T. F. Eck, I. Slutsker, D. Tanré, J. P. Buis, A. Setzer, E. Vermote, J. A. Reagan, Y. J. Kaufman, T. Nakajima, F. Lavenu, I. Jankowiak, and A. Smirnov (1998), AERONET - A federated instrument network and data archive for aerosol characterization, *Remote Sensing of Environment*, *66*(1), 1-16, doi: 10.1016/s0034-4257(98)00031-5.

Jemmett-Smith, B. C., J. H. Marsham, P. Knippertz, and C. A. Gilkeson (2015), Quantifying global dust devil occurrence from meteorological analyses, *Geophysical Research Letters*, 2015GL063078, doi: 10.1002/2015gl063078.

Jickells, T. D., Z. S. An, K. K. Andersen, A. R. Baker, G. Bergametti, N. Brooks, J. J. Cao, P. W. Boyd, R. A. Duce, K. A. Hunter, H. Kawahata, N. Kubilay, J. laRoche, P. S. Liss, N. Mahowald, J. M. Prospero, A. J. Ridgwell, I. Tegen, and R. Torres (2005), Global Iron Connections Between Desert Dust, Ocean Biogeochemistry, and Climate, *Science*, *308*(5718), 67-71, doi: 10.1126/science.1105959.

Jones, C., N. Mahowald, and C. Luo (2003), The Role of Easterly Waves on African Desert Dust Transport, *Journal of Climate*, *16*(22), 3617-3628, doi: 10.1175/1520-0442(2003)016<3617:troewo>2.0.co;2.

Kallistratova, M. A., and R. D. Kouznetsov (2012), Low-Level Jets in the Moscow Region in Summer and Winter Observed with a Sodar Network, *Boundary-Layer Meteorology*, *143*(1), 159-175, doi: 10.1007/s10546-011-9639-8.

Knippertz, P. (2008), Dust emissions in the West African heat trough the role of the diurnal cycle and of extratropical disturbances, *Meteorologische Zeitschrift*, *17*(5), 553-563, doi: 10.1127/0941-2948/2008/0315.

Knippertz, P., and A. H. Fink (2006), Synoptic and dynamic aspects of an extreme springtime Saharan dust outbreak, *Quarterly Journal of the Royal Meteorological Society*, *132*(617), 1153-1177, doi: 10.1256/qj.05.109.

Knippertz, P., and M. C. Todd (2010), The central west Saharan dust hot spot and its relation to African easterly waves and extratropical disturbances, *J. Geophys. Res.*, *115*(D12), D12117, doi: 10.1029/2009jd012819.

Knippertz, P., and M. C. Todd (2012), Mineral dust aerosols over the Sahara: Meteorological controls on emission and transport and implications for modeling, *Reviews of Geophysics*, *50*(1), doi: 10.1029/2011RG000362.

Knippertz, P., C. Deutscher, K. Kandler, T. Müller, O. Schulz, and L. Schütz (2007), Dust mobilization due to density currents in the Atlas region: Observations from the Saharan Mineral Dust Experiment 2006 field campaign, *J. Geophys. Res.*, *112*(D21), D21109, doi: 10.1029/2007jd008774.

Koch, J., and N. O. Renno (2005), The role of convective plumes and vortices on the global aerosol budget, *Geophys. Res. Lett.*, *32*(18), L18806, doi: 10.1029/2005gl023420.

Laurent, B., B. Heinold, I. Tegen, C. Bouet, and G. Cautenet (2008), Surface wind accuracy for modeling mineral dust emissions: Comparing two regional models in a Bodélé case study, *Geophysical Research Letters*, *35*(9), L09804, doi: 10.1029/2008gl033654.

Lavaysse, C., C. Flamant, S. Janicot, D. J. Parker, J. P. Lafore, B. Sultan, and J. Pelon (2009), Seasonal evolution of the West African heat low: a climatological perspective, *Climate Dynamics*, *33*(2), 313-330, doi: 10.1007/s00382-009-0553-4.

Lensky, I. M., and D. Rosenfeld (2008), Clouds-Aerosols-Precipitation Satellite Analysis Tool (CAPSAT), *Atmos. Chem. Phys.*, *8*(22), 6739-6753, doi: 10.5194/acp-8-6739-2008.

Lunt, D. J., and P. J. Valdes (2002), The modern dust cycle: Comparison of model results with observations and study of sensitivities, J. Geophys. Res., 107(D23), 4669, doi:10.1029/2002JD002316.

Marcella, M. P., and E. A. B. Eltahir (2010), Effects of mineral aerosols on the summertime climate of southwest Asia: Incorporating subgrid variability in a dust emission scheme, *Journal of Geophysical Research: Atmospheres*, *115*(D18), D18203, doi: 10.1029/2010jd014036.

Marsham, J. H., D. J. Parker, C. M. Grams, C. M. Taylor, and J. M. Haywood (2008), Uplift of Saharan dust south of the intertropical discontinuity, *J. Geophys. Res.*, *113*(D21), D21102, doi: 10.1029/2008jd009844.

Marsham, J. H., P. Knippertz, N. S. Dixon, D. J. Parker, and G. M. S. Lister (2011), The importance of the representation of deep convection for modeled dust-generating winds over West Africa during summer, *Geophys. Res. Lett.*, *38*(16), L16803, doi: 10.1029/2011gl048368.

Marsham, J. H., M. Hobby, C. J. T. Allen, J. R. Banks, M. Bart, B. J. Brooks, C. Cavazos-Guerra, S. Engelstaedter, M. Gascoyne, A. R. Lima, J. V. Martins, J. B. McQuaid, A. O'Leary, B. Ouchene, A. Ouladichir, D. J. Parker, A. Saci, M. Salah-Ferroudj, M. C. Todd, and R. Washington (2013), Meteorology and dust in the central Sahara: Observations from Fennec supersite-1 during the June 2011 Intensive Observation Period, *Journal of Geophysical Research: Atmospheres*, *118*, 4069–4089, doi: 10.1002/jgrd.50211.

Miller, R. L., J. Perlwitz, and I. Tegen (2004), Feedback upon dust emission by dust radiative forcing through the planetary boundary layer, *Journal of Geophysical Research: Atmospheres*, *109*(D24), D24209, doi: 10.1029/2004jd004912.

Miller, R. L., R. V. Cakmur, J. Perlwitz, I. V. Geogdzhayev, P. Ginoux, D. Koch, K. E. Kohfeld, C. Prigent, R. Ruedy, G. A. Schmidt, and I. Tegen (2006), Mineral dust aerosols in the NASA Goddard Institute for Space Sciences ModelE atmospheric general circulation model, *Journal of Geophysical Research: Atmospheres*, *111*(D6), D06208, doi: 10.1029/2005jd005796.

Miller, S. D., A. P. Kuciauskas, M. Liu, Q. Ji, J. S. Reid, D. W. Breed, A. L. Walker, and A. A. Mandoos (2008), Haboob dust storms of the southern Arabian Peninsula, *Journal of Geophysical Research D: Atmospheres*, *113*(1), doi: 10.1029/2007JD008550.

Nunalee, C. G., and S. Basu (2013), Mesoscale modeling of coastal low-level jets: implications for offshore wind resource estimation, *Wind Energy*, *17*, 1199-1216, doi: 10.1002/we.1628.

Oke, A. M. C., N. J. Tapper, and D. Dunkerley (2007), Willy-willies in the Australian landscape: The role of key meteorological variables and surface conditions in defining frequency and spatial characteristics, *Journal of Arid Environments*, *71*(2), 201-215, doi: 10.1016/j.jaridenv.2007.03.008.

Pérez, C., S. Nickovic, G. Pejanovic, J. M. Baldasano, and E. Özsoy (2006), Interactive dust-radiation modeling: A step to improve weather forecasts, *Journal of Geophysical Research: Atmospheres*, *111*(D16), D16206, doi: 10.1029/2005jd006717.

Prospero, J. M., P. Ginoux, O. Torres, S. E. Nicholson, and T. E. Gill (2002), Environmental characterization of global sources of atmospheric soil dust identified with the NIMBUS 7 Total Ozone Mapping Spectrometer (TOMS) absorbing aerosol product, *Rev. Geophys.*, *40*(1), 1002, doi: 10.1029/2000rg000095.

Reinfried, F., I. Tegen, B. Heinold, O. Hellmuth, K. Schepanski, U. Cubasch, H. Huebener, and P. Knippertz (2009), Simulations of convectively-driven density currents in the Atlas region using a regional model: Impacts on dust emission and sensitivity to horizontal resolution and

convection schemes, *Journal of Geophysical Research: Atmospheres*, *114*(D8), D08127, doi: 10.1029/2008jd010844.
Renno, N. O., M. L. Burkett, and M. P. Larkin (1998), A Simple Thermodynamical Theory for Dust Devils, *Journal of the Atmospheric Sciences*, *55*(21), 3244-3252, doi: 10.1175/1520-0469(1998)055<3244:asttfd>2.0.co;2.
Roberts, A. J., and P. Knippertz (2014), The formation of a large summertime Saharan dust plume: Convective and synoptic-scale analysis, *Journal of Geophysical Research: Atmospheres*, *119*(4), 1766-1785, doi: 10.1002/2013jd020667.
Ryder, C. L., E. J. Highwood, T. M. Lai, H. Sodemann, and J. H. Marsham (2013), Impact of atmospheric transport on the evolution of microphysical and optical properties of Saharan dust, *Geophysical Research Letters*, *40*(10), 2433-2438, doi: 10.1002/grl.50482.
Ryder, C. L., J. B. McQuaid, C. Flamant, R. Washington, H. E. Brindley, E. J. Highwood, J. H. Marsham, D. J. Parker, M. C. Todd, J. R. Banks, J. K. Brooke, S. Engelstaedter, V. Estellés, P. Formenti, L. Garcia-Carreras, C. Kocha, F. Marenco, P. Rosenberg, H. Sodemann, C. J. T. Allen, A. Bourdon, M. Bart, C. Cavazos-Guerra, S. Chevaillier, J. Crosier, E. Darbyshire, A. R. Dean, J. R. Dorsey, J. Kent, D. O'Sullivan, K. Schepanski, K. Szpek, and A. Woolley (2015), Advances in understanding mineral dust and boundary layer processes over the Sahara from Fennec aircraft observations, *Atmos. Chem. Phys. Discuss.*, *15*(1), 199-290, doi: 10.5194/acpd-15-199-2015.
Schepanski, K., and P. Knippertz (2011), Soudano-Saharan depressions and their importance for precipitation and dust: a new perspective on a classical synoptic concept, *Quarterly Journal of the Royal Meteorological Society*, *137*(659), 1431-1445, doi: 10.1002/qj.850.
Schepanski, K., I. Tegen, B. Laurent, B. Heinold, and A. Macke (2007), A new Saharan dust source activation frequency map derived from MSG-SEVIRI IR-channels, *Geophys. Res. Lett.*, *34*(18), L18803, doi: 10.1029/2007gl030168.
Schepanski, K., P. Knippertz, S. Fiedler, F. Timouk, and J. Demarty (2014), The sensitivity of nocturnal low-level jets and near-surface winds over the Sahel to model resolution, initial conditions and boundary-layer set-up, *Quarterly Journal of the Royal Meteorological Society*, n/a-n/a, doi: 10.1002/qj.2453.
Schepanski, K., I. Tegen, M. C. Todd, B. Heinold, G. Bönisch, B. Laurent, and A. Macke (2009), Meteorological processes forcing Saharan dust emission inferred from MSG-SEVIRI observations of subdaily dust source activation and numerical models, *J. Geophys. Res.*, *114*(D10), D10201, doi: 10.1029/2008jd010325.
Shao, Y., K.-H. Wyrwoll, A. Chappell, J. Huang, Z. Lin, G. H. McTainsh, M. Mikami, T. Y. Tanaka, X. Wang, and S. Yoon (2011), Dust cycle: An emerging core theme in Earth system science, *Aeolian Research*, *2*(4), 181-204, doi: 10.1016/j.aeolia.2011.02.001.
Solomos, S., G. Kallos, E. Mavromatidis, and J. Kushta (2012), Density currents as a desert dust mobilization mechanism, *Atmospheric Chemistry and Physics*, *12*(22), 11199-11211, doi: 10.5194/acp-12-11199-2012.
Todd, M. C., R. Washington, J. V. Martins, O. Dubovik, G. Lizcano, S. M'Bainayel, and S. Engelstaedter (2007), Mineral dust emission from the Bodélé Depression, northern Chad, during BoDEx 2005, *J. Geophys. Res.*, *112*(D6), D06207, doi: 10.1029/2006jd007170.
Todd, M. C., C. J. T. Allen, M. Bart, M. Bechir, J. Bentefouet, B. J. Brooks, C. Cavazos-Guerra, T. Clovis, S. Deyane, M. Dieh, S. Engelstaedter, C. Flamant, L. Garcia-Carreras, A. Gandega, M. Gascoyne, M. Hobby, C. Kocha, C. Lavaysse, J. H. Marsham, J. V. Martins, J. B. McQuaid, J. B. Ngamini, D. J. Parker, T. Podvin, A. Rocha-Lima, S. Traore, Y. Wang, and R. Washington (2013), Meteorological and dust aerosol conditions over the Western Saharan region observed at Fennec supersite-2 during the Intensive Observation Period in June 2011, *Journal of Geophysical Research: Atmospheres*, *118*, 8426–8447, doi: 10.1002/jgrd.50470.
Walters, D. N., M. J. Best, A. C. Bushell, D. Copsey, J. M. Edwards, P. D. Falloon, C. M. Harris, A. P. Lock, J. C. Manners, C. J. Morcrette, M. J. Roberts, R. A. Stratton, S. Webster, J. M. Wilkinson, M. R. Willett, I. A. Boutle, P. D. Earnshaw, P. G. Hill, C. MacLachlan, G. M. Martin, W. Moufouma-Okia, M. D. Palmer, J. C. Petch, G. G. Rooney, A. A. Scaife, and K. D. Williams (2011), The Met Office Unified Model Global Atmosphere 3.0/3.1 and

JULES Global Land 3.0/3.1 configurations, *Geosci. Model Dev.*, *4*(4), 919-941, doi: 10.5194/gmd-4-919-2011.

Washington, R., M. C. Todd, N. J. Middleton, and A. S. Goudie (2003), Dust-Storm Source Areas Determined by the Total Ozone Monitoring Spectrometer and Surface Observations, *Annals of the Association of American Geographers*, *93*(2), 297-313, doi: 10.1111/1467-8306.9302003.

Washington, R., M. C. Todd, S. Engelstaedter, S. Mbainayel, and F. Mitchell (2006), Dust and the low-level circulation over the Bodélé Depression, Chad: Observations from BoDEx 2005, *J. Geophys. Res.*, *111*(D3), D03201, doi: 10.1029/2005jd006502.

Washington, R., C. Flamant, D. J. Parker, J. H. Marsham, J. B. McQuaid, H. Brindley, M. C. Todd, E. Highwood, C. Ryder, J. P. Chaboureau, C. Kocha, M. Bechir, and A. Saci (2012), Fennec - The Saharan Climate System, *CLIVAR Exchanges*, *17*(3), 31-33.

Wilks, D. S. (2006), *Statistical Methods in the Atmospheric Sciences*, 627 pp., Academic Press, London.

9. Thesis Conclusions

This final chapter discusses the overall findings of the research chapters and their wider implications. The first two subsections answer the research aims and present a general discussion. This is followed by a subsection addressing the implications of the research for our understanding of Saharan dust. Lastly, future directions for research are suggested.

9.1. Research aims and results

Six research aims were stated in the Motivation (Chapter 3). An examination of the main results associated with each aim is presented below.

1. *To use Fennec ground-based observations to identify the atmospheric mechanisms that cause dust emission and transport in the Sahara in summer, first at the dust maximum, then across the Fennec instrument network.*

The comprehensive instrumentation available at BBM, particularly in June 2011, made it possible to identify the atmospheric mechanisms responsible for making it the dustiest location in the world in summer. The mechanisms identified were cold pool outflows (both transporting and emitting dust), LLJs, monsoon surges and dry convective plumes (Chapters 5-7). The individual mechanisms could be distinguished because they have distinctive meteorological 'signatures'; for example, dry convective plumes cause a pressure well and LLJs have distinctive wind profiles. The structure and temporal evolution of the lidar backscatter also aided identification; for example, some cold pools have a raised 'nose'. In June 2011 at BBM the instrumentation available made it possible to distinguish between dust advection caused by cold pools and a low-dust 'background' dust loading that was dust in suspension (i.e. wind speeds below the emission threshold) but not possible to attribute.

The Fennec AWS network provided the opportunity to expand the analysis from a point (BBM) to a wider domain (across the CWS). To do this, a methodology was developed to identify atmospheric dust mechanisms at the AWSs (Chapter 8). It was based on the meteorological signature concept but had to incorporate model output, primarily because there were no wind profile observations at the AWSs with which to detect LLJs. Cold pools and LLJs were by far the most frequently occurring dust mechanisms in the CWS, and BBM experienced more than any other station. Monsoon surges were not detected at any Fennec stations in the CWS in June 2011 except BBM. It is likely that they would be detected more frequently in July and August, after the monsoon 'jump', when the ITCZ shifts to a quasi-stationary location around 10°N [*Sultan and Janicot*, 2000].

2. *To ascertain the relative importance of the different atmospheric dust mechanisms.*

Three different metrics can be used to assess the importance of each mechanism: the frequency of occurrence, the total time that each mechanism is present, and the amount of dust associated with each mechanism. The first metric is the most easy to calculate, the last is the most difficult and requires much more comprehensive instrumentation. The metrics do not give the same results, which is in itself informative.

Across the Fennec stations in the CWS, LLJs were the most frequently detected mechanism overall. The proportion of LLJs actually resulting in dust emission could be calculated and studied in detail at BBM in June 2011, thanks to the nephelometer, lidar and radiosondes (Chapter 6). Out of 28 mornings, LLJs were detected on 21 (i.e. 75% mornings). However, only five (i.e. 24% detected jets) resulted in momentum mix-down and dust emission at the surface. Thus the presence of a LLJ wind profile is not enough

to predict dust emission. At BBM in June 2011, LLJ-induced emission was responsible for 14% of the total dust burden.

Across the Fennec stations in the CWS, cold pool outflows were the second most frequently detected dust mechanism (except at BBM, where they were first equal with LLJs). At BBM, the total duration of time occupied by cold pools and their contribution to the dust burden could also be estimated (Chapter 5). In June 2011, cold pool emission occurred for 17% of the IOP, but was responsible for the single largest percentage of dustiness: 45%. By comparison, LLJ-induced dust emission occurred for 12% of the IOP, but was responsible for only 14% dustiness. Therefore not only is cold pool emission the largest single contributor to dustiness in the summer dust maximum region, it is also very 'efficient' at producing dust: more dust is produced per hour of cold pool emission than any other mechanism (average nephelometer scattering 0.047 m^{-1} $hour^{-1}$).

Cold pool dust advection in June 2011 was responsible for 27% dust at BBM, making it the second most important cause of dust presence. The 'background' unattributable dust loading[19] comprised 13% dust, almost as much as the LLJ emission contribution (14%).

Only two monsoon surges were observed at BBM in June 2011, but these were responsible for an impressive 10% nephelometer scattering, with almost the same high 'dust efficiency' as cold pool emission (average nephelometer scattering 0.046 m^{-1} $hour^{-1}$). Dry convective plumes were both infrequent in the Fennec observations across the CWS and responsible for very little dust. Only 7 were detected across all stations in June 2011; the five that occurred at BBM were responsible for < 2% total dust. Note however that the definition of dry convective plumes only extends to

[19] i.e. periods when nephelometer scattering $\leq 2 \times 10^{-4}$ m^{-1} (see Chapter 5)

dust raised by afternoon gustiness (e.g. Section 2.6.3): dry convection is additionally responsible for mixing LLJ momentum down to the surface and this is implicitly included in the LLJ partitioning category.

AWS measurements were used together with SEVIRI, ALAM and GLOBAL to detect atmospheric dust mechanisms in June 2011 across the wider CWS (Chapter 8). LLJs and cold pools were by far the most frequently occurring atmospheric mechanisms, and more occurred at BBM than at any other station. No estimates can be made of the contribution of the mechanisms to the dust burden at the AWSs however, because the local dust emission thresholds are not known and there were no dust detection instruments or observers.

3. *To examine in detail the operation of the LLJ as a dust emission mechanism.*

This examination was motivated in part by the finding that whilst LLJs occur frequently at BBM in June 2011 (75% mornings), they are only responsible for 14% of the dust burden. By explicitly calculating momentum exchanges through the atmospheric column, it was shown that momentum mix-down is indeed the mechanism through which LLJs induce dust emission, but that this can only happen if the LLJ is particularly strong ($\geq$16 m s^{-1}) (Chapter 6). At midnight on dusty mornings, the LLJ is already stronger than the maximum strength the LLJ reaches on nondusty mornings. The depth of wind speeds > 8m s^{-1} is also twice as great, 90–1500m agl compared to 90–700m agl. A 100 metre-deeper convective boundary layer promotes momentum mix-down to the surface in the morning, where post-sunrise surface wind speeds display a Gaussian increase and decay, closely matched by the lidar backscatter from 0700 to 1300. Strong pressure gradients associated with the SHL are the main synoptic-scale control on the

strength of the LLJs. Only 5/21 (24%) LLJs detected at BBM in June 2011 were strong enough to lead to dust emission.

Using the characteristics of dust-emitting LLJs found at BBM, GLOBAL and ALAM wind profiles above the AWSs were screened to detect 'dust-emitting' LLJs (Chapter 8). 12% of the GLOBAL wind profiles and 36% of the ALAM wind profiles were 'dust emitting' LLJs. Although the characteristics of LLJs that lead to dust emission may change across the domain, it still seems reasonable to conclude that only a minority of LLJs result in dust emission across the CWS.

4. *To document the variability of the atmospheric dust mechanisms from one summer to another.*

Chapter 7 addressed this research aim by developing a methodology that could identify atmospheric dust mechanisms at BBM in June 2012 (when limited instrumentation was available) and then compared these results with those from June 2011. Validation of the detection methodology for June 2012 (using a data-denial method applied to the June 2011 results) shows that detection uncertainty is low for all mechanisms except advected dust. This exception is because transported dust often does not have clear meteorological signals at the surface and can be missed by satellite retrieval if the dust loadings are low.

The findings show that although June 2012 is more dusty overall than June 2011 (up to 63% dustier), the ranking of the different atmospheric mechanisms is the same in both June months. This is the case when the total duration of the different mechanisms is compared, and when their total contribution to the dust burden is compared. In both years, emission by cold pool outflows from deep convection causes most dust, followed by dust advection, monsoon surges, LLJ emission and lastly dry convective plumes. The

uncertainties in the June 2012 detection scheme do not change the comparison between the two field seasons. The reason June 2012 is more dusty overall than June 2011 is probably due to the stronger WAM in June 2012, which would have promoted more cold pools and monsoon surges.

5. *To evaluate the fidelity of different measurement approaches to detect dust under central Saharan atmospheric conditions.*

It is possible to infer the presence of atmospheric dust emission mechanisms using routine meteorological instruments, human observers and satellite data; however such approaches struggle to detect advected dust and cannot quantify dust burden (Chapter 7). The limited instrumentation and lack of observers at the AWSs precluded an assessment of the contribution of advected dust at the AWSs (by any metric). It also precluded the calculation of dust burden attributable to each mechanism, although estimates of the frequency of each emission mechanism could be obtained (Chapter 8). It is therefore - unsurprisingly - important that dedicated dust instrumentation is deployed for detailed observational studies of atmospheric dust mechanisms. More important, however, is the choice of dust instrumentation.

Chapter 7 evaluated the different dust detection instrumentation deployed at BBM for the Fennec IOPs. A major finding is that sun photometers – a benchmark dust detection instrument – miss about half of the dust, because of the predominance of atmospheric mechanisms that occur at night or under cloud. In June 2012 at BBM, 16% cold pool emission, 35% dust advection and 64% monsoon surge emission occurred under cloud. Additionally, because of the diurnal cycle of deep convection, cold pool outflows very frequently occurred at night (67% time in June 2011 and 43% in June 2012), when the sun photometer cannot retrieve and when (in general) observers do not report.

As a result, monthly-mean AOD values from regions like the central Sahara where cold pools dominate are highly suspicious. This is particularly important to know when validating satellite retrievals or models: flawed observations could lead to the wrong conclusions about the fidelity of the model. The lidar and nephelometer are particularly useful instruments for dust detection, but whilst the lidar has the advantage of providing height-resolved dust profiles, its size and air conditioning requirement make it a less practical instrument for fieldwork in hot remote desert environments than the nephelometer.

6. *To assess the ability of numerical models to capture the characteristics of LLJs and surface winds in the central Sahara*

Validation of numerical models being particularly important in remote regions where they are heavily relied upon to be accurate, Chapters 6 and 8 examined model simulation of LLJs and of surface wind speeds. The ALAM model simulates the wind profiles of Harmattan LLJs at BBM very successfully, but ERAI reanalyses underestimate the Harmattan profile at all heights. Both ALAM and ERAI significantly underestimate the wind profiles of monsoon LLJs at BBM (by up to 8.5 m s^{-1}). Across the Fennec radiosonde network in the CWS, the GLOBAL model simulates LLJ core wind speeds slightly more accurately than ALAM.

The models evaluated here have difficulties in simulating morning and early-afternoon surface wind speed increases associated with LLJ momentum mix-down. The highest resolution model (ALAM) does best, but on 38% cases at the Fennec stations across the CWS in June 2011 the momentum mix-down is still not captured. This rises to 79% for the GLOBAL model. Both models have the same boundary layer configuration, so this cannot be the cause of the difference, although it will likely be the reason why there is a

problem to begin with. The reason for the poorer performance of GLOBAL is in large part due to the fact that the model does not output data at 0900, the crucial time for momentum mix-down, as also identified by *Fiedler et al.* [2013].

Observations of surface wind speeds from BBM and the AWSs show that there is a 'long tail' of wind speeds greater than about 6 m s^{-1}. ALAM and GLOBAL significantly underpredict the frequency of these high wind speeds compared to the observations. This is partly because ALAM and GLOBAL do not simulate cold pools, but also due to their deficiencies in simulating LLJ momentum mix-down as noted above. Underpredicting the occurrence of wind speeds > 6 m s^{-1} will result in significant underestimates of dust emission, as emission is a threshold process and proportional to the cube of wind speed.

9.2. Discussion

9.2.1. Atmospheric dust mechanisms

This thesis has sought to explain the atmospheric mechanisms that make the central Sahara the dustiest place in the world in boreal summer, principally using observational data from the Fennec Project. Four different atmospheric mechanisms are responsible in unequal proportion for dust emission: cold pool outflows, low level jets, monsoon surges and dry convective plumes. In addition, dust in suspension (i.e. wind speeds too low for emission) is a large contributor to the dust burden. This dust may be in transport (most frequently advected by aged cold pools) or may be a 'background' environmental dust loading whose provenance cannot be identified.

At BBM, it is very clear that only the strongest LLJs (core wind speed ≥ 16 m s^{-1}) lead to dust emission. *Fiedler et al.* [2013], who use ERAI and an offline dust emission model over North Africa, find that the median LLJ wind speed during dust emission

ranges from 14-16 m s^{-1}, in good agreement with the 16 m s^{-1} threshold found at BBM. It is interesting that this threshold is similar but that ERAI tends to underestimate LLJ wind profiles at BBM, suggesting that ERAI may simulate fewer jets of dust-emitting strength than observed. Calculations presented here show that LLJ-induced dust emission is responsible for 14% nephelometer scattering at BBM in June 2011. However, in the vicinity of BBM in June-August *Fiedler et al.* [2013] calculate a LLJ contribution of about 30% to dust emission. This higher contribution than observed may be because ERAI has too coarse spatial resolution to simulate cold pools, which are the prime dust mechanism at BBM. Therefore, in percentage terms, the importance of LLJ emission is inflated when using ERAI. Indeed, if cold pools were removed from the nephelometer data, LLJ emission would be responsible for 50% nephelometer scattering. In this like for like scenario, the 30% estimate of ERAI underestimates the LLJ contribution to dust emission, consistent with the reanalysis underestimating LLJ wind profiles compared with observations.

R L Miller et al. [2004] examine feedbacks on dust emission by dust radiative forcing by using an AGCM with interactive dust. They find that the dust reduces incoming shortwave radiation to the surface, reducing the flux of turbulent heat into the troposphere and hence suppressing turbulent mixing. As a result, downward transport of momentum to the surface is reduced and so is dust emission. This may explain why the observations presented here find that LLJs are frequently present but only lead to a relatively small amount of dust emission (14% nephelometer scattering). BBM is, after all, within kilometres of the boreal summer dust maximum [*Ashpole and Washington*, 2012]. The results of *R L Miller et al.* [2004] may also explain why the estimate of LLJ-induced dust emission calculated by *Heinold et al.* [2013] over West Africa in late summer (40%) is higher than the estimate presented here. Although *Heinold et al.* [2013]

drive the *Tegen et al.* [2002] dust emission scheme with a NWP model that can simulate cold pools, dust is calculated offline and therefore does not contribute to radiative interactions – interactions which may reduce the dust emission from LLJs.

The results presented in this thesis show that cold pools are the most 'efficient' dust producing mechanism: more dust is produced per hour of cold pool emission than any other mechanism. In Chapter 5 (Figure 5-12) it is shown that in general, for the same wind speed, cold pool outflows raise more dust than any other mechanism. Why this should be the case would be an interesting avenue for further research. It is possible that cold pools contain particularly high levels of dust because both advected and locally emitted dust can be present during the passage of a gust front. Another possibility is that the high air density of cold pool outflows results in more dust emission than other mechanisms (for the same wind speed). Indeed, cold pool outflows are a class of density current [*Charba*, 1974] and are often simply called density currents in the meteorological literature [e.g. *Moncrieff and Liu*, 1999; *Grandpeix and Lafore*, 2009; *Emmel et al.*, 2010]. A density term is used in most dust emission parameterisation schemes [e.g. *Marticorena and Bergametti*, 1995]; increasing the density increases emission. The density dependence is thought to be limited in general [e.g. *Kok et al.*, 2014], but perhaps it is important in regions where cold pools dominate dust emission. Ignoring air density – as with an 'uplift potential' approach [e.g. *Marsham et al.*, 2011] – may underestimate dust emission.

Since monsoon surges also behave like density currents [*Bou Karam et al.*, 2008], their high air density may also explain their very high dust production efficiency. The importance of monsoon surges is also highlighted by *Ashpole and Washington* [2013a],

who find using SDF that monsoon surges are associated with days of particularly high dust detection frequency.

Dust advection has been found to be a particularly important feature of the central Saharan observations. In both field seasons at BBM, dust advection occupied the single largest amount of time (19% total hours in June 2011, 18-30% in June 2012) and caused the second largest amount of scattering. *Cowie et al.* [2014] also emphasize the importance of dust advection from their examination of existing station data, particularly in the southern Sahara. Ignoring the contribution of dust advection by focusing solely on fresh emission [e.g. *Marsham et al.*, 2013] will underestimate the total dust burden, and would lead to errors in radiative forcing if this is calculated.

By contrast, dry convective plumes and dust devils are infrequently detected in the Fennec observations and directly responsible for very little dust. Only 7 are detected across all stations in June 2011; the five that occur at BBM are responsible for < 2% total dust. These values are certainly an underestimate because of missing AWS data and because the small spatial scale of dry convective plumes makes them easy to miss. However, the predominance of larger-scale atmospheric mechanisms in the summer suggests that dry convective plumes will only be responsible for a small fraction of the dust overall. *Koch and Renno* [2005] suggest a global contribution of 35%; the work here is in much better agreement with the 3.4% best estimate of *Jemmett-Smith et al.* [2015] as discussed in Chapter 8. As mentioned above, the 'dry convective plume' category is not the total influence of dry convection which is much broader and in particular is a cause of momentum mixdown from LLJs.

The opportunity to undertake a second field season at BBM in June 2012 allowed for a comparison of the relative importance of the dust mechanisms to be made with June

2011. Although June 2012 was up to 63% dustier than June 2011, the ranking of the dust mechanisms (by both total duration and total dustiness) is identical. This result increases confidence that June 2011 was not an unusual season and that cold pools (emitting and advecting dust) are the main contributor to the dust burden in the central Sahara in June, even with interannual variability in total dustiness.

9.2.2. Links to synoptic- and regional-scale phenomena

There is an interesting geographical distribution of the atmospheric dust mechanisms in the CWS. Apart from at BBM, LLJs are more frequent than cold pools across the CWS (although, as discussed, most of these will probably not lead to dust emission). LLJs are particularly frequent to the north-west and north-east of the CWS, and are likely promoted by Atlantic ventilation in the north-west and the extensive Harmattan flow in the north-east. Cold pool outflows are most frequent at BBM, but are also detected in the central and northern CWS. The high frequency of cold pool occurrence at BBM is because of its location closest to WAM convection; however cold pools can travel hundreds of kilometres which explains their presence in the central CWS and in the northern CWS (at AWS 138, 58% cold pools originate from the Atlas Mountains). *Ashpole and Washington* [2012] show that the June dust maximum in SDF is roughly centred on BBM and that relatively lower dust loadings are found over the AWS locations (see also Figures 4-1 and 4-2). Since BBM has exceptionally high cold pool activity compared to the other Fennec stations, the SDF map probably also points to cold pools being more important contributors to summer Saharan dust loadings than LLJs.

Although both cold pools and LLJs are meso-scale phenomena, they are linked inseparably with two regional-scale phenomena: the SHL and the WAM. These

themselves are linked since the low surface pressure at the surface of the SHL is a driving force of the southerly summer monsoon [e.g. *Sultan and Janicot*, 2003]. The SHL organises surface flow around it broadly cyclonically, resulting in easterly and north-easterly LLJs to its north and southerly and south-westerly LLJs to its south. Indeed, the orientation of LLJs at BBM has been shown here to depend on the geographic location of the SHL (Chapter 6). The role of the monsoon in summer dust emission in north Africa has been addressed by many studies previously [e.g. *Engelstaedter and Washington*, 2007; *Flamant et al.*, 2007; *Bou Karam et al.*, 2008; *Knippertz*, 2008; *Flamant et al.*, 2009; *Ashpole and Washington*, 2013a; *Fiedler et al.*, 2013]. However, these studies were all based on satellite-derived or model data, or on aircraft results from the Sahel. This thesis confirms and quantifies the importance of the monsoon for driving dust emission and advection using central Saharan observations, both directly (monsoon surges) and indirectly (cold pool outflows, LLJs embedded in the monsoon flow). The importance of the monsoon for dust was highlighted by contemporaneous Fennec research at BBM [*Marsham et al.*, 2013]. By contrast Fennec results from Zouerat, which is not influenced by WAM, show that dust loadings here in June 2011 were generally low [*Todd et al.*, 2013]. It would be reasonable to speculate that summers when the WAM is stronger should be more dusty; this is the case at BBM in June 2012 compared with June 2011. Developing a formal statistical association or prediction scheme would be an interesting avenue for further research.

9.2.3. Moisture in the desert

It is a somewhat endearing finding that, in the hyper-arid central Sahara, moist processes are the ones that are predominantly responsible for the high levels of dust in summer. Indeed, the only dust mechanisms that are not associated with moisture in some way are Harmattan LLJs and dry convection, which are together responsible for

less than 9% observed dust at BBM in June 2011. There is an interesting scale dimensionality too, since moist processes play a role on a very small scale (evaporation of rain droplets leads to latent cooling which causes cold pool outflows [*Krumm*, 1954]) and on the continental scale (the WAM circulation). A bolder argument would be that a more distant monsoon system also deserves credit. *Rodwell and Hoskins* [1996] propose that large scale descent over the Sahara is a result of a Rossby wave response to diabatic heating in the Asian summer monsoon region. Since adiabatic descent over the Sahara is a major cause of the SHL which drives the WAM, and WAM is directly or indirectly responsible for most of the dust in the central Sahara in summer, the case could even be made that the Asian monsoon is partly responsible for the central Sahara being the summer global dust maximum!

More prosaically, the importance of moisture for dust in the central Sahara makes it very important that models are able to accurately simulate moist processes, from evaporation to WAM dynamics. Numerical models without explicit convection cannot simulate cold pool outflows [e.g. *Reinfried et al.*, 2009], the prime dust mechanism in the central Sahara. The results presented here show that numerical models and reanalyses also significantly underestimate the strength of LLJs embedded in the moist monsoon flow. *Engelstaedter et al.* [2015] examine moisture transport in the SHL from Fennec aircraft observations and find that ALAM mixes moisture too deeply, and transports it in two perpendicular directions, neither of which is the same as observed. This is concerning since even if models with explicit convection become more commonly used, the location of the convection is particularly important from an erodibility perspective.

Improving the modelling of moist processes will have other benefits beyond dust. For example, *Marcella and Eltahir* [2008] find substantial improvements in model rainfall over Kuwait when a more realistic sub-cloud evaporation scheme is included. When cold pools occur at BBM, Met Office Global Model temperature and humidity errors at BBM increase by a factor of up to 5 compared to other periods [*Garcia-Carreras et al.*, 2013], incentivising their representation even without regard to dust. Much more broadly, accurate forecasting of the WAM is an important societal goal given the dependence on rain-fed agriculture in the Sahel [*FAO*, 2009].

Moisture presents a difficulty for observing dust as well as modelling it. No high temporal resolution satellite product has the capability to detect dust under cloud [*Ashpole and Washington*, 2013b]. Sun photometers cannot retrieve dust when cloud is present. Because of the diurnal cycle of deep convection, cold pool outflows very frequently occur at night, when the sun photometer cannot retrieve and when observers do not usually report. It is important to take this into consideration when planning field campaigns in the central Sahara and regions where cold pools are frequent. Likewise, it is important to be aware of the potential biases of sun photometer measurements when using them to validate models or satellite algorithms.

Observations of surface wind speeds from across the CWS show that there is a 'long tail' of wind speeds greater than about 6 m s^{-1}. ALAM and GLOBAL significantly underpredict the frequency of these high wind speeds. Dust emission schemes driven by these model winds will therefore underestimate dust greatly because (i) 6 m s^{-1} is probably the minimum dust emission threshold across the Sahara [e.g. *Callot et al.*, 2000] (ii) dust emission is more closely proportional to the third power of wind speed than wind speed alone, as has been found by many studies from *Bagnold* [1941]

onwards and confirmed here at BBM. At stations dominated by cold pools the underprediction of the long tail is likely due to the fact that cold pools are not represented in ALAM or GLOBAL; at stations where LLJs are more frequent it is likely that LLJ momentum mix-down is poorly represented, or that the model output is not archived at 0900 (the case for GLOBAL). Including subgrid-scale wind speed variability to the models may lead to more accurate dust emission fluxes, as found by several studies [*Cakmur et al.*, 2004; *R L Miller et al.*, 2006; *Marcella and Eltahir*, 2010].

9.3. Implications

The research presented in this DPhil points to a thought-provoking thesis: that summertime North Africa is probably a great deal dustier than current estimates suggest. This argument arises from the fact that almost all the techniques that are currently used to study dust in the region are systematically biased to result in underestimates of dust burden.

Observations presented here show that cold pool outflows – which both emit and advect dust – are by far the most important atmospheric dust mechanism in the central Sahara. However, because of the high (~7 km) horizontal resolution required for their simulation, cold pool outflows are not resolved in most numerical models used for weather prediction and certainly not in climate projections. Cold pools rarely occur during the daytime or in cloud-free conditions in the central Sahara. As a result, sun photometer measurements will underestimate dust here and also in the Sahel, because they cannot retrieve at night or below cloud. Taking monthly-mean photometer AOTs is therefore not representative of the true dust burden in these regions.

Cold pool outflows occurring under cloud will also be missed by satellites that cannot retrieve below cloud (i.e. any that use infrared, visible or ultraviolet wavelengths). Cold pool outflows occurring at night will be missed by satellites that only pass over the central Sahara during daylight hours. This is all of the A-train satellites (including the MODIS, OMI[20], POLDER[21] and CALIOP[22] dust-retrieving instruments); Nimbus 7 (including the TOMS instrument) and Terra (including the MODIS and MISR[23] instruments), in other words most of the satellite instruments used to estimate dust loadings. Developed using an instrument on a geostationary satellite exploiting the infrared spectrum, the SEVIRI false-colour dust detection algorithm [*Lensky and Rosenfeld*, 2008] can retrieve over North Africa at night but the false-colour dust detection algorithm suffers from limitations that cause it to miss dust under conditions of high (relatively speaking) column water vapour (>20 mm) [*Brindley et al.*, 2012]. Since cold pool outflows are usually associated with higher levels of water vapour than their environments, SEVIRI false-colour dust detection will therefore also underestimate cold pool contribution to Saharan dustiness. Somewhat strangely, SEVIRI-derived dust AOTs overestimate AOT under moist conditions [*Banks et al.*, 2013], but SEVIRI AOTs are currently only available during daylight hours [*Banks and Brindley*, 2013] so will not detect the frequently-occurring night-time cold pools.

Although the Fennec field observations suggest that LLJs only contribute moderately to central Saharan dust totals, their wind profiles and core wind speeds are usually underestimated by the models and reanalysis examined here, by more than 10 m s^{-1} in some cases. Even if the models do not have problems mixing momentum to the surface (which is probably not the case), this will result in an underestimate of dust emission

[20] Ozone Monitoring Instrument (on board the Aura satellite)
[21] Polarization and Directionality of the Earth's Reflectance instrument (on board the Parasol satellite)
[22] Cloud-Aerosol Lidar with Orthogonal Polarization (on board the Calipso satellite)
[23] Multi-angle Imaging SpectroRadiometer

because the observations at BBM show that only the very strongest LLJs result in dust emission. Therefore modelled LLJ dust emission is likely to be underestimated in the summertime central Sahara. Furthermore, ALAM and GLOBAL underpredict the frequency of surface wind speeds > 6 m s^{-1} compared with Fennec observations. Given the threshold cubic nature of dust uplift, emission schemes driven with these models will severely underestimate dust emission. Modelling groups can recalibrate their calculated emission upward, which may be a suitable approach if the goal is to calculate the climate impact of dust radiative forcing. However, the unintended effect is that recalibrated models have the wrong mechanistic sensitivity, which is a liability in climate change projections.

The results from BBM have demonstrated that advected dust is a very important component of the Saharan dust burden. However, this is missed by 'uplift potential' type approaches [*Marsham et al.*, 2011; *Marsham et al.*, 2013; *Roberts and Knippertz*, 2014], which estimate dust emission but do not consider the lifetime of the dust in the atmosphere after emission. Since advected dust frequently carried very large particles to BBM[24], this dust will have important radiative impacts: *Ryder et al.* [2013] document an exceptional abundance of coarse-mode dust (up to 300μm diameter) during the Fennec 2011 aircraft campaign and demonstrate that this results in much more absorption over the Sahara than previously thought. Finally, thick dust also compromises active remote sensing because it attenuates the electromagnetic signal. This was a problem with the lidar at BBM, but is also a problem with airborne and satellite lidar instruments. In all cases, the result will be an underestimation of dust loadings.

[24] Possibly caused by the unusual situation of having an elevated cold pool propagate above the nocturnal temperature inversion then break-down to the surface at sunrise, as discussed in Chapter 5.

As described, almost all of these techniques and technologies are systematically biased to underestimate dust loadings in the summertime central Sahara. The inference is therefore that the central Sahara is much dustier than current estimates suggest. These conclusions would not be possible without the remote observations provided by Fennec (or an assessment of their limitations). In Chapter 3, a case was made for observations as a way of choosing between disparate views provided by models or satellite retrievals. This still holds – we could now suggest that the upper estimate of dust emission from North Africa provided by [*Huneeus et al.*, 2011] is probably closer to the truth than the lower estimate. However, the thesis has also identified a more insidious problem: agreement between estimates does not imply accuracy. Sun photometer, model and satellite dust retrievals may give similar results over the central Sahara, but they share the same bias – they all underestimate the contribution of cold pool outflows. So their agreement must not be assumed to imply accuracy. Certainly care should be taken when tuning models to satellite observations and sun photometer measurements, because these are themselves biased.

9.4. Further work

There are of course many areas where this research could be expanded. Potential future work can be grouped into four general categories: (i) temporal expansion (ii) greater depth and breadth (iii) specific scientific questions arisen (iv) application to other dust source regions. These four categories will be addressed in turn.

The thesis has focused on June 2011 and, to a lesser extent, June 2012. This is because summer is the dustiest month in the central Sahara and because June was when the most comprehensive instrumentation was available. However, an investigation of the dust mechanisms operating in the central Sahara during late summer and other seasons

would be worthwhile, to establish whether the contribution of the dust mechanisms differs, as would be expected outside the monsoon season. It would be difficult because - beyond June 2011 and June 2012 - the instrumentation at BBM is very basic. However, the methods used in Chapter 8 provide a possible way forward. In the same chapter, model and observed surface wind speed distributions were compared at three stations in June 2011; this work could be expanded to include June 2012 when AWS data was more complete and more stations could be compared.

A limitation of this research in general has been the data availability. With only one month when all the instruments were available at BBM, dust burden estimates beyond June 2011 - particularly for dust advection - have come with uncertainties, although these have been explicitly identified and quantified as far as possible (Chapter 7). Having no dust instruments at the AWSs is a significant limitation, as is their frequent periods with missing data (Chapter 8). Nonetheless, the AWS network has now generated several years of data, meaning that a longer assessment of interannual variability is now a real possibility. It should be mentioned that organising and operating a large-scale field campaign across a remote, hyper-arid and politically unstable region roughly the size of Argentina is hugely difficult!

A number of avenues could be explored to deepen and broaden the research. A more extensive model validation exercise from the Fennec data would be valuable. GLOBAL, ALAM and ERAI have been compared with regard to their simulation of LLJ wind profiles at BBM and at the Fennec radiosonde stations (Chapters 6 and 8), but a detailed assessment of the causes of model errors has not been attempted. The boundary layer schemes may be one cause of the problem. For LLJs, correct simulation of the stable nocturnal boundary layer is particularly important, but NWP simulation of stable

stratification is surprisingly difficult [*Sandu et al.*, 2013]. It would be very informative to validate a larger suite of NWP models and reanalyses. A validation of ERAI surface wind speeds across the CWS is currently in progress: the research shows that ERAI does not generally capture the amplitude of the diurnal cycle and underestimates surface wind speeds on LLJ mornings [*Caton-Harrison and Washington*, in prep.]. It would also be interesting to see whether incorporation of sub-grid scale variability improves the model surface wind speeds evaluated here, and to assess the magnitude of surface wind speed errors on days when cold pools occur.

Direct calculations of dust burden were not made in this thesis: (close) proxies of dustiness such as lidar backscatter and nephelometer scattering have been used. Converting these proxies into dust concentrations would in theory provide a more accurate measure of dust burden; certainly it should make it easier for the model community to evaluate modelled dust loadings. However, these calculations would require certain assumptions about the size distribution and optical characteristics of the dust, which would be a source of uncertainty; converting lidar backscatter into AOT may require fewer assumptions and be a more appropriate 'half-way' point.

This thesis has focused on the erosivity side of the dust cycle, therefore a deeper analysis would need to incorporate some view of erodibility. Given that the central Sahara is hyper arid, it seems a fair assumption that erodibility here does not display significant interannual variability. However, our understanding of the spatial variability of erodibility in the Sahara is fairly poor due to the lack of surface observations [e.g. *Shao et al.*, 2011]. Correct specification of dust source regions is important because strong winds acting on supposedly but wrongly specified non-erodible regions will underestimate dust emission (and vice versa for wrongly specified erodible regions).

Tuning the model emissions to match satellite estimates provides a 'fix' but the satellite observations may be biased, as argued in Section 9.3. Unfortunately, the size of the Sahara and the current dangers of travel there make field work a difficult proposition; high resolution satellite source maps [e.g. *Ginoux et al.*, 2012; *Ashpole and Washington*, 2013b] are an attractive alternative provided their limitations are not overlooked.

The third category of further work discussed here consists of three specific and intriguing scientific questions that have arisen from the research, although there could be many more. Firstly, why are cold pool outflows and monsoon surges particularly efficient dust producers (i.e. more dust produced per hour) compared with the other mechanisms? The hypothesis is that, because the air is more dense during cold pool and monsoon surge events, more dust can be lifted for the same wind speed. It might also be the case that denser air reduces the settling of dust particles back to the surface, explaining why cold pool advection can contain such large particles and high concentrations of dust. Alternatively, the particularly high dust loadings during cold pools could be because they can contain both advected and locally emitted dust during the passage of the gust front. These hypotheses could be tested in a number of ways including theoretical or laboratory approaches, numerical modelling and field work.

For Saharan dust to have remote effects (radiative and biogeochemical) in other parts of the world it must be transported out of the desert. In summer this requires the dust to be lifted above the southerly monsoon flow and transported westward across the Atlantic [*Goudie and Middleton*, 2006; *Schepanski et al.*, 2009]. The second intriguing puzzle is therefore to establish which of the atmospheric dust mechanisms examined in this thesis ultimately results in the most long-range transport. It seems likely that the direction of the flow may be more important than the precise nature of the dust mechanism:

southward propagating cold pools and LLJs should result in more dust being lifted above the monsoon layer to the south of the Sahara, ready for westward transport in the SAL. However, this may not always be necessary: aircraft observations have documented a cold pool 'injecting' dust into or even above the SAL [*Flamant et al.*, 2007]. Events that emit or advect dust higher up into the atmosphere are more likely to result in dust penetrating above the CBL and thus being available for long-range transport. There is evidence from the lidar to suggest that dry convective plumes took dust higher into the atmosphere than cold pools and LLJs (typically over 1km, Table 5-1), but frequently the lidar signal was attenuated during cold pools and LLJs so the confidence in this result is low.

The third question is, given that the key dust mechanisms found here are associated with the monsoon, is it possible to develop a statistical prediction scheme that estimates summer Saharan dust production using the monsoon as a predictor? SDF would be a suitable dataset for an initial investigation of this possibility. Such a prediction scheme would have useful applications, not least because increased dust from the Sahara may suppress tropical cyclone formation in the North Atlantic [e.g. *Evan et al.*, 2006].

Finally, if dust in the central Sahara is underestimated, as argued in this thesis, an obvious follow-up question is whether this could be the case at other dust sources. It would likely be the case in other regions where cold pools are important. These include the Sahel [e.g. *Williams*, 2008], the Arabian Peninsula [e.g. *S D Miller et al.*, 2008], Australia [e.g. *McTainsh et al.*, 2005] and the south-western USA [e.g. *Idso*, 1973]. Likewise, models might be expected to underestimate dust emission from regions where LLJs are particularly important if they underestimate LLJ wind profiles and/or surface winds in these regions. This has been found to be the case for some regional models in

the Bodélé Depression, in the eastern Sahara [*Todd et al.*, 2008a; *Todd et al.*, 2008b; *Heinold et al.*, 2011]. These hypotheses would be worthwhile investigating with targeted and carefully instrumented ground campaigns. If they are correct, an intriguing possibility is that not only could the dustiest region in the world be more dusty than previously thought, but that dust regions globally may produce more dust than we have imagined.

9.5. References

Ashpole, I., and R. Washington (2012), An automated dust detection using SEVIRI: A multiyear climatology of summertime dustiness in the central and western Sahara, *J. Geophys. Res.*, *117*(D8), D08202, doi: 10.1029/2011jd016845.

Ashpole, I., and R. Washington (2013a), Intraseasonal variability and atmospheric controls on daily dust occurrence frequency over the central and western Sahara during the boreal summer, *Journal of Geophysical Research: Atmospheres*, *118*(23), 2013JD020267, doi: 10.1002/2013jd020267.

Ashpole, I., and R. Washington (2013b), A new high-resolution central and western Saharan summertime dust source map from automated satellite dust plume tracking, *Journal of Geophysical Research D: Atmospheres*, *118*(13), 6981-6995, doi: 10.1002/jgrd.50554.

Bagnold, R. A. (1941), *The Physics of Blown Sand and Desert Dunes*, Methuen, London.

Banks, J. R., and H. E. Brindley (2013), Evaluation of MSG-SEVIRI mineral dust retrieval products over North Africa and the Middle East, *Remote Sensing of Environment*, *128*(0), 58-73, doi: 10.1016/j.rse.2012.07.017.

Banks, J. R., H. E. Brindley, C. Flamant, M. J. Garay, N. C. Hsu, O. V. Kalashnikova, L. Klüser, and A. M. Sayer (2013), Intercomparison of satellite dust retrieval products over the west African Sahara during the Fennec campaign in June 2011, *Remote Sensing of Environment*, *136*(0), 99-116, doi: 10.1016/j.rse.2013.05.003.

Bou Karam, D., C. Flamant, P. Knippertz, O. Reitebuch, J. Pelon, M. Chong, and A. Dabas (2008), Dust emissions over the Sahel associated with the West African monsoon intertropical discontinuity region: A representative case-study, *Quarterly Journal of the Royal Meteorological Society*, *134*(632), 621-634, doi: 10.1002/qj.244.

Brindley, H., P. Knippertz, C. Ryder, and I. Ashpole (2012), A critical evaluation of the ability of the Spinning Enhanced Visible and Infrared Imager (SEVIRI) thermal infrared red-green-blue rendering to identify dust events: Theoretical analysis, *Journal of Geophysical Research D: Atmospheres*, *117*(7), doi: 10.1029/2011JD017326.

Cakmur, R. V., R. L. Miller, and O. Torres (2004), Incorporating the effect of small-scale circulations upon dust emission in an atmospheric general circulation model, *Journal of Geophysical Research: Atmospheres*, *109*(D7), D07201, doi: 10.1029/2003jd004067.

Callot, Y., B. Marticorena, and G. Bergametti (2000), Geomorphologic approach for modelling the surface features of arid environments in a model of dust emissions: Application to the Sahara desert, *Geodinamica Acta*, *13*(5), 245-270, doi: 10.1016/S0985-3111(00)01044-5.

Caton-Harrison, T., and R. Washington (in prep.), ERA-Interim representation of summertime winds in the Saharan heat low region: an evaluation against ground observations from the Fennec Campaign.

Charba, J. (1974), Application of Gravity Current Model to Analysis of Squall-Line Gust Front, *Monthly Weather Review*, *102*(2), 140-156, doi: 10.1175/1520-0493(1974)102<0140:aogcmt>2.0.co;2.

Cowie, S. M., P. Knippertz, and J. H. Marsham (2014), A climatology of dust emission events from northern Africa using long-term surface observations, *Atmos. Chem. Phys.*, *14*(16), 8579-8597, doi: 10.5194/acp-14-8579-2014.

Emmel, C., P. Knippertz, and O. Schulz (2010), Climatology of convective density currents in the southern foothills of the Atlas Mountains, *J. Geophys. Res.*, *115*(D11), D11115, doi: 10.1029/2009jd012863.

Engelstaedter, S., and R. Washington (2007), Atmospheric controls on the annual cycle of North African dust, *J. Geophys. Res.*, *112*(D3), D03103, doi: 10.1029/2006jd007195.

Engelstaedter, S., R. Washington, C. Flamant, D. Parker, C. J. T. Allen, and M. C. Todd (2015), The Saharan heat low and moisture transport pathways in the central Sahara – multi-aircraft observations and Africa-LAM evaluation, *Journal of Geophysical Research-Atmospheres 120*, doi:10.1002/2015JD023123.

Evan, A. T., J. Dunion, J. A. Foley, A. K. Heidinger, and C. S. Velden (2006), New evidence for a relationship between Atlantic tropical cyclone activity and African dust outbreaks, *Geophysical Research Letters*, *33*(19), L19813, doi: 10.1029/2006gl026408.

FAO (2009), *Food and Agriculture Organisation of the United Nations Statistical Yearbook 2009*, United Nations, Rome.

Fiedler, S., K. Schepanski, B. Heinold, P. Knippertz, and I. Tegen (2013), Climatology of Nocturnal Low-Level Jets over North Africa and Implications for Modeling Mineral Dust Emission, *Journal of Geophysical Research: Atmospheres*, *118*, 6100–6121, doi: 10.1002/jgrd.50394.

Flamant, C., P. Knippertz, D. J. Parker, J. P. Chaboureau, C. Lavaysse, A. Agusti-Panareda, and L. Kergoat (2009), The impact of a mesoscale convective system cold pool on the northward propagation of the intertropical discontinuity over West Africa, *Quarterly Journal of the Royal Meteorological Society*, *135*(638), 139-159, doi: 10.1002/qj.357.

Flamant, C., J. P. Chaboureau, D. J. Parker, C. M. Taylor, J. P. Cammas, O. Bock, F. Timouk, and J. Pelon (2007), Airborne observations of the impact of a convective system on the planetary boundary layer thermodynamics and aerosol distribution in the inter-tropical discontinuity region of the West African Monsoon, *Quarterly Journal of the Royal Meteorological Society*, *133*(626), 1175-1189, doi: 10.1002/qj.97.

Garcia-Carreras, L., J. H. Marsham, D. J. Parker, C. L. Bain, S. Milton, A. Saci, M. Salah-Ferroudj, B. Ouchene, and R. Washington (2013), The impact of convective cold pool outflows on model biases in the Sahara, *Geophysical Research Letters*, *40*(8), 1647-1652, doi: 10.1002/grl.50239.

Ginoux, P., J. M. Prospero, T. E. Gill, N. C. Hsu, and M. Zhao (2012), Global-scale attribution of anthropogenic and natural dust sources and their emission rates based on MODIS Deep Blue aerosol products, *Reviews of Geophysics*, *50*(3), doi: 10.1029/2012RG000388.

Goudie, A. S., and N. J. Middleton (2006), *Desert Dust in the Global System*, 287 pp., Springer, Berlin.

Grandpeix, J.-Y., and J.-P. Lafore (2009), A Density Current Parameterization Coupled with Emanuel's Convection Scheme. Part I: The Models, *Journal of the Atmospheric Sciences*, *67*(4), 881-897, doi: 10.1175/2009jas3044.1.

Heinold, B., I. Tegen, S. Bauer, and M. Wendisch (2011), Regional modelling of Saharan dust and biomass-burning smoke Part 2: Direct radiative forcing and atmospheric dynamic response, *63*(4).

Heinold, B., P. Knippertz, J. H. Marsham, S. Fiedler, N. S. Dixon, K. Schepanski, B. Laurent, and I. Tegen (2013), The role of deep convection and nocturnal low-level jets for dust emission in summertime West Africa: Estimates from convection-permitting simulations, *Journal of Geophysical Research: Atmospheres*, *118*, 4385–4400, doi: 10.1002/jgrd.50402.

Huneeus, N., M. Schulz, Y. Balkanski, J. Griesfeller, J. Prospero, S. Kinne, S. Bauer, O. Boucher, M. Chin, F. Dentener, T. Diehl, R. Easter, D. Fillmore, S. Ghan, P. Ginoux, A. Grini, L. Horowitz, D. Koch, M. C. Krol, W. Landing, X. Liu, N. Mahowald, R. Miller, J. J. Morcrette, G. Myhre, J. Penner, J. Perlwitz, P. Stier, T. Takemura, and C. S. Zender (2011), Global dust model intercomparison in AeroCom phase I, *Atmos. Chem. Phys.*, *11*(15), 7781-7816, doi: 10.5194/acp-11-7781-2011.

Idso, C. W. (1973), Haboobs in Arizona, *Weather*, *28*(4), 154-155, doi: 10.1002/j.1477-8696.1973.tb02253.x.

Jemmett-Smith, B. C., J. H. Marsham, P. Knippertz, and C. A. Gilkeson (2015), Quantifying global dust devil occurrence from meteorological analyses, *Geophysical Research Letters*, 2015GL063078, doi: 10.1002/2015gl063078.

Knippertz, P. (2008), Dust emissions in the West African heat trough the role of the diurnal cycle and of extratropical disturbances, *Meteorologische Zeitschrift*, *17*(5), 553-563, doi: 10.1127/0941-2948/2008/0315.

Koch, J., and N. O. Renno (2005), The role of convective plumes and vortices on the global aerosol budget, *Geophys. Res. Lett.*, *32*(18), L18806, doi: 10.1029/2005gl023420.

Kok, J. F., S. Albani, N. M. Mahowald, and D. S. Ward (2014), An improved dust emission model – Part 2: Evaluation in the Community Earth System Model, with implications for the

use of dust source functions, *Atmos. Chem. Phys.*, *14*(23), 13043-13061, doi: 10.5194/acp-14-13043-2014.
Krumm, W. R. (1954), On the cause of downdrafts from dry thunderstorms over the plateau area of the United States, *Bull. Am. Meteorol. Soc*, *35*(3), 122-125.
Lensky, I. M., and D. Rosenfeld (2008), Clouds-Aerosols-Precipitation Satellite Analysis Tool (CAPSAT), *Atmos. Chem. Phys.*, *8*(22), 6739-6753, doi: 10.5194/acp-8-6739-2008.
Marcella, M. P., and E. A. B. Eltahir (2008), Modeling the Hydroclimatology of Kuwait: The Role of Subcloud Evaporation in Semiarid Climates, *Journal of Climate*, *21*(12), 2976-2989, doi: 10.1175/2007jcli2123.1.
Marcella, M. P., and E. A. B. Eltahir (2010), Effects of mineral aerosols on the summertime climate of southwest Asia: Incorporating subgrid variability in a dust emission scheme, *Journal of Geophysical Research: Atmospheres*, *115*(D18), D18203, doi: 10.1029/2010jd014036.
Marsham, J. H., P. Knippertz, N. S. Dixon, D. J. Parker, and G. M. S. Lister (2011), The importance of the representation of deep convection for modeled dust-generating winds over West Africa during summer, *Geophys. Res. Lett.*, *38*(16), L16803, doi: 10.1029/2011gl048368.
Marsham, J. H., M. Hobby, C. J. T. Allen, J. R. Banks, M. Bart, B. J. Brooks, C. Cavazos-Guerra, S. Engelstaedter, M. Gascoyne, A. R. Lima, J. V. Martins, J. B. McQuaid, A. O'Leary, B. Ouchene, A. Ouladichir, D. J. Parker, A. Saci, M. Salah-Ferroudj, M. C. Todd, and R. Washington (2013), Meteorology and dust in the central Sahara: Observations from Fennec supersite-1 during the June 2011 Intensive Observation Period, *Journal of Geophysical Research: Atmospheres*, *118*, 4069–4089, doi: 10.1002/jgrd.50211.
Marticorena, B., and G. Bergametti (1995), Modeling the atmospheric dust cycle: 1. Design of a soil-derived dust emission scheme, *J. Geophys. Res.*, *100*(D8), 16415-16430, doi: 10.1029/95jd00690.
McTainsh, G., Y.-c. Chan, H. McGowan, J. Leys, and K. Tews (2005), The 23rd October 2002 dust storm in eastern Australia: characteristics and meteorological conditions, *Atmospheric Environment*, *39*(7), 1227-1236, doi: 10.1016/j.atmosenv.2004.10.016.
Miller, R. L., J. Perlwitz, and I. Tegen (2004), Feedback upon dust emission by dust radiative forcing through the planetary boundary layer, *Journal of Geophysical Research: Atmospheres*, *109*(D24), D24209, doi: 10.1029/2004jd004912.
Miller, R. L., R. V. Cakmur, J. Perlwitz, I. V. Geogdzhayev, P. Ginoux, D. Koch, K. E. Kohfeld, C. Prigent, R. Ruedy, G. A. Schmidt, and I. Tegen (2006), Mineral dust aerosols in the NASA Goddard Institute for Space Sciences ModelE atmospheric general circulation model, *Journal of Geophysical Research: Atmospheres*, *111*(D6), D06208, doi: 10.1029/2005jd005796.
Miller, S. D., A. P. Kuciauskas, M. Liu, Q. Ji, J. S. Reid, D. W. Breed, A. L. Walker, and A. A. Mandoos (2008), Haboob dust storms of the southern Arabian Peninsula, *Journal of Geophysical Research D: Atmospheres*, *113*(1), doi: 10.1029/2007JD008550.
Moncrieff, M. W., and C. Liu (1999), Convection initiation by density currents: Role of convergence, shear, and dynamical organization, *Monthly Weather Review*, *127*(10), 2455-2464.
Reinfried, F., I. Tegen, B. Heinold, O. Hellmuth, K. Schepanski, U. Cubasch, H. Huebener, and P. Knippertz (2009), Simulations of convectively-driven density currents in the Atlas region using a regional model: Impacts on dust emission and sensitivity to horizontal resolution and convection schemes, *Journal of Geophysical Research: Atmospheres*, *114*(D8), D08127, doi: 10.1029/2008jd010844.
Roberts, A. J., and P. Knippertz (2014), The formation of a large summertime Saharan dust plume: Convective and synoptic-scale analysis, *Journal of Geophysical Research: Atmospheres*, *119*(4), 1766-1785, doi: 10.1002/2013jd020667.
Rodwell, M. J., and B. J. Hoskins (1996), Monsoons and the dynamics of deserts, *Quarterly Journal of the Royal Meteorological Society*, *122*(534), 1385-1404, doi: 10.1002/qj.49712253408.

Ryder, C. L., E. J. Highwood, P. D. Rosenberg, J. Trembath, J. K. Brooke, M. Bart, A. Dean, J. Crosier, J. Dorsey, H. Brindley, J. Banks, J. H. Marsham, J. B. McQuaid, H. Sodemann, and R. Washington (2013), Optical properties of Saharan dust aerosol and contribution from the coarse mode as measured during the Fennec 2011 aircraft campaign, *Atmos. Chem. Phys.*, *13*(1), 303-325, doi: 10.5194/acp-13-303-2013.

Sandu, I., A. Beljaars, P. Bechtold, T. Mauritsen, and G. Balsamo (2013), Why is it so difficult to represent stably stratified conditions in numerical weather prediction (NWP) models?, *Journal of Advances in Modeling Earth Systems*, *5*(2), 117-133, doi: 10.1002/jame.20013.

Schepanski, K., I. Tegen, and A. Macke (2009), Saharan dust transport and deposition towards the tropical northern Atlantic, *Atmos. Chem. Phys.*, *9*(4), 1173-1189, doi: 10.5194/acp-9-1173-2009.

Shao, Y., K.-H. Wyrwoll, A. Chappell, J. Huang, Z. Lin, G. H. McTainsh, M. Mikami, T. Y. Tanaka, X. Wang, and S. Yoon (2011), Dust cycle: An emerging core theme in Earth system science, *Aeolian Research*, *2*(4), 181-204, doi: 10.1016/j.aeolia.2011.02.001.

Sultan, B., and S. Janicot (2000), Abrupt shift of the ITCZ over West Africa and intra-seasonal variability, *Geophysical Research Letters*, *27*(20), 3353-3356, doi: 10.1029/1999gl011285.

Sultan, B., and S. Janicot (2003), The West African monsoon dynamics. Part II: The "preonset" and "onset" of the summer monsoon, *Journal of Climate*, *16*(21), 3407-3427, doi: 10.1175/1520-0442(2003)016<3407:TWAMDP>2.0.CO;2.

Tegen, I., S. P. Harrison, K. Kohfeld, I. C. Prentice, M. Coe, and M. Heimann (2002), Impact of vegetation and preferential source areas on global dust aerosol: Results from a model study, *Journal of Geophysical Research: Atmospheres*, *107*(D21), 4576, doi: 10.1029/2001jd000963.

Todd, M. C., R. Washington, S. Raghavan, G. Lizcano, and P. Knippertz (2008a), Regional model simulations of the Bodélé low-level jet of Northern Chad during the Bodélé dust experiment (BoDEx 2005), *Journal of Climate*, *21*(5), 995-1012, doi: 10.1175/2007JCLI1766.1.

Todd, M. C., D. Bou Karam, C. Cavazos, C. Bouet, B. Heinold, J. M. Baldasano, G. Cautenet, I. Koren, C. Perez, F. Solmon, I. Tegen, P. Tulet, R. Washington, and A. Zakey (2008b), Quantifying uncertainty in estimates of mineral dust flux: An intercomparison of model performance over the Bodélé Depression, northern Chad, *Journal of Geophysical Research: Atmospheres*, *113*(D24), D24107, doi: 10.1029/2008jd010476.

Todd, M. C., C. J. T. Allen, M. Bart, M. Bechir, J. Bentefouet, B. J. Brooks, C. Cavazos-Guerra, T. Clovis, S. Deyane, M. Dieh, S. Engelstaedter, C. Flamant, L. Garcia-Carreras, A. Gandega, M. Gascoyne, M. Hobby, C. Kocha, C. Lavaysse, J. H. Marsham, J. V. Martins, J. B. McQuaid, J. B. Ngamini, D. J. Parker, T. Podvin, A. Rocha-Lima, S. Traore, Y. Wang, and R. Washington (2013), Meteorological and dust aerosol conditions over the Western Saharan region observed at Fennec supersite-2 during the Intensive Observation Period in June 2011, *Journal of Geophysical Research: Atmospheres*, *118*, 8426–8447, doi: 10.1002/jgrd.50470.

Williams, E. (2008), Comment on "Atmospheric controls on the annual cycle of North African dust" by S. Engelstaedter and R. Washington, *J. Geophys. Res.*, *113*(D23), D23109, doi: 10.1029/2008jd009930.

10. List of co-author papers

The following is a list of the papers on which I have been a co-author during my DPhil.

Ryder, C. L., McQuaid, J. B., Flamant, C., Washington, R., Brindley, H. E., Highwood, E. J., Marsham, J. H., Parker, D. J., Todd, M. C., Banks, J. R., Brooke, J. K., Engelstaedter, S., Estellés, V., Formenti, P., Garcia-Carreras, L., Kocha, C., Marenco, F., Rosenberg, P., Sodemann, H., **Allen, C. J. T.**, Bourdon, A., Bart, M., Cavazos-Guerra, C., Chevaillier, S., Crosier, J., Darbyshire, E., Dean, A. R., Dorsey, J. R., Kent, J., O'Sullivan, D., Schepanski, K., Szpek, K., and Woolley, A **(2015)** Advances in understanding mineral dust and boundary layer processes over the Sahara from Fennec aircraft observations, *Atmospheric Chemistry and Physics Discussions* doi: 10.5194/acpd-15-199-2015

Todd, M.C., **Allen, C.J.T**., Bart, M., Bechir, M., Bentefouet, J., Brooks, A.B.J., Cavazos-Guerra, C., Clovis, T., Dieh, M.F., Engelstaedter, S., Flamant, C., Garcia-Carreras, L., Gandega, A., Gascoyne, M., Hobby, M., Kocha, C., Lavaysse, C., Marsham, J.H., Martins, J.V., McQuaid, J.B., Ngamini, J.B., Parker, D.J., Podvin, T., Rocha-Lima, A., Traoré, S., Wang, Y. and Washington, R. **(2013)** Meteorological and dust aerosol conditions over the Western Saharan region observed at Fennec supersite-2 during the Intensive Observation Period in June 2011. *Journal of Geophysical Research: Atmospheres* doi 10.1002/jgrd.50470.

Marsham, J.H., Hobby, M., **Allen, C.J.T**., Banks, J.R., Bart, M., Brooks, B.J., Cavazos-Guerra, C., Engelstaedter, S., Gascoyne, M., Lima, A.R., Martins, J.V., McQuaid, J.B., O'Leary, A., Ouchene, B., Ouladichir, A., Parker, D.J., Saci, A., Salah-Ferroudj, M., Todd, M.C., and Washington, R. **(2013)** Meteorology and dust in the central Sahara: Observations from Fennec supersite-1 during the June 2011 Intensive Observation Period. *Journal of Geophysical Research: Atmospheres*, doi 10.1002/jgrd.50211.

Hobby, M., Gascoyne, M., Marsham, J.H., Bart, M., **Allen, C.J.T.**, Engelstaedter, S., Dieh, M.F., Seddik, F., Gandega, A., Lane, R., McQuaid, J.B., Ouchene, B., Parker, D.J., Rosenberg, P., Salah Ferroudj, M., Saci, A., Todd, M.C., Walker, D. and Washington, R. **(2013)** The Fennec Automatic Weather Station (AWS) Network: monitoring the Saharan Climate System. *Journal of Atmospheric and Oceanic Technology* doi 10.1175/JTECH-D-12-00037.1.

Engelstaedter, S., Washington, R., Flamant, C., Parker D. J., **Allen, C.J.T.**, Todd, M.C. **(2015)** The Saharan heat low and moisture transport pathways in the central Sahara - multi-aircraft observations and Africa-LAM evaluation. *Journal of Geophysical Research: Atmospheres 120,* doi:10.1002/2015JD023123.